MEKELLE UNIVERSITY

COLLEGE OF NATURAL AND COMPUTATIONAL SCIENCES

SCHOOL OF EARTH SCIENCES

A

Thesis

On

Landslide Susceptibility Mapping Using Frequency Ratio (FR) and Weight of Evidence (WoE) Methods, and Verification Using the Limit Equilibrium (LE) Method: A Case Study along the Bonga - Felegeselam Road.

By

Hagos Kidanemariam Gebregewergs

ID No.: CNCS/PS196/09

Submitted to the Department of Earth Science in Partial Fulfillment of the Requirements for the Degree of Master of Science in Geological Engineering

Under the supervision of

Advisor: Gebremedhin Berhane (Ph.D.)

Co-advisor: Gebreslassie Mebrahtu (M.Sc.)

September 2025

Mekelle, Ethiopia.

APPROVAL SHEET

MEKELLE UNIVERSITY

COLLEGE OF NATURAL AND COMPUTATIONAL SCIENCES

SCHOOL OF EARTH SCIENCES

Landslide Susceptibility Mapping Using Frequency Ratio (FR) and Weight of Evidence (WoE) Methods, and Verification Using the Limit Equilibrium (LE) Method: A Case Study along the Bonga - Felegeselam Road.

SUBMITTED BY:

Hagos Kidanemariam Gebregewergs	CNCS/PS196/09	_____	_____
Student's Name	ID. No.	Signature	Date

APPROVED BY:

1. Dr. Gebremedhin Berhane (Assoc. Prof.)	_____	_____
Advisor's Name	Signature	Date
2. _____	_____	_____
Department Head	Signature	Date
3. Mr. Tesfahunegn Abera (Asst.Prof.)	_____	_____
Chairperson	Signature	Date
4. Dr. Asmelash Abay (Assoc.Prof.)	_____	_____
Internal Examiner	Signature	Date
5. Mr. Yonas Hadush	_____	_____
External Examiner	Signature	Date

Declaration

I, the undersigned, declare that this thesis entitled "***Landslide Susceptibility Mapping Using Frequency Ratio (FR) and Weight of Evidence (WoE) Methods, and Verification Using the Limit Equilibrium (LE) Method: A Case Study along the Bonga - Felegeselam Road***" is my original work and has not been presented for any other award, and that all sources of materials used in this thesis are duly acknowledged. This thesis was carried out under the supervision of my principal advisor Gebremedhin Berhane (Ph.D.), Department of Geology, College of Natural and Computational Sciences, Mekelle University in the academic year of 2025.

Name of student candidate: Hagos Kidanemariam Gebregewergs

Signature with date: _____

This thesis has been submitted for examination with my approval as university **advisor/co-advisor**.

Name of the advisor: Dr. Gebremedhin Berhane (Assoc.Prof.)

Signature of the Advisor with date: _____

Name of the co-advisor: Mr. Gebreslassie Mebrahtu (Asst.Prof.)

Signature of the co-advisor with date: _____

Place: **Mekelle University, Mekelle, Ethiopia**

Date of submission: _____

ACKNOWLEDGEMENTS

Above all, I want to sincerely thank to Almighty God for his blessings and strength from the start to end of this thesis work; without him, this research would not have been possible. I am highly grateful to my advisor, Gebremedhin Berhane (Ph.D.), who has relentlessly shaped my professional knowledge and offered constant support and direction during my thesis work. I would like to express my gratitude to my co-advisor, Assistant Professor Gebreslassie Mebrahtu, for his support and encouragement. Great thanks to Mekelle University, particularly the Department of Earth Sciences, and Civil Works Consulting Engineers Plc (CWCE), for providing me with the chance to pursue a Master of Science in Geological Engineering. I sincerely thank CWCE and Core Consulting Engineers Plc for sharing their priceless data. I am also grateful for the free online data available by institutions such as the United States Geological Survey (USGS), Alaska Satellite Facility (ASF), Ethiopian Geological Survey (EGS), Ethiopia Geospatial Agency (EGA), and Ethiopian Meteorological Institute (EMI). I honestly appreciate Stadia Engineering Works Consultant PLC for allowed me laboratory testing services and provided vehicle for the field work. Special thanks to the field team and technical staff for helping to successfully complete the site work. I would like to express my sincere gratitude for the amazing people of Bonga, Felegeselam, and Amaya for their help and giving directions throughout the fieldwork. I am incredibly grateful to my friends, colleagues, and coworkers for their solid moral support and inspiration during trying times. Finally, I would like to express my sincere gratitude to my wife, Mahlet, my sons, Elnathan and Nabel, and my entire family for their patience, love, and sacrifice. I have benefited greatly from their unwavering support.

TABLE OF CONTENTS

LIST OF TABLES

LIST OF FIGURES

ACRONYMS

Acronym	*Explanations*	*Acronym*	*Explanations*
AAHSTO	American Association of State Highway and Transportation Officials	LE	Limit Equilibrium Method
AHP	Analytical Hierarchy Process	LHS	Left-Hand Side
ARCSDM	Arc Spatial Data Modeler	LSM	Landslide Susceptibility Mapping
ASTM	American Society for Testing and Materials	LSI	Landslide Susceptibility Index
AUC	Area Under the Curve	LULC	Land Use Land Cover
BH	Borehole	M	Medium Risk Zone
C	Cohesion	MER	Main Ethiopian Rift
CGCOC	China Geo-Engineering Corporation	MH	Silt, High Plasticity
CH	Clay, High Plasticity	ML	Silt, Low Plasticity
CI	Consistency Index	MPa	Mega Pascal
CL	Clay, Low Plasticity	MSEW	Mechanically Stabilized Earth Wall
CNCS	College of Natural and Computational Science	NMC	Natural Moisture Content
CR	Consistency Ratio	NNW	North-Northwest (direction)
CWCE	Civil Works Consulting Engineers PLC	NS	North-South (direction)
DEM	Digital Elevation Model	NW	Northwest (direction)
EIGS	Ethiopian Institute of Geological Survey	PHI	Friction Angle
EMI	Ethiopian Meteorological Institute	PLC	Private Limited Company
ERA	Ethiopian Roads Administration	RHS	Right-Hand Side
ES-EN	Ethiopian Standard - based on Eurocode 8	ROC	Receiver Operating Characteristic
FAO	Food and Agriculture Organization	RQD	Rock Quality Designation
FEM	Finite Element Method	RMR	Rock Mass Rating
FOS	Factor of Safety	SE	Southeast (direction)
FR	Frequency Ratio	SG	Specific Gravity
GIS	Geographic Information System	UCS	Unconfined Compressive Strength
GPS	Global Positioning System	UNDRR	United Nations Office for Disaster Risk Reduction
GSE	Geological Survey of Ethiopia	UNICONE	United Consulting Engineers plc
GSI	Geological Strength Index	USCS	Unified Soil Classification System
GWL	Groundwater Level	USGS	United States Geological Survey
H	High Risk Zone	UTM	Universal Transverse Mercator
ITCZ	Intertropical Convergence Zone	W^C	Weigh of contrast
Kn/m^3	Kilonewtons per Cubic Meter	WGS	World Geodetic System
LA	Limit Analysis	WOE	Weight of Evidence

ABSTRACT

Landslides are a critical geohazards in Ethiopia, particularly along mountainous and rift-margin road corridors, where they frequently disrupt transportation, damage infrastructure, and pose serious threats to human life. The study aims to generate landslide susceptibility mapping and slope stability analysis along the Bonga – Felegeselam road corridor. Initially, a total of 120 landslides were inventoried and mapped based on field visits and Google Earth image interpretation, and subsequently divided into two subsets: 70% for model training and 30% for validation. Eight landslide causative factors including slope angle, aspect, elevation, lithology, land use, distance to road, distance to stream and precipitation were selected based on geomorphological relevance and site verification. The relationship between landslide occurrence and causative factors was analyzed using frequency ratio (FR) and weight of evidence (WoE) models. Based on these models, landslide susceptibility maps were generated by integrating the weighted values of all factors and reclassified into five susceptibility zones: very low, low, moderate, high, and very high. The high and very high susceptibility zones accounted for 17.8% and 24.1% of the area in the FR and WoE models, respectively. The accuracy of the models was validated using the relative operating characteristic (ROC) curve and the area under the curve (AUC) values. The frequency ratio (FR) model achieved a prediction rate of 80.6%, while the WoE model yielded 79.1%, both indicating strong predictive capability. Geotechnical verification of eight road slope failures within moderate to very high susceptibility zones was performed using limit equilibrium method (LEM) based stability analyses. Secondary borehole and eight test pit data, supported by laboratory test results, were used to establish subsurface profiles and geotechnical parameters of the slope materials. Stability analyses using Bishop and Spencer methods under both dry and saturated conditions produced factors of safety ranging from 1.15 to 0.78 and 0.96 to 0.54, respectively. These results confirm the consistency of the susceptibility models by indicating strong agreement between mapped zones and stability analysis results. This approach provides a strong framework for landslide hazard management and informed infrastructure planning in Ethiopia and similar mountainous regions.

***Key Words**: Landslide inventory, Causative factors, Soil Properties, Factor of Safety (FoS), and Remedial measures.*

1 INTRODUCTION

1.1 BACKGROUND OF THE STUDY

Landslides continue to be a major global concern and are one of the most common and destructive geohazards. They involve the gravitational movement of rock, soil, or debris downslope and are caused by both natural and man-made factors (Cruden, 1996; Varnes, 1984). According to the United Nations Office for Disaster Risk Reduction (UNDRR, 2025), disasters result in direct economic losses of more than $202 billion every year, with environmental and cascade effects totaling more than $2.3 trillion. Particularly in steep and mountainous areas, landslides have caused numerous fatalities and severe damage to livelihoods.

Despite tremendous advancements in understanding of landslides, they still have a serious impact, causing enormous financial damage in developed countries and a high death toll in underdeveloped ones (Gariano & Guzzetti, 2016; Petley, 2012). Landslides are common in Ethiopia, particularly in the northern and southwestern highlands, where human activity exacerbates slope instability caused by complex geology, steep slopes, and heavy rainfall (Ayalew, 1999; Woldearegay, 2013).

In order to achieve the goals of national development, Ethiopia's road networks have grown significantly in recent years. However, much of this expansion has taken place without basic geotechnical investigation and landslide hazard mapping. Numerous highland routes have experienced costly and frequent failures as a result. Data on landslide hazards along these corridor are scarce; however, (Ayalew, 1999; Redshaw et al., 2017) reported that, landslides had harm transportation infrastructure by about USD 300,000 every year. In addition to causing significant damage to road infrastructure, neighborhoods, and agricultural land. Landslides are caused by a combination of natural and man-made elements have killed over 300 people and destroyed 100 kilometers of road (Ayalew, 1999).

Although landslide susceptibility mapping has been studied extensively around the world, it is still not widely used in Sub-Saharan Africa, especially in East Africa (Broeckx et al., 2017; Pal & Chowdhury, 2019). In order to address these issues, thorough mapping of landslide susceptibility has become an essential technique for identifying high-risk regions before they occur. These methods are particularly helpful in situations when there is a lack of equipment or comprehensive historical data, which may limit the adoption of deterministic techniques. According to Lee & Pradhan (2007) and Regmi et al., (2010), landslide susceptibility mapping uses statistical influences to determine the causes of prior landslip events, such as slope angle,

lithology, rainfall, land cover, and proximity to roads or streams. Although susceptibility maps indicate where landslides are likely to occur, they do not explain why or how a slope may fail in specific situations. To evaluate susceptibility data and offer viable mitigation techniques, slope stability analysis must be included, taking into consideration shear strength, pore water pressure, and factor of safety.

However, several researchers (e.g. Abay & Barbieri, 2012; Berhane et al., 2020, 2023; Hailu et al., 2024) emphasize the importance of hazard zonation maps as a planning tool for reducing landslide-related impacts, despite the fact that no integrated study has yet combined landslide susceptibility mapping with slope stability analysis of road corridors. More recently, Woldearegay (2025) highlighted the importance of comprehensive geological and geotechnical studies, proposing both surface and subsurface methods such as groundwater level monitoring, drilling, and geophysical surveys to better identify and mitigate slope failures.

In order to address the growing need for road connection in Ethiopia's mountainous regions and the increased dangers from rainfall extremes brought on by climate change, this study combines geotechnical stability analysis with landslide susceptibility mapping using FR and WoE models. In road design, planning, and maintenance, the goal is to create a strong foundation for proactive landslide hazard control.

1.2 STATEMENT OF THE PROBLEM

Landslides remain one of the key challenges hindering the growth and sustainability of road infrastructure in many parts of Ethiopia highlands. The Bonga-Felegeselam road in southwestern highland Ethiopia has become known for its susceptibility to landslides, due to its steep slope, thick soil deposit, weak bedrock, and the intense seasonal rainfall that beat the region year after year (Ayalew & Yamagishi, 2004; Nyssen et al., 2002; Woldearegay et al., 2004). Currently, many parts of road stretches have been heavily damaged and some entirely blocked due to continuing landslide activity fig. 1 and 2.

The situation has caused a series of damaging social, economic, and environmental problems: (1) peoples living in the risk zone have been forced to move into neighboring villages; (2) that move leaves them far from schools, clinics, and markets they relied on daily; (3) slopes still sliding and eroding are disturbed the environment; (4) heavy rain continues to claim lives and destroy homes year after year; and (5) ongoing repair and reconstruction efforts are progressively draining public financial resources.

Though previous geotechnical and geophysical investigations have been conducted, while

informative, failed to reliably locate the high-hazard zones.

Figure 1: Damage along Bonga–Felegeselam road, showing (a) distorted side ditch, (b) gully erosion, (c) tension cracks, and (d) asphalt differential settlement

Figure 2: Debris flow blocks Bonga–Felegeselam road near Km 17+340, triggered by heavy rainfall, covering the asphalt.

To fill this gap, incorporating landslide susceptibility mapping (LSM) is now crucial, because the technique highlights valuable spatial information by pinpointing hazard prone sections.

Once the hazardous zones are marked, engineers can design safer cuts and less costly drainage systems in much shorter time and with smaller budgets. However, such integrated approaches have not been implemented in the Bonga – Felegeselam corridor, leaving the road vulnerable to further disasters.

Therefore, this study aims to develop landslide susceptibility map for the Bonga–Felegeselam road corridor, using GIS based spatial analysis, and to integrate the results with appropriate slope stability and mitigation approaches. The findings will contribute to improving future road design and slope stabilization practices in similar geological settings, ultimately enhancing the resilience of transportation infrastructure in landslide-prone regions.

In light of this challenge, the present research aims to produce a landslide susceptibility map (LSM) for the Bonga - Felegeselam road corridor by using GIS tools and then integrate the map with practical slope-stability guidelines and risk-reduction actions. By sharing these products, road planners and engineers in similar geologies can refine design standards and protection techniques, making transport systems less vulnerable to future landslides.

1.3 OBJECTIVE OF THE STUDY

1.3.1 GENERAL OBJECTIVE

The main objective of this study was to create a landslide susceptibility map, evaluate slope failures, and recommend possible remedial measures for the Bonga–Felegeselam Road corridor.

1.3.2 SPECIFIC OBJECTIVE

- To prepare landslide inventory map,
- To identify the major landslide causative and triggering factors along the road corridor,
- To produce landslide susceptibility map (LSM) using statistical methods,
- To characterize the geological and geotechnical properties of slope-forming materials,
- To assess slope stability on selected sections of the road corridor, and
- To propose appropriate remedial measures based on the findings.

1.4 DESCRIPTION OF THE STUDY AREA

1.4.1 LOCATION AND ACCESSIBILITY

The study area is located in the newly formed southwestern regional state of Ethiopia. Geographically, it is located between 2035000E, 796800N and 235000E, 7968000N (Fig. 3). Its extents an area of 180 sq. km, characterized by rugged hills and mountain terrains covered in dense rainforest. Bonga town, the capital of Keffa zone, is located 465.0 km far from Addis

Ababa. The study area traverses 70km to southeastern parts of Bonga and linking the towns of Bonga - Felegeselam and Amaya. The road project frequently experiences landslides during heavy rainfall, particularly along its route, due to its construction.

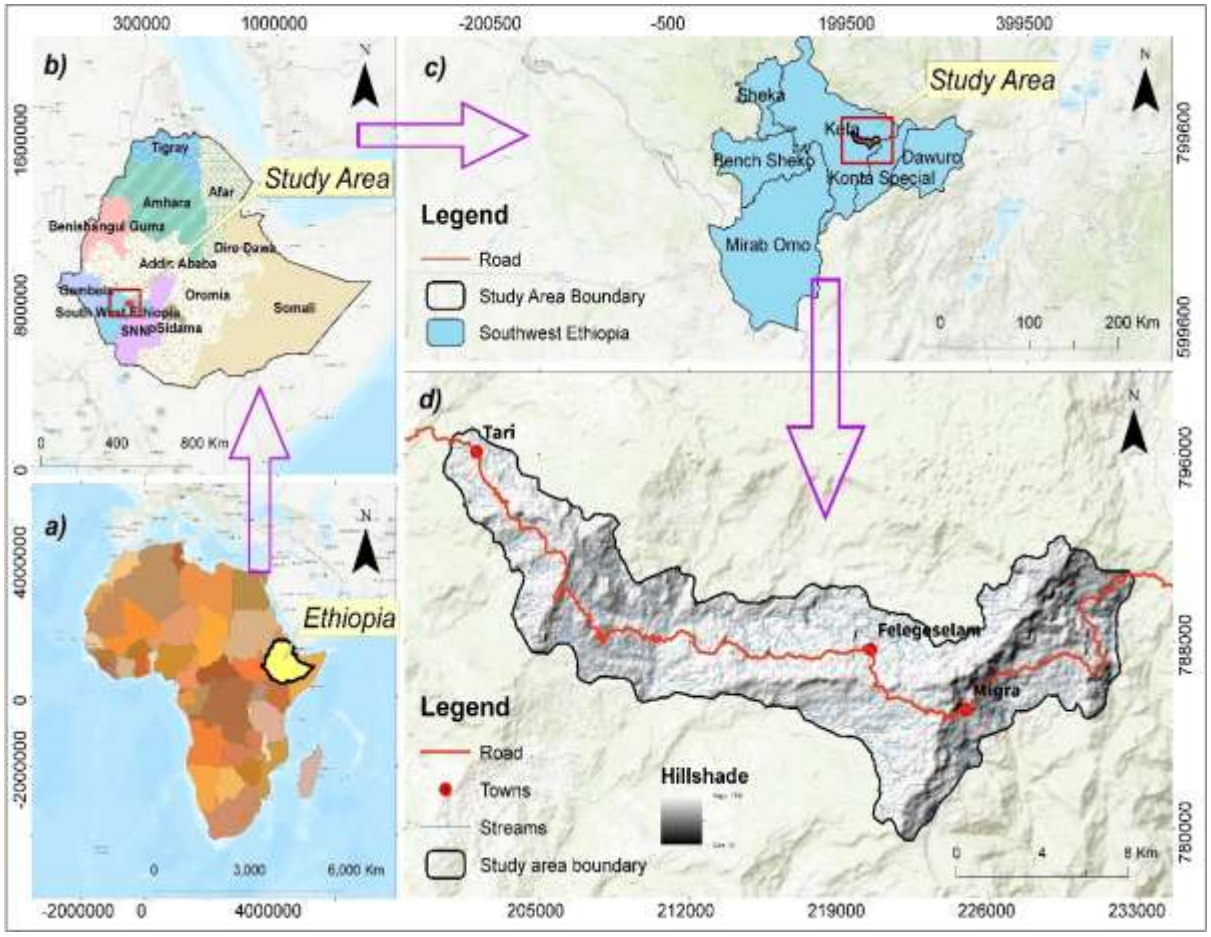

Figure 3: Location of the study area. (a) Map of Africa showing Ethiopia (source: https://hub.arcgis.com/datasets/geoduck:africa-boundaries); (b) Map of Ethiopia with regional states, including Southwest Ethiopia (source: https://data.humdata.org/dataset/cod-ab-eth); (c) Administrative map of Southwest Ethiopia showing zonal administration; (d) Map of the study area and its surroundings overlaid on hill shade of a digital elevation model (DEM source: www.earthexplorer.usgs.gov).

1.5 PHYSIOGRAPHY AND DRAINAGE

The main rift valley separates Ethiopia's physiographic features, which can be roughly categorized into two regions: the northwest and southeast highlands. As part of the East African Rift System, the current study area is located in the southwestern highlands and is characterized by its wide elevation ranges, rugged volcanic terrain, and rugged volcanic terrain (Tsige et al., 2017). Over geological time, both internal processes like tectonic and volcanic activity as well as external influences sculpted the route corridor's geomorphology, which includes a mix of

highlands, escarpments, and flat to rolling plains. The relief is dominated by mountainous formations and deep gorges, interspersed with gently rolling landforms. Several streams with a dendritic drainage pattern (Fig. 4) cut through the region, with elevations ranging from 1517 to 3331 meters above mean sea level. Many of these streams cross the main road. These tributary streams contribute significantly to the initiation of various-sized earth slides and shallow debris.

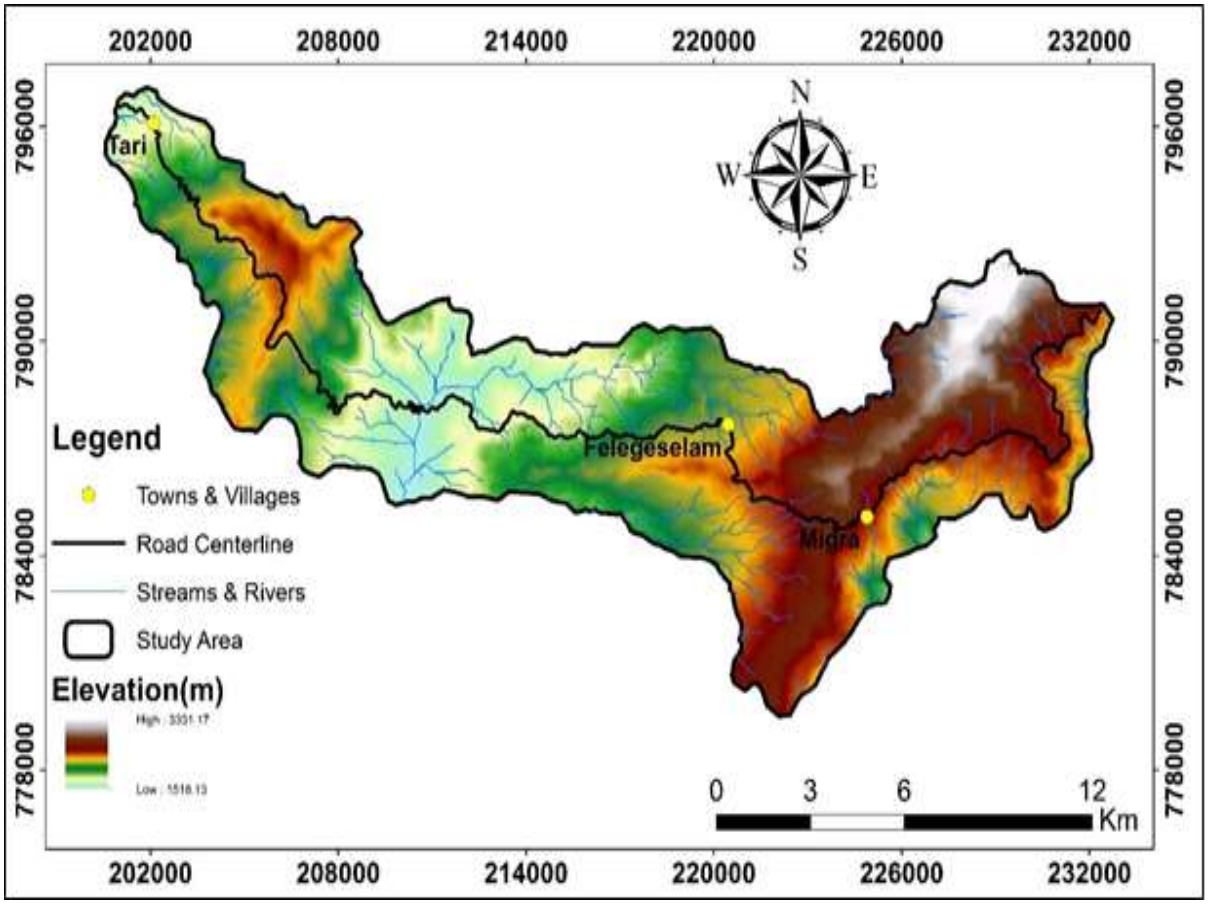

Figure 4: Physiographic features and Drainage network overlaid on DEM. Source of DEM: earthexplorer.usgs.gov.

1.5.1 RAINFALL AND TEMPERATURE

The Ethiopian highlands have a diverse climate, with mean annual rainfall exceeding 1200 mm and accounting for nearly 70% of total precipitation, which is largely controlled by the Inter Tropical Convergence Zone's (ITCZ) seasonal migration and the country's rugged topography (Ayalew, 1999). In the southwestern highlands, where the study area is located, the climate is warm, humid, and subtropical, with an average annual rainfall of 304.9 mm observed between 2001 and 2021 and summer temperatures reaching up to 22.7 °C. Rainfall occurs throughout the year but has two distinct peaks: the main rainy season from July to September and a shorter one in April–May, resulting in maximum stream flows during the summer months. The timing, intensity, and distribution of rainfall strongly influence surface runoff and groundwater

conditions, which are critical for slope stability in the region.

Table 1: Mean monthly rainfall of Bonga, Felegeselam, and Amaya Stations (2000–2024). Source: Ethiopian Meteorological Institute (EMI).

Month	Jan	Feb	Mar	Apr	May	Jun	Jul	Aug	Sep	Oct	Nov	Dec
Bonga	38.1	70.6	134.9	208.5	231.5	204.4	202.7	194.2	208.0	165.7	123.1	59.5
Felegeselam	41.1	94.5	158.2	228.5	275.4	200.0	231.4	241.5	234.0	212.3	112.4	51.5
Amaya	33.6	68.0	141.6	216.1	259.8	186.7	235.6	248.1	221.3	193.2	83.9	37.5

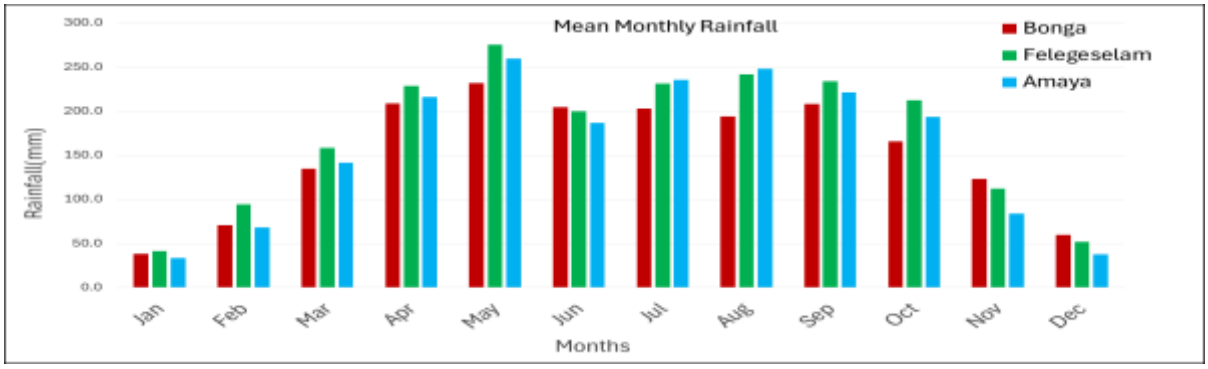

Figure 5: Mean monthly rainfall of Bonga and Felegeselam metrological stations (2000-2024). Source: Ethiopian Meteorological Institute (EMI).

Table 2: Mean monthly max. and min. temperature of Bonga and Felegeselam stations (2000-2024). Source: Ethiopian Meteorological Institute (EMI).

Month	Month	Jan	Feb	Mar	Apr	May	Jun	Jul	Aug	Sep	Oct	Nov	Dec
Bonga	T^0 Max	20.3	21.6	21.7	20.3	20.7	17.4	16.8	16.9	17.4	18.4	19.2	18.6
	T^0 Min	16.4	17.5	18.4	18.0	17.4	16.4	15.9	15.8	16.3	16.2	15.6	15.2
Felegeselam	T^0 Max	22.7	23.6	23.3	22.2	20.6	19.3	19.4	19.4	20.5	21.8	21.6	21.4
	T^0 Min	17.8	19.1	19.4	18.6	18.1	17.3	16.9	17.2	17.8	17.8	17.3	16.8

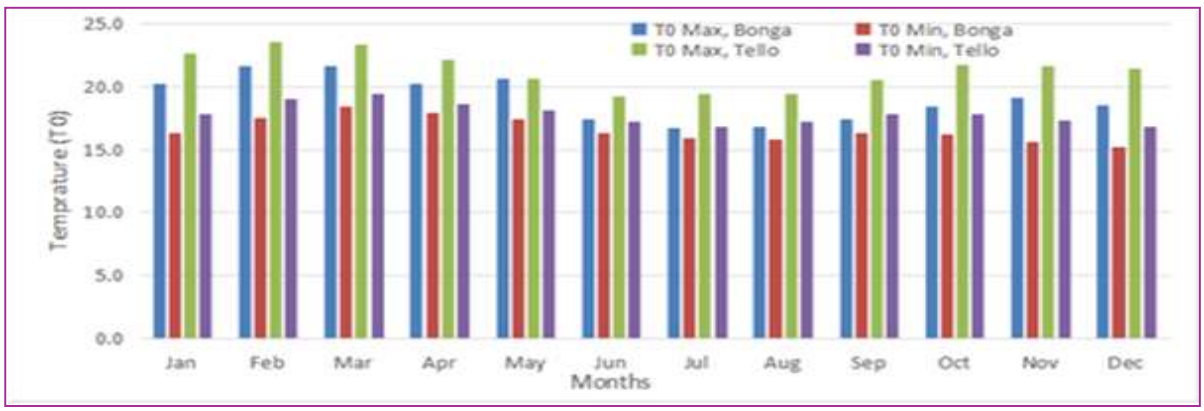

Figure 6: Mean min. and max. temperatures of Bonga and Felegeselam stations (2000-2024). Source: Ethiopian Meteorological Institute (EMI).

1.5.2 LAND USE - LAND COVER

The occurrence of landslides is greatly influenced by changes in land-use and land-cover, such as deforestation and slope disruption from road construction (Reichenbach et al., 2014). The project region spans rugged and forested terrain, with steep hills, deep gorges, and stream systems. Road construction-related excavation and embankment operations change the natural slope profiles, raising the possibility of landslides, instability, and soil erosion. Despite the rugged topography, the area also contains residential and agricultural lands. The region's vegetation varies; dense bushes and grasses dominate riverbanks, ridges, and uncultivated places, while thick forests with bamboo strewn throughout the central and eastern highlands. Along the route, in addition to the natural vegetation, there are often tree plantations, and many sections that were formerly forests have been turned into coffee plantations.

1.5.3 SEISMICITY OF THE STUDY

Earthquakes are the key damaging geohazards, capable of triggering ground shaking and severely impacting infrastructure. In countries like Ethiopia, the seismic risk is mainly concentrated along the Main Ethiopian Rift (MER), a tectonically active, fault-bounded zone spanning from the Afar Depression in the northeast to the southwest (Ayele et al., 2007). This rift system is the main source of earthquake activity and forms the basis for countrywide seismic hazard zoning. Historical records demonstrate that the MER has experienced several damaging earthquakes, including the 1961 Karakore earthquake (M6.5) and the 1969 Sardo event (M6.2), both of which caused property damage and loss of life (Ayele, 2017; Spall, 1981). Seismic events of up to magnitude 6.8 have been reported in the region. Earthquakes in Ethiopia have also been recognized to cause landslides, types of rock falls and debris slides (Abay & Barbieri, 2012). However, earthquake-induced landslides are less documented in the country (Woldearegay, 2013), with their impact on infrastructure in seismic zones, necessitating well designed and risk reduction measures.

According to the Ethiopian Standard (ES EN 1998-1:2015) the country is classified into five seismic zones according to probabilistic ground acceleration (0.04g – 0.025g) with a 475-year return period. The Bonga–Felegeselam road alignment passes through Zone 0 to 1, and is known as a low seismic hazard zone with design acceleration ranging between 0.0 and 0.04g.

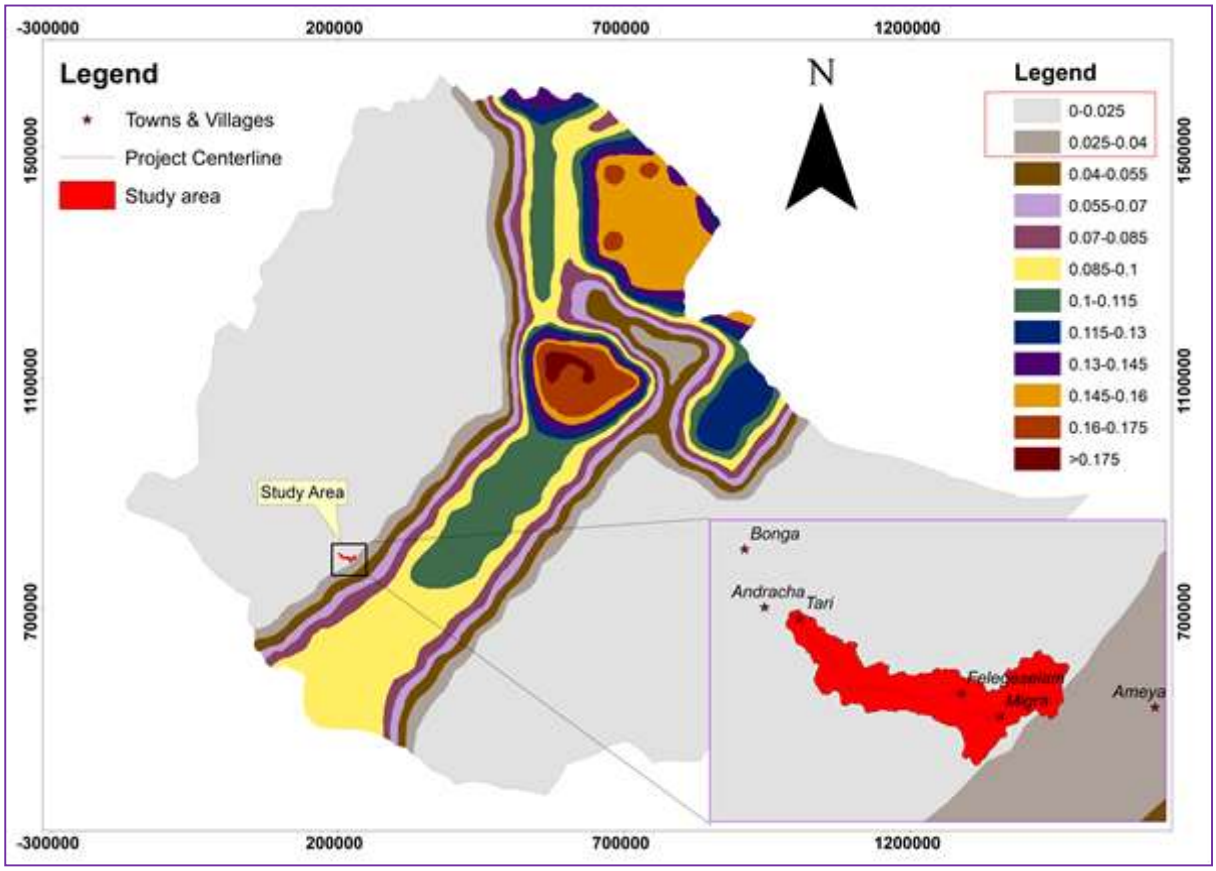

Figure 7: Seismic hazard map of Ethiopia along the study area, numbers in the legend area peak gravitational acceleration values (ES EN 1998:2015)

1.6 SIGNIFICANCE OF THE STUDY

In order to reduce costs and avoid misdirected investments, landslide susceptibility maps provide a useful tool for choosing safer paths, lowering risk, and forecasting future landslides. In addition to supporting future study and risk prevention, this thesis improves knowledge of the landslide factors along the Bonga–Felegeselam road. Participants in the study, including the Ethiopian Roads Administration (ERA), researchers, academic institutions, and local businesses, will gain from the findings.

1.7 STRUCTURE OF THE THESIS

This thesis is typically divided into six main chapters, as outlined below:

Chapter one - presents about background of the study, statement of problem, general and specific objectives, overall description of the study area, significance and limitations of the study area.

Chapter two - discuss about literature review of landslides such as definitions and terminology of landslides, types, causes and failure mechanisms of landslides, triggering factors of

landslides, landslide inventory and hazard zonation mapping.

Chapter three - discuses all over in detail about the methods, approaches and materials followed to achieve the objectives and the results.

Chapter four - deals with the geological history of Ethiopia and the main lithological units in the Bonga-Felegeselam area.

Chapter five - this chapter concerned with results and discussion of the study, which focus on landslide causative factor, analysing of the inventory maps of the study and generating of landslide susceptibility maps based on GIS-approach using frequency ratio (FR), Weight of Evidence (WoE) and limit equilibrium (LE) methods. Analysing and interpretation of geotechnical properties of soils is the other section. In addition to this mitigation measures based on the result obtained is recommended.

Chapter six - deals with recommendation and conclusion of the study area that drawn from this research and outlines future research directions.

2 LITERATURE REVIEW

This literature review aims to provide an overview of the current state of research on landslides, with a particular focus on their types and failure mechanisms, landslide influencing factors, characteristics, assumptions and methods of landslide hazard assessments.

2.1 LANDSLIDE: TYPES AND CAUSES

Landslides can cause a variety of ground mass movement, from very slow to very fast (USGS, 2004; Varnes, 1978). Though landslides are classified using a variety of criteria, the broadest and widely used one considers the material involved, the type of movement, activity, and velocity. Generally, landslides are broadly categorized in to mass movements and subsidence (Hutchinson, 1991; Sharp, 1958; Varnes, 1978, 1984). According to Varnes (1978), which was later improved by (Cruden & Varnes, 1996), three material classification (soil, debris and rock) and six distinct movement mechanisms can be used to simulate the complexity of a landslide (Table 3). If the nature of the movement changes as the movement goes on, the material should be introduced at the beginning of each successive movement.

Table 3: Varnes classification of slope movements (Cruden and Varnes, 1996)

Types of movement		**Types of material**		
		Bed rock	**Engineering soils**	
			Coarse soil	**Fine soil**
Falls		Rock fall	Debris fall	Earth fall
Topples		Rock topples	Debris topple	Earth topples
Slides	**Rotational**	Rock slide	Debris slide	Earth slide
	Translational			
Lateral spread		Rock spread	Debris spread	Earth spread
Flows		Rock flow	Debris flow	Earth flow
Complex		Combination of two or more principal types of movement (Nature movement varies with time)		
Composite		Nature of movement varies in different parts of the failed slopes		

2.1.1 FALLS

It is the sudden detachment of rocks from a cliff along discontinuities, joints, or bedding planes, with least or no shear displacement (Cruden & Varnes, 1996; Hungr et al., 2014; Rotaru et al., 2007; USGS, 2004). It frequently happens when roads are being built on steep slopes, steep hill slopes, and rocky mountainous terrain, and is typically caused by rivers or waves undercutting the slopes toe or face.

2.1.2 TOPPLES

When a mass of soil or rock topples, it rotates forward out of the slope around an axis that is below the center of gravity of the displaced material before it falls to the ground (Bobrowsky et al., 2014; Cruden & Varnes, 1996; USGS, 2004; Varnes, 1978). High narrow blocks topple while wide low blocks slide. Rocks with steep joints have structures that affect this failure mechanism. The number of discontinuities, the type of rock being toppled, and its geometry all affect how long it will stay in place before falling away down a slope (Rotaru et al., 2007). The majority of topples take place in columnar jointed volcanic terrain, as well as nearly steep banked streams and rivers.

2.1.3 SLIDES

A slide is a downward movement of soil or rock mass that occurs on rupture surfaces or relatively thin zones of severe shear strain (Cruden & Varnes, 1996; Rotaru et al., 2007; USGS, 2004). Depending on the geology, structure, and hydrogeology, they can be rotational, translational, or a combination of both (Crozier & Glade, 2005).

Rotational slides have a semicircular shear surface with a curved upward surface of rupture and move rotationally about an axis parallel to the contour of the slope. Under certain conditions, the displaced mass may move as a relatively cohesive mass along the rupture surface with little internal deformation. According to Cruden & Varnes (1996) rotational slides are the most common landslide occurring in fill materials because they occur most frequently in homogeneous materials. Hutchinson (1991) also pointed out that the activity of rotational slides caused by erosion at the toe of slopes in cohesive soils is often cyclic.

Translational slides: When a mass is displaced on a relatively planar slip surface with little rotational movement or backward tilting, translational slides occur (Cruden, 1996). This type of slide can travel long distances if the surface of rupture is sufficiently inclined. Translational slides frequently fail along geologic discontinuities such as faults, joints, bedding surfaces, or rock-soil contact. Translation slip planes can occur in all types of rock and soil, ranging from minor soil slips to deep-seated landslides (Sidle & Ochiai, 2006). Translational slides are more harmful than rotational slides because they are shallower and move faster and further distances.

2.1.4 FLOWS

Flows are the most destructive and turbulent slope failures, containing a high water content that causes the slope material to lose cohesion and transform into a fluid (Bobrowsky et al., 2014). These types of movement could be classed as debris flow, debris avalanche, earth flow, mud

flow and creep based on material type and velocity of flow (Rotaru et al., 2007; USGS, 2004). The percentage of particle sizes and the volume of water within them differentiate the flow types. For example, debris flow is made up of loose soil, rock, organic matter, and water (50% fine materials), whereas mudflow is made up of materials that contain at least 50% sand, silt, and clay sized particles and are moist enough to flow quickly (USGS, 2004).

2.1.5 SPREADS

A spread is an extension of a cohesive soil or rock mass combined with a general subsidence of the fractured cohesive mass into softer underlying material. The low angled slopes involved, as well as the distinctive form and rate of movement, set it apart. Spreads can occur as a result of the liquefaction process in which saturated loose sediments such as sands or silts are converted to a liquid-like state (Bobrowsky et al., 2014). This process is frequently triggered by rapid ground motion, such as earthquake tremors, and/or can be deliberately induced.

2.1.6 COMPLEX

Varnes (1978) offered a sixth form of movement as well: complicated failures. These are failures in which one of the five types of movement described above is followed by another type (or several types). In such cases, the name of the first type of movement should be followed by the name of the next type of movement, e.g., rock fall and debris flow. Practically all landslides involve various forms of movement, either concurrently in separate portions of the failure or evolving down slope into different failures over time.

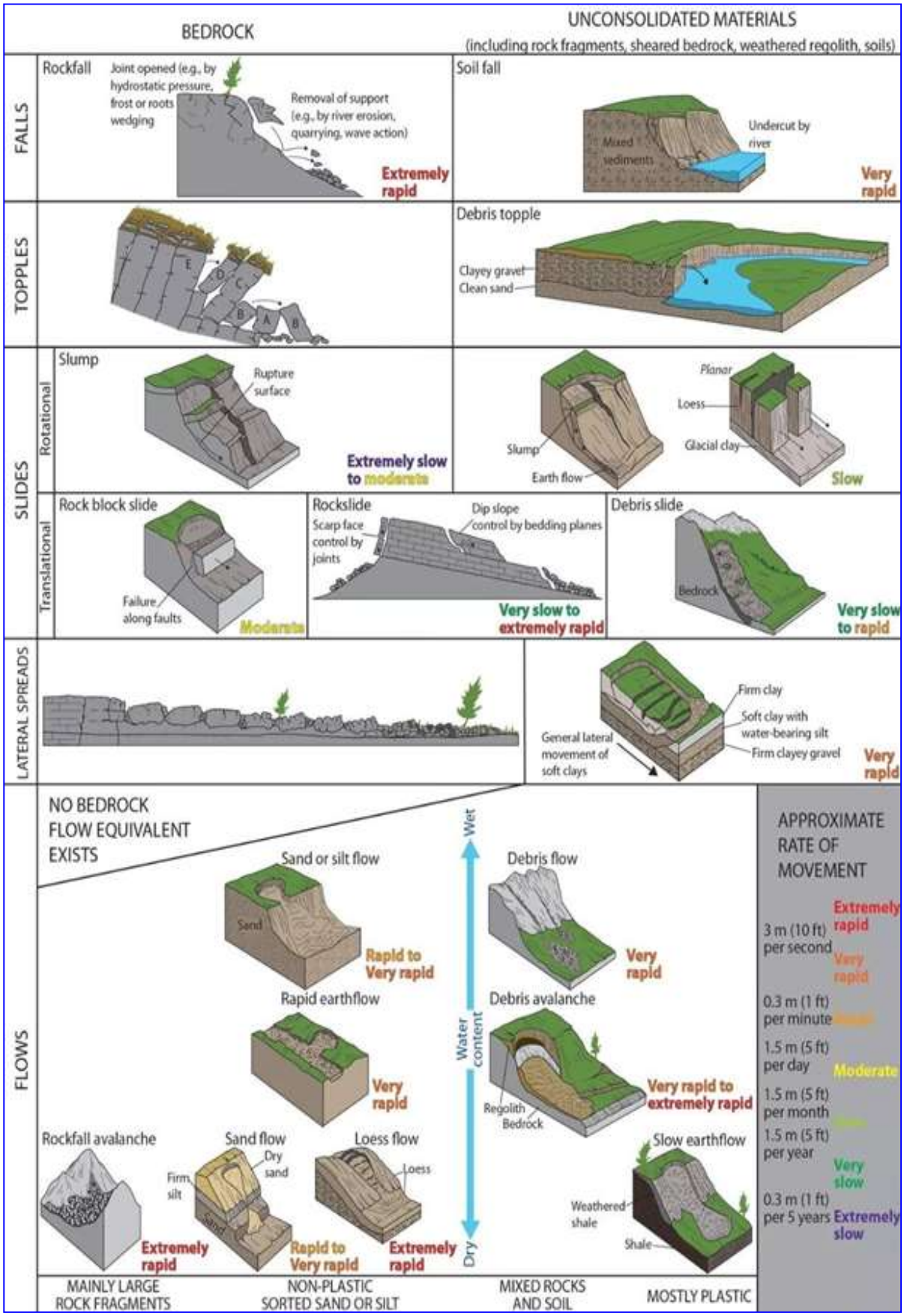

Figure 8: Varnes classification of slope movements (Cruden and Varnes, 1996), Source: https://www.linkedin.com/company/engineering geology

2.2 LANDSLIDE INFLUENCING FACTORS

Several causative and triggering factors impact landslides, which vary significantly from place to place (Pardeshi et al., 2013). These factors either reduce shearing resistance or increase shearing stress (Corominas et al., 2014; Dai et al., 2002; Terzaghi, 1950, 1953; Varnes, 1984). According to Cruden & Varnes (1996) classify the factors that influence the occurrence of landslides in a given area categorized in to two; (1) the internal variables, which include bedrock geology, geomorphology, soil, land use/land cover, and hydrologic conditions; and (2) external factors such as rain, earthquakes, blasting and drilling, cloudbursts, and flash floods (Ali et al., 2019; Chau et al., 2004; Huabin et al., 2005; Kumar & Anbalagan, 2015). The controlling variables tend the slope to a marginally stable condition without actually causing failure (McColl, 2022). However, the triggering variables move the slope from a marginally stable to an unstable state, causing failure (Kanungo & Sharma, 2014; Wu & Sidel, 1995). Some of the key components that influence slope stability are as follows:

2.2.1 LANDSLIDE INTRINSIC FACTORS

The internal variables show the basic properties of the ground that make slopes prone to landslides. According to Varnes (1984), there are a number of variables that affect slope stability and should be taken into consideration when evaluating landslide risks. These aspects were categorized by (Lee W. Abramson, et al., 2002; van Westen et al., 2008), as (1) geological concerns, (2) geomorphological considerations, (3) topographical considerations, (4) hydrological considerations, and (5) land use issues. Other inherent parameters for slope instability, according to several authors e.g., (Basharat et al., 2016; Ghosh et al., 2012; Raghuvanshi et al., 2014; Wang & Niu, 2010), include slope geometry (slope inclination, aspect, elevation, and curvature), land use and land cover, as well as lithology, soil type, structural discontinuity characteristics, and shear strength of the material. By making the slope susceptible to failure without actually initiating it, these factors help the slope reach a relatively stable condition (Chau et al., 2004). Some of the inherent parameters are described here.

2.2.1.1 GEOMORPHOLOGICAL FACTORS

Geomorphological characteristics including slope inclination, slope curvature or shape, slope length, and slope aspect enhance slope instability (Moradi & Rezaei, 2014; Nechyba et al., 2016). The most important terrain related risk element that influences slope stability is the slopes steepness (Chen & Lee, 2003). As slope angle and height increase, the occurrence of a landslide typically rises while other regulatory elements remain constant (Lee & Min, 2001; Seyed et al., 2011). In soils and unconsolidated materials, shear stress normally rises as the

slope angle does (Lee & Min, 2001). Steep slope terrains are responsible for high runoff, deeply incised gully erosion, and the reactivation of previous landslides (Nechyba et al., 2016). Slope aspect greatly affects slope failures, especially in mountainous terrains, through variations in precipitation and air temperature (Nyssen et al., 2002). The angle of the slope affects the amount of sunlight, wind, and precipitation that it receives, which in turn influences other landslide-causing factors such soil moisture, vegetation cover, and soil thickness (Meten et al., 2015). Slope curvature is the curve of a slope in a particular direction. This affects a terrains hydrological condition because, after a rainstorm, a concave slopes soil cover may hold more water and hold it for longer than a convex slope (Moradi & Rezaei, 2014). The upward concave, flat, and upward convex forms in that cell are represented by positive, zero, and negative values, respectively.

2.2.1.2 GEOLOGICAL FACTORS

The types of landslides that may occur and their movements can be controlled using the properties of slope forming the underlying geological materials. Terzaghi (1950, 1953) have emphasized the relation between geology and slope instability. The key geologic factors that affect slope stability, however, are the geotechnical properties of soils and rocks, the existence and kind of geological structures, the degree of weathering, and the type of rocks (Anbalagan, 1992; Corominas et al., 2014; Lee W. Abramson, et al., 2002). The chance of a landslide is increased when bedrock is fractured, jointed, faulted, or bedded in a direction parallel to the hill slope. It was further recognized by (Cruden & Varnes, 1996) that if the geologic components of the slope are weak, sensitive, weathered, or sheared, mass movement may be clearly happened.

2.2.1.3 HYDROLOGICAL FACTORS

Slopes become unstable as a result of water infiltration because it raises pore water pressure (load) and lowers shear strength (Kanungo & Sharma, 2014). When it rains heavily or for a long time, the soil becomes saturated, the pore water pressure rises, the grains are forced apart, and slips are likely to occur. When all other factors are equal, slopes in moist climates tend to be more prone to landslides. Though water saturation of a slope is the main factor in different types of slope failures (USGS, 2004), the extent of that saturation is influenced by factors such as topographic slope, soil type, permeability, porosity, humidity, the amount of organic matter in the soil, land cover, and weather conditions. Pourghasemi et al. (2013; Wu & Sidel, 1995) reported a large number of recent landslides in southern Ethiopia along river channels that were caused by stream incision as a result of elevated peak flow discharges in their catchments.

2.2.1.4 MANMADE ACTIVITIES

The majority of disastrous landslides are brought on by human activity; like mining, deforestation, artificial excavation, loading on slopes crests, and their toes, modifying surface runoff routes, and artificial excavation and mining (Cruden & Varnes, 1996; Sidle & Ochiai, 2006; USGS, 2004). According to Dai et al. (2002), as development advances, human activities like clearing land for building sites or cut and fill slopes for road construction have become key landslide causes.

Vegetation cover has also an impact on the frequency of landslides. Deep rooted plants may increase soil shear strength and contribute to the stability of slopes. Dense vegetation cover lowers the amount of water by catching the rain while barren slopes are more vulnerable to landslides, which tend to buffer the effects of climatic agents like rain and other factors, such the natural anchorage provided by tree roots (Saha et al., 2002). In the highlands of Ethiopia, cultivated lands with little forest cover were the sites of the majority of landslides (Woldearegay, 2013). Therefore, the physical and biological slope qualities that affect its stability may be changed as a result of forest management strategies.

2.2.2 LANDSLIDE TRIGGERING FACTORS

Landslides are influenced by a variety of external variables, such as heavy rainfall, earthquakes, and rapid stream erosion. The triggering variables, however, may be change over a very short time of period, making them very challenging to evaluate (Dai et al., 2002).

2.2.2.1 TEMPERATURE

Through its effects on slope materials and hydrological conditions, temperature is thought to be a significant yet indirect landslide-triggering factor. Predisposing slopes to failure, processes including fast snow or ice melt, permafrost deterioration, and freeze-thaw weathering can raise pore-water pressure and decrease shear strength. Slope instability can be exacerbated in warmer climates by temperature induced drying and cracking of clay rich soils, which can also improve infiltration after rainfall. As a result, even while temperature rarely acts alone, it significantly alters slope stability and promotes the onset of landslides (Crozier, 2010; Huggel et al., 2012).

2.2.2.2 RAINFALL

Despite the fact that there is no direct relationship between rainfall and slope instability, rainfall is the most common cause of landslides in the majority of the literature (Crozier & Glade, 2005; Fell et al., 2008) claim that rainfall caused shallow landslides are a risky phenomenon that can damage both infrastructure and individuals. Though the size of the event is determined by the

intensity of the rain, the amount of rainfall that triggers landslides can differ from one location to another and can change depending on the average annual precipitation (Caine, 1980; Campbell, 1975; Crozier, 1986; Dubois, 1987; Monteleone & Sabatino, 2014; Polemio & Petrucci, 2012). However, triggering conditions can be identified for a variety of landslide categories (shallow, medium, and deep) and in geologically uniform areas (Gill et al., 2008; Terranova et al., 2007). According to several scholars, rainfall is the primary cause of different types of mass movements, particularly in highlands and rift escarpments of Ethiopia (Abebe et al., 2010; Fisseha & Mewa, 2016; Meten et al., 2015; Woldearegay, 2013).

2.2.2.3 EARTHQUAKE

Earthquake is a main factor that triggers landslides (Huang et al., 2012). Most of the landslides occur after earthquakes are directly related to the activity of faults (Moradi & Rezaei, 2014). There are comparatively few records of earthquake-induced landslides in Ethiopia, despite the fact that they are frequent in tectonically active areas (Woldearegay, 2013).

2.3 LANDSLIDE RISK ASSESSMENT

Though mapping methodologies for landslide hazard are subjective; numerous methods have been developed to assess the possibility of landslides. These methods can be categorized into deterministic, statistical, heuristic, and inventory approaches (Atkinson & Massari, 1998; Ayalew et al., 2004; Baeza & Corominas, 2001; Pardeshi et al., 2013). Generally speaking, there are two types of methodologies: qualitative and quantitative (Kanungo & Sharma, 2014). On the other hand, these methods classified further as qualitative, semi-quantitative, and quantitative techniques (Kumar & Anbalagan, 2015). However, the assessment of landslide risk has routinely employed by quantitative techniques.

2.3.1 QUALITATIVE METHODS

Geologists and geomorphologists evaluate the risk of landslides using qualitative techniques based on their knowledge and field observations. It is a conventional and simple method that enables instant field application (Aleotti & Chowdhury, 1999). Classifying the risk of landslides using geological and geomorphological criteria, particularly at the regional level, is a commonly adopted approach. Field analysis and the utilization of index maps or parameter maps, with or without weights, are the two primary techniques employed. However, it is important to acknowledge the limitations of this approach, including the reproducibility of results and the subjectivity inherent in decision rules.

2.3.1.1 INVENTORY METHODS

Inventory methods considered as one of the most straightforward qualitative techniques for identifying the location and scale of landslide events in real world settings (Pardeshi et al., 2013). Through the utilization of data obtained from field surveys, historical records, satellite imagery analysis, aerial photography, and topographic map contours, this approach demonstrates the distribution of previously occurred landslides (Kanungo & Sharma, 2014; Kumar & Anbalagan, 2015; van Westen et al., 2008). However, this method is both time consuming and costly due to the absence of information on temporal variations in landslide distribution within inventory maps (Kanungo & Sharma, 2014).

2.3.1.2 HEURISTIC METHODS

The expert driven heuristic method is utilized to assess the susceptibility of landslides. It relies on overlaying qualitative map layers such as geology, hydrology, slope, land use, soil maps, and others (Ahmed, 2015). By employing this technique, it becomes possible to generate landslide maps of high quality for extensive areas without requiring in depth geotechnical knowledge. However, it is important to note that a substantial amount of geomorphological mapping is still necessary (Roslee et al., 2017). This qualitative approach, which involves a considerable degree of subjectivity and heavily relies on the individual's expertise, assigns distinct values to each terrain variable (Rengers et al., 2016; Zhou et al., 2013). According to Dai et al. (2002), his methodology employs expert judgment that relies on knowledge of preparatory variables to evaluate the likelihood of landslides. Consequently, it may prove challenging to determine the accuracy of maps generated through the utilization of these techniques (Pardeshi et al., 2013). An issue with these models is the necessity for extensive data on landslides and their underlying causes over an extended period, either for a specific location or for areas characterized by similar environmental conditions.

2.3.2 SEMI-QUANTITATIVE METHODS

2.3.2.1 ANALYTICAL HIERARCHY PROCESS

The analytical hierarchy process, invented by (Saaty, 1980), serves as a valuable tool for the hierarchical formalization of our complex and multifaceted perception of reality. Through the integration of diverse viewpoints and experiences of researchers, the AHP technique offers a statistical reflection of the decision-making process. This technique enables the selection of a preference scale from a provided list of choices (Saaty, 2008). By utilizing a matrix and conducting pairwise comparisons, the AHP method facilitates the evaluation of the

contributions made by various factors (Intarawichian & Dasananda, 2010).

AHP procedures must now follow four levels of hierarchy: problem definition, goal, and alternative selection, pair-wise comparison matrix construction, weight selection, and overall priority selection (Pardeshi et al., 2013). Based on relative importance, each landslide-related parameter is assigned an absolute number (from 1 to 9), and comparison matrices are constructed to determine the consistency ratio (CR) and consistency index (CI) (Intarawichian & Dasananda, 2010; Pardeshi et al., 2013).

This number changes between 1 and 9 when the factor on the vertical axis is more important than the factor on the horizontal axis, and between 1/2 and 1/9 when the factor on the horizontal axis is more important than the component on the vertical axis (Saaty, 2008). The reliability of a matrix is measured by the consistency ratio, which must be smaller than 0.1 for the estimated weights to be accepted. The consistency ratio (CR), which has a scale of 0 to 1, contrasts the matrix's consistency index and random index.

2.3.3 QUANTITATIVE METHODS

This technique involves identifying the combinations of variables that were the main cause of past instability. Once identified, these tactics are then applied to stable slopes and areas with similar conditions (Dai et al., 2002; Pardeshi et al., 2013). Quantitative techniques are used to assign weights to different parameters based on their relationship to landslide incidence.

2.3.3.1 STATISTICAL METHODS

Statistical analyses are widely utilized due to their ability to offer a quantitative approach and effectively assess the individual impacts of different factors. In the context of landslide hazard zonation, statistical analysis can be conducted using both bivariate and multivariate methodologies (Roslee et al., 2017).

In the context of bi-variate statistical analysis for landslide hazard zonation, the data layers about each causative component are compared to the existing distribution of landslides (Kanungo & Sharma, 2014). The factors contributing to landslides are assigned weights based on landslide density. Various prominent bivariate statistical methods such as the frequency ratio method, weight of evidence model, weighted overlay model, and others have been employed in the mapping of landslide hazard zonation (Chung & Fabbri, 2003; Guzzetti et al., 1999; Pardeshi et al., 2013). Similarly, multi-variate statistical analysis evaluates how each contributing element contributes differently to the total vulnerability to landslides (Kanungo & Sharma, 2014). These techniques compute the landslide area percentage for every pixel and provide a

data layer that illustrates the locations of landslides and their absences. The logistic regression model, discriminant analysis, multiple regression models, conditional analysis, and artificial neural networks are just a few of the many techniques commonly employed for landslide hazard mapping.

2.3.3.2 DETERMINISTIC APPROACHES

Deterministic methods are used to assess slope stability in areas with relatively uniform ground conditions and clearly defined landslides (Dai et al., 2002). Common techniques include limit equilibrium method (LEM), limit analysis (LA), finite element method (FEM), and finite difference method (Kaur et al., 2016). LEM, widely used for its simplicity, compares driving and resisting forces along an assumed failure surface but does not account for stress-strain behavior (Duncan, 2014). LA offers safety bounds based on plasticity theory without assuming a failure surface, though it is more theoretical (H. Chen & Lee, 2003). FEM and FDM use numerical modeling to simulate slope behavior FEM for deformation analysis (Griffiths & Lane, 1999), and FDM for dynamic problems.

Table 4: Summary of Limit Equilibrium methods (Abramson et al. 2002)

Method	**Equilibrium Type**	**Slip Surface**	**Key Assumptions**
Ordinary/Fellenius	Moment only ($\sum M = 0$)	Circular	Ignores both interslice normal (E) and shear (T) forces
Bishop Simplified	Moment only ($\sum M = 0$, vertical $\sum F \neq 0$)	Circular, some non-circular*	Includes E, neglects T
Janbu Simplified	Horizontal force only ($\sum F = 0$)	Circular, non-circular	Includes E, neglects T
Janbu Generalized (GPS)	Both moment and force ($\sum M$ & $\sum F$)	Circular	Includes both E and T; T and E act at line of thrust (LoT)
Lowe - Karafiath	Not fully defined	Non-circular	Inclined resultant, $\theta = ½ (\alpha + \beta)$
Corps of Engineers	Not fully defined	Non-circular	Inclined resultant, $\theta = ½ (\alpha_1 + \alpha_2)$
Sarma	Both moment and force ($\sum M$ & $\sum F$)	Non-circular	$T = c + E \cdot \tan\varphi$ (Mohr-Coulomb), considers interslice shear
Spencer	Both moment and force ($\sum M$ & $\sum F$)	Circular, non-circular	Constant interslice inclination, $T = \tan\theta \cdot E$
Morgenstern-Price	Full equilibrium ($\sum M$ & $\sum F$)	Circular	T and E defined by functions: $T = f(x) \cdot \lambda \cdot E$
Note: * Methods marked with (*) are applicable for both circular and non-circular surfaces.			

These methods require detailed geotechnical input (e.g., cohesion, friction, permeability) and are suitable for site specific studies (Van Westen et al., 2003). While they offer precise physical

representation, they often overlook broader factors like climate, vegetation, and human activity. The results reflect only the stability at the time of data collection and do not predict landslide timing or size.

Despite the variety of methods, LEM remains the most commonly used, especially for analyzing road cut slopes (Lee W. Abramson, et al., 2002). All LEMs are based on assumptions about interslice forces (normal and shear), differing mainly in how these are treated, the shape of the failure surface, and the equilibrium conditions used to calculate the factor of safety. A summary of selected LE methods and their assumptions are presented in Table 4.

2.3.3.3 GEOTECHNICAL APPROACH

This technique is deterministic in nature and enables examination of individual slope rather than regional scale measurements. It also requires a detailed input data set including slope geometry, borehole drilling and geotechnical parameters such as cohesion, internal friction angle and pore water pressure (Duncan & Wright, 2005). The numerical value of the Factor of Safety (FoS) which is a measurement of inherent stability of the slope material, is calculated by coupling the slope stability models with groundwater flow solutions (Lee W. Abramson, et al., 2002). Due to its computational complication, this method typically relies on specialized geotechnical software e.g., Slide, Plaxis, GeoStudio for precise results (Griffiths & Lane, 1999). As a result, it offers a precise and site-specific evaluation of slope stability under various hydrological and loading conditions (Wyllie & Mah, 2004).

2.4 ROCK MASS CHARACTERIZATION

Various rock mass classification systems have been established for engineering applications, each with distinct criteria and methodologies. The most commonly used systems include RMR, Q-system, GSI, and RQD, all of which are derived from empirical case studies. These classifications play a crucial role in tunnel design, slope stability assessments, and foundation engineering (Barton et al., 1974; Bieniawski, 1989; Deere, 1964; Hoek & Brown, 1980). The RMR system developed by (Bieniawski, 1989), is one of the most widely used classification methods. It incorporates parameters such as uniaxial compressive strength of the rock, rock quality designation (RQD), spacing of discontinuities, condition of discontinuities, groundwater conditions, and orientation of discontinuities. The parameters are easily obtained from drill holes and surface geological mapping which is applicable and adaptable to different situations.

An essential parameter in assessing rock material strength and classifying rock strength is the uniaxial compressive strength (UCS), serving as a fundamental cornerstone in geotechnical

analysis (Hoek & Brown, 1980). A Schmidt Hammer Rebound Test (also called the Rebound Hammer Test) is a quick and practical way to estimate the Uniaxial Compressive Strength (UCS) of rocks and concrete in the field. It works by measuring the rebound of a spring-loaded mass impacting the rock surface, which correlates with the material's strength (Aydin, 2009; Katz et al., 2000; Yermukhanbetov et al., 2021).

2.5 LANDSLIDE REMEDIAL STRATEGIES

Globally pervasive and damaging geohazards like landslides occur regularly in tectonically active and mountainous regions (Cruden & Varnes, 1996). The need for effective mitigation and remedial interferences becomes apparent through the impacts on infrastructure, human lives, and natural systems (Turner & Schuster, 1996). Over years, experts in research and practical fields have framed multiple approaches to mitigate landslide hazards while enhancing slope stability. The categorization of remedial measures typically involves their division into structural engineering solutions, bio-engineering approaches, and planning or regulatory interventions.

In Ethiopia, several scholars have made key contributions to understanding and reducing landslide risks. Woldearegay and Fubelli studied drainage related water harvesting and afforestation to help control soil erosion and improve slope stability in the highlands (Abebe et al., 2010; Woldearegay et al., 2005). Abay worked on integrated land use planning and building retaining structures to boost community resilience, especially in the Debresina area (Abay & Barbieri, 2012). Raghuvanshi used GIS based statistical methods to map landslide-prone areas, which supports more focused efforts to prevent landslides (Raghuvanshi et al., 2014).

Selecting the right remedial techniques depends on several factors, like the soil and rock properties, water conditions, slope shape, and the specific environment of the site (Duncan & Wright, 2005; Popescu, 2001). Common engineering solutions include retaining walls, reshaping slopes, improving drainage, and stabilizing with soil nails or anchors. These methods are still widely used in infrastructure projects, especially in areas with high risk (Kazmi et al., 2017). It can enhance slope stability by adding measures like installing rock bolts for deeper support, constructing check dams to manage water flow, and using reinforced earth structures to strengthen at risk slopes (Cornforth, 2005). Furthermore, there's a growing trend towards integrated strategies that combine structural solutions with bio-technological and planning methods to promote long term slope resilience and sustainability (Stokes et al., 2014).

Bio-engineering techniques, such as planting vetiver grass for root reinforcement and creating live crib walls with innate vegetation, along with the use of vegetated gabions to combine

ecological and structural benefits, is becoming more popular (Nyssen et al., 2009; Stokes et al., 2014). When it comes to planning interventions, we can really step things up with strategies like zoning laws to limit development in high-risk areas, implementing early warning systems that use real-time monitoring, and encouraging community-based reforestation programs to help reduce soil erosion and stabilize slopes (Abay & Barbieri, 2012; Woldearegay et al., 2005). Overall, these studies reinforce the importance of a comprehensive, site-specific strategy that blends engineering works, ecological stabilization, and informed planning to sustainably manage landslide hazards across Ethiopia's highlands.

2.6 LANDSLIDES STUDIES IN ETHIOPIA

In Ethiopia, landslides occur often because of the subtle landscape and complex geological shifts. According to several authors (Abebe et al., 2010; Ayalew, 1999; Ayalew et al., 2004; Ayele et al., 2007; Fisseha & Mewa, 2016; Hearn, 2019; Tsige et al., 2017; Woldearegay et al., 2005) have identified several factors contributing to the prevalence of landslides in the Ethiopian highlands, including irregular morphology, high relief energy, and the characteristics of protruding rocks.

Woldearegay (2013) conducted a study on the analysis of the occurrence and underlying factors of landslides in the highlands of Ethiopia, with particular implications for infrastructural development. The findings of this study indicate that rainfall plays a significant role as a primary trigger for various types and sizes of landslides, including debris/earth slides, debris/earth flows, and medium to large-scale rockslides.

The hilly and mountainous nature of Ethiopia has regularly faced landslides due to precipitation (Ayalew, 1999; Woldearegay et al., 2005). These landslides primarily occur in three forms: medium- to large-scale rockslides, debris/earth slides, and debris/earth flows. All of these types of landslides are closely linked to heavy rainfall events. As per (Hearn, 2019), Ethiopia perceived a substantial expansion of its road network. However, this development also led to the occurrence of new landslides and the reactivation of older ones in multiple areas. The issue of conducting comprehensive landslide inventories and addressing the resulting property damage and loss of life has not received sufficient attention from the public administration and decision-makers.

Most of the research publications on landslides in Ethiopian highland terrains have focused on evaluating landslide inventories and their causal variables in specific areas. However, there has been limited attention given to susceptibility mapping, despite the importance of reducing landslide-related risks and damages for strategic land use planning. Some studies e.g. (Abay et

al., 2019; Ayenew & Barbieri, 2005; Berhane et al., 2020, 2023) have conducted susceptibility mapping, investigating the relationships between landslide frequency and their underlying causes (such as slope, soil type, and water flow influence). These findings suggest that future slope collapses are more likely to occur under similar conditions that have led to historical and current instability.

The assessment of landslide hazard must therefore take into account historical failures (Carrara et al., 1997; Guzzetti et al., 1999; Hutchinson, 1995). The validity of the findings, however, is yet largely unknown.

No published research articles on landslide susceptibility mapping in the study region were found, except slope stability analysis in Bonga Town, Southwestern Ethiopia (Tsige et al., 2017). However, relevant technical reports were available, including slope stability analyses conducted by Civil Works and Consulting Engineers (2019) for the project road area.

3 METHODS AND MATERIALS

The thesis aimed to accomplish its objectives through the application of various approaches and methodologies, including: (a) literature review, (b) field investigations, (c) laboratory analysis, and (d) landslide susceptibility mapping and e) slope stability analysis.

3.1 LITERATURE REVIEW

The study reviewed previous works and relevant literatures such as spatial databases, journals, and academic papers related to landslides for the area. This involved analyzing varied geological, topographical, hydrological, meteorological and geotechnical records from various sources (Table 6). The purpose is to better understand the types of landslides, their causes, causative factors, susceptibility mapping methods, and possible mitigation strategies in the area. Furthermore, existing geological maps, topographical data, satellite imagery, and previous reports were reviewed in accordance with ASTM D420 to identify critical slope sections and guide field investigations.

3.2 FIELD INVESTIGATION

Primary data such as, landslide inventory, geological, hydrological, geotechnical, and structural information, along with soil samples for lab testing were gathered, with relevant notes and photographs documented concurrently. Both primary field measurements and secondary data (2019–2023) were used in the study. While geomorphological and geological parameters were considered stable, dynamic variables such as land cover and rainfall were standardized using recent satellite data, field inspections, and multi-year averages. By combining all spatial datasets to a single coordinate system and resolution, discrepancies were minimized and reliable integrated analysis was ensured.

The primary tasks were to identify the key factors contributing to landslides and to delineate the study area based on these insights. The selection of causative factors was based on a literature review, prior studies, and field observations. Eight landslide causative factors including, slope gradient, aspect, elevation, lithology, distance from roads, distance from streams, land use/land cover, and precipitation were selected. A total of 120 inventory of landslides were initially identified using Google Earth, followed by validation field verification. Several characteristics that could not be determined solely through google image analysis were assessed during field investigations (Appendix-1), with some having their GPS coordinates recorded along with details of their failure mechanisms. Additionally, their approximate dimensions, including length and width, were measured. To further analyze the landslides,

traverse routes were established in the field, and classification was carried out based on the frameworks proposed by (Cruden & Varnes, 1996; Varnes, 1978).

All the spatial datasets were converted to raster format and resampled to a uniform cell size of 30 m × 30 m. Subsequently, all layers were projected to WGS84 (UTM Zone 37N) and clipped to the study area boundary to ensure spatial consistency. This preprocessing facilitated accurate overlay and analysis of the causative factors for landslide susceptibility modeling using the Frequency Ratio and Weight of Evidence methods.

Another main task was identifying lithological units, resulting in the classification of six distinct units. Each unit was described in detail following BS 5930-1990 (Howard, 1987) soil and characterizations, and a geological map of the area was generated at a 1: 50,000 scale. The geological map of the study area was obtained from Geological map of Jimma area at a scale of 1:250,000. It was digitized and projected to WGS84 (UTM Zone 37N) to maintain consistency with other spatial datasets. Lithological units were reclassified where necessary to correspond with the landslide causative factor categories used in this study. Geological structures (faults and joints) were identified and described. The raw data of faults and joints were analyzed using software's rockworks 16 and Georose 0.5.2 respectively.

Due to the presence of thick soil deposits across all landslide sections, detail rock mass characterization and classification were not carried out. However, for some exposed rock sections were trying to characterized based on field weathering degree observations while for the subsurface soil layering characterization, secondary data from borehole logs, and laboratory results, including core weathering, RQD, and UCS data from underlying layers were analyzed.

Eight representative soil samples were collected by trial pits with depth ranging from 0.5-1.0m from face of selected slope failure sections for detail description and slope stability analysis. While collecting the samples there is in situ densities was calculated at field using sand replacement method following the procedures and empirical formulas suggested by ASTM-D 1556, 2000. On top of that, the water content of the soils also calculated using oven dry method (ASTM-D 1556).

In addition to this, secondary data of subsurface investigations of each failed landslide sections were collected CWCE & Core (2019). Boring (in depth in situ testing, rock/soil sampling) and subsequently laboratory testing is compiled to define the subsurface profile and their geotechnical properties. For the present study, these secondary subsurface data have been compiled and used for landslide stability analysis to supplement the high susceptibility mapped sections to have better complete information about the subsurface conditions.

Table 5: Collected soil samples

S. ID	Station, (KM)	Coordinates [WGS84 / UTM Zone 37N]		Elevation, m	Sample Depth, m
		Eating, m	Northing, m		
PS-01	17+160 LHS	203278	794049	2111.0	0.8
PS-02	20+510 LHS	205327	792340	2310.0	1.5
PS-03	35+220RHS	212270	787809	1727.0	1.2
PS-04	52+200 LHS	224000	784745	2710.0	0.5
PS-05	53+160 LHS	224382	784909	2652.0	3.0
PS-06	57+600 LHS	226919	786768	2462.0	3.0
PS-07	63+400 LHS	231269	787343	2475.0	1.6
PS-08	65+620 LHS	230324	789039	2448.0	2.2

3.3 LABORATORY ANALYSIS

The current study focused on the areas where failures occurred and collected laboratory test results from two private companies, Civil Works and CORE Consulting Engineers, in addition eight soil samples were collected for further lab analysis. Disturbed samples were subjected to index property tests, including natural moisture content (ASTM D2216), Atterberg limits (ASTM D4318), grain size distribution (ASTM D422), and specific gravity (ASTM D854), as well as strength tests such as direct shear (ASTM D3080) to determine the shear strength parameters cohesion (c) and friction angle (φ). The shear strength parameters were calculated using the Mohr-Coulomb failure criterion and were utilized as input data for slope stability analysis. The uniaxial compressive strength (UCS) tests were conducted using rock core samples recovered, each with a diameter twice that of the cylindrical rock core samples.

3.4 LANDSLIDE SUSCEPTIBILITY MAPPING

To evaluate the probability of landslides occurring in a specific area, it is crucial to map causative factors and the locations of past landslides (Fumagalli, 2025; Guzzetti et al., 2022). To map and evaluate the current study area, GIS based overlay analysis, utilizing models such as frequency ratio (FR) and Weight of Evidence (WoE) were employed.

Frequency Ratio (FR):

Using equation (1), the frequency ratio value for each category of causative factors was determined (Lee & Talib, 2005). Based on the relative frequency of landslides and the criteria taken into consideration, this model assists in identifying locations that are more or less susceptible to landslides.

$$\mathrm{FR} = \frac{\%\ \text{of landslide area in a given sub class (b)}}{\%\ \text{of total area in a given sub class (a)}} \ldots\ldots\ldots\ldots\ldots\ldots\ldots\ldots\ldots\ldots (1)$$

Where,

$$a = \frac{Number\ of\ class\ pixles\ in\ a\ given\ subclass}{Total\ number\ of\ sub\ class\ pixles}$$

$$b = \frac{Number\ of\ landslide\ pixles\ in\ a\ given\ subclass}{Total\ number\ of\ landslide\ sub\ class\ pixles}$$

To create the landslide susceptibility index (LSI), the FR values of eight factors were combined under raster calculator using ArcGIS toolbox using equation (2) (Lee & Pradhan, 2007).

$$\boldsymbol{LSI} = \sum_{\boldsymbol{i=1}}^{\boldsymbol{n}} \boldsymbol{FR_{Class\ i}} = (FR_{slope} + FR_{aspect} + FR_{elevation} + FR_{lithology} + FR_{LULC} + FR_{distance\ to\ road} + FR_{distance\ to\ streams} + FR_{precipitation} \ldots\ldots\ldots\ldots\ldots\ldots\ldots (2)$$

Finally, the landslide inventory, literature study, and natural breaks (Jenks) were used to classify the LSI map into five susceptibility zones (very low to very high) using ArcGIS 10.8.2.

Weight of Evidence (WoE):

The second method used was weight of evidence (WoE), which is a statistical approach based on Bayesian probability that is commonly used for landslide susceptibility modeling and other natural hazard assessments. The WoE value for each causative factors was calculated using Equation (3) and 4) (Regmi et al., 2010; Van Westen et al., 2003).

$$\mathbf{W}^{+} = ln\left\{\frac{(\frac{\mathbf{N[pix1]}}{\mathbf{N[pix1]\ +\ N[pix2]}})}{(\frac{\mathbf{N[pix3]}}{\mathbf{N[pix3]\ +\ N[pix4]}})}\right\} \ldots\ldots\ldots\ldots\ldots\ldots\ldots\ldots\ldots\ldots\ldots\ldots (3)$$

$$\mathbf{W}^{-} = ln\left\{\frac{(\frac{\mathbf{N[pix2]}}{\mathbf{N[pix1]\ +\ N[pix2]}})}{(\frac{\mathbf{N[pix4]}}{\mathbf{N[pix3]\ +\ N[pix4]}})}\right\} \ldots\ldots\ldots\ldots\ldots\ldots\ldots\ldots\ldots\ldots\ldots\ldots (4)$$

Where,

Npix1 = Number of pixels where the factor is **present inside** landslide areas,

Npix2 = Number of pixels where the factor is **absent inside** landslide areas,

Npix3 = Number of pixels where the factor is **present outside** landslide areas,

Npix4 = Number of pixels where the factor is **absent outside** landslide areas.

Final weight expressed with W^{c} was calculated using Equation (5),

$$\boldsymbol{C} = \boldsymbol{W}^{+} - \quad \boldsymbol{W}^{-} \ldots\ldots\ldots\ldots\ldots\ldots\ldots\ldots\ldots\ldots\ldots\ldots\ldots\ldots\ldots\ldots\ldots\ldots\ldots\ldots\ldots\ldots\ldots\ldots\ldots\ldots\ldots\ldots\ldots\ldots (5)$$

Where,

W+ **(Positive WoE)** → Influence of a factor **when present** in landslide areas.

W− **(Negative WoE)** → Influence of a factor **when absent** in landslide areas.

After completing all WOE calculations, the values were assigned with each causative factors in ArcGIS environment. The landslide susceptibility index (LSI) raster was obtained by summing the Woe contrast values of the eight causative factors using equation (6),

$$\boldsymbol{LSI} = \sum_{\boldsymbol{i=1}}^{\boldsymbol{n}} \boldsymbol{C_{Class\ i}} = (C_{slope} + C_{aspect} + C_{elevation} + C_{lithology} + C_{LULC} + C_{distance\ to\ road} + C_{distance\ to\ streams} + C_{precipitation}) \ldots\ldots\ldots\ldots\ldots\ldots\ldots\ldots\ldots\ldots\ldots\ldots\ldots\ldots\ldots . (6)$$

A total of 120 landslides was initially inventoried to assist as input for the susceptibility mapping. The inventory was prepared using field observations, interviews with local communities, and interpretations of Google Earth imagery (2021). Following this, the selection and prioritization of landslide conditioning factors were carried out. Though ranking such factors is often challenging in a single study, eight key factors were identified based on literature review, evidence from past landslide events and field verifications. The eight (8) factors were; slope gradient, slope aspect, elevation, lithology, land cover, distance to roads, distance to streams, and precipitation.

Table 6: Data sources used to prepare thematic maps using GIS Analysis

Prepared Map	**Source**	**Scale**	**Format**
Landslide Inventory map	Google Earth Imagery and field visits	1:50,000	Vector/shape file
Slope map	Ethiopian- Aster Digital Elevation Model	30X30 resolution	Raster/Grid
Aspect map			
Elevation map			
Lithological map	Geological map of Jimma area, GSE, (2012)	1:250,000	Vector/Shape file
Distance to streams	DEM with 30X30 resolution	30X30	Raster/Grid
LULC map	ESA Sentinel-2 imagery at 10m resolution	10X10	Raster/Grid
Distance to road map	Ethiopian Mapping Agency (EMA)	1:50, 000	Vector/Shape file
Geotechnical data	Civil works and Core Consulting Engineers plc	Data	Point/Lines

The factors were derived from various sources using tools like ArcGIS and Google Earth, with

DEM data (30x30m) used for terrain features and ESRI 10m LULC data for land cover analysis (2017-2022) available in the Google earth engine (GEE) Community Catalog, enabling detailed analysis and mapping.

3.5 LIMIT EQUILIBRIUM (LE) METHOD

Finally, in the stability analysis stage, eight representative failed cut slopes at km 17+160 LHS, km 20+510 LHS, mile 35+220RHS, km 52+200 LHS, km 53+160 LHS, km 57+600 LHS, km 63+400 LHS, and km 65+620 LHS were selected for stability analysis. Slope cross-sections were developed from field observations, survey data, test pits, geophysical survey results (SRT and ERT), borehole logs, and laboratory test results incorporating soil layering, and analyzed using Rocscience Slide 2D software. Data from surface springs and boreholes were used to determine the groundwater conditions. Laboratory test results were used to assign soil and rock parameters, such as cohesion (c), internal friction angle (φ), and unit weight (γ), to each layer. Limit equilibrium methods (Bishop's simplified and Spencer techniques) were applied in accordance with Eurocode 7 and the 2013 ERA Geotechnical Design Manual, evaluating stability under dry, and saturated scenarios. For circular failures such as Km 17+160, Km 20+510, Km 35+220, Km 52+200, Km 53+160, the Bishop simplified approach was employed whereas for complex semi-circular failures on layered soil and rock slopes (Km 57+600, Km 63+400, Km 65+620), the Spencer method was utilized. The methods were chosen, based on the observed failure type, material heterogeneity, and slope geometry. Furthermore, the stability of each slope was also modeled further in different worst-case scenarios (dry, and saturated state). The limit equilibrium method evaluates the stability of a slope by analyzing the equilibrium of forces and moments acting on individual slices within the slope (Fredlund & Rahardjo, 1993). The factor of safety (FOS) for the slope failures was calculated using equation (7) (Das, B.M. 2010). Factors of safety were interpreted against standard thresholds (FoS ≥ 1.3 for long-term stability and FoS ≥ 1.0 for short-term conditions) to identify critical sections, governing failure mechanisms, and possible remedial measures.

$$FOS = \frac{Sum\ of\ restisting\ forces\ (F)}{Sum\ of\ driving\ forces\ (D)} = \frac{Shear\ strength(\tau)}{shear\ stress\ (\sigma)} \ldots\ldots\ldots\ldots\ldots\ldots\ldots\ldots\ldots\ldots (7)$$

Critical slip surface and factor of safety against failure are determined based on the forces of gravity, soil shear strength (Duncan, J.M., and Wright, 2005), and external loads using equation (8).

$$\tau = c' + \sigma' \tan(\varphi') \ldots\ldots\ldots\ldots\ldots\ldots\ldots\ldots\ldots\ldots\ldots\ldots\ldots\ldots\ldots\ldots\ldots\ldots\ldots\ldots\ldots\ldots\ldots\ldots\ldots\ldots (8)$$

Where:

τ: Shear strength

c': Effective cohesion

σ': Effective normal stress

φ': Effective angle of internal friction

The bishop method is widely used due to its simplicity and practicality in assessing slope stability in engineering practice (Duncan, and Wright, 2005).

$$\mathbf{FOS} = \frac{\mathbf{\Sigma\ (c'\ \Delta l cos\alpha +\ (W\ -\ u\ \Delta l)\ tan\ \varphi')/m}}{\mathbf{\Sigma\ (W\ sin\ \alpha)}} \ldots\ldots\ldots\ldots\ldots\ldots\ldots\ldots\ldots\ldots\ldots\ldots\ldots\ldots\ldots\ldots\ldots\ldots (9)$$

Where:

Δl: Length of the base of a slice, c′: Effective cohesion of the soil, W: Weight of the slice, ϕ′: Effective angle of internal friction, u: Pore water pressure, α: Base inclination angle of the slice, m = cos α + (sin α tan φ') / FoS (solved iteratively)

The Spencer method used was illustrated as follows in equation (10)

$$\mathbf{FOS} = \frac{\sum_{i=1}^{n}[\boldsymbol{cili} + (\boldsymbol{Wicos\alpha i} - \boldsymbol{uili})\boldsymbol{tan\phi i}]}{\sum_{i=1}^{n}[\boldsymbol{Wisin\alpha i} - \boldsymbol{Xi}]} \ldots\ldots\ldots\ldots\ldots\ldots\ldots\ldots\ldots\ldots\ldots\ldots\ldots\ldots\ldots\ldots\ldots\ldots (10)$$

Where,

Wi = weight of slice I, li = base length of slice I, αi = base inclination of slice I, ci = cohesion along slice base, ϕi = friction angle along slice base, ui = pore-water pressure at base, Xi = inter-slice shear force, determined iteratively to satisfy horizontal and vertical equilibrium

Finally, results were interpreted to identify critical failure mechanisms and inform site-specific remedial measures.

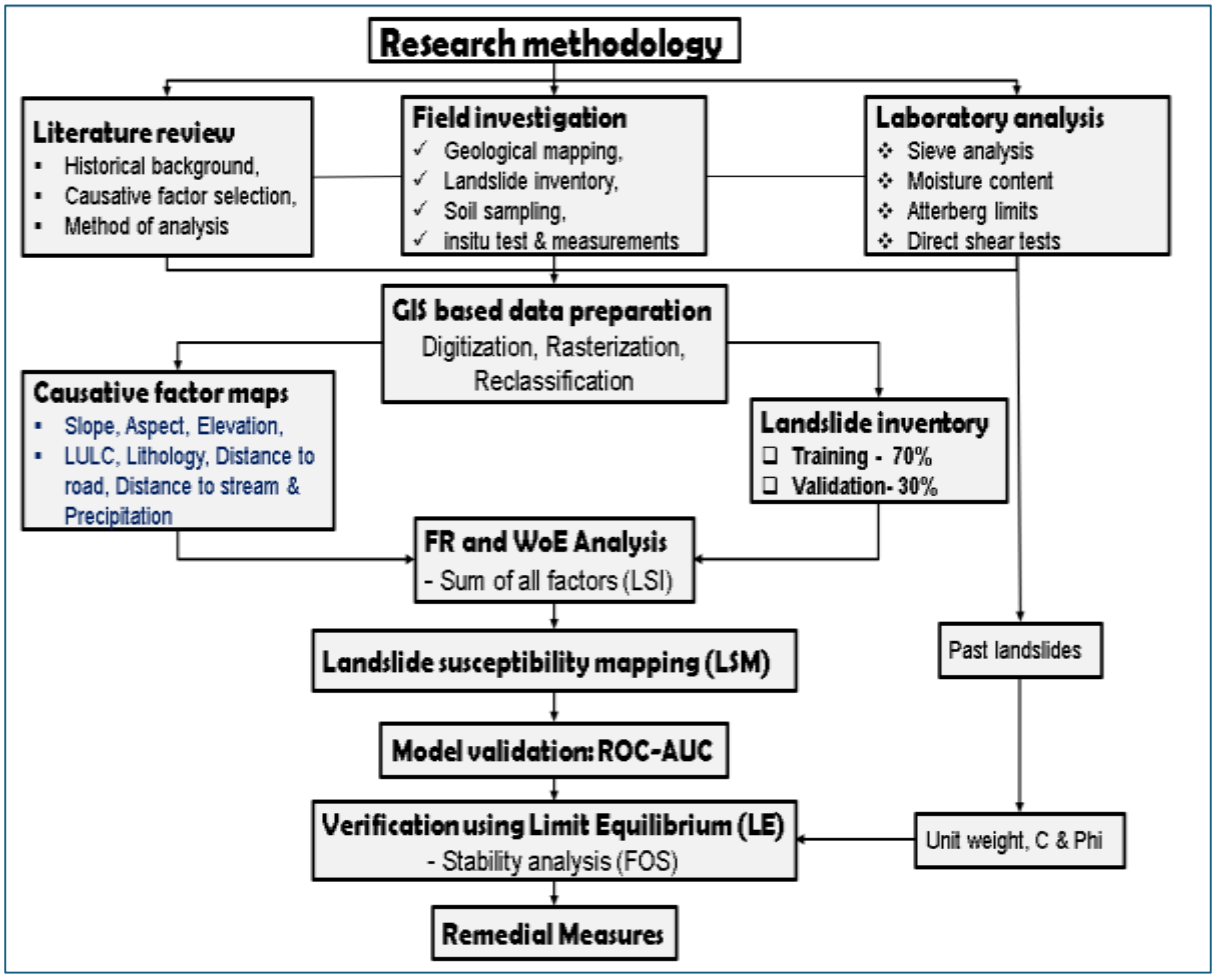

Figure 9: Flow chart showing the adopted research methods

4 GEOLOGY

4.1 REGIONAL GEOLOGY

Ethiopian geological structure comprises three main units: Precambrian bedrock, sedimentary rocks from the Late Paleozoic to Early Tertiary, and volcanic rocks from the Tertiary to Quaternary (Mengesha et al., 1996). The oldest, the Precambrian basement rocks, dating back 880 to 550 million years, serve as the region's crustal backbone (Abbate et al., 2015). This unit encompasses various igneous, volcanic, and sedimentary deposits that have undergone metamorphism and intrusion to different extents (Asrat et al., 2001; Kazmin et al., 1978).

The sedimentary rocks, ranging from the Late Paleozoic to the Early Tertiary era, found in various regions of Ethiopia including the north, west, south, and east, consist mainly of sandstones with some tillite, shale, siltstone, and conglomerate. These rocks, dated from the Upper Paleozoic to Lower Mesozoic, are supplemented by Jurassic and Cretaceous period deposits in the Blue Nile Basin beneath the Mekelle Outlier to the north. Research by (Gani et al., 2009) suggests that the Mesozoic rifting of Gondwana is linked to the NE-SW directed extensions from the Triassic to Cretaceous periods, resulting in the deposition of Mesozoic to Cenozoic rocks in Ethiopia.

Volcanic rocks from the Tertiary to Quaternary period dominate the Ethiopian highlands, with extensive flood basalts covering much of the area. These basalts are overlain by large shield volcanoes, which shape the landscape due to ongoing uplift and significant volcanic activity, as noted by (Abbate et al., 2015; Kieffer et al., 2004) estimate that the current extent of flood basalts covers 600,000 km2, previously reaching 750,000 km2 before erosion. Cenozoic volcanic formations and sediments constitute 56% of Ethiopia's land area, as highlighted by (Gerra & Hailemariam, 2000).

Structurally, the Ethiopian highlands comprise two distinct uplifted blocks, the Western and Eastern plateaus, separated by the Main Ethiopian Rift. According (Choi et al., 2016) various fault systems within these highlands create horsts, tectonic depressions, and fault scarps. Notably, fault activity is evident in the displacement of Tertiary - Quaternary volcanic rocks and Quaternary alluvial deposits, particularly along the Rift Valley and marginal basins.

The Cenozoic volcanic rocks are in turn classified into two series: the Aden series and the Trap series (Mohr, 1963), known as the Jima volcanics (Kazmin et al., 1978) where the current study area is located. The Trap series consists of intercalated felsic lava, pyroclastic rocks, and flood basalts from the Paleogene and Neogene periods that lying immediately on the Precambrian

basement. The Trachybasalt and rhyolites that make up the majority of southwest Ethiopia were named as Jima volcanic (Merla et al., 1979). Afterwards, the trap volcanic series was divided into the predominantly silicic lava Upper Jimma volcanic and the predominantly basaltic Lower Jima volcanic during the compilation of Ethiopian geology (EIGS, 1996).

As per the findings of many researchers (Davidson, 1983; Kazmin, 1972; Merla et al., 1979), the lower basalt flows, lower pyroclasts, lower volcanic flows, and Omo trachyte flows are pre-Oligocene. The middle basalt flows and middle trachyte flows may correspond to Oligocene Period. Miocene–Pliocene age is assigned to the younger flows.

The Quaternary stratified tuffs and alluvial deposits follow events of rifting and subsequent down warping & different graben formation to which they have accumulated. Quaternary alluvial deposits also occur in wide valleys on the plateau.

4.1.1 PRE-OLIGOCENE VOLCANIC ROCKS

The main lower tertiary (Pre-Oligocene) volcanic rock units exposed in the area are the Omo trachyte flows (TV1), Lower basalt flows (TV2); mainly basalts with rare pyroclasts, Lower trachyte flows (TV3); mainly trachyte with minor ignimbrite and Lower pyroclastic (TV4); mainly ignimbrite, minor lithic to bouldery tuffs.

4.1.2 OLIGOCENE VOLCANIC ROCKS

Volcanic rocks from the Oligocene period identified in this area include Middle basalt flows (TV5), primarily composed of basalt with some trachyte content, and Middle trachyte flows (TV6), consisting mainly of trachyte flows with minor basaltic components.

4.1.3 MIOCENE–PLIOCENE VOLCANIC ROCKS

The volcanic rocks from the upper tertiary period, which date back to the Miocene-Pliocene era, consist of several formations; Upper basalt flows (TV7); mainly layered basalts, with smaller amounts of trachyte interspersed within them, Upper trachyte flows (TV8); mainly massive trachyte flows, Rhyolite flows (TV9); mainly rhyolite with lower part rhyolitic ignimbrite, minor trachyte and tuffs, Upper pyroclastics (TV10); mainly ignimbrites, Kobech phonolite (TV11); flows with top part pyroclastic flows, Trachyte plugs (TV12), and Sentema basalt (TV13); layered basalts-aphanitic and porphyritic.

4.1.4 QUATERNARY VOLCANIC AND SEDIMENTARY DEPOSITS

Except for certain Quaternary alluvial deposits (Qal2) and small occurrences of Quaternary Lake sediments (Qal2), the region primarily features Quaternary stratified tuffs (Qa11), which

are visible in marshy areas and broad, winding flat valleys. These tuff formations also include layers of alluvial channel deposits (sand) up to 30cm thick, sandwiched between the tuff layers.

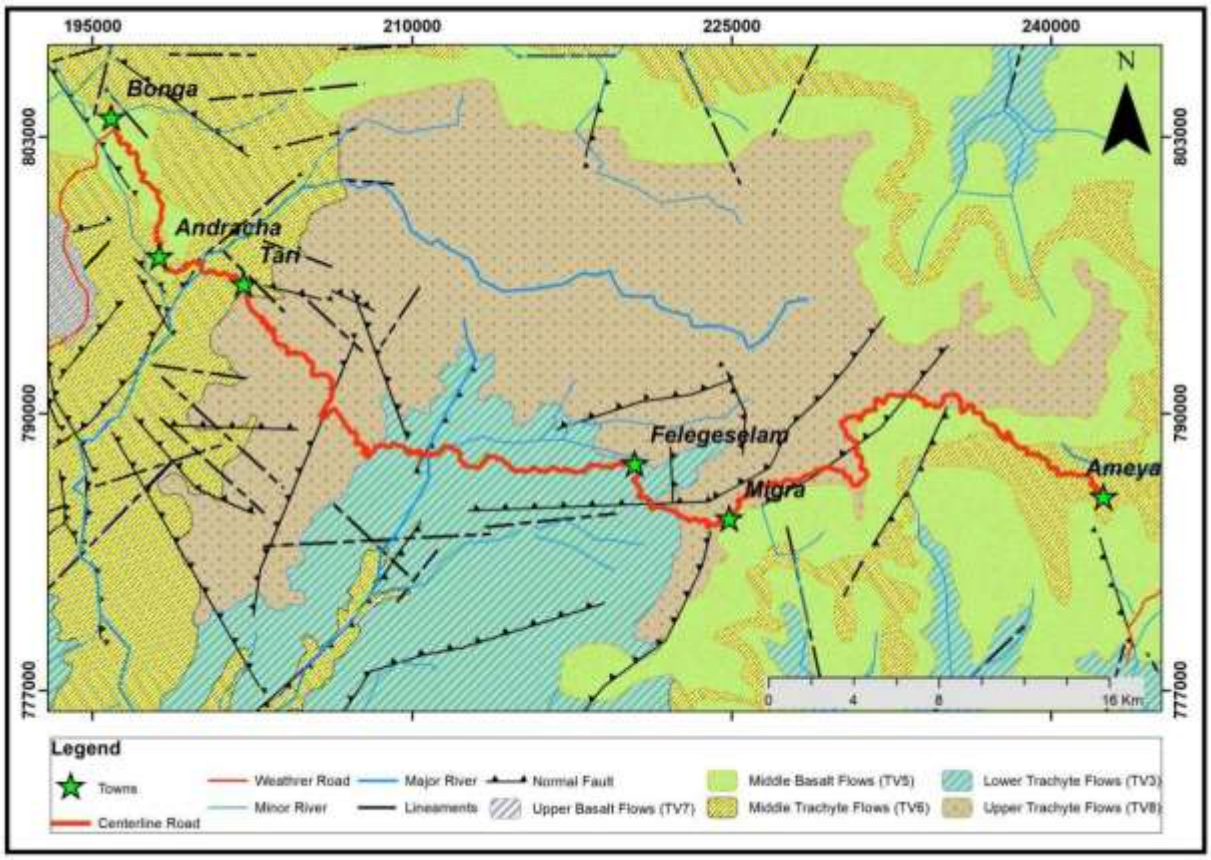

Figure 10: Simplified regional geological map of the study area. Extracted from the 1:250,000 Jimma sheet (adapted from GSE, 2012).

4.2 LOCAL GEOLOGY

By referencing the Jimma sheet geological map (NB 37-1 and 1: 250,000 scale) and detail fieldwork, the main local geologic setup of the road alignment was found to be basalt flows and trachyte flows as upper, middle, and lower trachyte. Quaternary unconsolidated deposits were found to be a minor supplement (Fig. 16). The following is a summary of each lithologic unit.

4.2.1 UNCONSOLIDATED DEPOSITS (QAL2)

The study area experiences fluctuating rainfall patterns and temperature variations. These conditions, coupled with diverse terrain, complex geological compositions, erosion and weathering processes, promote the formation of unconsolidated deposits. They were formed by weathering of volcanic rocks and undergo erosion then deposited in situ. They moved downhill towards gentler areas, such as valleys, rivers, and streams, driven by the combined forces of gravity and water action. They are distributed throughout the western, central, and eastern parts of the study area (Fig. 11).

Figure 11: Representative unconsolidated deposits. (a) Alluvial sediments within a riverbed; (b) Colluvial materials along the backslope of a road.

The road corridor crossed by numerous streams and rivers, resulting deep gully erosions and debris/earth slides. Such sections composed of loose materials of silty clay mixed with gravel textures (colluvium and alluvium), particularly at deep and box cut road sections. Moreover, the alluvial deposits are present in certain sections of the agricultural areas within residential zones and floodplains. It is exposed along the Shosha river km 32+940-33+360.

4.2.2 UPPER TRACHYTE FLOW (TV8)

This unit covers a significant section of the route, especially in the western and eastern parts of the study area, and is primarily located on hilltops and hillsides (Fig. 12). The thick saprolite soil cover and dense plants make it difficult to see. Basalt and pyroclastic rocks intercalate the unit in certain exposures, grading at depth into Trachybasalt as one descends. The trachyte is highly weathered, resulting in gap-graded material that is loose to firm and has light gray to pinkish colors. Debris flows frequently affect springs in rock outcrops, which are found between 2700 and more than 3300 meters above sea level.

Figure 12: Photographs showing road cut exposures of upper trachyte flows at different locations: (a) completely weathered trachyte at Km 17+000, (b) highly weathered trachyte with deep box cut at Km 51+100, and (c) loose and weathered trachyte exposure with steep slope face at Km 65+500.

4.2.3 MIDDLE TRACHYTE FLOW (TV6)

The middle trachyte is found west of the study area, close to Tari's village (northeast), and has little exposure. It appears on undulating to rugged terrain along the road at Km 12+740 and Km 63+460. The texture of the rock is often sandy, it is light grey, fine- to medium-grained, and its hue varies from light grey to yellowish and sometimes pinkish (Fig. 13). Although there are occasional fractures that result in rough to undulating terrain, it is usually huge. In certain places, ignimbrite and trachyte are intercalated, with paleosols that are 30 to 50 cm deep separating them. The primary layers are formed of trachyte, however there are frequently thin ignimbrite intercalations.

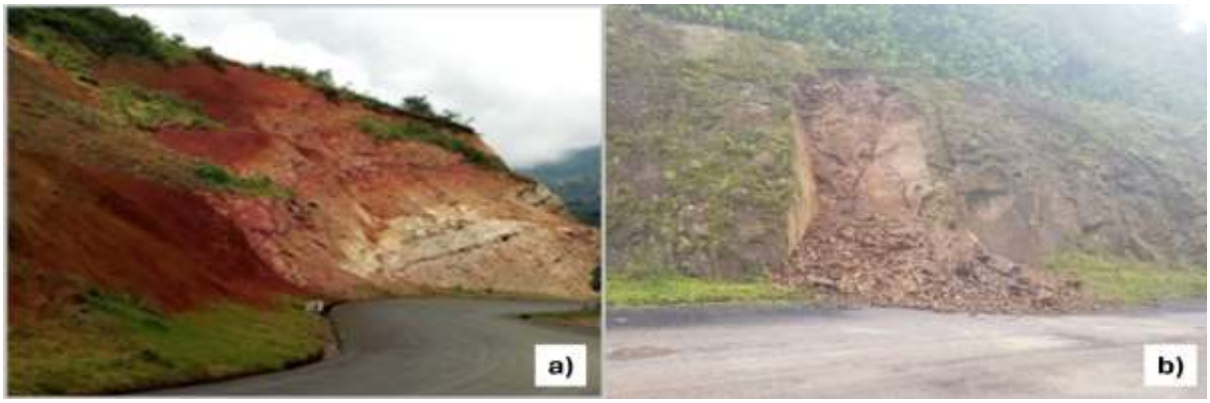

Figure 13: Middle trachyte flow exposures along the road. (a) With distinct paleosol horizon at Km 12+740, indicating ancient weathering surface; (b) Highly jointed and moderately weathered middle trachyte exposure at Km 63+460, showing slope face with potential for instability.

4.2.4 BASALT FLOW (TV5)

It is exposed to the extreme southeastern part of the study area, mainly in cut sections of the road (km 63+400-63+800). It is dark gray when fresh and dull gray when weathered. This unit has varied in color in some locations due to weathering, which may affect its strength (Fig. 14).

Figure 14: Middle Basalt Flows (TV5) at Km 63+600. Slightly weathered basalt exposure with random jointing observed along the left-hand side of the road.

The rock mass properties vary as per the weathering condition and topographical environment. It shows light to dark grey color, reflecting fresh to moderately weathered conditions. It is characterized by medium grained and intersected by deep, randomly oriented joints. As a result, some rock fragments suddenly hinder the main road, as well as side channels and road crossing structures. Occasionally, three set joint (110/40SE, 300/40NE and 140/45 SW trends) were observed on the rock unit.

4.2.5 LOWER TRACHYTE FLOW (TV3)

This unit mainly exposed in riverbanks, hillsides, and road cuts, showing light grey when weathered and dark grey when fresh, with fine to medium grains. The layers are separated by 10–20 cm thick paleosol horizons and characterized by fine to medium grain sizes. It covered the central part and west of Felegeselam along road cut sections at km28+660-32+940 and km33+360-49+100. The rock thickness varies from 5m to 10m while measures in the road sections. To the northwest of Shosha river, this unit exposed on cliff forming topography. Occasional columnar joints were observed. In the north of Shosha river, this unit intercalated with ignimbrite. The ignimbrite is weathered and shows light grey and medium grained texture. It shows flow layering and often tilts to the east (60^0) probably due faulting.

Figure 15: Representative lower trachyte flows. a) Km 31+960: Showing Lower Trachytes exposed around Felegeselam town with visible flow banding and distinct paleosol layers. b) Km 39+480: Highlighting the separation of lower trachyte by paleosol layers and surrounding vegetation.

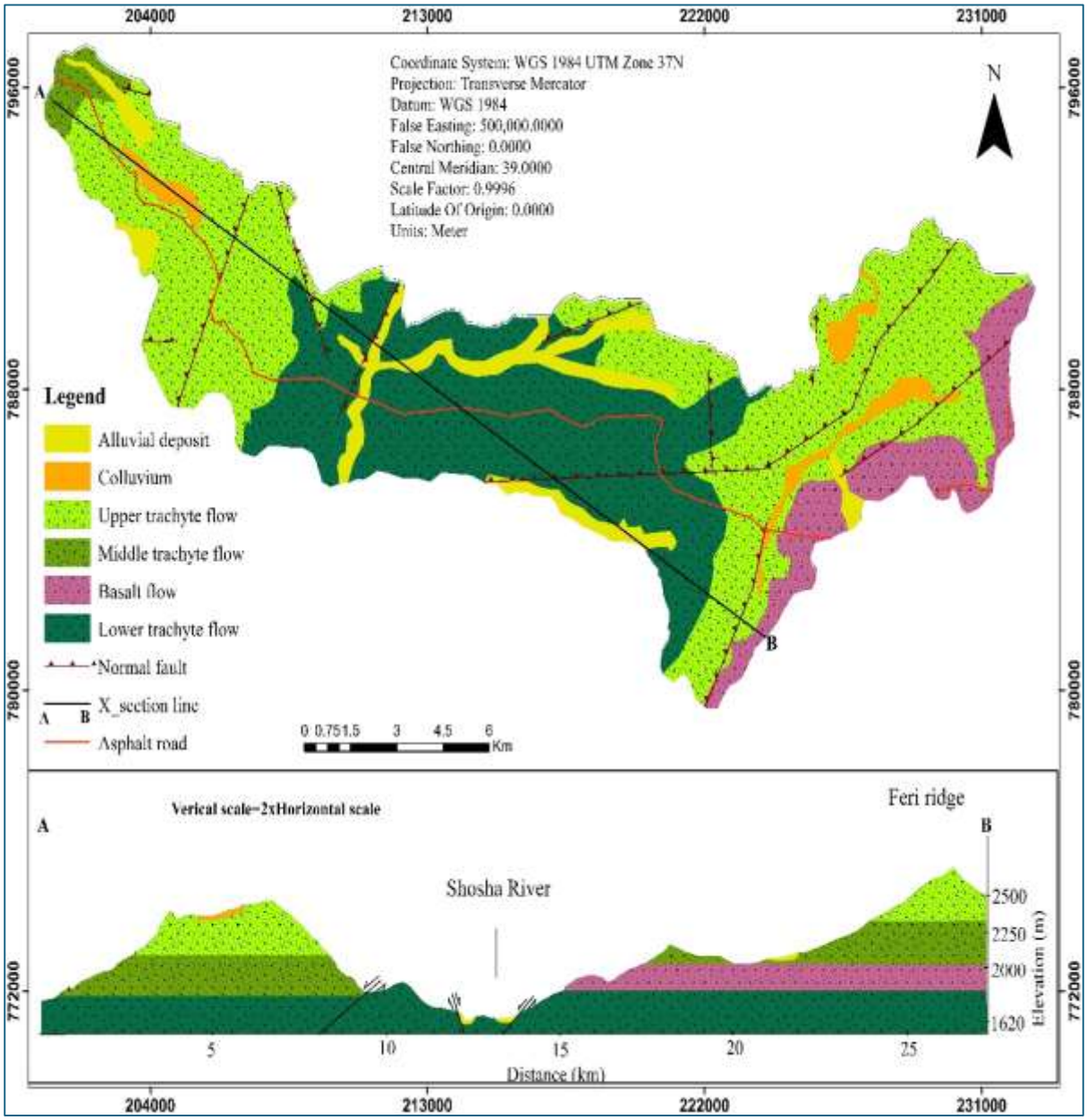

Figure 16: Local geological map of the study area (1:50,000 scale), combining field data from traverses and digitizing from existing map of the Jimma area sheet at a 1:250,000 scale map (GSE 2012).

4.3 GEOLOGICAL STRUCTURES

The structural setting of the southwestern Ethiopian plateau is closely related to tectono-volcanic activity and rift related tensional fractures. Dominant ENE–WSW structural trends, as noted by Workineh (1998), control local grabens and influence faulting, joints, and lineaments along the road.

4.3.1 FAULTS

There are three major fault orientations, NW-SE, NNW-SSE, and N-S (Fig. 17), affecting the ridges, grabens and dissected gorges. The normal faults are traced on a hill shade derived from

a digital elevation model (DEM) by observing linear scarps, aligned valleys, or abrupt topographic breaks that indicate down dropped blocks and fault-related offsets. The grabens are formed due to the normal faults while the dissected gorges are also formed from both the lineaments and the normal faults.

4.3.2 JOINTS

Joints are quite rare in the study area because of the existence of a thick residual and colluvial cover. Three joint sets were observed, however, in road cut sections specifically at Km 57+600 and Km 65+620, while two joint sets were observed at Km 63+400. The joints orientation was usually NNW–SSW for the first, WSW for the second, and SW for the third. These fractures and joints were seen within the trachytic and basaltic rock units, which increase rock permeability. Thus, the occurrence of these fractures and joints is the reason for seasonal contact springs and colluvial seepages in the region.

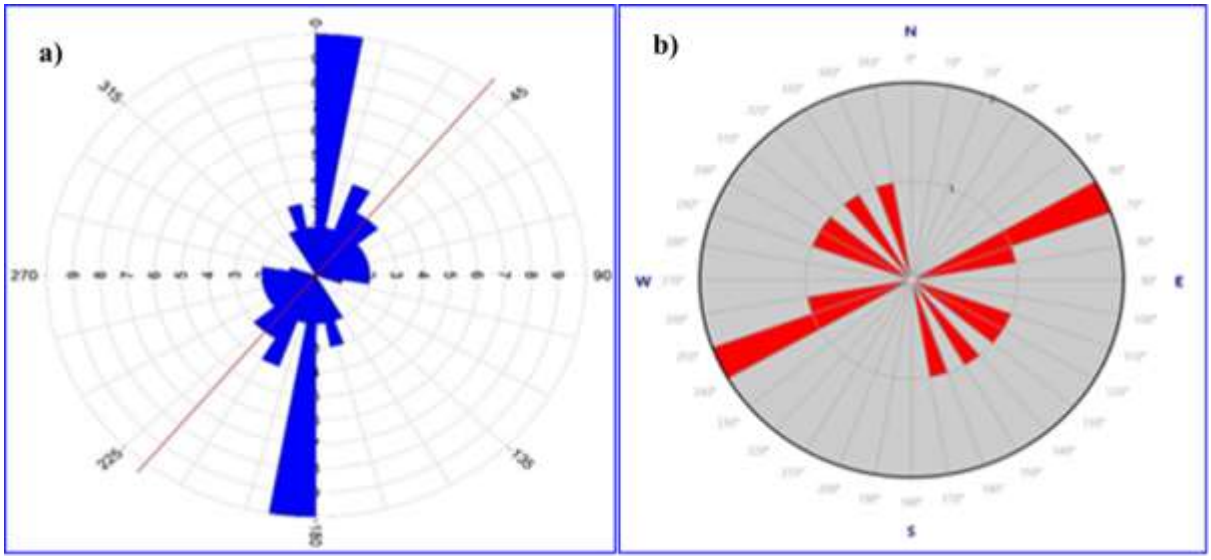

Figure 17: Strike direction of faults (a), and joints (b)

5 RESULTS AND DISCUSSIONS

5.1 INTRODUCTION

This section presents and discusses the findings obtained from the landslide susceptibility mapping (LSM) and slope stability analyses carried out in the study area.

5.2 LANDSLIDE INVENTORY

The study area was started by generating landslide inventory map of 120 landslides through field assessment and Google earth imagery interpretations. The landslide inventory map is illustrated the size and geographical distribution of landslides within a specific area (Cruden, 1991; Fell et al., 2008). It covered 180 km^2. The predominant types of landslides observed along the route were earth/debris flow and earth/debris slides, with some complex slides and creeping movements (Fig. 18).

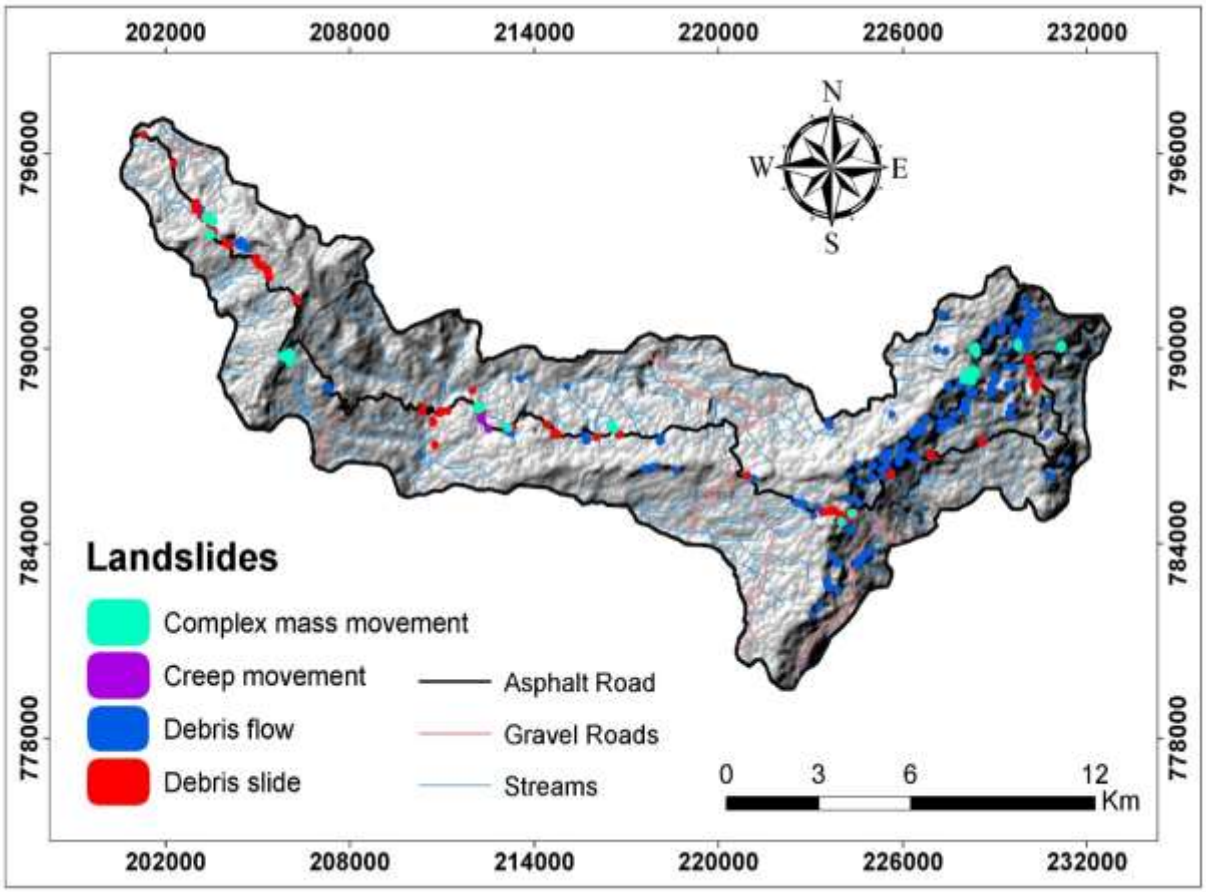

Figure 18: Landslide inventory locations in the study area, superimposed on a hill shade derived from DEM. Source of DEM: http://www.earthexplorer.usgs.gov/

The areal coverage of each landslide types is 53 (44.2%) debris flow, 39 (32.5%) earth slide, 21 (17.5%) complex slides, and 7 (5.8%) creeping movements from the total landslide inventory.

Debris flows and earth/debris slides frequently result damage to roads, villages, farms, and grazing fields, with agricultural areas being particularly susceptible to damage from debris flows.

5.2.1 DEBRIS/EARTH FLOW

The primary type of failure identified in the study area is debris /earth flows commonly observed in steep hilly and mountainous areas. From site investigation and observation, the presence of various sizes of rock fragments mixed with fine particles flowing down onto the slope and immediately affected the road. The accumulation of thick colluvium deposits and rock fragments within the slope mass are contributing factors to these debris and earth flows. Indicators of instability in the study area includes road damages, clogged drainage systems, and damaged retaining structures among others and frequently observed in Tari, Migra within forested areas, and Washa localities (Fig. 19).

Figure 19: Overview of debris and earth flows from a steep hillside near Migra down to the road. (a) Satellite view from google earth; (b) ground photo showing debris flow paths; and (c) Earth/mud flows along the road cut slope blocking the road (Photographs taken in August 2021).

5.2.2 DEBRIS/EARTH SLIDE

The second most common type of failure is debris/earth slides. It is composed of loose residual deposits mainly silty clay and has occurred at the interface of soil masses and the underlying weathered trachytic and basaltic rock units. The depths of these failures range from approximately 0.5m to 10m, with an average travel distance of 5m to 10m along the road cut sections. Rotational slides are the most common mode of instability, although in areas with thicker residual/alluvial deposits, more complex failure types were also observed. These slides primarily occur around river banks and road cut/fill slopes, resulting in the destruction of road parts and disturbed the surrounding ecosystem. The undercutting of streams and rivers, especially the Shosha river, and bank collapse are the primary causes of these failures. Predominantly observed along cut sections near Gomera, east of Migra, and close to Washa village. In many of the debris/earth slides, several cracks (1-2m openings) were observed at the zone of depletion between the crown and the zone of accumulation.

Figure 20: Overview of observed landslides in the study area. (a) general view of rotational landslides, triggered by road cutting, impacting the roadway, (b) additional view of rotational landslide activity, that damaged retaining structure. (Photographs were taken in August 2021).

5.2.3 GULLY EROSION

The unconsolidated soil materials are primarily composed of residual and colluvial deposits, with over 50% silty clay soil that is highly susceptible to erosion due to heavy rainfall and steep slope. The erosion leads to the formation of gullies which affecting roads, farmland, and the natural environment. In stream sections, these unconsolidated deposits can be as thick as 12 meters, contributing to active erosion and deep gullying. The thick residual deposits found in road cut sections have resulted in gullies up to 9.0 m deep, damaging drainage structures and nearby farmland (Fig. 21). Most of the gully erosions were relatively recent, having developed after the road excavations. The road excavation changed the existing surface and shallow

groundwater drainage patterns on the topography, which in turn affects the stability of the road. As a result, the risk of gully erosion and landslide activity were increased following the road construction.

Figure 21: Typical examples of gully erosion. (a) and (b) Gully erosion damaging cultivated areas and causing deep erosion along the roadway near Washa; (c) and (d) widening and scouring around crossing structures near Tari and Mecha. (Photographs were taken in August 2021).

5.2.4 PAVEMENT DEFECTS

The asphalt road from Bonga - Felegeselam was recurrently damaged by different defects. The most commonly observed types of road damage include raveling, rutting (vertical depressions or settlements), shoving (longitudinal surface depressions), and potholes (bowl-shaped holes of varying sizes on the pavement surface). These road failures resulted from several interrelated factors, such as weak subgrade soils, steep and complex terrain, inadequate drainage of surface and subsurface water, and substandard embankment fill materials. Due to these factors the riding quality are reducing from time to time especially during rainy seasons. Previously implemented rock fill and drainage measures not fully addressed the problem. As can be seen in Fig. 22a) a typical rutting (vertical depressions or settlements) observed around km20+200 and Fig. 22b) longitudinal cracking and sliding of underlying fill section around km35+220 that affected the traffic flow.

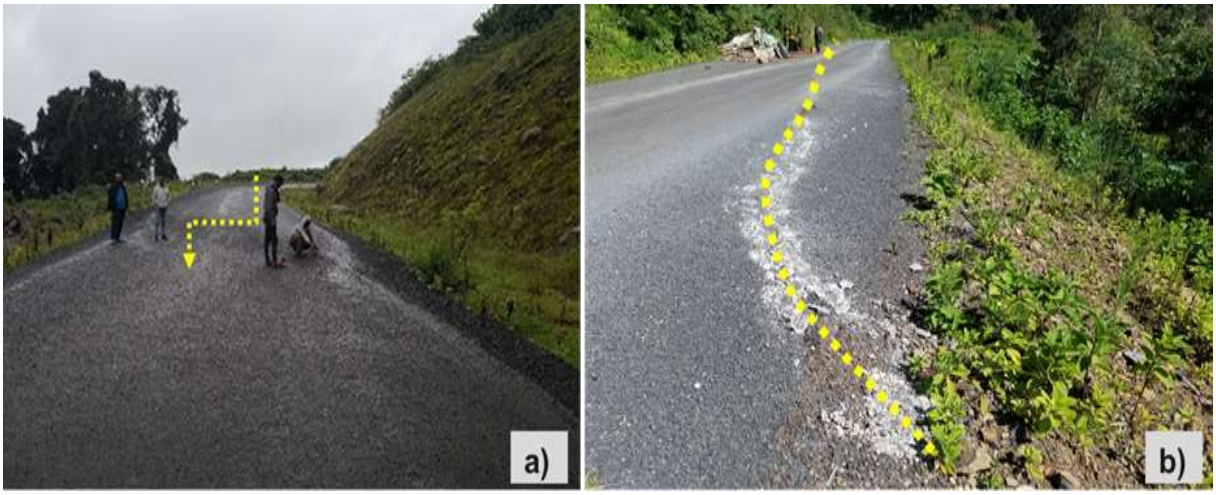

Figure 22: Pavement defects observed along the study area. (a) Rutting and (b) Longitudinal cracking. (Photographs were taken in August 2021).

5.3 LANDSLIDE CAUSATIVE FACTORS

The selection of causative factors for landslide susceptibility mapping depends on the study context, area characteristics, and landslide types (Berhane et al., 2020, 2023; Corominas et al., 2014; Manzo et al., 2013). Though the challenges, eight influencing factors, including slope, aspect, lithology, distance to roads and streams, LULC, and precipitation, were chosen based on field surveys, expert opinions, literature reviews, and their relation to previous landslides (Ayalew & Yamagishi, 2004; Moradi & Rezaei, 2014). Each factor was gathered from different sources (Table 6), standardized, rasterized using ArcGIS 10.8.2 software, and classified into subclasses to assess their impact on landslide occurrences. The selected conditioning factors are detailed with maps in the following subsections.

5.3.1 SLOPE

Slope gradient is considered as primary cause of landslides in several studies (Ayalew et al., 2004; Berhane et al., 2023; Çellek, 2020; Woldearegay et al., 2004), as it influences the downward flow of materials due to gravity, especially in hilly and mountainous regions. The relationship between landslide types and slope classes shows that shallow landslides and debris flow predominantly occur on moderate to steep slopes (20–45°), while deep-seated rotational and translational slides are more common on steep to very steep slopes (>30–45°). Gentle slopes (<10–20°) generally experience fewer or minor landslides, often triggered by local saturation or human activity. As per FAO (1976) the study area slope were divided into six subclasses: a) very gentle slopes (0–10°), b) gentle steep slopes (10–20°), c) moderately steep slopes (20–30°), d) steep slopes (30–45°), and e) very steep slopes (>45°).

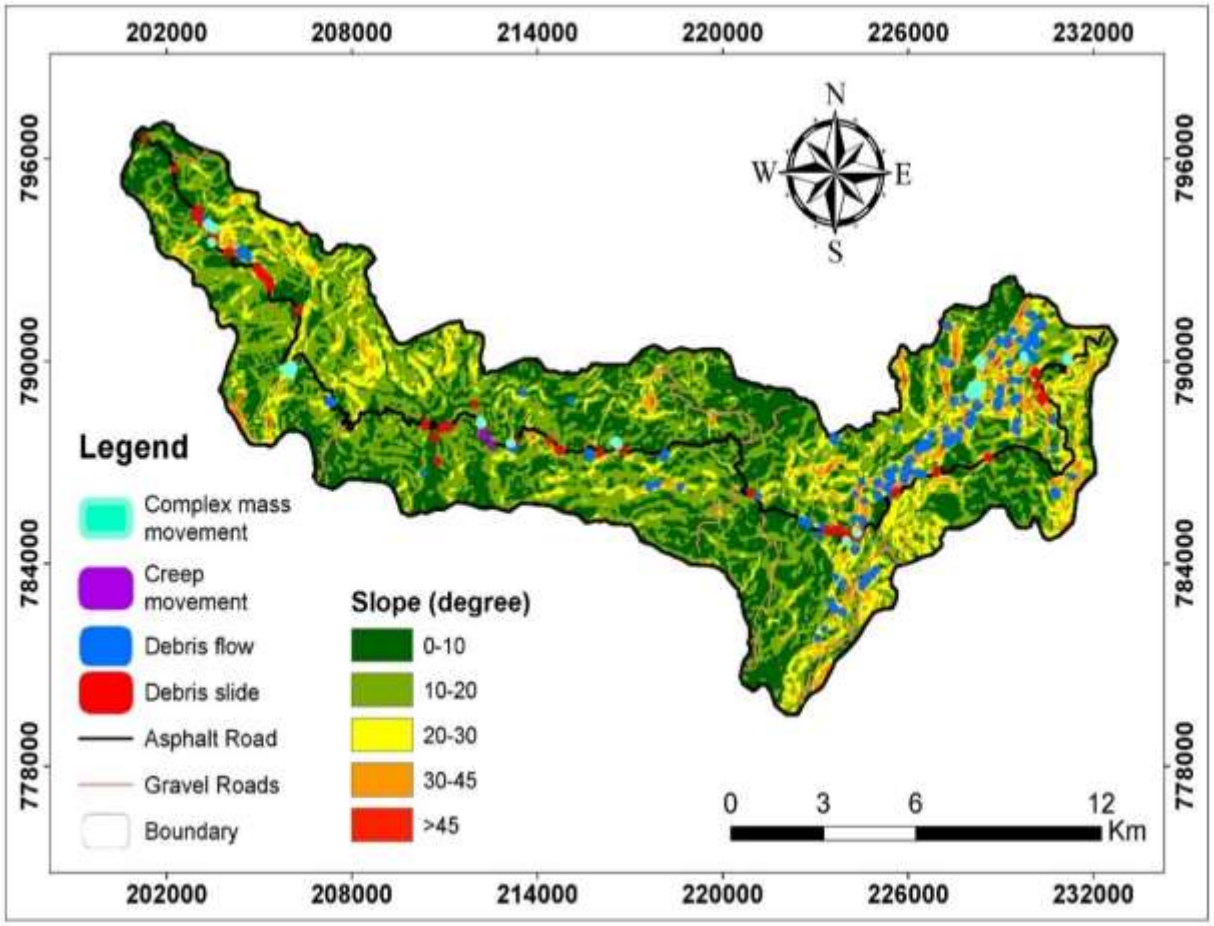

Figure 23: Causative factor map displaying the slope gradient in the study area

5.3.2 ASPECT

The slope direction of a terrain is commonly known as its aspect. Numerous studies have identified slope aspect as a significant factor in landslides (Berhane et al., 2023; Abay et al., 2019, Capitani et al., 2013; Moradi & Rezaei, 2014; Woldearegay, 2013). As a result, slope aspect is considered as essential element in the development of landslide susceptibility mapping. The climate in the study area is characterized by extended periods of precipitation, sunlight exposure, wet and dry conditions, variations in soil moisture, and weathering. Climatic pattern is profoundly influenced by the topographic aspect and the frequency of landslides (Dai & Lee, 2001; Komac, 2006). The aspect map was categorized into nine distinct classes: flat (-1°), north (0°-22.5°; 337.5°-360°), northeast (22.5°-67.5°), east (67.5°-112.5°), southeast (112.5°-157.5°), south (157.5°-202.5°), southwest (202.5°-247.5°), west (247.5°-292.5°), and northwest (292.5°-337.5°).

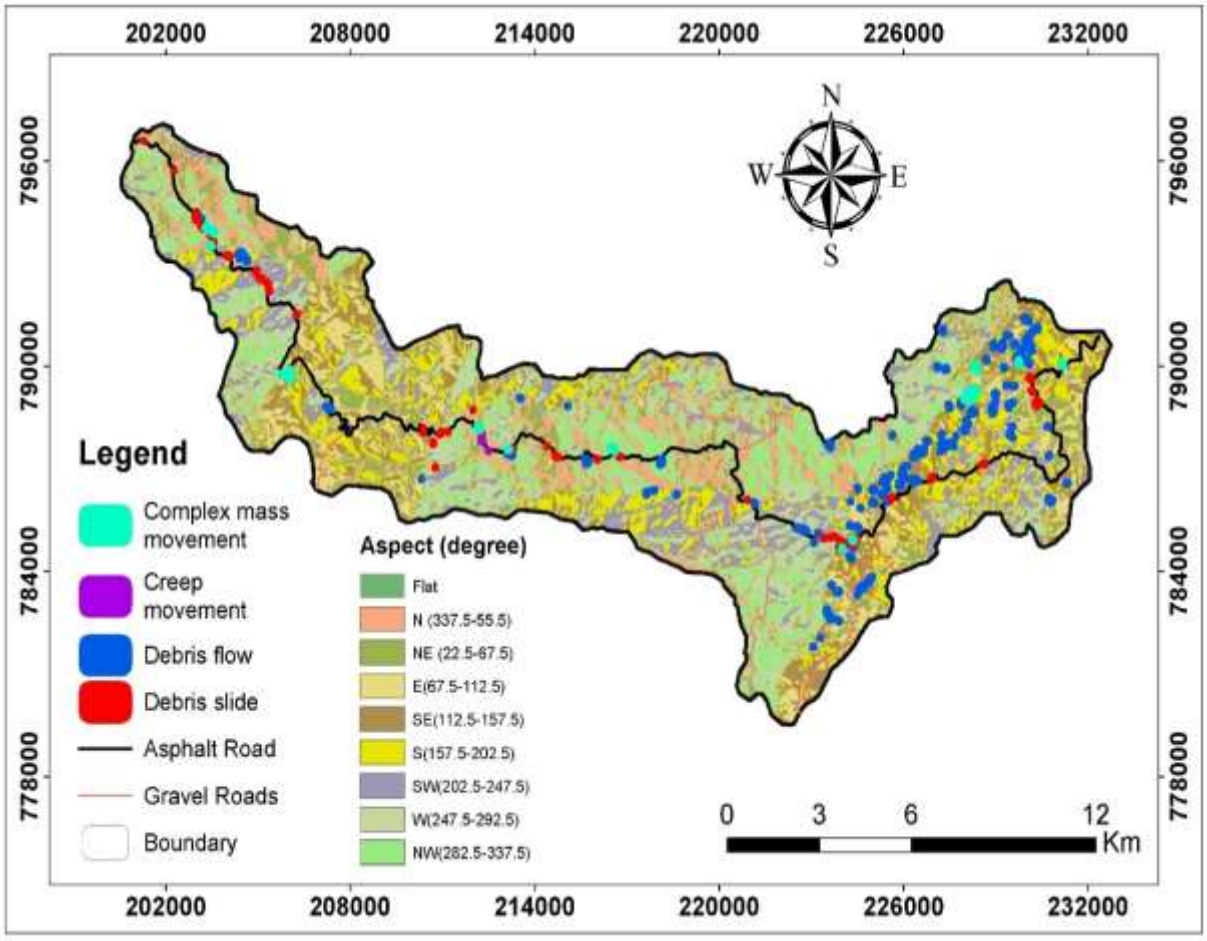

Figure 24: Causative factor map displaying the slope aspect in the study area

5.3.3 ELEVATION

Elevation plays a critical role for landslides occurrence; hence it should be given certain attention in cartographic representations. It represents the variation in vertical distance between the lowest point of a valley and the highest point of a ridge, designating a substantial change in slope (Anbalagan, 1992). Most of the landsides occurred with higher elevation (>2500m above sea level). This is due to higher mountains that extend to great heights often consist of weathered rocks that possess higher shear strengths. However, shear strength of mountain rocks depends on lithology, weathering, and structural features, and is not necessarily higher at greater elevations. On the other hand, slopes at intermediate elevations commonly exhibit thin colluvium, rendering them susceptible to landslides (Dai & Lee, 2001; Yalcin et al., 2011). Elevation in the study area was classified into five different interval categories based on expert opinion and field observations to reflect local topographic conditions: very low (1,500–1,800 m), low (1,800–2,000 m), medium (2,100–2,500 m), high (2,500–3,000 m), and very high (>3,000 m). These intervals were selected to reflect differences in terrain slope and the likelihood of landslide occurrence.

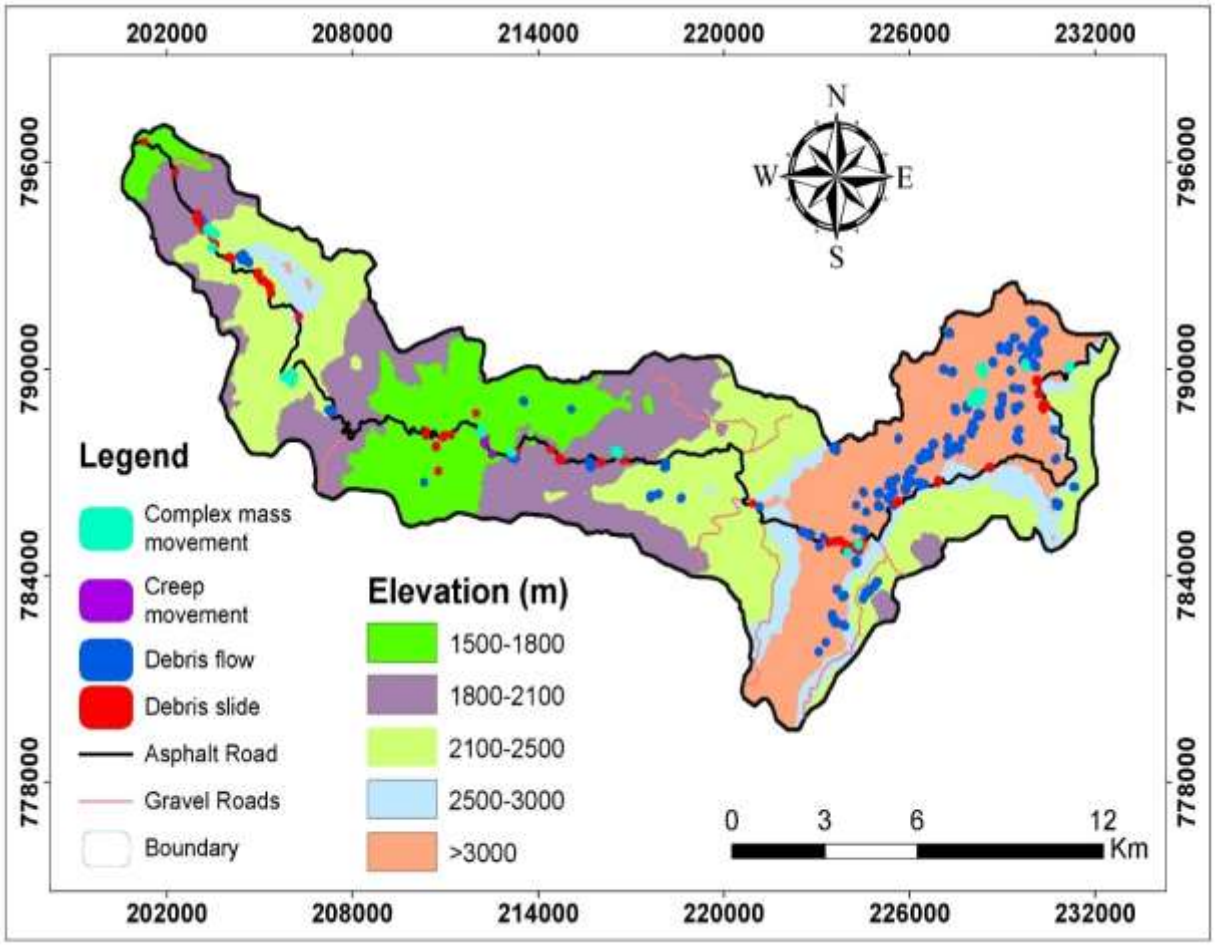

Figure 25: Causative factor map displaying the elevation of the study area

5.3.4 LITHOLOGY

The occurrence of landslides is significantly influenced by lithology, which alters the permeability, weathering susceptibility, and mechanical strength of materials. Weak and highly weathered lithology, such clay rich soils, marls, shales and tuffs, are more likely to fail, particularly when they are covered by more impermeable or competent layers that increase pore pressure and water retention (Dai et al., 2002; Guzzetti et al., 2006). The geological map of the study area was developed based on interpretations from the 2021 Google Earth imagery, field observations, and the 1: 50,000 scale geological map of the Jimma region (Fig. 26). It is mainly characterized by a variety of lithologic units, especially Jimma volcanic (trachyte and basaltic) flows and quaternary deposits. It is commonly accepted that each rock unit responds differently to the degree of weathering, the erosion process, the nature of discontinuities, soft rock intercalations and the intact rock strength value, and hence these differences affect the stability of slopes (Ayalew, 1999).

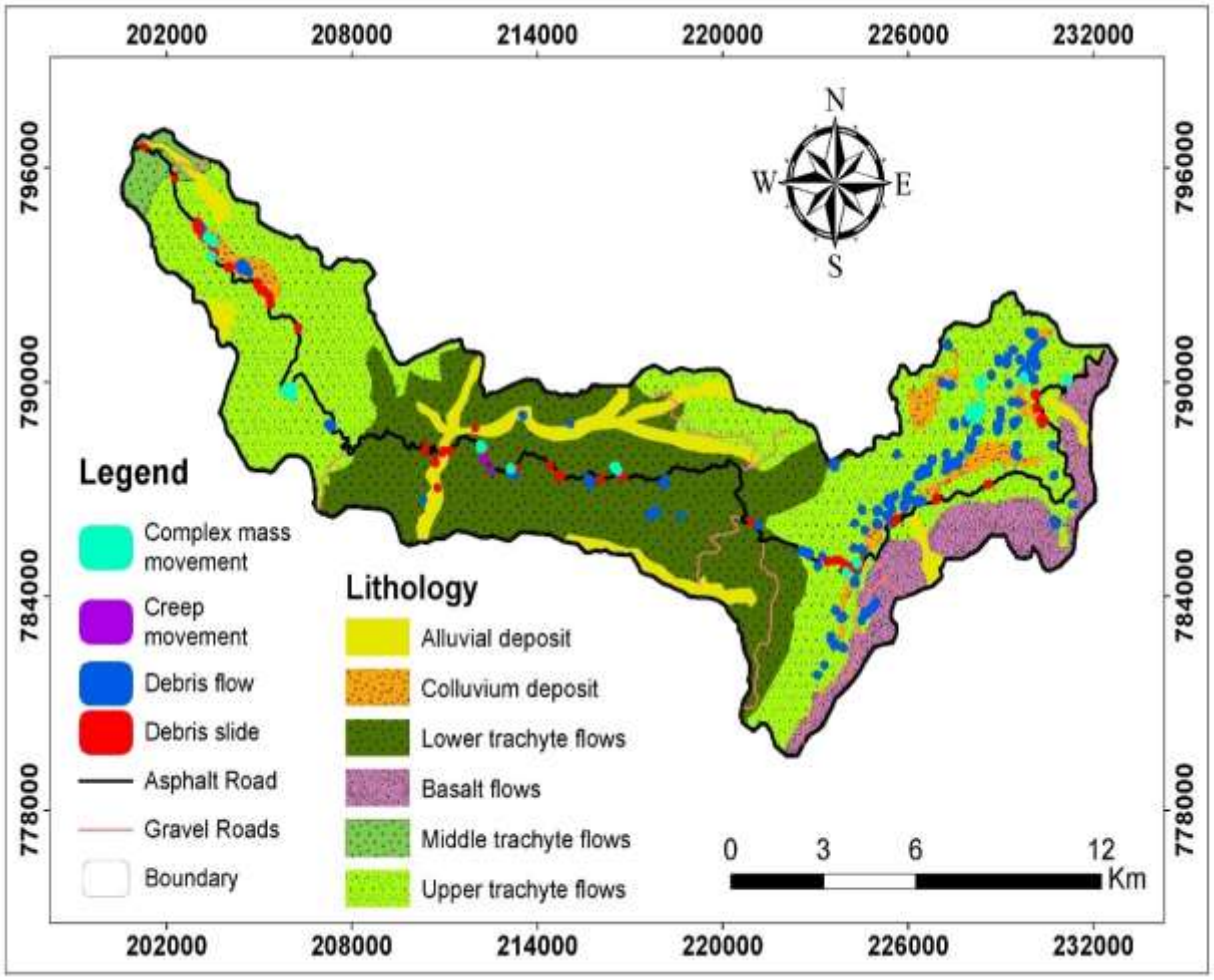

Figure 26: Causative factor map displaying the lithological units in the study area

5.3.5 DISTANCE TO STREAMS

As suggested by different authors (Ayalew & Yamagishi, 2004; Ayenew & Barbieri, 2005; Berhane et al., 2020; Dai & Lee, 2001; Saha et al., 2002; Woldearegay et al., 2004), the proximity of slopes to streams may negatively impact the stability by either eroding the toe or saturating the lower slope material until the water level increases or both. Slope stability and erosion processes are also impacted by the moisture content of the slope materials, which increases when groundwater levels rise (Yalcin et al., 2011).

Distance to streams map was created using DEM with a spatial resolution of 30x30m and divided into six buffer zones. The distance to streams map of the area was categorized into seven classes with 50m interval for the first two then a 100 m interval, ranging from 0 to 100 to >500 m.

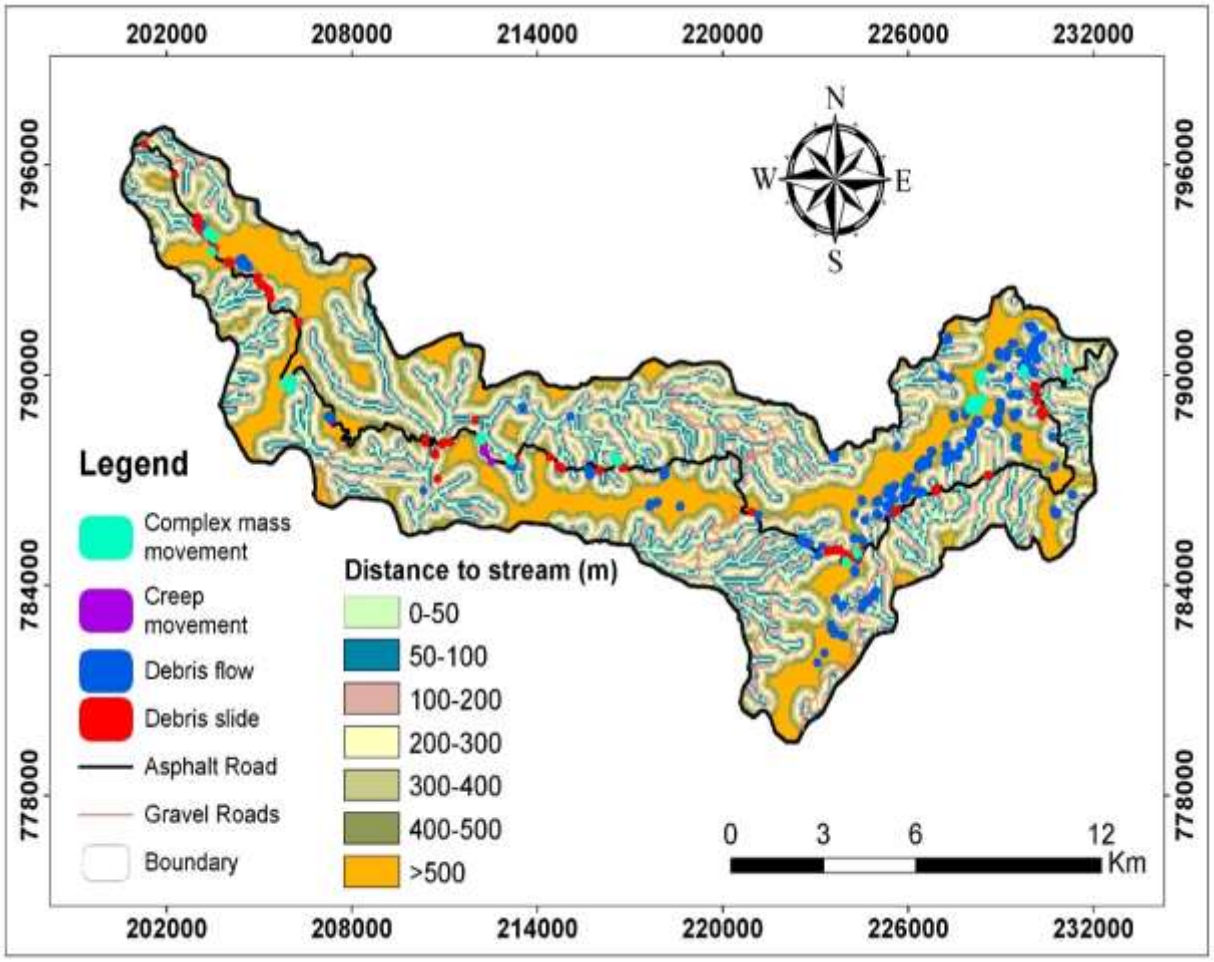

Figure 27: Causative factor map displaying distance to drainage of the study area

5.3.6 DISTANCE TO ROAD

Landslide occurrence is strongly influenced by proximity to roads, as construction activities often disturb natural slope stability through excavation, loading, and inadequate drainage. Studies have shown that landslides are significantly more frequent within the first few hundred meters of roads, particularly within 100–200 m, where slope undercutting and concentrated runoff are common triggers (Ayalew et al., 2004; Moeyersons et al., 2019; Yalcin et al., 2011).

The closer the road, the greater is the landslide probability. It also tends to change the current pattern of the slope surface and shallow groundwater drainage. Near roadways, both effects are anticipated to occur. Therefore, following road construction, there is a higher chance of soil erosion and landslide activity. The Ethiopian Road network map and road alignment centerline was used to create the road proximity map. Subsequently, distance from the road was computed from the road at the interval 100 m using ArcGIS software.

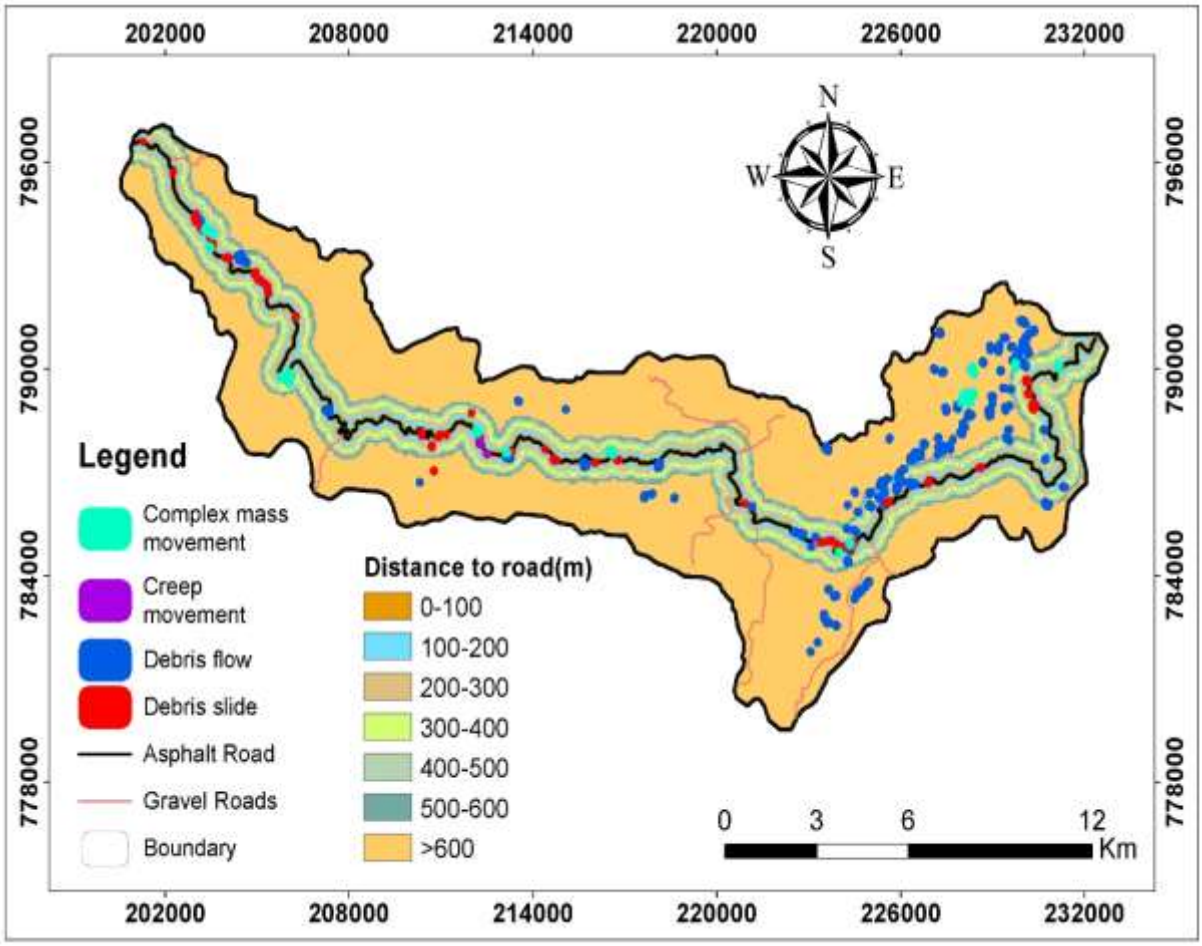

Figure 28: Causative factor map displaying distance to road of the study area

5.3.7 LAND USE AND LAND COVER

Variations in land use and vegetation cover affect a slopes probability of failure. However, on bare and periodically vegetated land, the landslide movements become high due to relatively high weathering intensity, erosion and other related activities (Berhane et al., 2020; Raghuvanshi et al., 2014). However, in the study area landslides are more common in the forest and bushland regions. This is due to the nature of steep terrain with loose colluvium deposits and shallow springs. Forest areas, where some scattered houses are built and road excavations at the base of mountains, are severely impacted by various sizes of debris and earth flows, which degrade agricultural land and block access roads and their crossing structures.

The study area was characterized into six distinct land use/land cover (LULC) classes namely: forest land, bare land, settlements, agricultural land, and bushland. The LULC map was developed based on Sentinel-2, 10-Meter Land Use/Land Cover 2017-2024 and was further distinguished through field verification surveys.

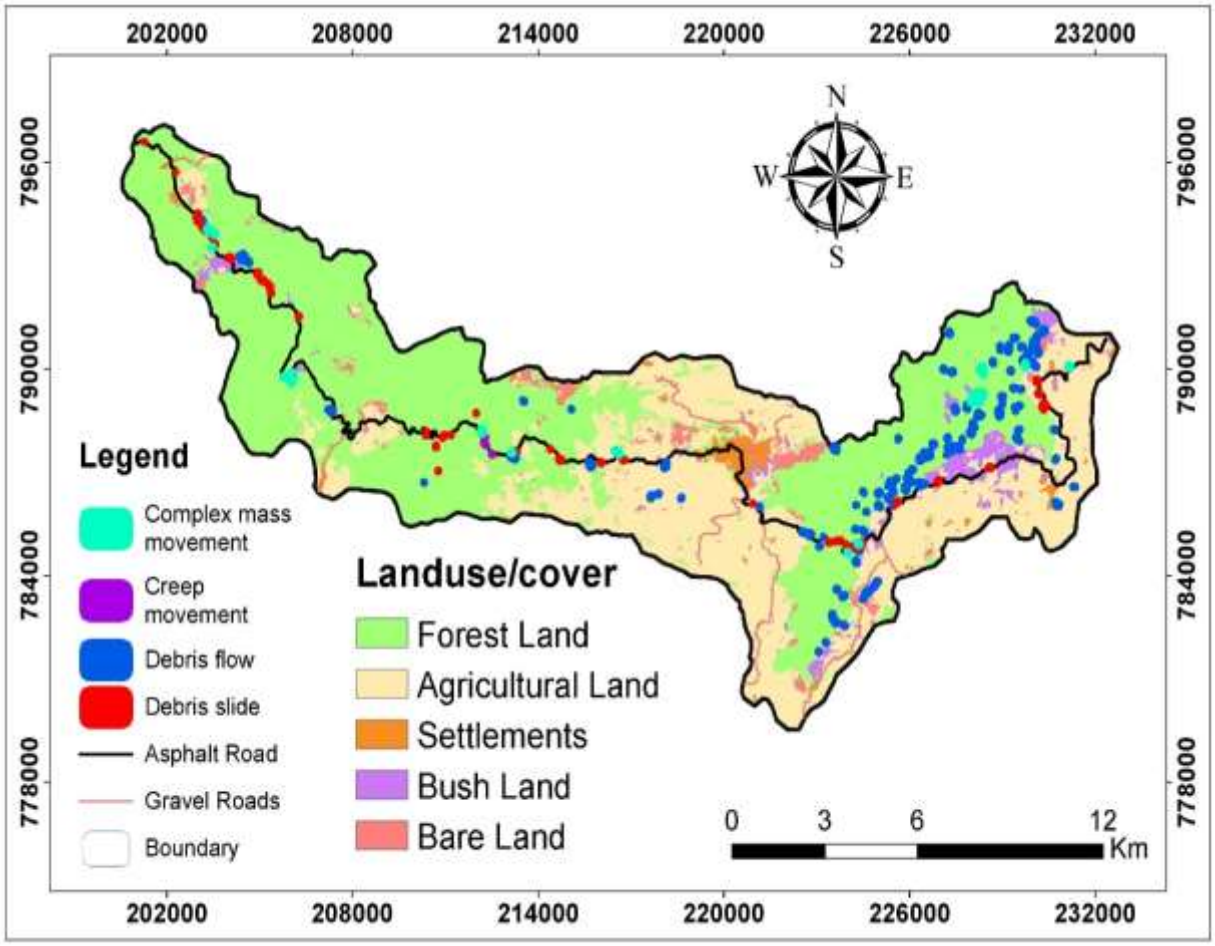

Figure 29: Causative factor map displaying Land Use Land Cover of the study area

5.3.8 PRECIPITATION

Precipitation is a major natural component that triggers landslides. Intense and continuous rainfall permeates into the ground, increasing pore water pressure and decreasing soil shear strength, ultimately causing slope failures (Dai et al., 2002).

Rainfall data of 24 years (2000-2024) were attained from four neighboring meteorological stations (Bonga, Felegeselam, Amaya, and Migra) to assess the geographical variability of rainfall and its relationship to landslide distribution. The equal interval method was used to create an interpolated rainfall map and classified into four categories. These classifications ranges from 1840 mm to over 2200 mm, with regions receiving more than 2100 mm of rainfall being more vulnerable to landslides due to increased saturation and decreased slope stability as shown Fig. 30.

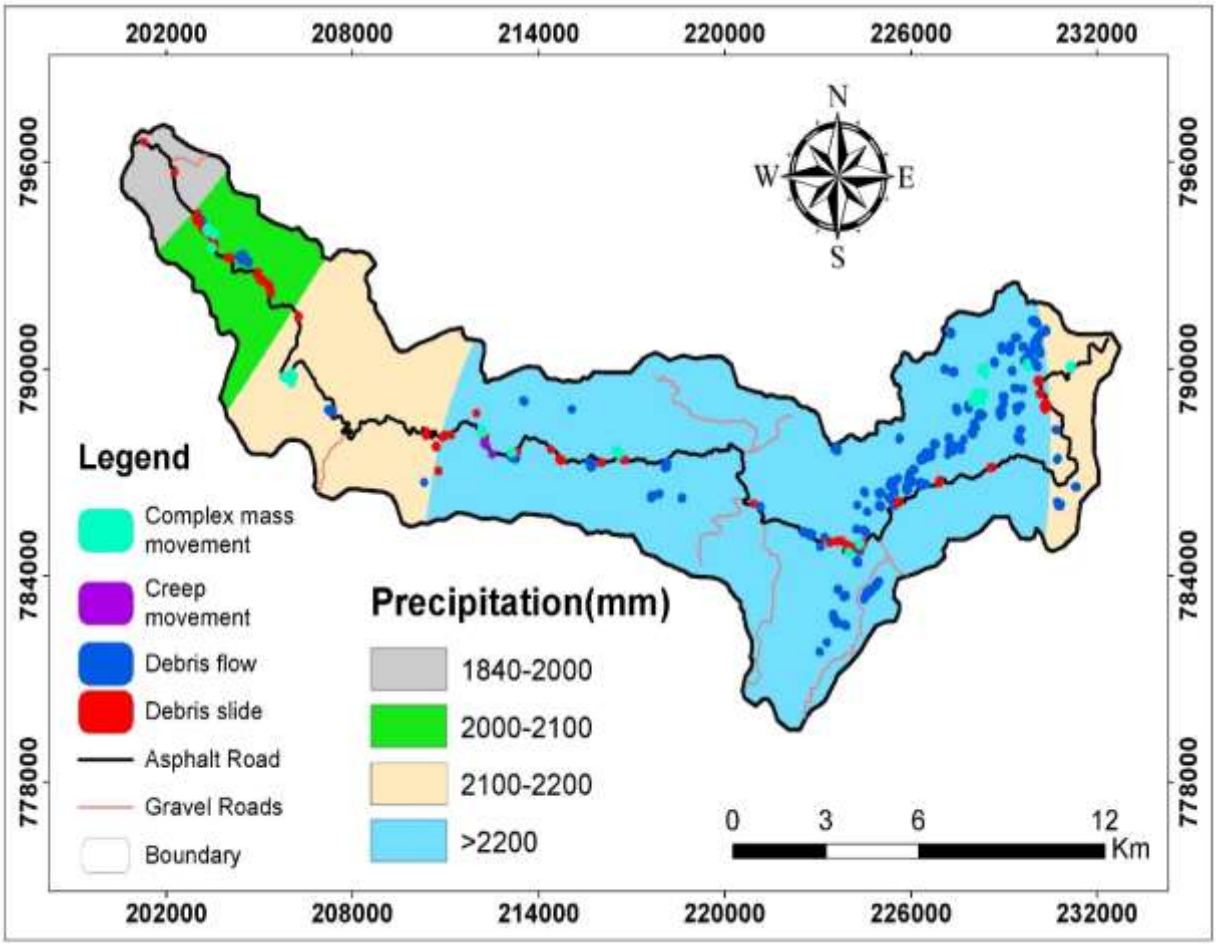

Figure 30: Causative factor map showing Precipitation of the study area

5.4 LANDSLIDE SUSCEPTIBILITY MAPPING

5.4.1 INFLUENCE OF THE CAUSATIVE FACTORS

Each subclass of the causative factors was given a frequency ratio (FR) and weight of evidence (WoE) value in order to evaluate their contribution to the incidence of landslides. Moreover, each subclass of landslide density was determined, and weights were assigned appropriately. Subclasses with FR > 1.0 and WoE > 0.1 are significantly related with landslides, whereas lower values show a weaker relationship, according to several research (e.g. Abay et al., 2019; Berhane et al., 2020; Kumar & Anbalagan, 2015; Lee & Pradhan, 2007) as shown in table (7) below.

Table 7: Calculation result of FR and WoE for factor classes

Parameter	Classes	Pixel Classes	Landslide Pixels	FR (b/a)	W+	W-	C
Slope (Deg.)	0^0-10^0	68446	165	0.41	-0.90	0.27	-1.17
	10^0-20^0	88456	410	0.61	-0.50	0.27	-0.77
	20^0-30^0	31850	352	1.79	0.60	-0.16	0.76
	30^0-45^0	11571	570	4.95	1.69	-0.28	1.97

Parameter	Classes	Pixel Classes	Landslide Pixels	FR (b/a)	W+	W-	C
	$>45^0$	765	37	6.06	1.92	-0.02	1.94
Aspect (deg.)	Flat (-1)	316	4	0.59	-0.53	0.00	-0.53
	N (337.5-22.5)	8509	83	1.06	0.06	0.00	0.06
	NE (22.5-67.5)	15198	107	1.03	0.03	0.00	0.03
	E (67.5-112.5)	19916	255	1.29	0.26	-0.03	0.29
	SE (112.5-157.5)	25813	421	2.08	0.75	-0.18	0.93
	S (157.5-202.5)	28827	220	1.57	0.47	-0.10	0.57
	SW (202.5-247.5)	27115	235	0.83	-0.19	0.03	-0.21
	W (247.5-292.5)	62539	121	0.30	-1.23	0.28	-1.52
	NW (292.5-337.5)	12855	88	0.83	-0.19	0.01	-0.21
Elevation (m)	<1800	30217	36	0.47	-0.76	0.09	-0.85
	1800-2100	47141	183	0.42	-0.88	0.16	-1.05
	2100-2500	61307	443	0.79	-0.24	0.09	-0.33
	2500-3000	16754	79	1.63	0.50	-0.06	0.56
	>3000	48748	793	1.94	0.68	-0.35	1.04
Lithology	Alluvial deposit	15653	38	0.53	-0.64	0.04	-0.68
	Colluvium deposit	7424	282	3.12	1.18	-0.09	1.27
	Basalt flow	17500	73	0.51	-0.69	0.05	-0.73
	Upper trachyte	94120	995	1.46	0.39	-0.51	0.90
	Middle trachyte	3193	4	1.18	0.17	0.00	0.17
	Lower trachyte	66265	142	0.34	-1.11	0.28	-1.39
LULC	Forest land	114973	1029	1.02	0.02	-0.02	0.04
	Agricultural land	72464	337	0.86	-0.15	0.08	-0.23
	Settlements	4908	2	0.52	-0.66	0.01	-0.67
	Bush land	6903	142	2.53	0.96	-0.06	1.02
	Barren land	4895	24	1.00	0.00	0.00	0.00
Distance to Road (m)	0-100	12213	304	4.46	1.57	-0.25	1.83
	100-200	11309	119	1.80	0.60	-0.05	0.65
	200-300	10970	44	1.35	0.31	-0.02	0.33
	300-400	10425	48	0.68	-0.39	0.02	-0.40
	400-500	10209	53	0.46	-0.79	0.03	-0.81
	500-600	9858	95	0.55	-0.61	0.02	-0.63
	>600	139143	871	0.70	-0.37	0.51	-0.88
Distance to streams (m)	0-50	23818	211	1.42	0.36	-0.06	0.42
	50-100	23074	177	1.18	0.17	-0.02	0.19
	100-200	41182	223	0.90	-0.11	0.03	-0.13
	200-300	33343	194	0.59	-0.53	0.08	-0.61
	300-400	25996	173	0.75	-0.29	0.04	-0.33
	400-500	12063	190	0.88	-0.13	0.01	-0.14
	>500	36351	366	1.34	0.30	-0.08	0.38
Precipitation (mm)	1840-2000	23818	211	0.67	-0.41	0.01	-0.42
	2000-2100	23074	177	0.84	-0.18	0.02	-0.20
	2100-2200	41182	223	0.78	-0.25	0.07	-0.31
	>22000	33343	194	1.12	0.11	-0.25	0.36

The frequency ratio for slope classes, 30-45° and >45° had the highest susceptibility, with values of 4.95 and 6.06, respectively. These classes had the highest WoE positive weights (W^+ = 1.689 and W^+ = 1.92, respectively), demonstrating a strong correlation with landslide pixels despite the limited coverage of slopes >45°. In comparison, moderate slopes (0-10°) have a FR of only 0.41 and a WoE of -0.90, indicating very low susceptibility. These findings are reliable with (Ayalew & Yamagishi, 2004; Lee & Pradhan, 2007), who revealed that steep slopes are greatly related with landslides due to higher shear stress, shallow soil depth, and water concentration on inclined planes.

The aspect classes of SE (112.5-157.5°) and E (67.5-112.5°) exhibit relatively more landslide susceptibility, with FR values of 2.08 and 1.29, and WoE contrast values of 0.75 and 0.26, respectively. These orientations are probably to receive more severe rainfall or sun radiation, which may degrade surface materials. In contrast, NW and W facing slopes have the lowest FR values (0.83 and 0.30, respectively) and negative WoE contrasts, indicating decreased susceptibility. Yalcin (2008) stated that similar aspect related tendencies, emphasizing that SE- and E-facing slopes in mountainous regions are more prone to failures caused by rainfall induced weathering and saturation.

The elevation class ranging from 2500-3000 m and >3000 m has FR values of 1.63 and 1.94, with WoE contrasts of 0.56 and 1.04, respectively. This could be due to the existence of loose colluvium soil or weathered rock in high elevation areas with rugged terrain. Lower elevation zones (<2100 m) have significantly lower FR values (0.42–0.79) and negative WoE contrasts (-0.85 to -1.05). These findings are consistent with those of (Abay & Barbieri, 2012; Regmi et al., 2010), who also showed greater landslide activity in elevated, geologically fractured terrains.

Based on the frequency ratio, the colluvial deposits have a very high value of 3.12 and WoE contrast of 1.27, indicating high landslide occurrence. Upper trachyte has a FR of 1.46 and WoE of 0.904, owed to its fractured and weathered condition. Lower trachyte and intermediate basalt, on the other hand, are less susceptible, with FR values of 0.34 and 0.51, respectively, indicating a stronger, more strong rock mass. Aleotti & Chowdhury (1999) and Guzzetti et al., (2006) obtained similar results, highlighting that loose materials and weathered volcanic rocks are among the most failure prone geological units.

Bush land is the most susceptible of the LULC classes, with a FR of 2.53 and WoE contrast of 1.020. This could be attributed to sparse root systems and inadequate surface binding. Agricultural land is moderately susceptible (FR = 0.86), but forest land is nearly neutral (FR = 1.02). This is because the forest land lies on colluvial deposits with steep terrain and contains

springs, which have led to the loss of vegetation roots. Settlement areas have a low FR (0.52), but caution is advised due to the short sample size. These patterns are consistent with (Berhane et al., 2020; Lee & Pradhan, 2007) findings, which revealed that removing vegetation cover increases landslide susceptibility, particularly in transitional zones such as bush or cleared land.

Distance to road is one of the most important causative factors for slope instability. The first 100 m class had a FR of 4.46 and WoE value of 1.827, suggesting that closeness to roadways significantly increases landslide hazard. This is most likely owing to cut and fill operations, slope undercutting, and concentrated runoff. Classes beyond 400 m had FRs < 1 and negative WoE values, indicating decreased hazard with distance. These results support findings by Lee & Talib (2005), who observed road cut failures are common triggers, especially in areas with steep topography and weak soil/rock interfaces.

Distance to stream revealed a moderate relationship. The closest class (0–100 m) had a FR of 1.42 and WoE of 0.419, indicating higher susceptibility due to toe erosion and increased soil saturation. Middle classes (100–400 m) had FR below 1 and negative WoE values, suggesting reduced influence. This agrees with studies by Dahal et al. (2008), which highlight that stream erosion and water saturation near channels promote slope failures. However, areas farther than 500 m again showed increased FR and WoE, due to steep slopes, weak soil/rock layers, and runoff accumulation that promote slope instability.

Higher precipitation correlates with increased susceptibility. The class >2200 mm has an FR of 1.12 and WoE of 0.362, indicating slightly elevated hazard. Other rainfall ranges show FR < 1, suggesting they contribute less to land sliding. According to Berhane et al., (2023); and Crozier & Glade, (2005), precipitation intensity and cumulative impacts are significant triggers in both shallow and deep-seated landslides.

Overall, slope, distance to road, lithology and land cover (especially bush land) were the most significant causative factors based on both FR and WoE results, consistent with previous studies (Berhane et al., 2023; Regmi et al., 2010).

5.4.2 FREQUENCY RATIO (FR)

To create the landslide susceptibility index (LSI), all conditioning factors and their respective weights derived from the frequency ratio (FR) method, were combined using raster calculator tool in the ArcGIS toolbox, as detailed in equation 2 (Section 3.4). Subsequently, the final products were examined. The landslide susceptibility map (LSM) was then created, and the output map values were classed into five susceptibility zones: very low, low, moderate, high,

and very high. The 180 km² research area is divided into five landslide susceptibility zones based on the generated LSM (Fig. 32): very Low (34.42% or 61.95 km²), low (27.53% or 49.56 km²), moderate (20.23% or 36.41 km²), high (9.92% or 17.86 km²), and very high (7.90% or 14.21 km²). The total area is made up of approximately 17.81% or 32.07 km2 of high and very high susceptibility zones.

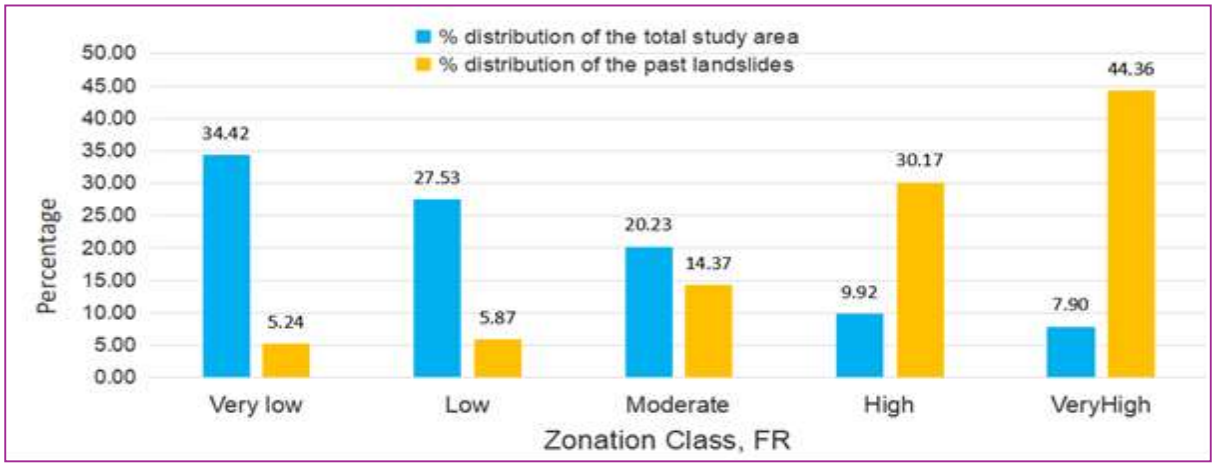

Figure 31: Percentages of areas that represent the different landslide susceptibility zones of the study area using FR

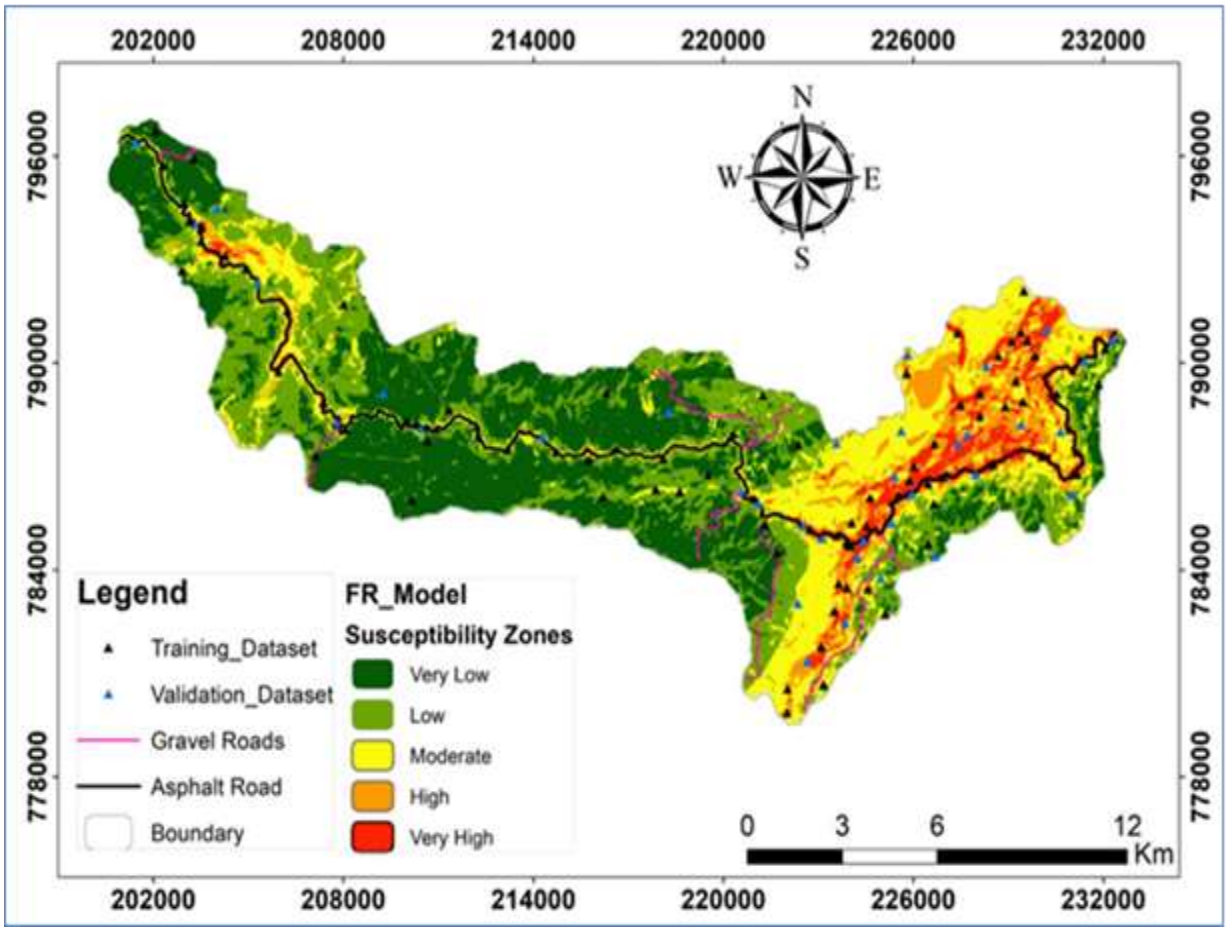

Figure 32: Landslide susceptibility mapping derived from RF method

5.4.3 WEIGHT OF EVIDENCE (WOE)

The landslide susceptibility index (LSI) raster was obtained by summing the WoE of the eight causative factors using equation (6). The values of the landslide susceptibility map using weight of Evidence were reclassified in to five zonation classes; very low, low, moderate, high, and very high. As can be noted from Fig. 34, below, the 180 km² study area is divided into five landslide susceptibility zones based on the generated LSM: very low (26.1% or 47.2 km²), low (28.1% or 50.9 km²), moderate (21.7% or 39.2 km²), high (14.9% or 27.0 km²), and very high (9.20% or 16.6 km²). The total study area comprises about 24.1% or 43.6 km² of high and very high susceptibility zones.

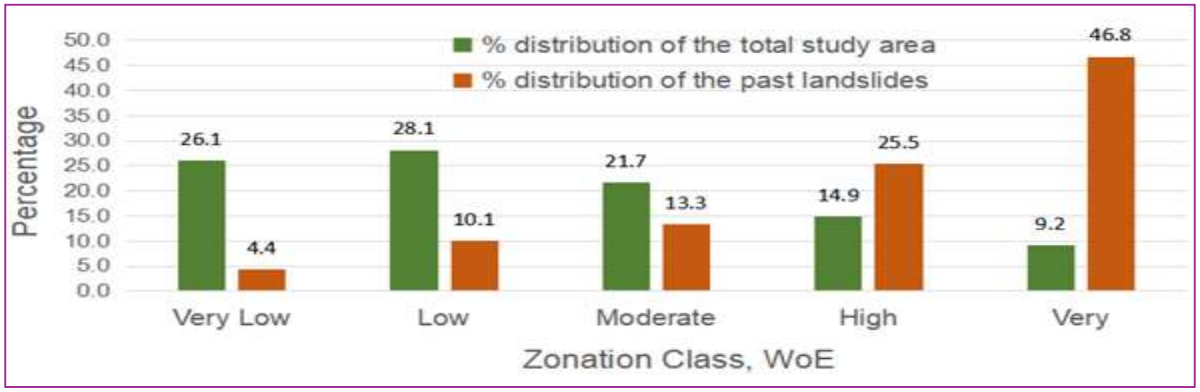

Figure 33: Percentages of areas that represent the different landslide susceptibility zones of the study area using WoE

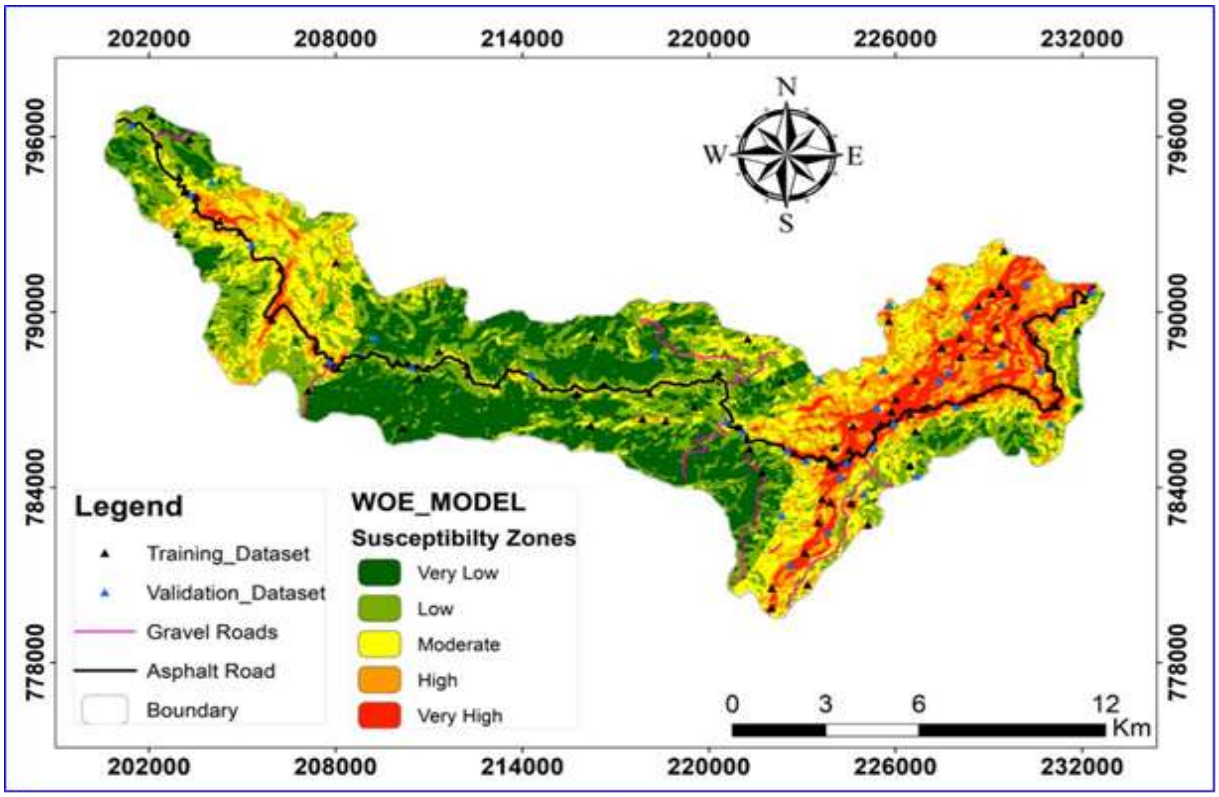

Figure 34: Landslide susceptibility mapping derived from WOE method

5.5 VALIDATION OF LSM

To ensure accuracy, landslide susceptibility models must be validated (Chung & Fabbri, 2003). The overlay approach and Receiver Operating Characteristic (ROC) curve with the Area Under the Curve (ROC-AUC) analysis were used to validate the map (Hosmer & Lemeshow, 2000). The first method used for validation of LSM was overlay method by superimposed the past landslide locations onto the final LSM map, based on the principle that past landslides predict future risks (Varnes, 1984). The LSM, produced using FR and WoE methods, was assessed by analyzing how well landslide locations fitted the susceptibility zones. For the model to be reliable, most landslides should fall in high or very high susceptibility zones. By overlaying past landslides on the LSM, we found FR had slightly better accuracy (74.53%) than WoE (72.26%) in identifying known landslides, as shown in the distribution across five susceptibility classes in the results tables (Table 8 & 9).

Table 8: Area coverage of past landslides on each susceptibility class using FR method

Landslide Susceptibility Class	Area (Km^2) of total study area	% distribution of the total study area	Area (km^2) of past landslides	% distribution of the past landslides
Very low	61.95	34.42	0.31	5.24
Low	49.56	27.53	0.34	5.87
Moderate	36.41	20.23	0.84	14.37
High	17.86	9.92	1.76	30.17
Very High	14.21	7.90	2.59	44.36

Table 9: Area coverage of past landslides on each susceptibility class using WoE method

Landslide Susceptibility Class	Area (Km^2) of total study area	% Distribution of the total study area	Area (km^2) of past landslides	% Distribution of the past landslides
Very Low	47.2	26.09	0.26	4.41
Low	50.9	28.15	0.59	10.07
Moderate	39.2	21.68	0.77	13.26
High	27.0	14.92	1.49	25.47
Very High	16.6	9.15	2.73	46.79

AUC is the second validation method which involved comparing the predicted landslide susceptibility zones (LSZ) with the 30% landslide locations. The AUC quantifies the models ability to predict landslide occurrence, with values close to 1.0 indicating high accuracy, and values near 0.5 reflecting random performance (W. Chen et al., 2018). Sewts (2016) further categorized AUC values: weak (0.5–0.6), moderate (0.6–0.7), good (0.7–0.8), very good (0.8–0.9), and excellent (0.9–1.0). Using the ArcGIS environment and the ARCSDM tool with a Monte Carlo simulation of 10,000 iterations, both the Frequency Ratio (FR) and Weight of

Evidence (WoE) models were evaluated. The results showed the FR model outperformed the WoE model, achieving an accuracy of 80.6%, slightly surpassing the WoE model's accuracy of 79.1% (Fig. 35). This confirms the strong predictive power of both models for landslide susceptibility.

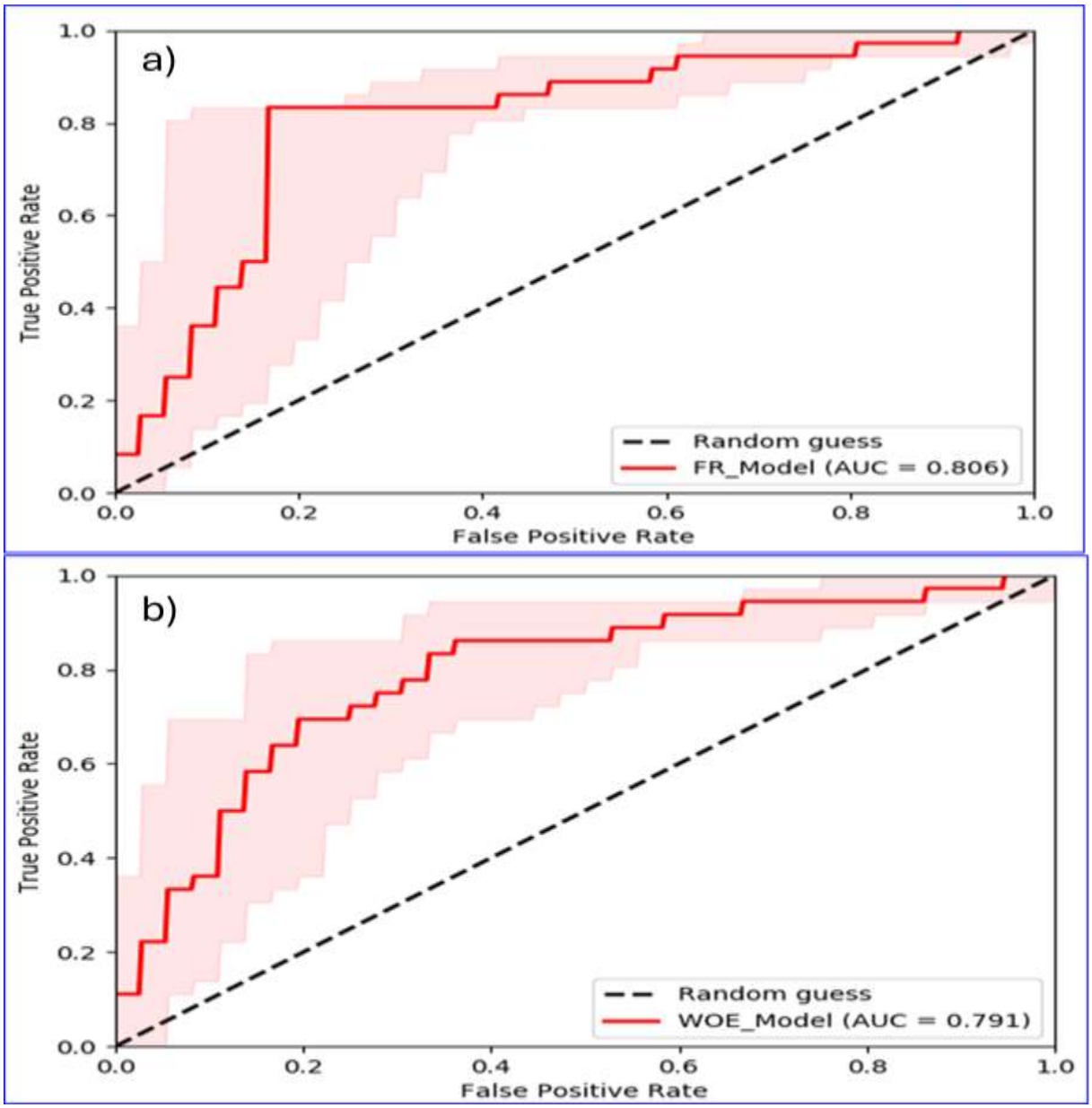

Figure 35: AUC success rate curve for FR model (a), and for WoE model (b)

5.6 ENGINEERING PROPERTIES OF SOILS AND ROCKS

5.6.1 ENGINEERING PROPERTIES OF SOILS

5.6.1.1 PHYSICAL PROPERTIES OF SOILS

Natural moisture content, atterberg limits, grain size distribution, and soil classification tests were tested on eight landslide failed sections specifically from the susceptibility mapping

(moderate, high and very high-hazard zones). As can be seen in table 10, the natural moisture content of these soils varies from 20.90% to 48.0%, liquid limits range from 46.0 - 58.0%, and plasticity indices fluctuated from 16.0 - 25.25%. According to the Unified Soil Classification System (USCS, ASTM D2487), soils are classed as CH, CL, MH, and ML, designating highly plastic clays, low plasticity clays, and highly and low plastic silts.

Table 10: Gradation, atterberg limits and NMC of soils derived from failed sections

ID	Co-ordinates [WGS84 / UTM Zone 37N]		NMC AASHTO (T-265)	Gradation (AASHTO T-88)				Atterberg Limits (%)		USCS, (ASTM -D2487)
	Eating, m	Northing, m		4.75	2.00	0.425	0.075	LL	PI	
PS-01	203277	794048	37.0	99.0	97.0	96.0	94.4	51.0	25.0	CH
PS-02	205327	792339	38.00	94.0	92.0	90.0	86.0	53.0	31.0	CH
PS-03	212269	787808	42.00	100.0	99.0	96.0	93.0	46.0	24.0	CL
PS-04	223999	784744	22.75	84.0	74.0	72.0	60.0	35.5	16.0	CL
PS-05	224381	784908	45.00	93.0	92.0	90.0	78.0	47.0	22.0	CL
PS-06	226919	786767	26.45	93.00	90.0	88.00	83.00	51.0	18.0	MH
PS-07	231268	787342	20.90	100.0	97.0	46.0	38.0	53.0	23.0	MH
PS-08	230324	789039	36.60	97.0	96.0	94.0	93.0	46.0	18.0	ML

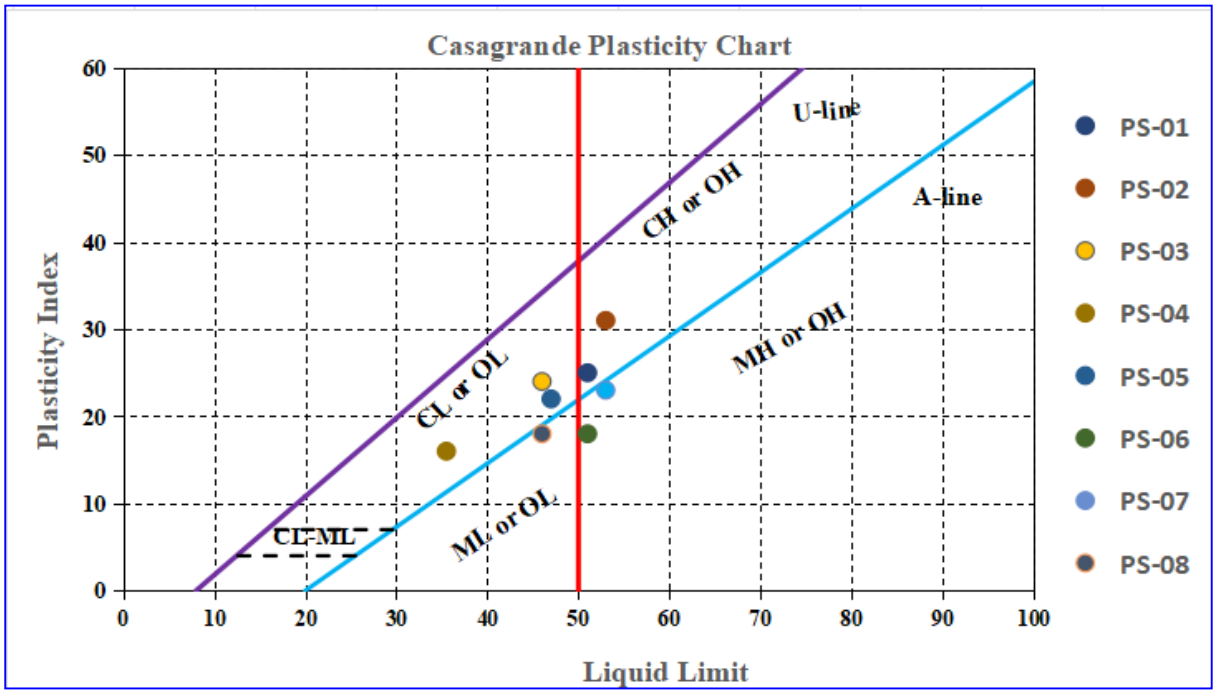

Figure 36: Plasticity chart of soil samples (PS = sample code) from the study area

5.6.1.2 SHEAR STRENGTH PROPERTIES OF SOILS

To determine the shear strength of the soils, direct shear tests were carried out on eight selected samples. In-situ field density tests, performed using the sand cone replacement method, revealed dry unit weights ranging from 15.0 kN/m³ (PS-01) to 19.0 kN/m³ (PS-08) and bulk

unit weights from 17.30 kN/m³ (PS-01) to 20.0 kN/m³ (PS-01). These variations suppose different levels of soil compaction, with lower values (e.g., PS-02) indicating loose soils potentially more susceptible to shear failure. Direct shear tests (ASTM T-236) showed cohesion (C) values ranging from 5.0 kN/m² (PS-07, PS-08) to 38.0 kN/m² (PS-06), and angle of internal friction (Φ) from 5.0° (M2) to 30° (PS-08). Particularly, PS-02 (C = 32.0 kN/m², Φ = 12.0°) and PS-08 (C = 5.0 kN/m², Φ = 30°) display varying shear strength parameters, suggesting differences in resistance to shear forces.

The failure mechanisms in these sections are likely influenced by the combination of variable soil compaction (low dry unit weight) and reduced shear strength, which, under increased pore water pressure from rainfall, may lower effective stress and trigger landslides along the slope.

Table 11: Results of dry, bulk density and shear strength soil tests

Sample ID	Co-ordinates [WGS84 / UTM Zone 37N]		Unit Weight (KN/m3)		Direct shear Test (ASTM T-236)	
	Eating, m	Northing, m	Dry	Bulk	C	Ø
PS-01	203278	794049	16.1	17.30	12.0	6.0
PS-02	205327	792340	15.0	18.90	32.0	12.0
PS-03	212270	787809	16.2	18.33	30.0	5.0
PS-04	224000	784745	16.1	18.75	34.0	9.0
PS-05	224382	784909	15.8	18.80	38.0	13.0
PS-06	226919	786768	16.8	17.0	5.0	30.0
PS-07	231269	787343	15.6	17.0	12.0	25.0
PS-08	230324	789039	19.0	20.0	5.0	30.0

5.6.2 ENGINEERING PROPERTIES OF ROCKS

Most of the slope cuts composed of residual and colluvial soils with few rock exposures. The exposed rocks were characterized by varying degree of weathering and occasionally intercalated with soil layers. As a result, most landslides were rotational failures confined to the soil with slip surfaces in the contact of the soil and rock and suggesting no movement occurred within the underlying rock, and rock falls/slides were rare along the cut sections.

5.6.3 SOIL AND ROCK INTERACTION WITH LANDSLIDES

The interaction between the soil and bedrock properties highlights the complex mechanisms driving landslides along the Bonga - Felegeselam road. The fine grained, highly plastic soils with high moisture content and low shear strength were the primary contributors to failure, as they could not withstand the driving forces of gravity and water pressure during rainfall. The shallow failure plane indicate that surface water infiltration was a key trigger, likely exacerbated

by seasonal rainfall patterns. The underlying trachytic and basaltic rock bed formations provided a relatively stable foundation. This suggests that both the soil and bedrock properties must be considered in designing mitigation measures, such as improved drainage systems, slope reinforcement, and the use of retaining structures to enhance stability.

5.7 LIMIT EQUILIBRIUM (LE) METHOD

This section presents a detailed the limit equilibrium-based slope stability analysis of eight cut slope failure locations based on landslide susceptibility mapping using the FR and WOE models, with hazard zones ranging from very low to very high.

5.7.1 FIELD INVENTORY

Landslide sections were selected based on the locations of slope failures in the field and their classification on the landslide susceptibility maps along the road corridor. The selection attempted to include a reasonable combination of sites across the moderate, high, and very high-hazard zones, ensuring that all hazard levels with actual failures were included (Table 12).

Table 12: Summary of the selected failed slope sections on hazard zones

Hazard zone	**No. of sections**	**Slope ID**	**Chainage, Km**	**Coordinates (WGS84 / UTM Zone 37N)**		**GWL, m (BH Log, 2019)**
				Easting, m	**Northing, m**	
Moderate	2	M1	Km20+510	205327.42	792339.80	3.3
		M2	Km35+220	212269.74	787808.74	6.0
High	2	H1	Km17+160	203277.84	203277.84	9.0
		H2	Km63+400	794048.51	794048.51	7.5
Very High	4	VH1	Km52+200	223999.55	223999.55	11.0
		VH2	Km53+160	784744.73	784744.73	5.0
		VH3	Km57+600	224381.54	224381.54	3.0
		VH4	Km65+620	784908.60	784908.60	0.8
Note: M-Moderate, V-High, VH-Very High Hazard, GWL-Ground Water Level, BH- Borehole						

As can be seen from the above table, two failures (M1, M2) have selected from the medium-hazard zone, two (H1, H2) in the high-hazard zone, and four (VH1, VH2, VH3, VH4) in the very high hazard zone. Areas designated as very low or low hazard were excluded since no failures occurred (Fig.37-38).

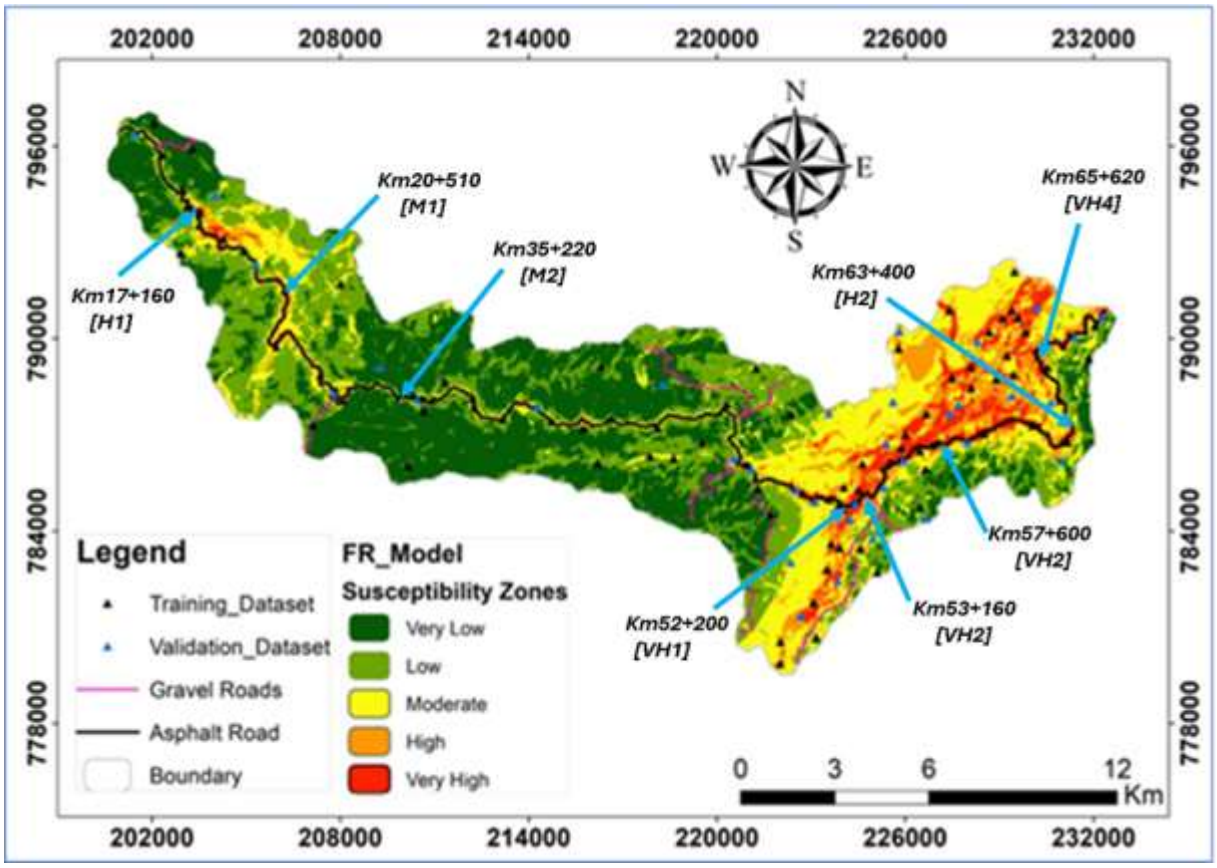

Figure 37: The eight selected failed slope sections on FR map susceptibility zones

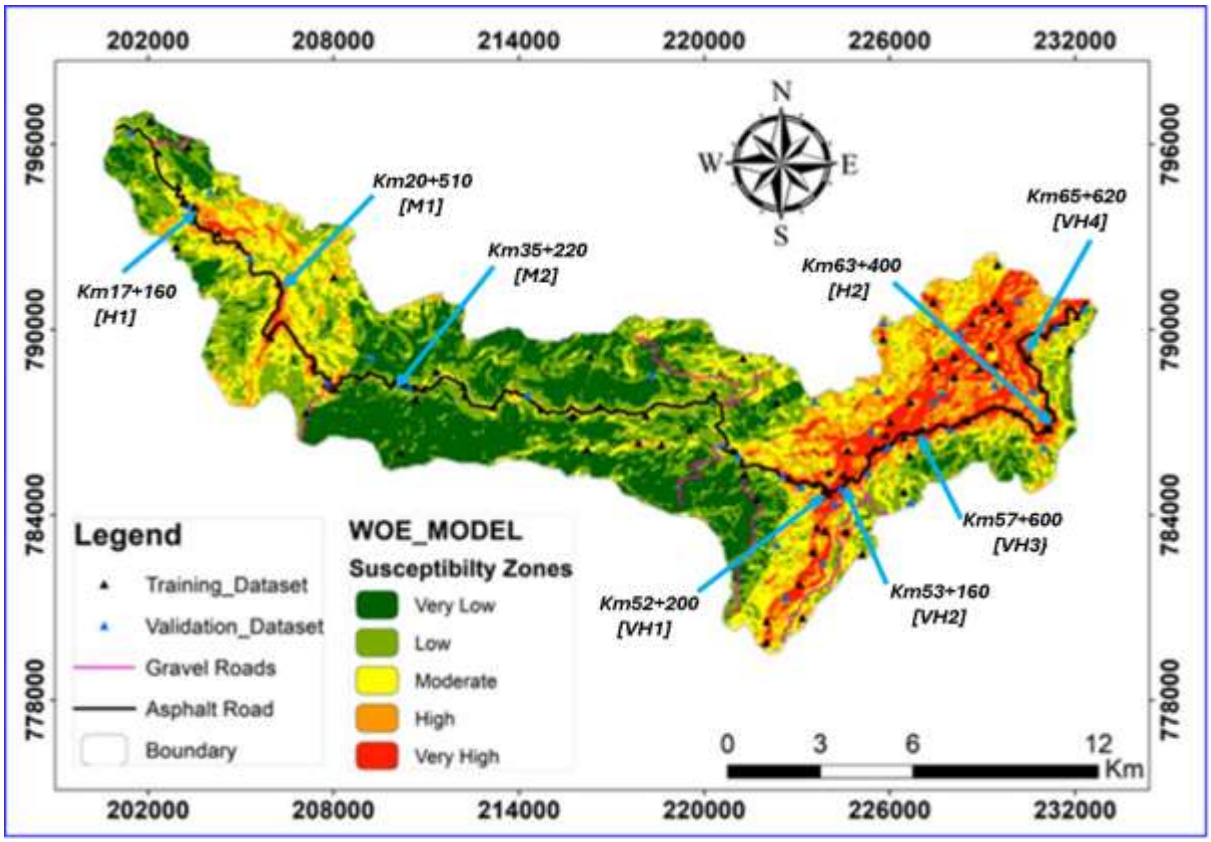

Figure 38: The eight selected failed slope sections on WoE map susceptibility zones

5.7.1.1 MODERATE HAZARD ZONE

M1 (Km 20+510):

As can be seen in fig. 39, this section is covered by dense vegetation, and spring waters which indicates that shallow groundwater is discharging near the surface, possibly contributing to soil saturation during rainy season. According to CWCE (2019) drilling data, shallow groundwater table is encountered at 3.3m depth. A retaining wall that was previously constructed along the slide section over the colluvium deposit has collapsed, and visible outward bulging of the road shoulder shows that movement is still occurring. The failure is mainly due low shear strength of the colluvial soil when saturated, which is exacerbated by inadequate slope drainage and a lack of proper toe support.

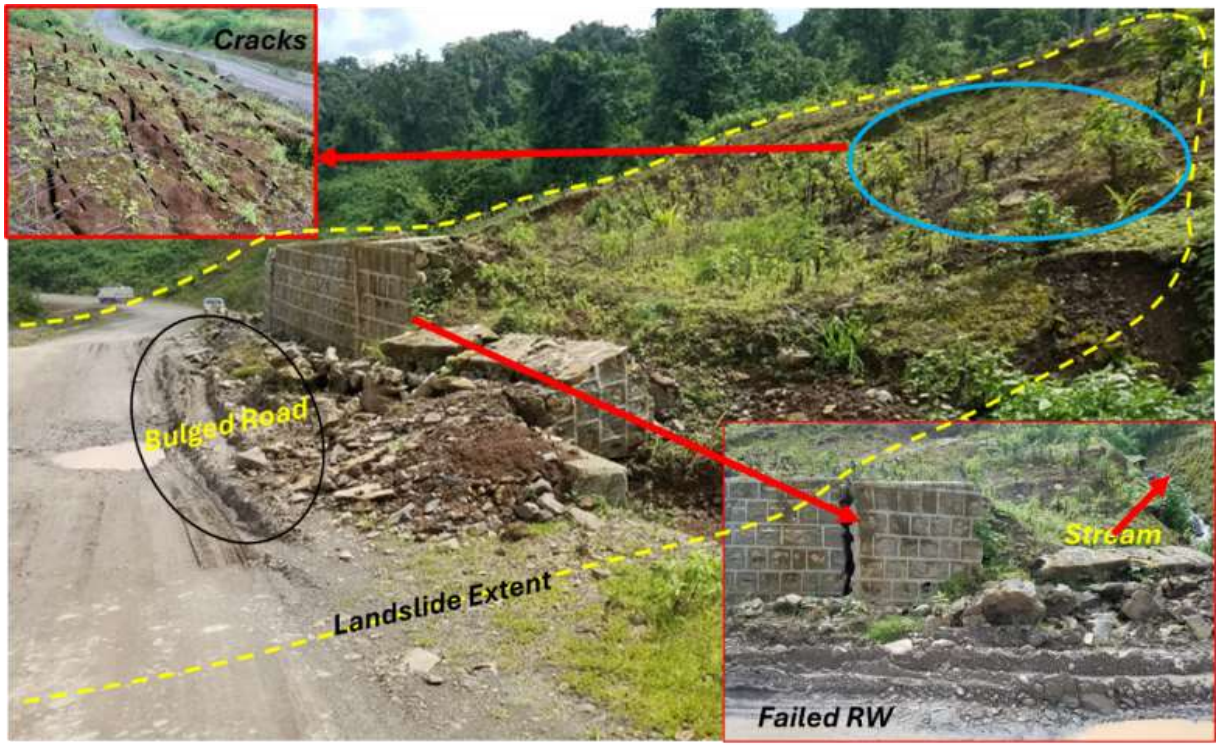

Figure 39: Photo showing failed retaining wall, tension cracks, and bulged road along M1 at Km 20+470, illustrating structural failure and ground deformation (Photo taken in August 2021).

M2 (Km 35+220):

Ground cracking has occurred along this section. The cracks moving parallel to the asphalt road. The ground has a typically gentle slope (Fig. 40). The cracking observed on the left side of the road facing to south, where an 8.0 high embankment founded on top of soft clay and decomposed rock. Differential settlement along the pavement, with surface depressions up to 20 cm deep, is an indicator of slope instability. These deformations are most often caused by poor compaction, water infiltration, or delayed settlement, which results in consolidation or

collapse of the fill material beneath. The fissures and uneven surface create recurring safety issues for road users.

Figure 40: Asphalt settlement over high fill section with longitudinal cracks along M2 at Km 35+220, indicating pavement distress (Photo taken in August 2021).

5.7.1.2 HIGH HAZARD ZONE

H1 (Km 17+160):

This section has a rotational landslide with a concave profile. The main scarp begins about 130m upslope to the left of the road centerline and continues about 65m downslope on the right side past the road toe. The landslide damaged a section of the road measuring 100m. Scarps, shifting soil blocks, toe bulging, and numerous tension cracks near the crest are all visible signs of continued movement in the failed material (Fig. 41). According to CWCE (2019) borehole data, the groundwater table is encountered at 9.0m. Runoff water from above crossing drainage structure directly discharged to the failure mass, contributing to high porewater pressures.

H2 (Km 63+400):

This failure occurred above the road on a very steep (~36°) slope underlain by light to dark brown silty clay over decomposed rock. The landslide stretches for 250m and it is a typical rotational type with a curved slip surface, tension cracks extending upslope, and evidence of active water seepage. Slope saturation and toe slumping suggest high pore pressures within the upper soil horizon. Borehole data indicates the groundwater table at 7.5 m depth (CORE, 2019), consistent with observed saturation indicators. The failed benching system highlights the

inadequacy of current mitigation efforts. The mechanism is dominantly rainfall induced, with subsurface water flow weakening the silty clay matrix over time.

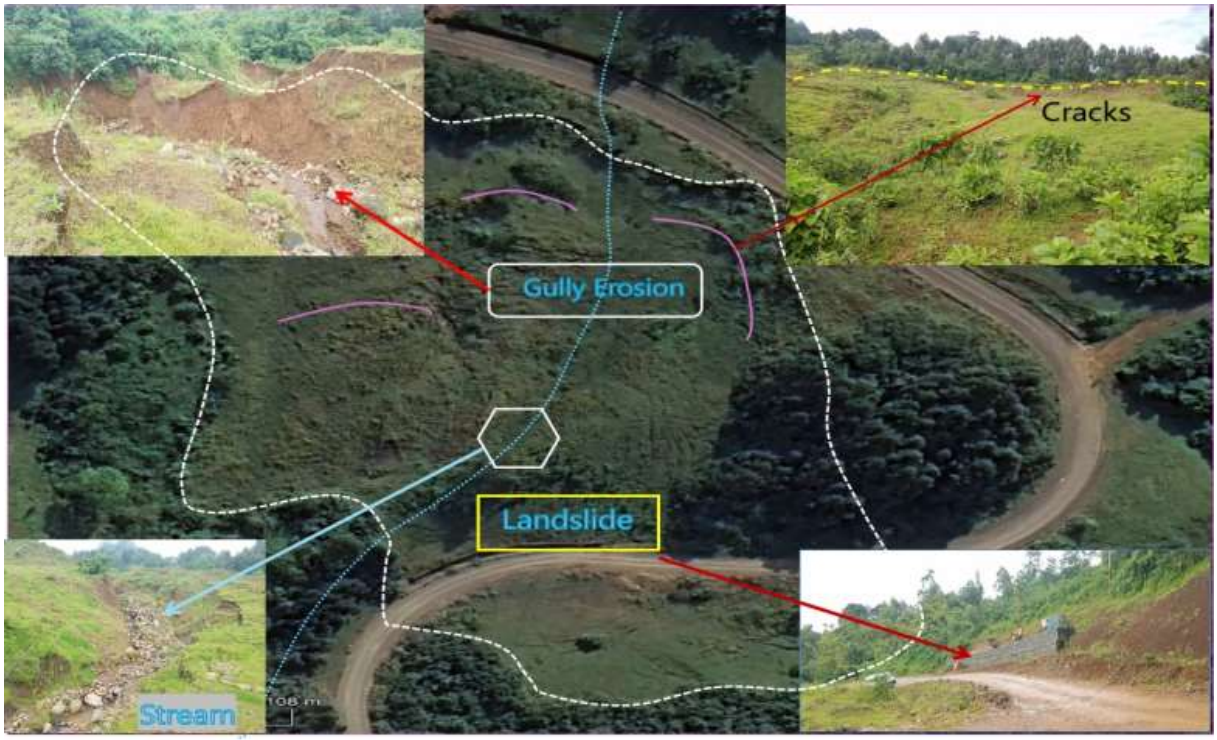

Figure 41: Rotational slope failure with deep gully erosion and cracks along H1 at Km 17+140, demonstrating significant slope instability (Photo taken in August 2021).

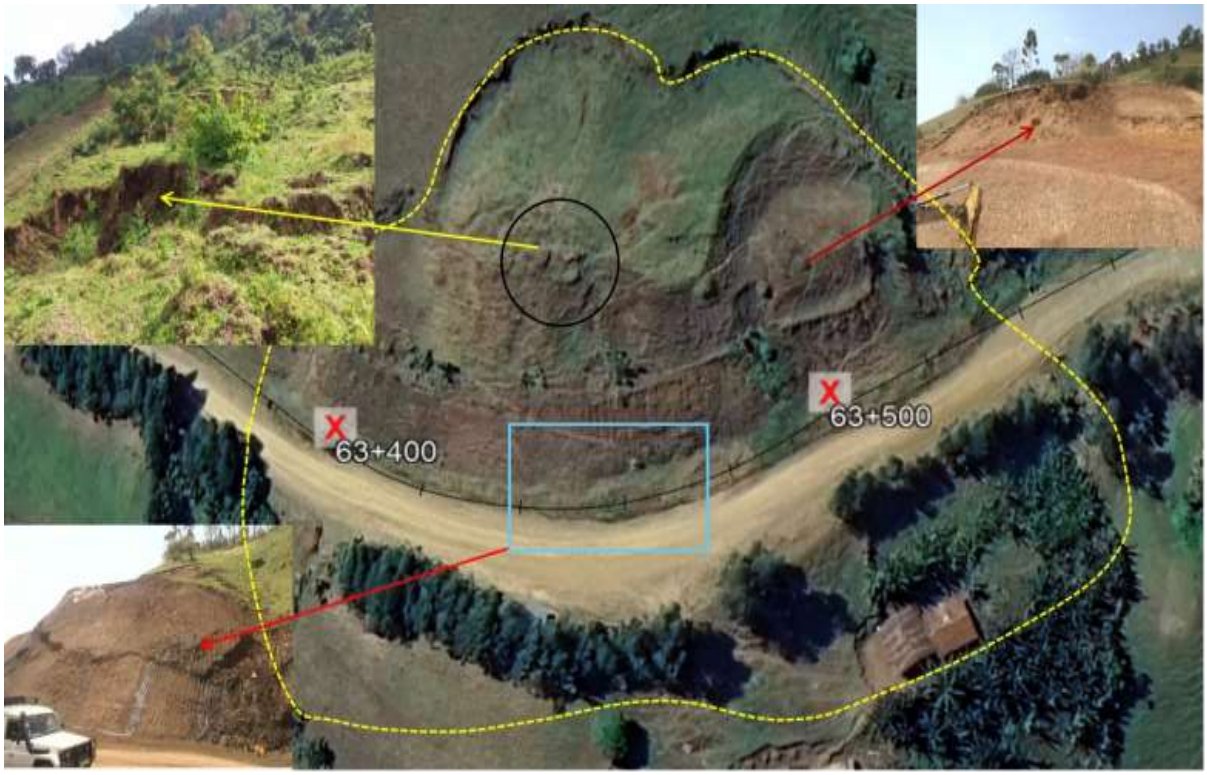

Figure 42: Slope failure with springs and cracks along H2 at Km 63+400, overlaid on a Google Earth image, showing water-induced instability (Photo taken in August 2021).

5.7.1.3 VERY HIGH-HAZARD ZONE

VH1 (Km 52+200):

This section situated on a rugged mountaintop top with steep slopes (30°–40°), densely vegetated. The failure was with in the top thick grayish brown sandy clay mixed with gravel. The landslide extends 200m along the road, with the main scarp located 30m to the left hand side and ranging 100m down the slope on the right hand side (Fig. 43). On the crown detachment occurred at ~3.0 m depth, with numerous tension cracks and seeps on the slope face. Borehole logs (CWCE, 2019) showed a water table at 11.0 m, with a highly fractured zone extending from 8 to 15 m and bedrock at ~20 m. A long active crack opening (30cm opening with 1.0m vertical detachment) were observed along the main road. The failure is attributed to lose slope material, subsurface flow, uncontrolled runoff, and absence of proper cut benching all contributing to reduced shear strength and increased driving forces.

Figure 43: Slope failure with big open cracks on top scarp and springs at slope toe along VH1 at Km 52+200, indicating active landslide with current traffic inaccessibility (Photo taken in August 2021).

VH2 (Km 53+160):

This is a large debris flow characterized by a complex rotational movement combined with debris and mud flow elements. In 2016, the mudflow traveled over 200m downslope from the road, causing severe damage to farmland, settlements and resulting in significant loss of life and property. The slope is 30.0m high, with a scarp located 90.0m behind the road centerline and extending 100.0m below the road (Fig. 44). The landslide affected a 100.0m stretch along the road. The surficial soil is composed of silty to sandy clay with gravel (colluvium),

transitioning to weathered volcanic rock. High moisture content, groundwater at 5.0 m (CWCE, 2019), and historical tension cracking triggered a progressive failure culminating in a rapid debris flow. The failure is related to improper excavation at the toe, insufficient drainage, and weak upper soil layers.

Figure 44: Old debris flow overflowing and cracks on the main scarp along VH2 at Km 53+180, with current road blockage due to active landslide (Photo taken in August, 2021).

VH3 (Km 57+600):

The landslide occurred upslope of the road, extending 200m along the road, with a back extension of 80.0m reaching up to the main scarp on the left-hand side above the road. It experienced a translational failure within a layer of brownish silty clay over decomposed rock (Fig. 45). The slope material is weakly consolidated and highly moisture sensitive and prone to erosion. Field evidence includes water seepage, planar joint sets with unfavorable dip direction, and a nearby stream on the LHS contributing to saturation. Active debris flow scars were observed downslope. Groundwater was recorded at 3.0 m CORE (2019), elevated pore pressure, and excavation at the toe are all contributing to the instability. The slope shows characteristics of shallow translational movement with potential to develop into deeper failures under prolonged wet conditions.

VH4 (Km 65+620):

This section is characterized by a compound landslide involving both rotational and translational movements across a steep hillslope (15°–25°). It stretches along the road for approximately 500.0m, featuring intermittent failure zones. Deep gully erosion including the road (~10 m) on the RHS and adjacent river-induced toe erosion are key triggers (Fig. 46). The

soil mass comprises grayish-brown silty clay mixed with gravel (talus). Borehole data (CORE, 2019) revealed a shallow groundwater table at 0.8 m, making the slope highly susceptible to saturation during rainfall. The failure progressed across the carriageway, highlighting the synergistic effect of intense surface runoff, erodible slope material, and poor drainage design.

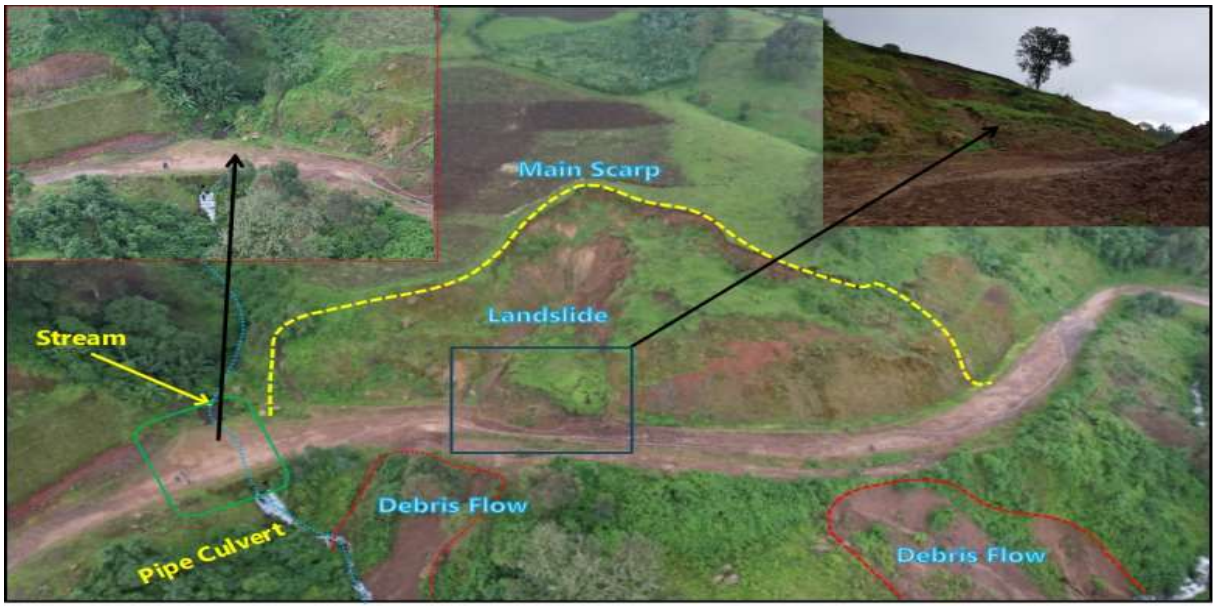

Figure 45: Rotational slope failure with tension cracks, several active minor scarps, and spring along VH3 at Km 57+600, indicating ongoing instability (Photo taken in August 2021).

Figure 46: Soil erosion on the face of the back slope and scouring due to roadside erosion and streams along VH4 at Km 65+620, showing significant surface degradation (Photo taken in August 2021).

5.7.2 INPUT PARAMETERS

Slope stability assessments were carried out once the geometry and material parameters of each unstable slope cut sections had been specified. In doing so, the geometrical characterization of

the landslide failed sections is based on surveying data that show both the present geometry and the design geometrical cuts. Trial pits were dug on top of each failed slope sections (0.50 to 1.0m) and soil samples were collected for laboratory investigation. The detailed subsurface soil profile and groundwater condition configurations for each section are also collected via laboratory test results and subsurface explorations CWCE and Core (2019). The geotechnical material layers provided in the slope stability analysis were identified using a combination of field observations and lab test findings (Tab. 13). The soil profiles were properly overlaid to match field conditions.

Table 13: Input parameters used for slope stability analysis of each hazard zones

ID.	Soil Type & Layer Thickness (m)	Soil Properties				Slope Profile	
		γ_d (kN/m^3)	γ_S (kN/m^3)	C, (kN/m^2)	Φ, (°)	Slope Angle (°)	Cut Height (m)
M1, Km20+510	L1: Lean CLAY - 7.0m	16.8	18.90	32	12	45	11.4
	L2: Fat CLAY – 2.0m	17.5	17.98	34	20		
	L3: Weathered Rock-11m	18.5	27.0	UCS – 5 MPa			
`M2, Km35+220	L1: Embankment Fill-4m	17.20	18.00	30	5	34	7.9
	L2: Lean CLAY-6m	17.50	18.33	20	5		
	L3: Decomposed Rock-9m	18.00	18.75	41	52		
H1, Km17+160	L1: Fat CLAY-8m	15.9	17.30	12	5	34	5.6
	L2: Lean CLAY-2m	16.5	17.18	37	11		
	L3: Weathered Rock-4m	17.8	28.00	UCS – 50 MPa			
H2, Km63+400	L1: Silty CLAY – 4.0m	16.2	17.0	12	25	45	21.5
	L2: Decomposed Rock- 8.0m	16.5	18.0	5	40		
	L3: Weathered Rock- 4.0m	23.0	27.0	UCS-34MPa			
	L4: Decomposed rock-14m	19.0	20.0	UCS-5MPa			
VH1, Km52+200	L1: Lean CLAY- 6.5m	14.5	18.75	34	9	45	16.5
	L2: Clayey SAND-8.5m	15.8	18.45	25	12		
	L3: Decomposed Rock-4.0m	16.5	18.43	36	53		
VH2, Km53+160	L1: Lean CLAY-5.0m	17.80	18.80	38	13	45	31.5
	L2: Sandy CLAY-13.0m	17.80	18.80	42	18		
	L3: Decomposed Rock-12m	21.0	23.0	UCS – 5 MPa			
VH3, Km57+600	L1: Silty CLAY-7.5m	16.5	17.0	5	30	45	21.5
	L2: Decomposed Rock-4.5m	19.2	20.0	70	5		
	L3: Weathered rock-8.0m	22.0	23.5	UCS-8.3MPa			
VH4, Km65+620	L1: Weathered Rock-13.0m	18.9	20.0	UCS-5MPa		53	48.9
	L2: Fresh Rock-7.0m	18.8	20.0	UCS-5MPa			
	L3: Colluvium Soil	17.0	18.0	5	30		

Table 14: Cross-sectional view of slope geometry for each failed section, derived from survey data.

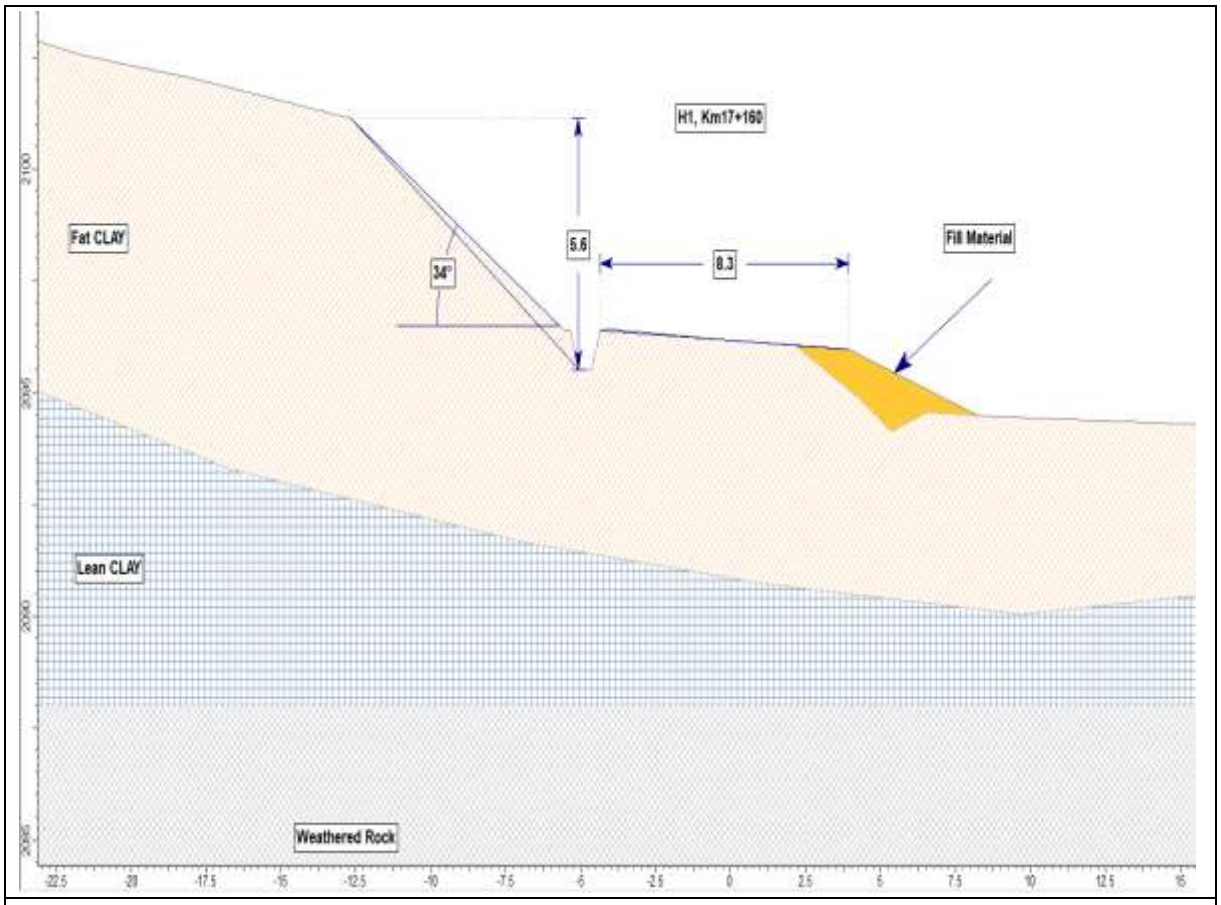

Slope profile at H1, Km17+160

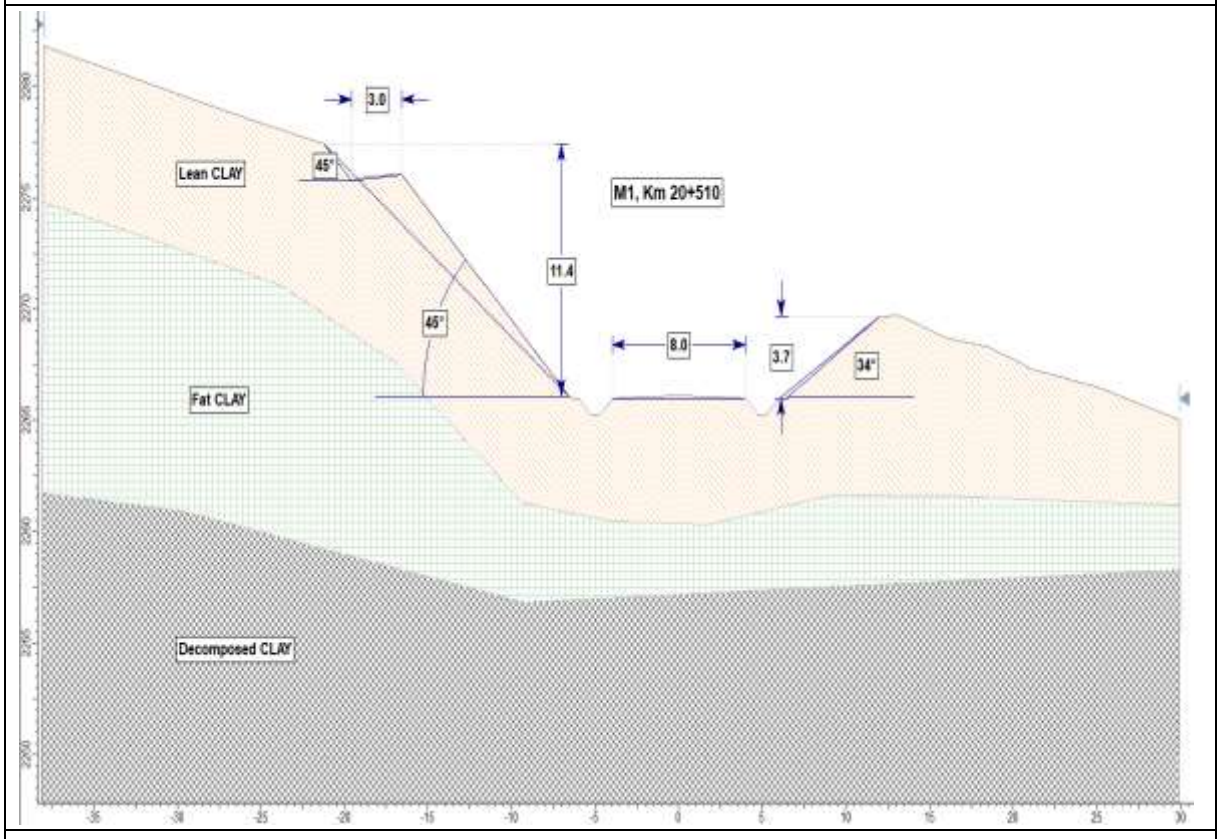

Slope profile at M1, Km20+510

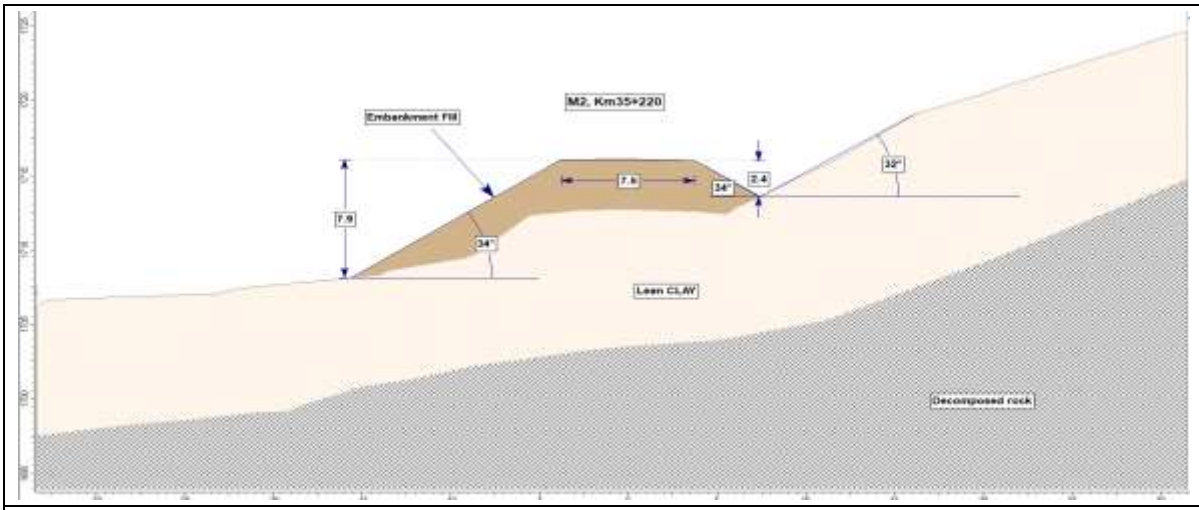

Slope profile at M2, Km35+220

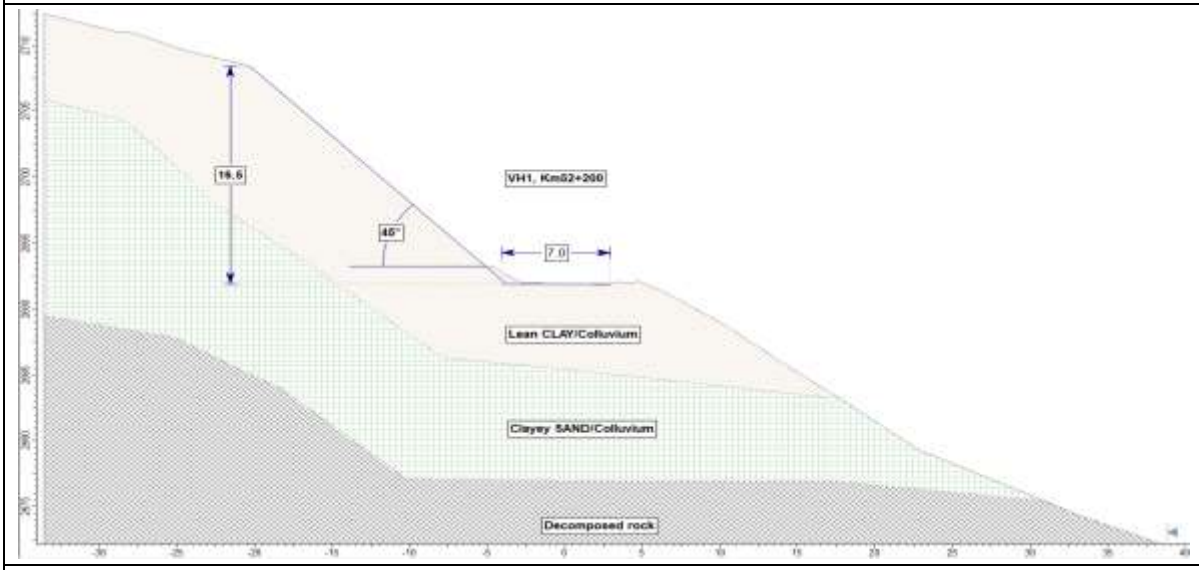

Slope profile at VH1, Km52+200

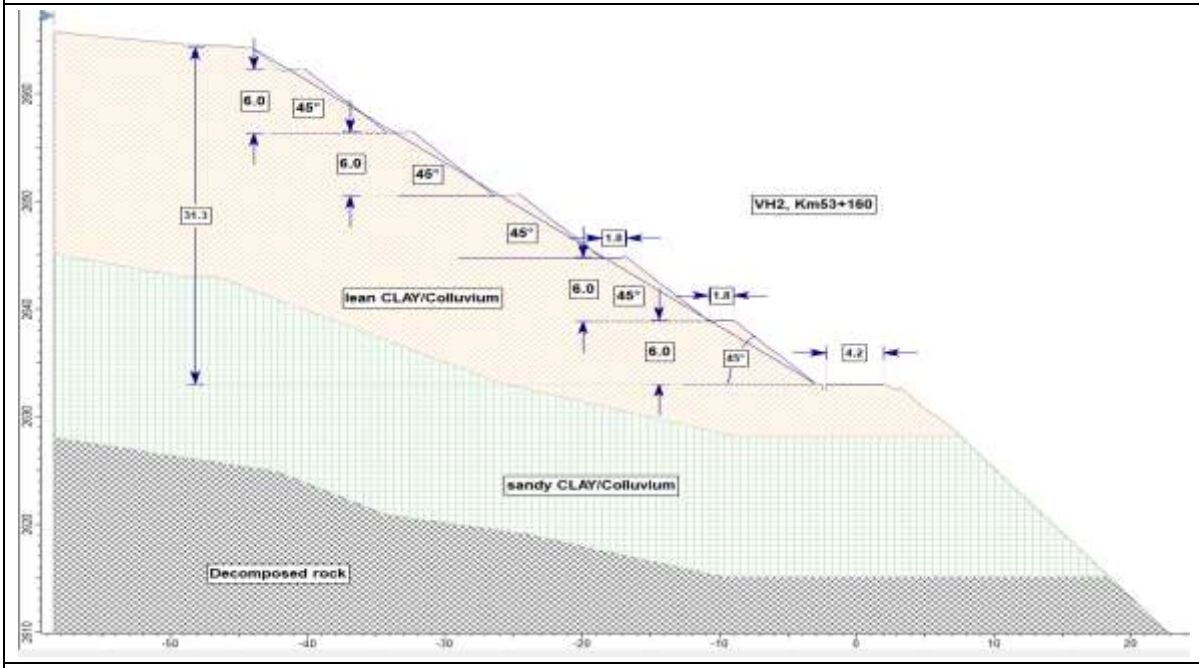

Slope Profile at HV2, Km53+160

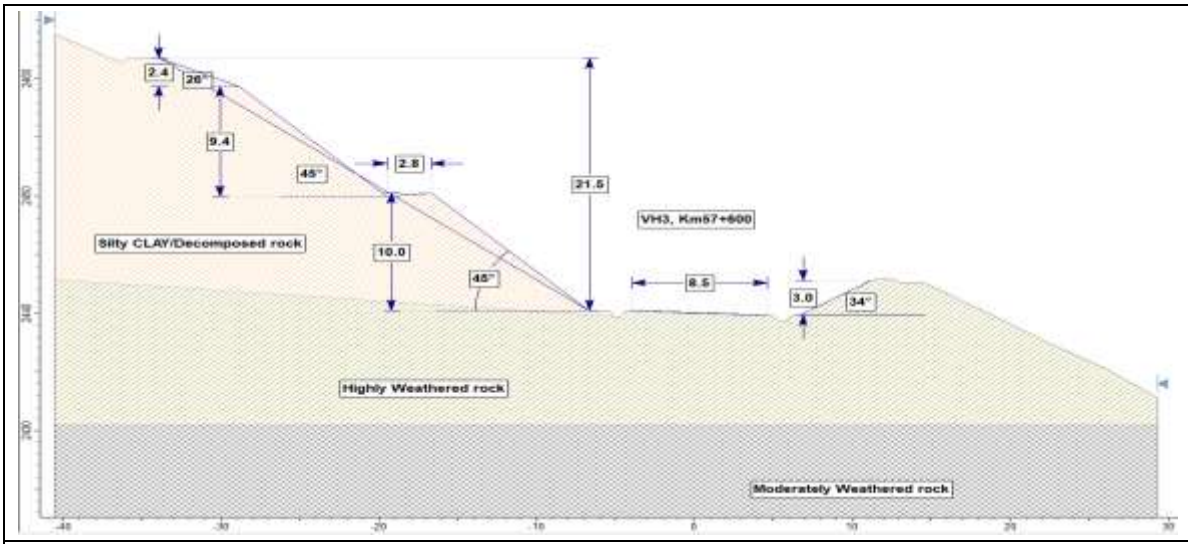

Slope profile at VH3, Km57+600

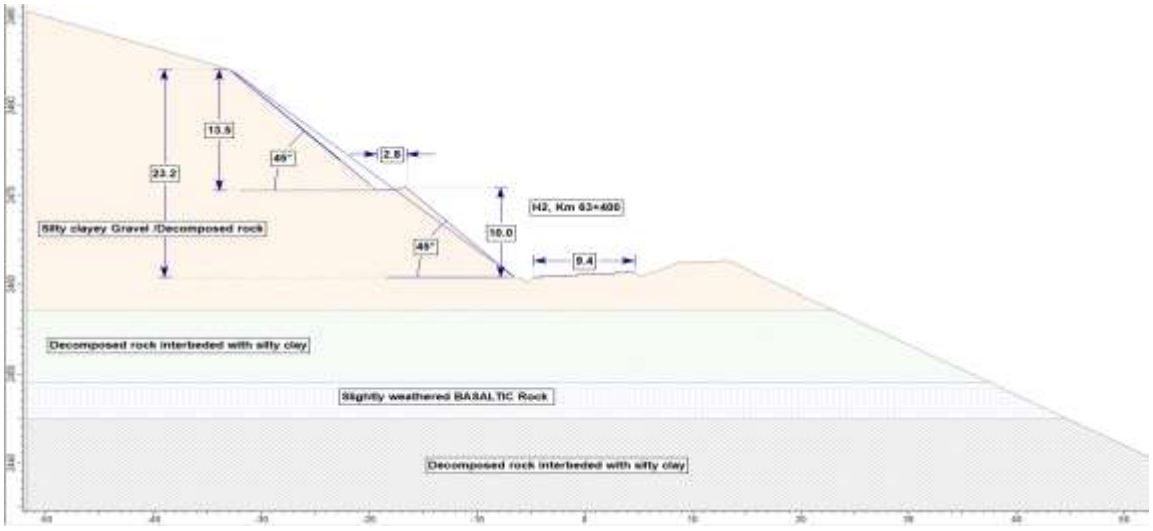

Slope profile at H2, Km63+400

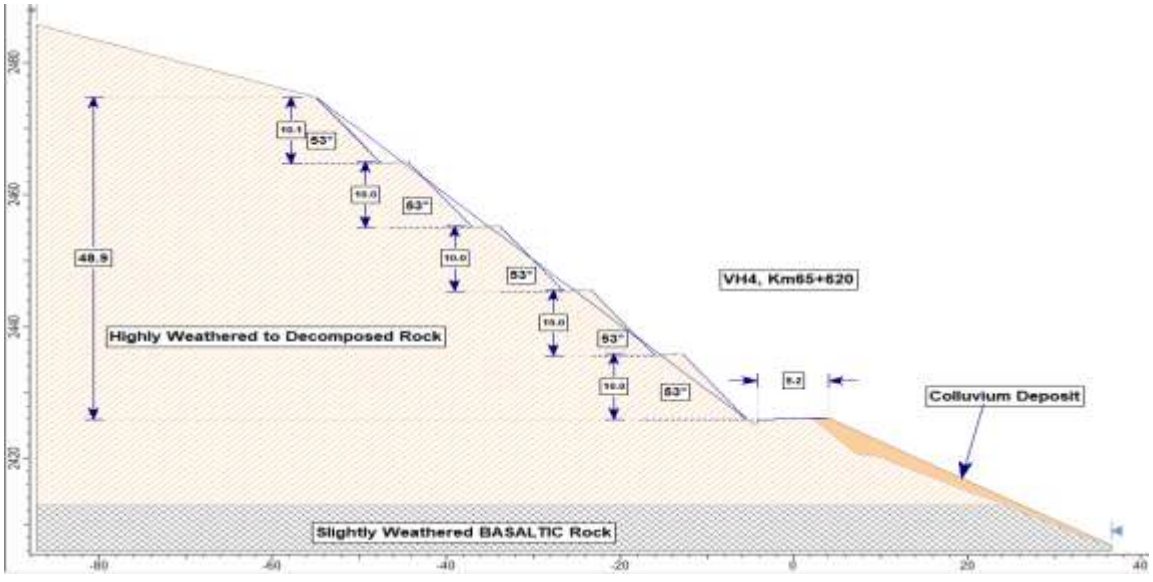

Slope profile at VH4, Km65+620

5.7.3 SLOPE STABILITY ANALYSIS

Limit equilibrium methods (Bishop's simplified and Spencer techniques) were applied. For circular failures such as Km 17+160, Km 20+510, Km 35+220, Km 52+200, Km 53+160, the Bishop simplified approach was employed whereas for complex semi-circular failures on layered soil and rock slopes (Km 57+600, Km 63+400, Km 65+620), the Spencer method was utilized. The methods were chosen, based on the observed failure type, material heterogeneity, and slope geometry. Furthermore, the stability of each slope was also modeled further in different worst-case scenarios (dry, and saturated state). The limit equilibrium method evaluates the stability of a slope by analyzing the equilibrium of forces and moments acting on individual slices within the slope (Fredlund & Rahardjo, 1993).

5.7.3.1 MODERATE HAZARD ZONE

- **M1 [Km20+510]**

This failed section is in the moderate susceptibility zone and has a 11.4 m high cut slope at a 1H:1V angle. The subsurface profile is composed of 3.0 m of silty clay, followed by 5.0 m of light gray fat clay, and underlying by 12.0 m of decomposed rock. Laboratory data reveal that the upper layer has high cohesive and a low angle of internal friction, resulting in lower shear strength when saturated. Slope stability analysis with slide software and the bishop limit equilibrium method generated a factor of safety (FOS) of 1.15 under dry conditions and 0.96 when saturated, as shown in Fig. 47 and 48. The critical slip surface was revealed inside the top two weak layers, consistent with field observations of surface cracks and minor deformations, indicating that the slope remains marginally stable, particularly during the wet season.

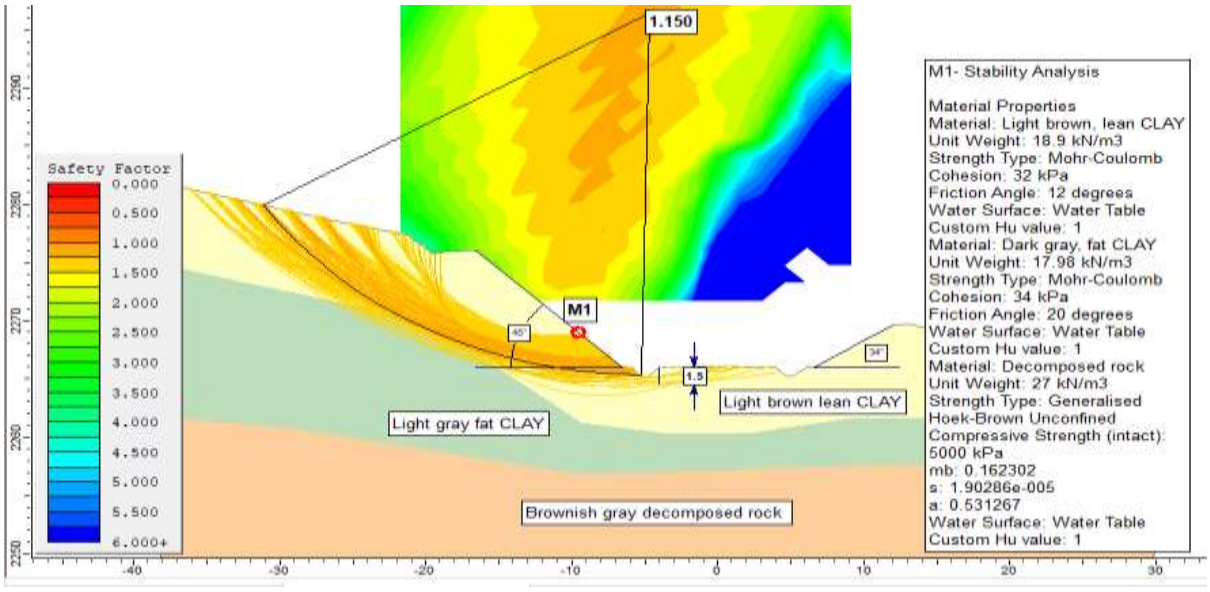

Figure 47: Slope stability analysis output of M1 under dry condition (FOS=1.15)

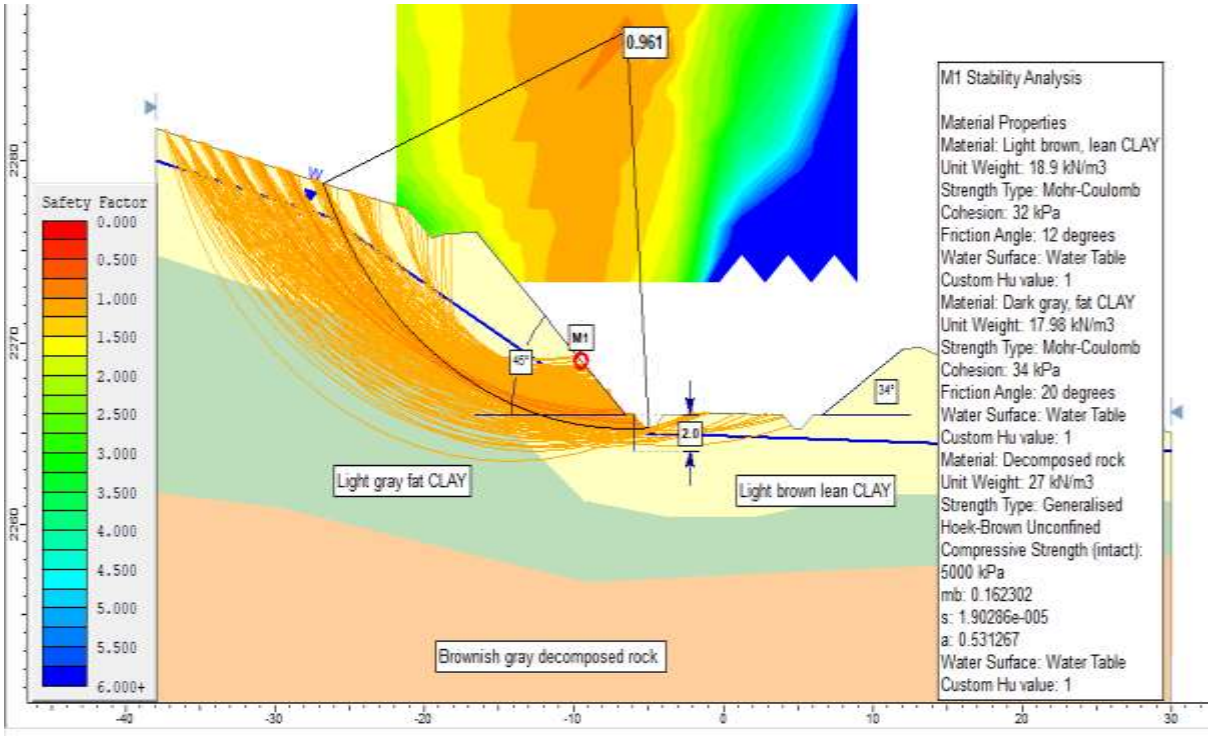

Figure 48: Slope stability analysis output of M1 under saturated condition (FOS=0.96)

- **M2 [Km35+220]**

The susceptibility map classifies this section as moderate susceptibility zone. It has a high fill section with 8.0m fill height and has a slope of 34^0 degrees. The geological formation along the sliding section is mainly reddish-brown lean clay underlying by decomposed material. The surrounding area is characterized by small bushes and medium forest. The major sliding has occurred within the embankment fill, implying that settlement could be due to water saturation at the surface or poor construction.

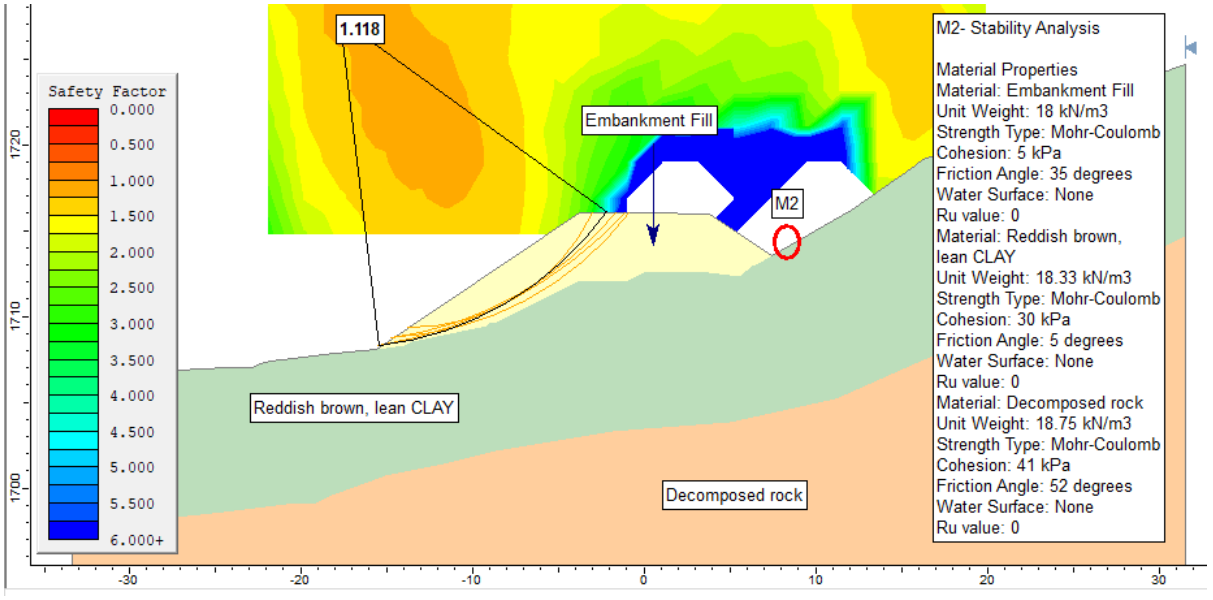

Figure 49: Slope stability analysis output of M2 under dry condition (FOS=1.11)

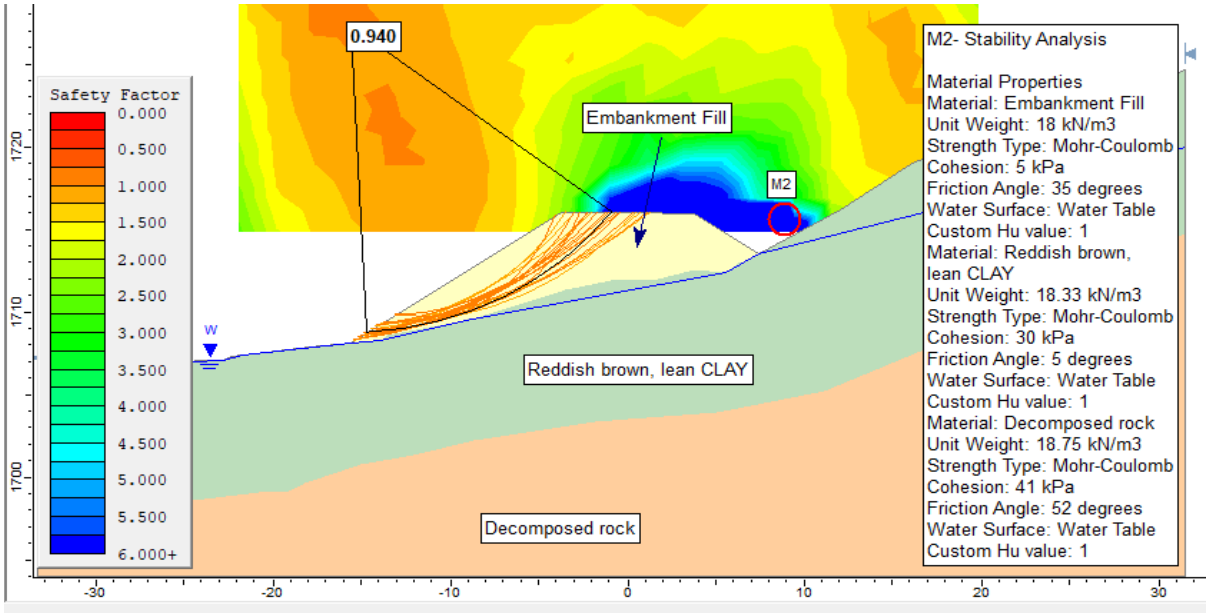

Figure 50: Slope stability analysis output of M2 under saturated condition (FOS=0.94)

The primary slip surface is visible on the road carriageway, indicated by longitudinal fissures and a 15-20 cm detachment in the asphalt toward the toe of high fill section. Using the slope profile and input parameters including unit weight, cohesion, and internal friction angle, the factor of safety was found to be 0.94 in dry conditions and decreased to 1.11 when saturated, as shown in Fig. 49 and 50.

5.7.3.2 HIGH HAZARD ZONE

- **H1 [Km17+160]**

Back slope and road carriageway failure has occurred along this section, which is located within a high susceptibility zone. The slope has a side cut of 11.40 m with a relatively gentle gradient of 1. 5H:1V. The sliding had propagated to the back slope material on LHS of the road and it has also damaged previously provided gabion wall including side drainage structure. The main scrap of the slip surface was observed on the road carriageway. The geological formations along the sliding section are mainly composed of 4.0 m of soft clay followed by 6.0 m of silty clay, underlying by decomposed tuff at greater depth. Laboratory test results revealed that low shear strength soils, especially the upper layer (soft clay), which contributes to the observed instability.

As demonstrated in Fig. 51 and 52, slope stability analysis utilizing slide software and Bishop approach yielded a factor of safety (FOS) of 1.10 under dry conditions, which reduced to 0.90 when saturated. The critical slip surface is located within the top weak clay layer and extends downward through the underlying silty clay. Shallow surface slumps, seepages, and indications of elevated pore water pressure, all suggesting a high potential for failure during wet periods as

confirmed during site investigation.

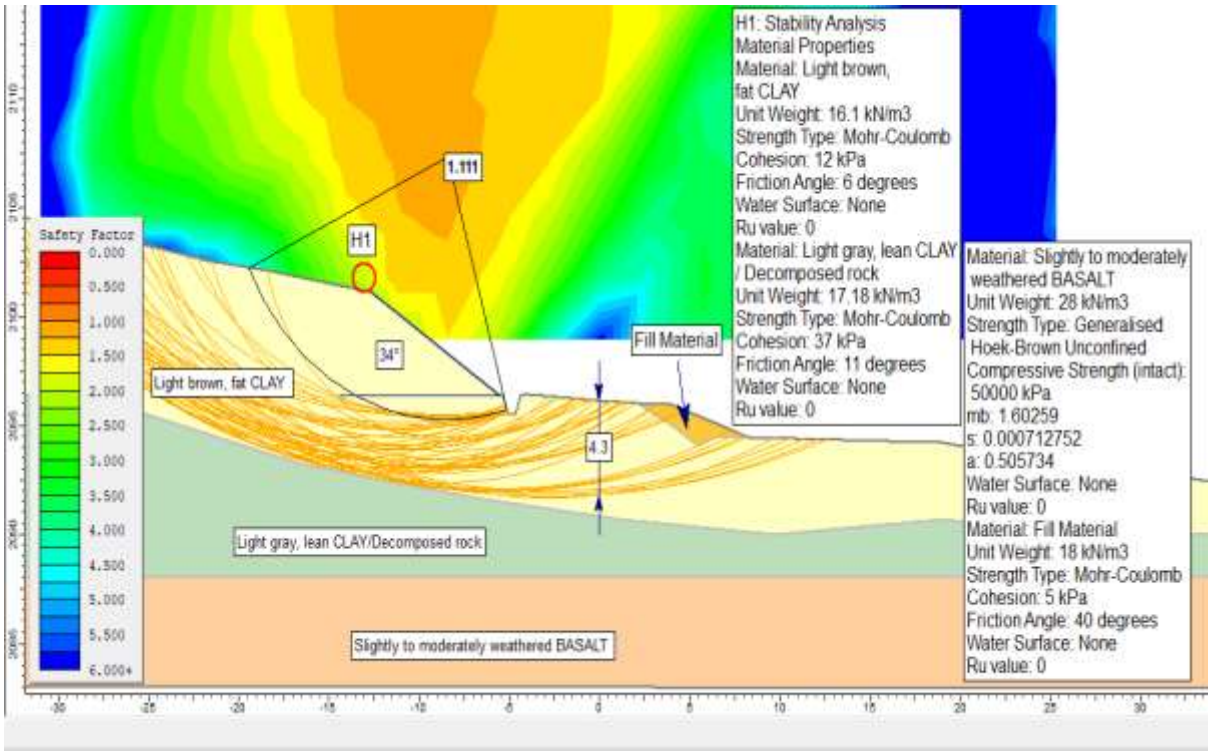

Figure 51: Slope stability analysis outputs of H1 under dry condition (FOS=1.11)

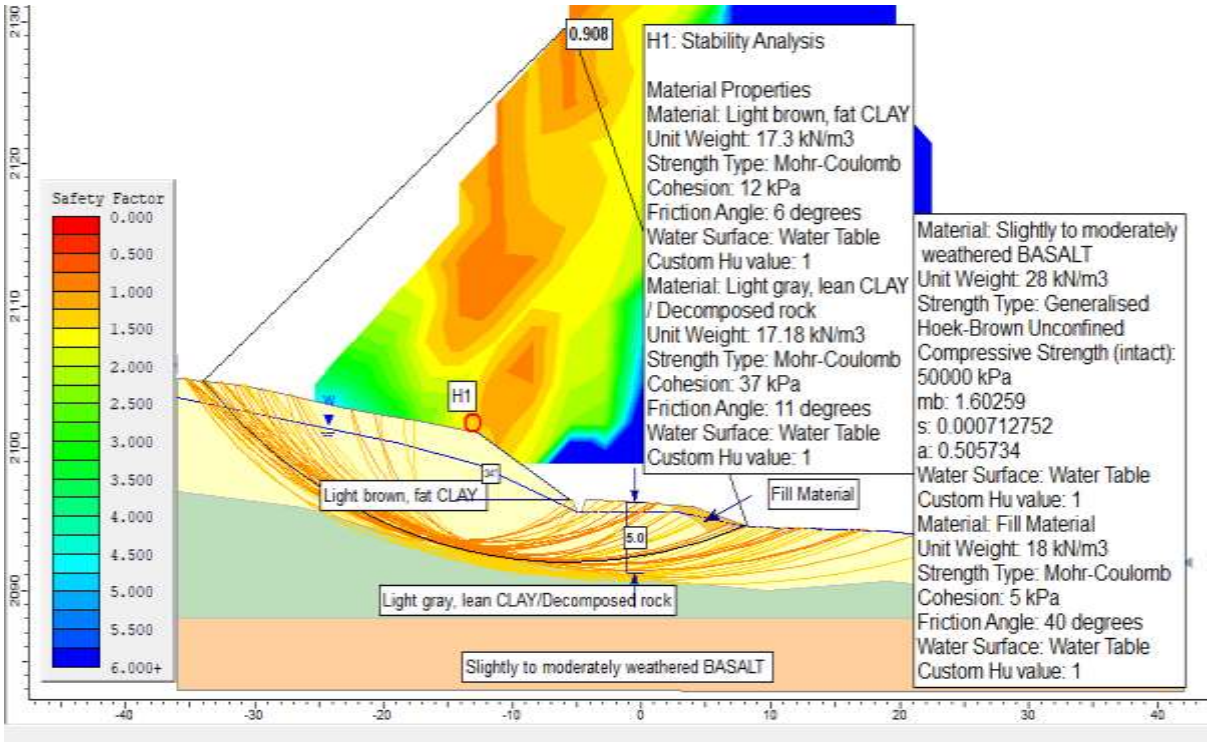

Figure 52: Slope stability analysis outputs of H1 under saturated condition (FOS=0.908)

- **H2 [Km63+400]**

A back slope failure occurred along this section, with the main scarp extending up to 30 m

upslope from the slope stake. The slope is 23.0 m high with a steep 1H:1V profile. The subsurface consists of residual soil over weathered rock, with lab tests showing low shear strength in the upper soft layer. Slope stability analysis using slide (Spencer method) produce a Factor of Safety of 1.06 (dry) and 0.88 (saturated). The slip surface is shallow relative to the road but deep in relation to the back slope, lying above the first and second benches in parts of the failure zone (Fig. 53 and 54).

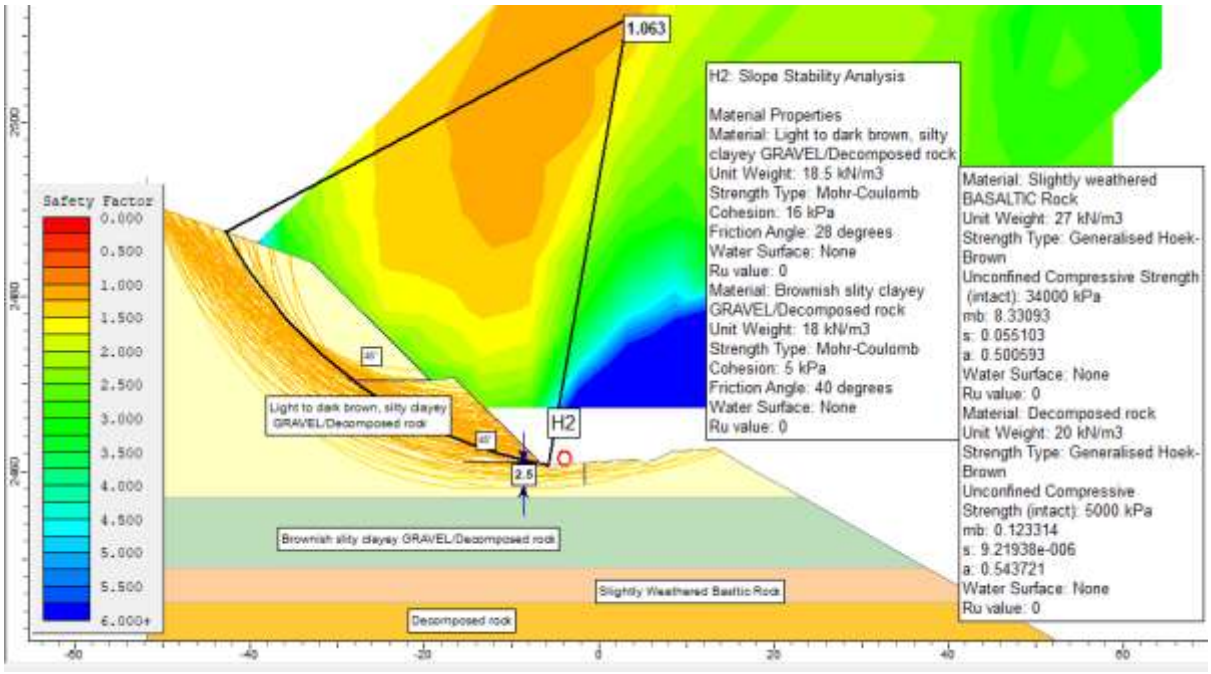

Figure 53: Slope stability analysis outputs of H2 under dry condition (FOS=1.06)

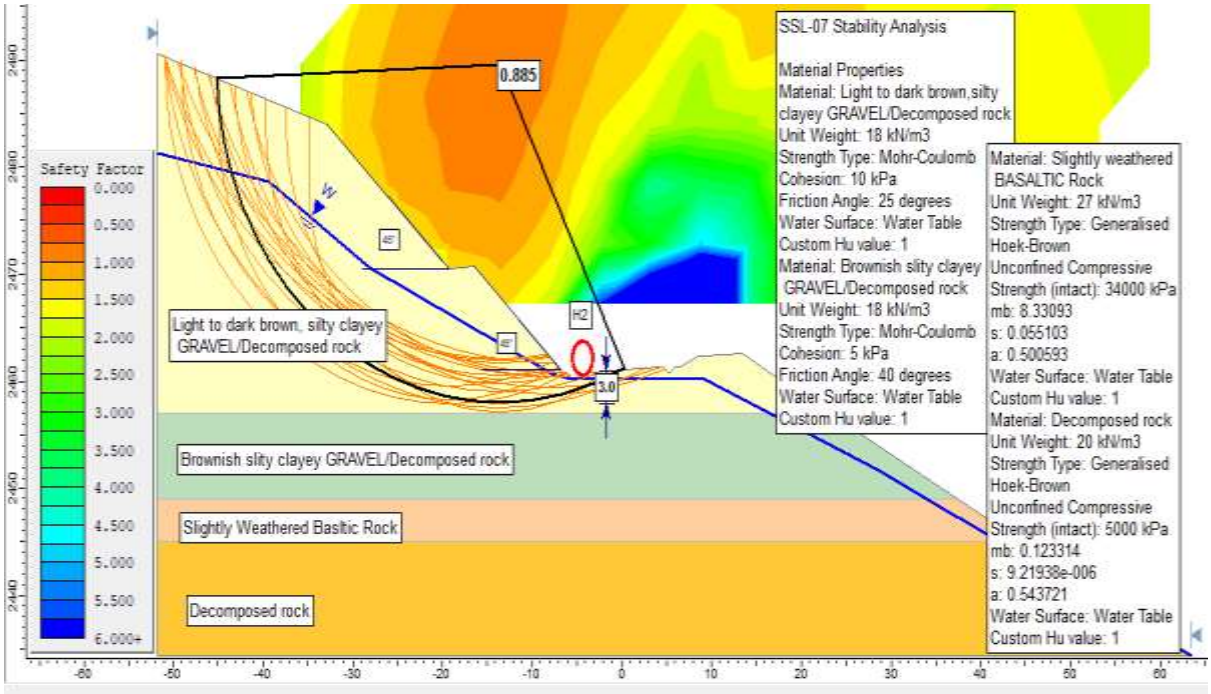

Figure 54: Slope stability analysis outputs of H2 under saturated condition (FOS=0.88)

5.7.3.3 VERY HIGH-HAZARD ZONE

- **VH1 [Km52+200]**

Landside has occurred in both sides of the road section. The cut slope is found in a very high susceptibility zone. The slope had a deep side cut height of 16.4 m high with a steep geometry of 1H:1V. The area is generally characterized by steep terrain with a deep colluvium soil deposit and covered with dense forest. The main scrap of the slip surface is located far away 15 - 20m from the road stake and propagated below the side slope of the road. The geological formation of the sliding mass is composed of 4.0 m of colluvial silty clay, underlain by 5.0 m of light gray silty clay developed from the highly weathered Tuff, and then underlying by 11m of decomposed rock.

Stability analysis in Slide showed an FOS of 0.90 (dry) and a low value of 0.81 when saturated as shown in Fig. 55 and 56. The critical slip surface passes through both the colluvium and marl layers. Field conditions confirm active slope deformation with fresh tension cracks, surface bulging, and swampy toe zones.

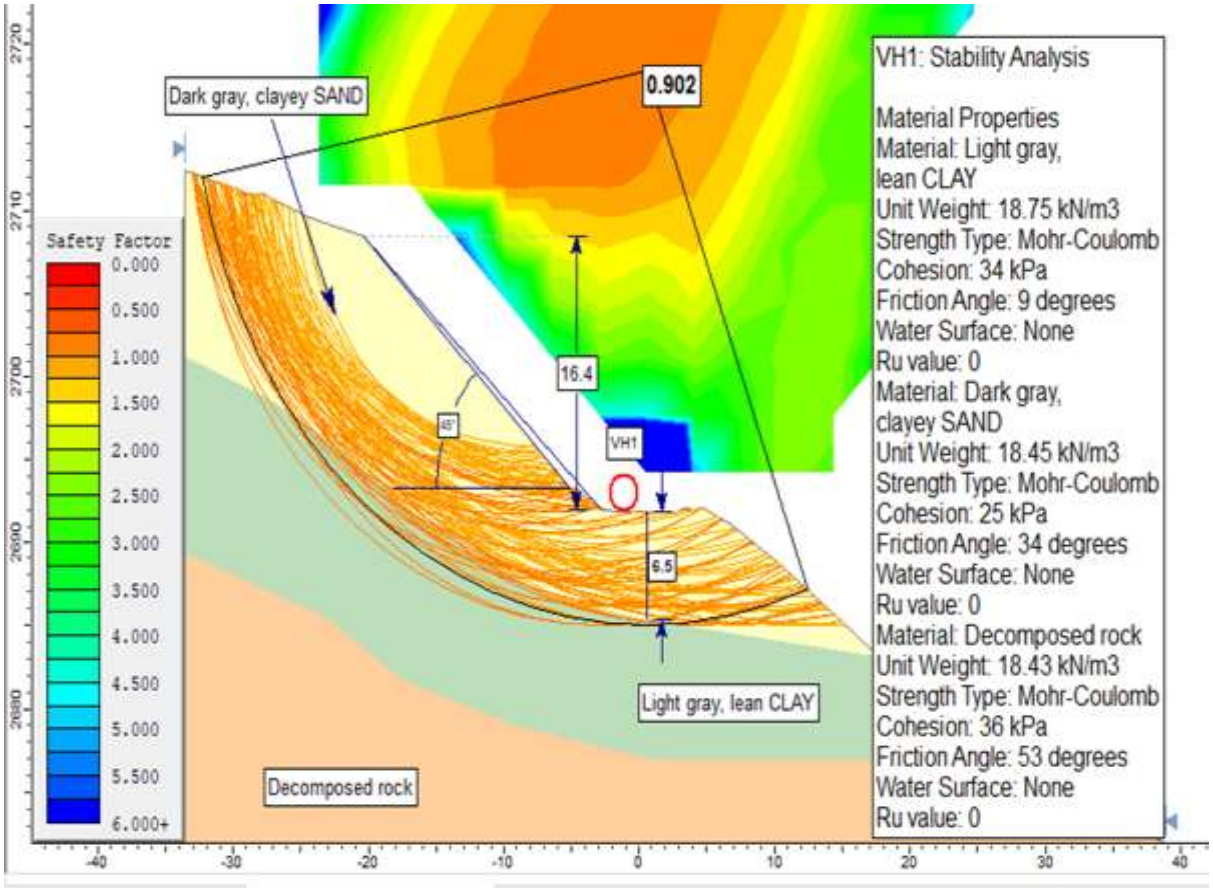

Figure 55: Slope stability analysis outputs of VH1 under dry condition (FOS=0.902)

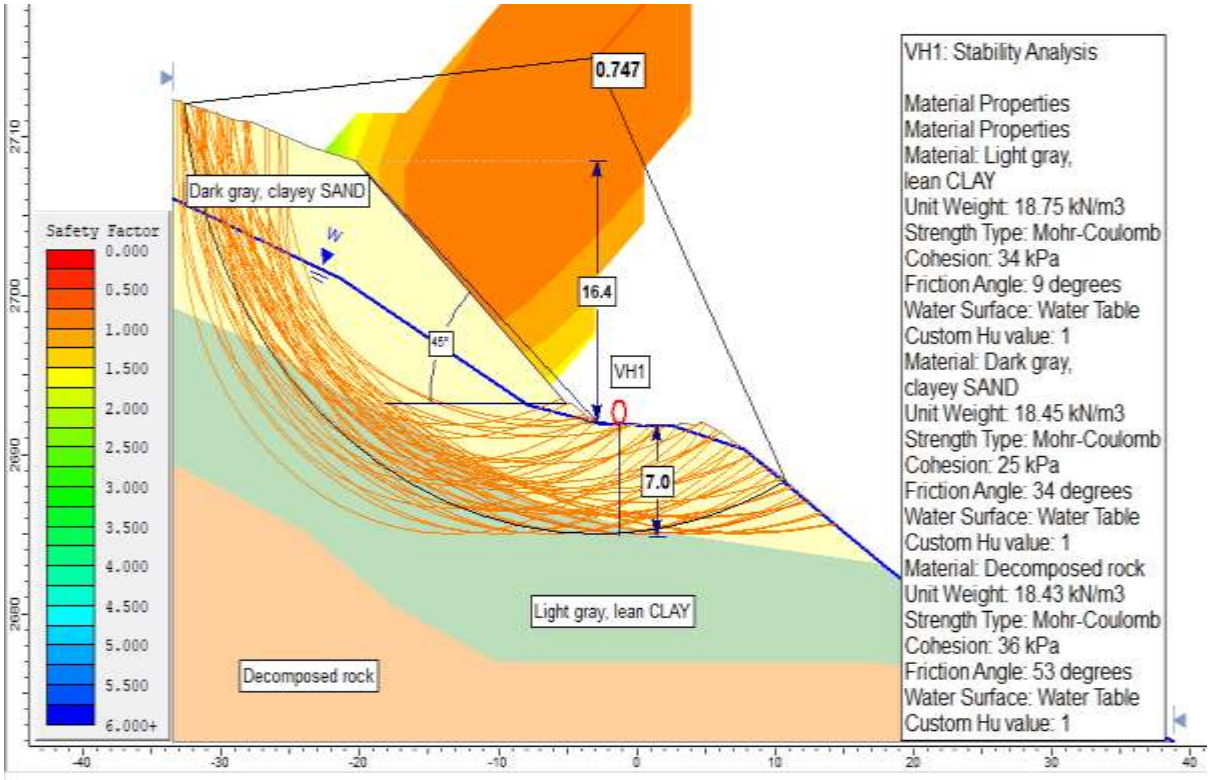

Figure 56:Slope stability analysis outputs of VH1 under saturated condition (FOS=0.747)

- **VH2 [Km 53+160]**

This section is categorized as extremely hazardous zone. A landslide has happened on the back slope on the left-hand side (LHS) of the road, where materials from the slope have slide down and affected the side slope as well. The incident caused fatalities as well as serious damage to surrounding homes. About 50 to 60m upslope from the slope stake, the major scarp of the slip surface was visible. The region has a steep side hill, and the geology is composed of decomposed material on top of a thick colluvial deposit. The area is covered by forest. Due to heavy rains, this incident caused a large landslide that later turned into a debris flow, disrupting the environment and killing many people downs the hill. The road's geometric design includes a deep side cut of 32m with a steep slope angle of 45°.

For slope stability analysis, the material layering was modeled using a combination of laboratory test results and in-depth field observations. According to the analysis, the slip surface extends through the entire back slope and beyond, and it is deep seated with respect to the road formation level. Slope stability analysis using the bishop limit equilibrium method and Slide software produced a factor of safety (FOS) of 0.64 in saturated conditions and 0.83 in dry conditions. Fig. 57 and 58 shows the slip surface's depth as established by the analysis.

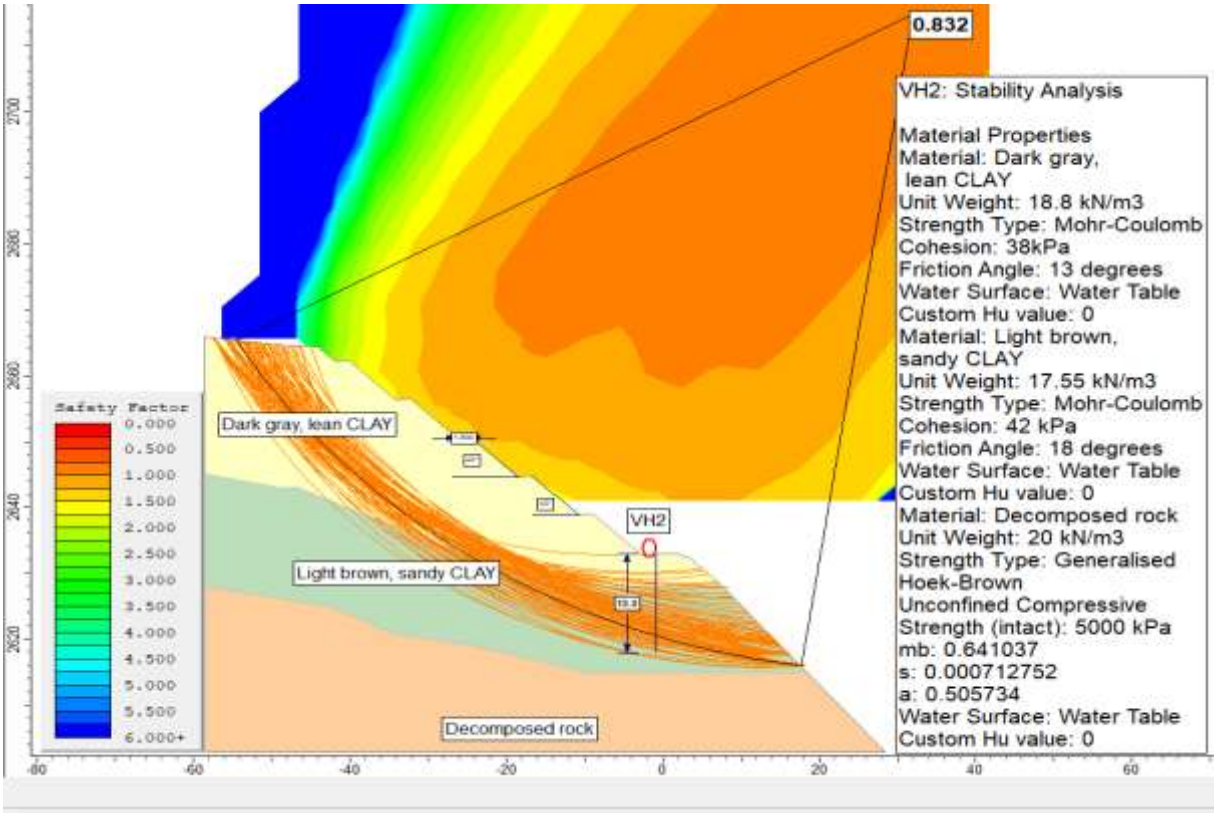

Figure 57: Slope stability analysis outputs of VH1 under dry condition (FOS=0.83)

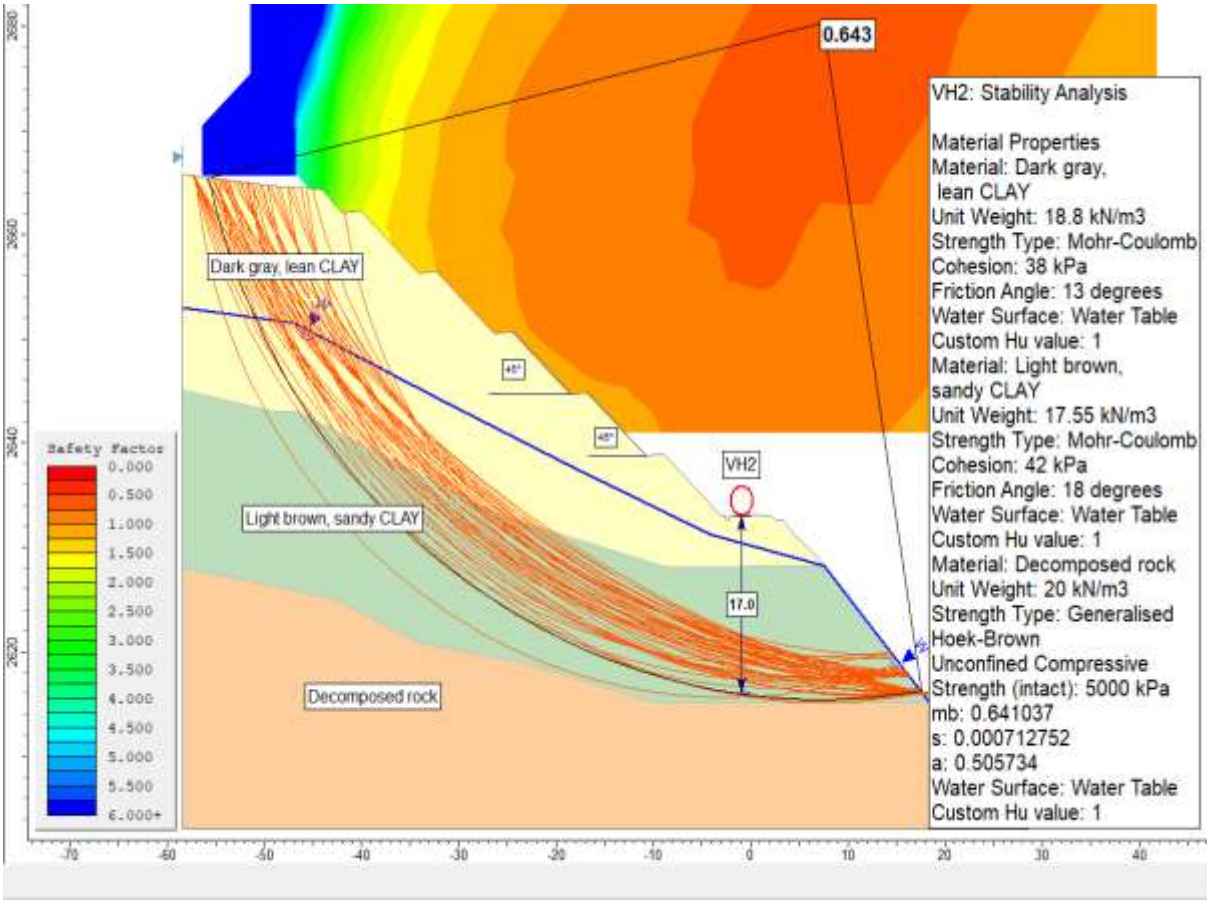

Figure 58: Slope stability analysis outputs of VH1 under saturated condition (FOS=0.64)

➢ **VH3 [Km57+600]**

A rotational back slope failure has occurred along this road section. The main scarp of the slip surface is located 30 to 40m upslope from the centerline. The geometric design along this section shows a 45° cut angle with a deep side cut depth of 21.0 m. Springs and minor cracks were also observed within the failed mass. The geological formation along the sliding section composed of decomposed rock underlying by highly weathered. A combination of trial pit test and previous borehole data is used in modelling the back slope material layering. Geotechnical data for stability analysis for this road section is based on the laboratory test results.

Based on the stability analysis, the possible depth of slip surface which is similar with the one observed during filed investigation at sliding section is within the back slope. Slope stability analysis using the Spencer method and Slide software produced a factor of safety (FOS) of 0.68 in saturated conditions and 0.94 in dry conditions. Fig. 59 and 60 shows the slip surface's depth as established by the analysis. This output will be used as input parameter in recommending remedial measure for the sliding.

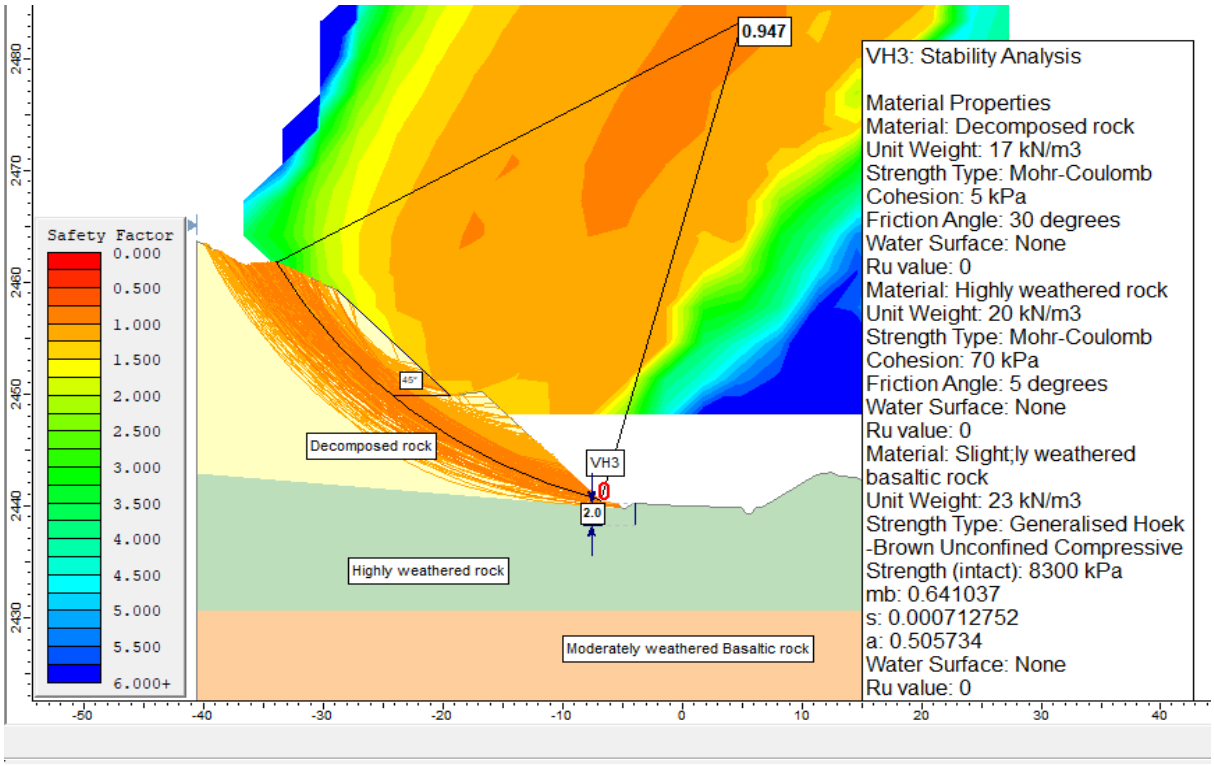

Figure 59: Slope stability analysis outputs of VH3 under dry condition (FOS=0.94)

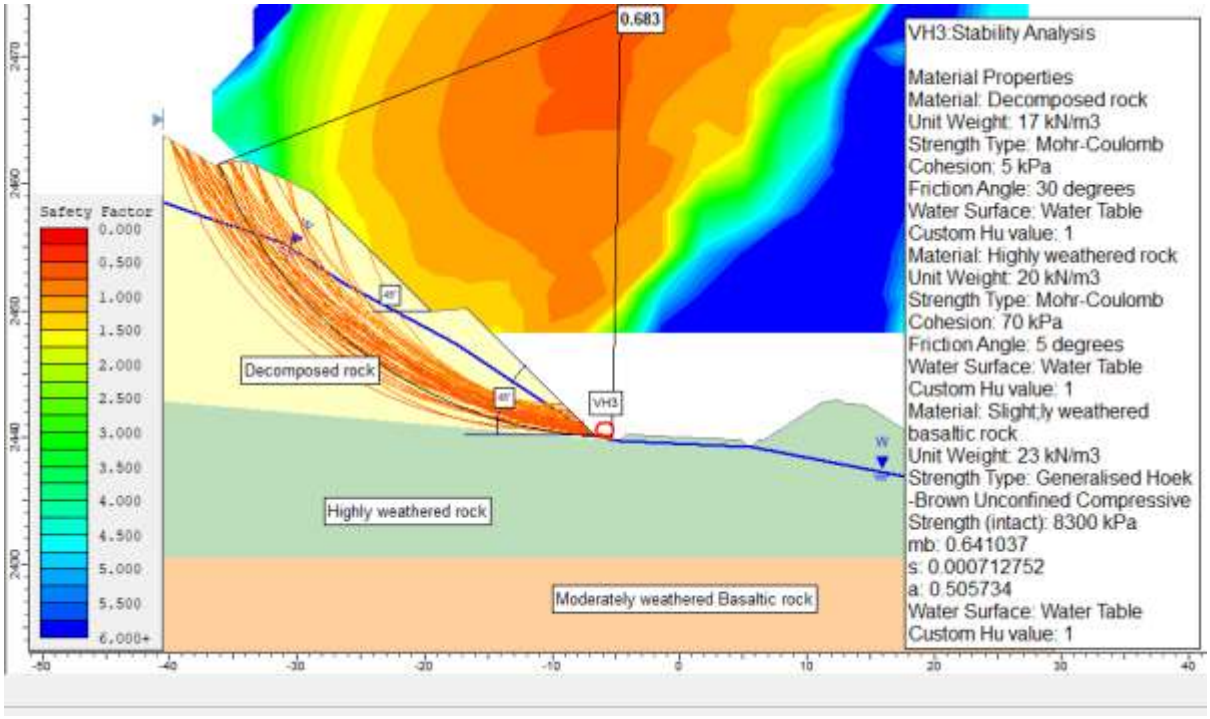

Figure 60: Slope stability analysis outputs of VH3 under saturated condition (FOS=0.68)

- **VH4 [Km65+620]**

A rotational side slope failure has occurred along this section. The geometrical design shows 53^0 slopes with 48.0m deep side cut. The geological formation along the sliding section is colluvium deposit underlying by weathered rock. The road passes through a desiccated valley, with a large stream on the right (RHS) and a very steep hillside on the left (LHS) that have eroded the terrain toe and disturbed the roads alignment. Deep gully erosion has developed along the carriageway as a result of intense runoff from the top hillside through multiple streams which crossing the road. The road is currently damaged and un able to pass. A combination of trial pit test and previous borehole data is used in modelling material layering in slope stability analysis. Geotechnical data for stability analysis is based on the laboratory test results.

Based on the stability analysis, the slip surface is located within the colluvium deposit, see Fig. 61 and 62. This indicates the slip surface is shallow seated and no movement is expected on the underling rock stratum but hazardous to the road. Slope stability analysis using the Spencer method and Slide software produced Factor of Safety (FOS) of 0.78 under dry conditions, which reduced to 0.54 when saturated.

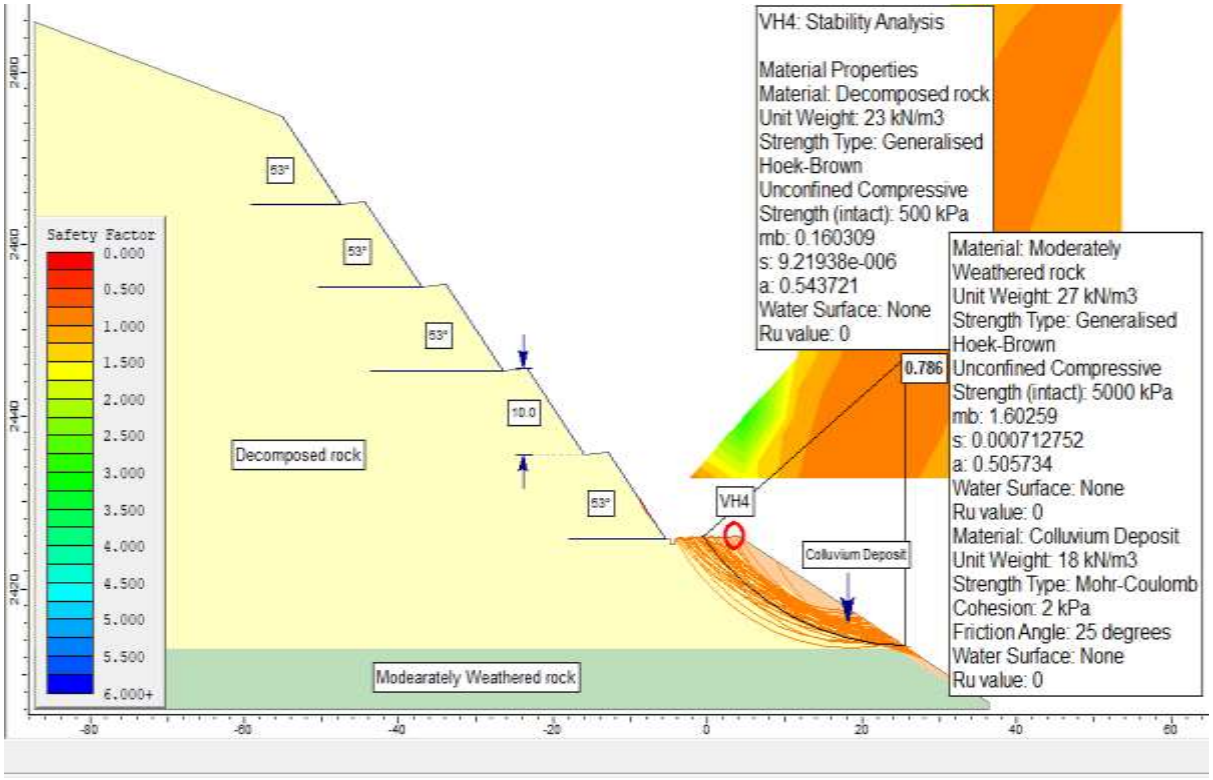

Figure 61: Slope stability analysis outputs of VH4 under dry condition (FOS=0.78)

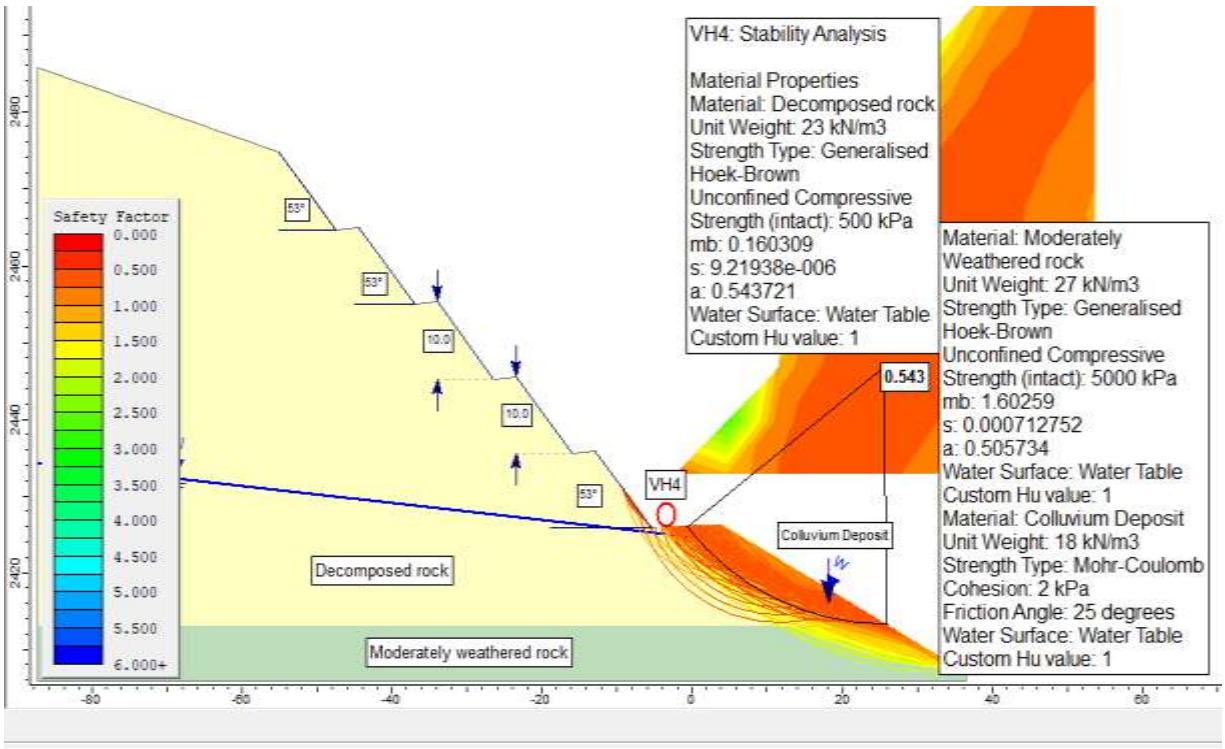

Figure 62: Slope stability analysis outputs of VH4 under saturated condition (FOS=0.54)

5.8 REMEDIAL MEASURES

Landslides pose a significant damage in Ethiopia, especially along road corridors crossing hilly and mountainous terrain (Woldearegay, 2013). These events consequence in substantial losses

of life, property, and agricultural land, primarily due to weak geological formations, steep slopes, poor drainage, spoil accumulation, and unfavorable soil or rock conditions (Dai et al., 2002; Guzzetti et al., 2022). External factors such as heavy rainfall and extensive excavation further exacerbate slope instability. Hence, detail landslide hazard assessments and risk evaluations are critical before commencing any developments, urban planning, or construction projects. In response to these challenges, the formulation and application of effective mitigation strategies are imperative to reduce vulnerability and enhance safety.

According to (FAO, 1993), slope instability measures are classified as control and restraint works. Control works reduce factors causing instability; such as drainage, slope flattening, and bioengineering while restraint works oppose driving forces, including retaining walls, anti-slide piles, and stone pitching. Effective remedial measures typically aim to increase the factor of safety to between 1.3 and 1.5 for temporary stability (Duncan, 1996), while a minimum safety factor of 1.5 or higher is generally recommended for long-term or permanent slope stability (Coduto et al., 2011).

For this study, both control and restraint approaches are applied according to the identified causes and slope conditions, with a combination of methods implemented across most sliding or destabilized slope sections. The correction actions for the encountered slope stability problems were based on the results of the slope stability analysis. The following sections provide details of the recommended remedial measures for each affected road section. Graphical representation of each section was attached in appendix-6.

5.8.1 MODERATE HAZARD ZONE

M1 [Km20+510]

The analysis of slope failure shows that the slip surface is shallow (2.0 m below finished road level), and is mainly attributed to slope overstepping and back slope material saturation by surface and spring water in this stretch. Remedial measures include flattening of the slope, removal of the failed mass above the first bench level, and construction of a 7.0 m high masonry retaining wall with an embedment depth of 3.0 m is recommended. Rock fill with 1.5m thickness provided under the wall for enhancing the bearing capacity of the foundation and facilitate subsurface drainage. Rock/granular backfill shall be provided behind the retaining wall which will discharge enough water. Subsurface flow will be conveyed to the pipe culvert at Km 20+410 in a channel buried through rock fill. Lined furrow ditches with chutes will also be recommended to regulate infiltration of surface water.

Based on the stability analysis, a minimum safety factor of 1.8 is obtained after the application of remedial measure.

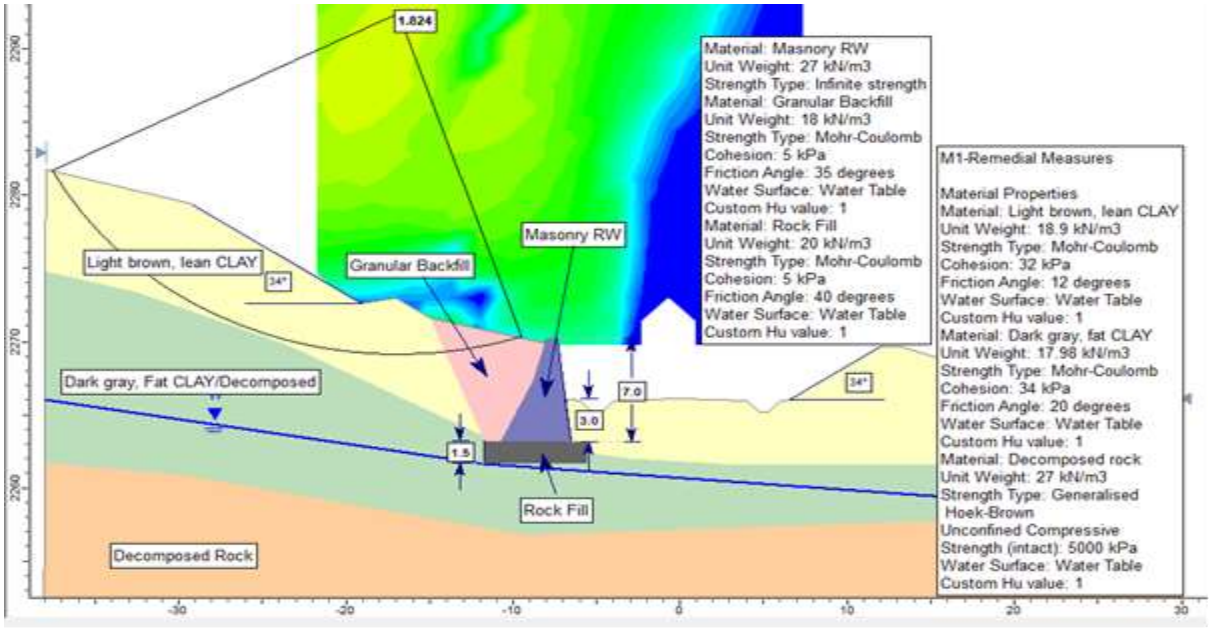

Figure 63: Stability analysis output with remedial measure along M1, Km20+510

M2 [35+200]

On the basis of the slope failure analysis, the slip surface occurred in the embankment fill mainly resulting from water saturation settlement and poor compaction. The suggested remedial action therefore involves the control of surface water runoff, removal of the failed fill section, and constructing masonry retaining wall at the fill toe.

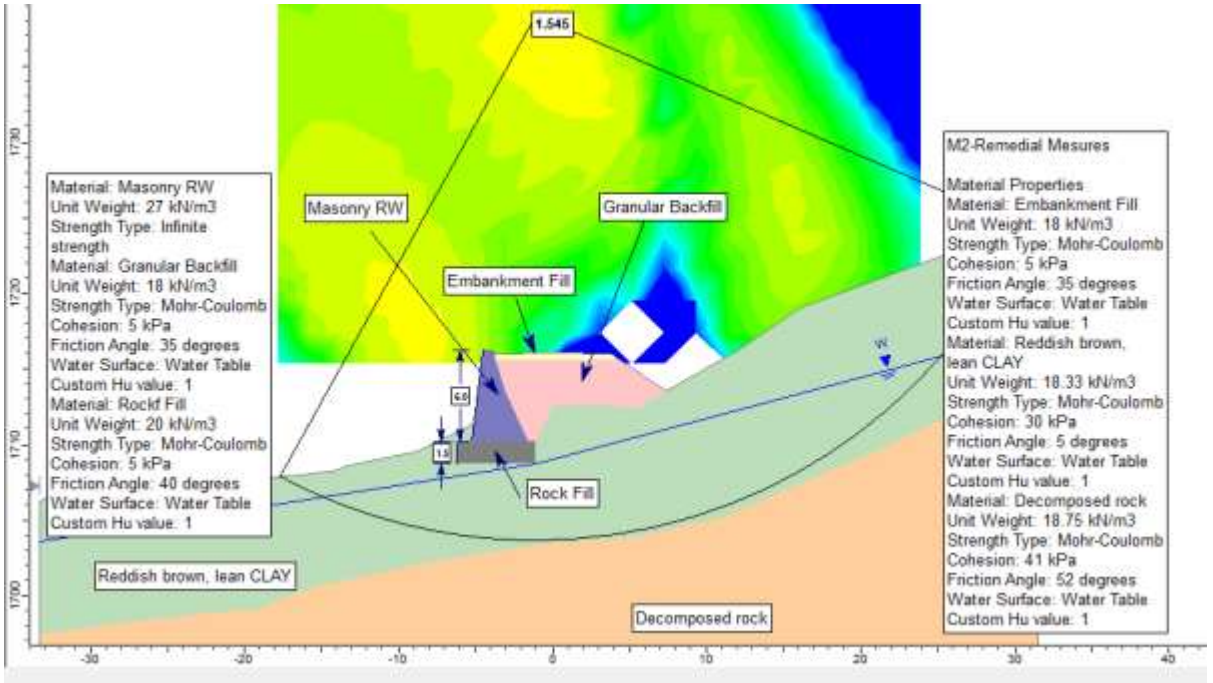

Figure 64: Stability analysis output with remedial measure along M2, Km35+220

A masonry retaining wall with a total height of 6.0m, including a 2.0m embedment depth is recommended. A 1.5m thickness of rock fill is proposed below the retaining wall for enhancing the stability of the foundation and allowing draining of ground water. Granular backfill shall be placed behind the wall and finished in the entire width of the road after the wall installation for enhancing effective drainage of the water. Further, a surface side ditch is recommended on the LHS to convey surface water. Based on the stability analysis, a minimum safety factor of 1.5 is obtained after the application of remedial measure.

5.8.2 HIGH HAZARD ZONE

H1 [Km17+160]

From the slope stability analysis, slip surface at this site is 5.0 m below the road level when the slope is saturated. The major reasons for the failure are removal of toe support, overstepping slope and saturation of material in the back slope. Therefore, a combination of control and restraint measures is suggested for slope stabilization.

The remedial works suggested are as follows: excavation of a section of the failed mass and constructing of a masonry retaining wall within the toe of the back slope with a height of 8.5 m out of which 6.0 m will be embedment. Rock fill of 1.0 m thickness also provided below the wall for strengthening the foundation and offering subsurface drainage. Granular backfill will be filled behind the wall to allow better water discharge. In addition, seepage of shallow groundwater beneath the retaining wall will be redirected to the pipe culvert inlet at Km 17+020 through a buried rock fill channel. Based on the stability analysis, a minimum safety factor of 1.8 is obtained after the application of remedial measures

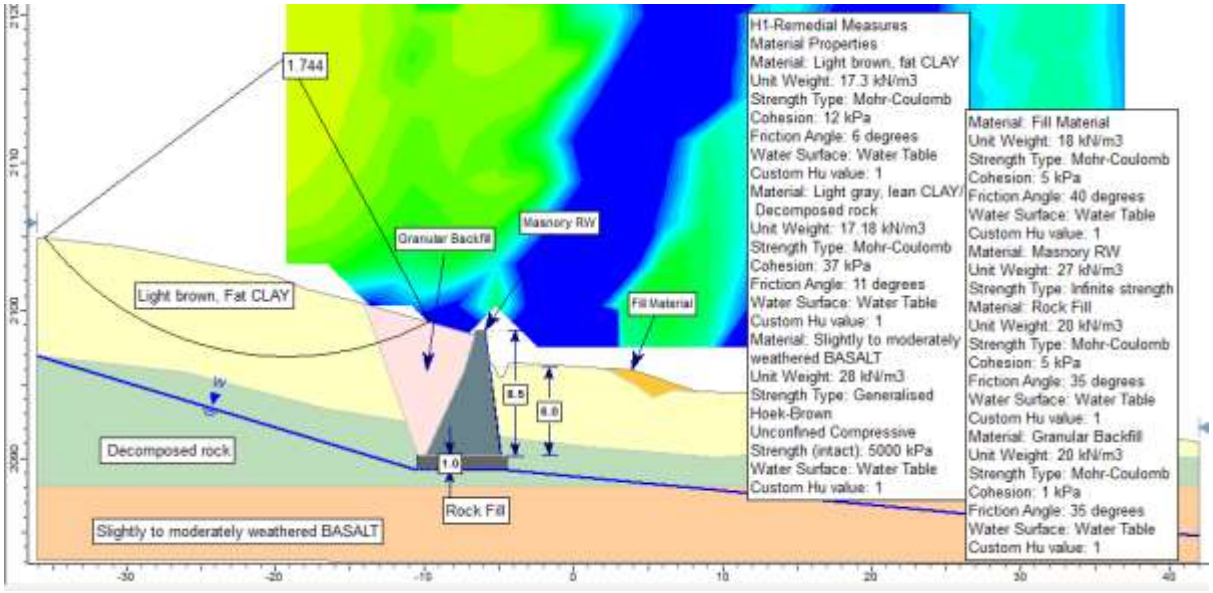

Figure 65: Stability analysis output with remedial measure along H1, Km17+160

.H2 [Km63+400]

Back slope material saturation due to spring water and old landslide reactivations are determined to be major triggering factor along this stretch. According to the slope failure analysis the slip surface depth is around 3.0 m below the finished road level. Thus, control and restraint works are advisable. The countermeasure is involved flattening of the slope adjacent to the scarp, removal of failed mass above the first bench, and constructing of 12.0 m high concrete retaining wall with 4.0 m embedment. Below the wall, there will be 1.0 m thick rock fill to enhance foundation stability and to assist subsurface drainage. Granular backfill behind the wall will be utilized for effective water discharge. Subsurface flow will be channelized to the pipe culvert at Km 63+560 through a buried rock fill channel. Apart from that, lined furrow ditches with chutes will also be incorporated on the back slope to reduce surface water ingress and abandon runoff safely.

Based on the stability analysis, a minimum safety factor of 1.5 is obtained after the application of remedial measure

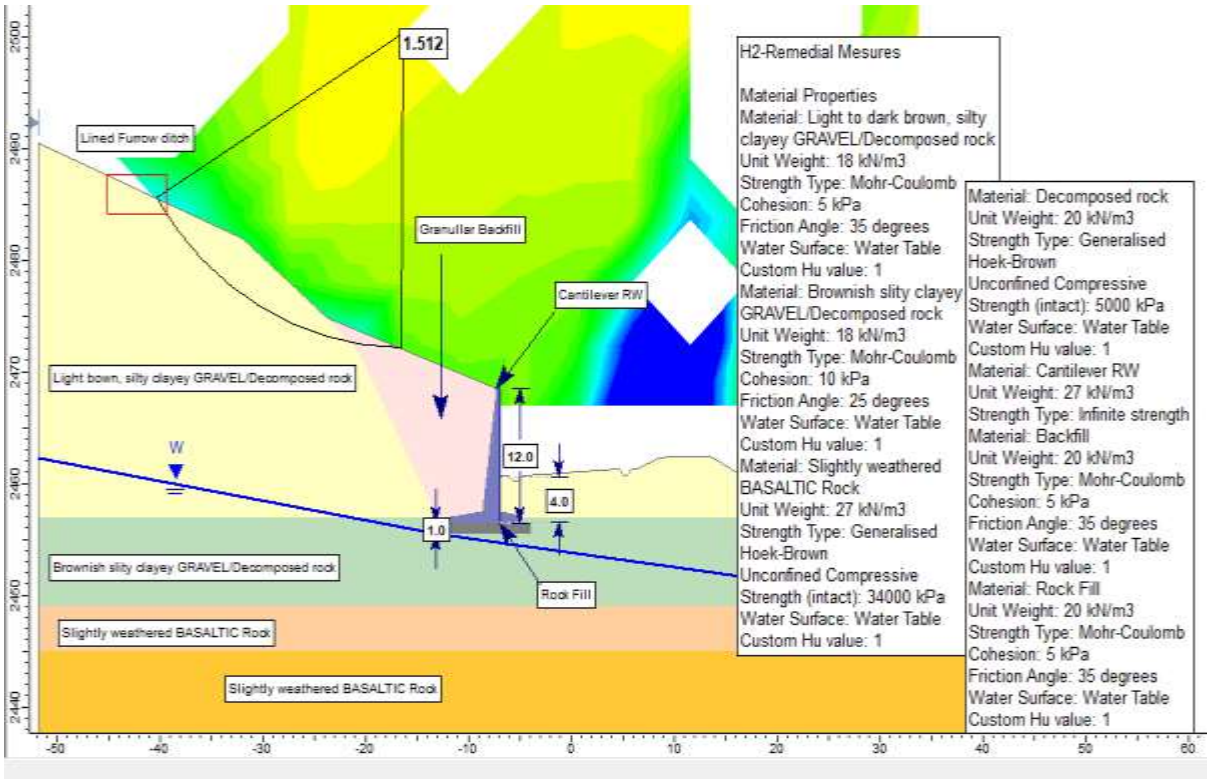

Figure 66: Stability analysis output with remedial measure along H2, Km63+400

5.8.3 VERY HIGH-HAZARD ZONE

VH1 [Km52+200]

Slope failure analysis shows a deep seated slip surface under saturation, which is approximated

to be 7.0 m below road formation level. The main reasons for the landslide along this section are poor slope design, removal of toe support, and inadequate drainage, all of which have promoted water overflow downhill. Hence, surface and subsurface water control, as well as structural resisting works, are required in order to suppress the landslide. The suggested remedial measures are removal of the failed mass, trimming and flattening of the first bench, and driving of continuous anti-slide piles (length 18 m, diameter 1.2 m, spacing 1.5 m) along the roads RHS. A lined furrow ditch at 3 m upslope distance from the slope stake, with side ditches connected through bench drain chutes, is also suggested for containing runoff as well as erosion. Accordingly, a minimum safety factor of 1.61 is obtained after the application of remedial measures.

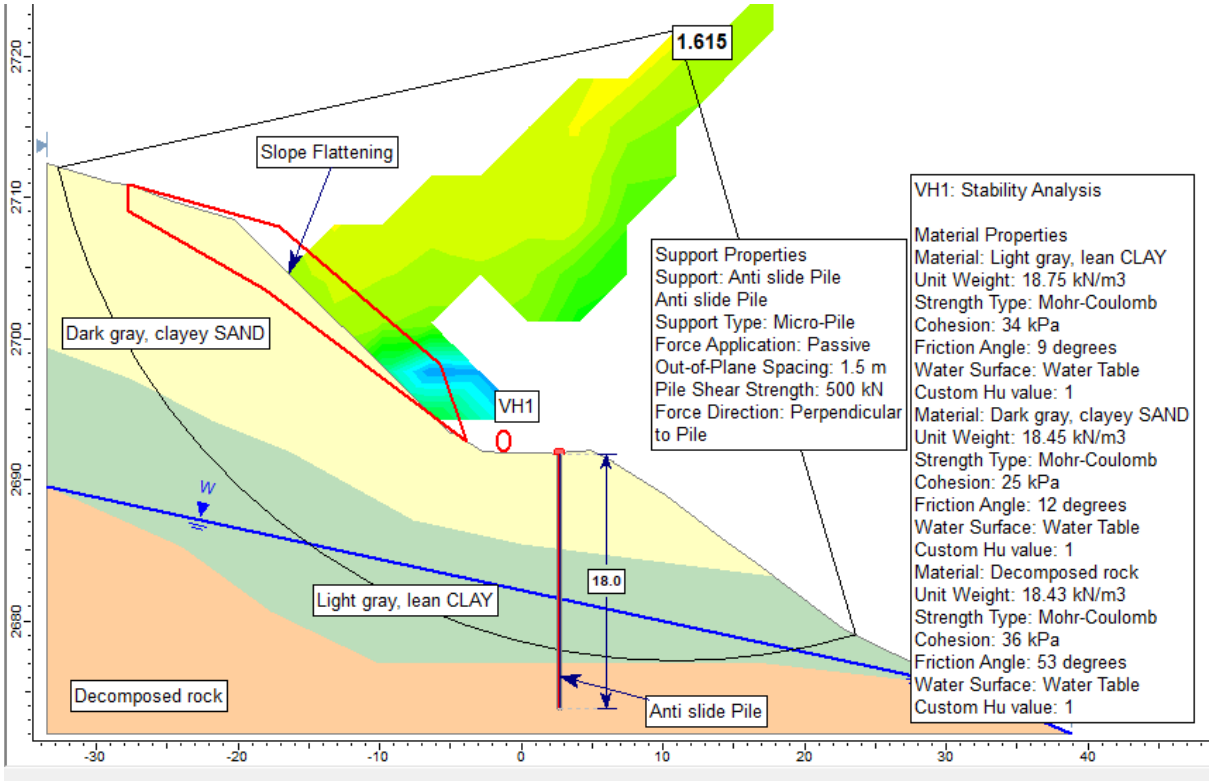

Figure 67: Stability analysis output with remedial measure along VH1, Km52+200

VH2 [Km53+160]

The main landslide causative factors along this stretch involved; over steepened cut slopes, loose thick back slope material, toe support removal, uncontrolled surface and subsurface flow, and heavy rainfall are the major triggering factors. Water saturated backslope material has resulted in debris flows and damage to nearby houses, and agricultural lands. This road is permanently block to traffic due to recurring of landslides every year. Analysis of slope failure indicated that a very deep-seated slip surface within the residual and colluvial deposits of soil, at about 17.0 m below road formation level.

Therefore, integrated control and restraint works are required. The recommended remedial measures are flattening of the steep slope, removal of the failed material above the first bench, and employment of anti-slide piles (25 m long, 8.0 m embedment, 1.2 m diameter, 1.5 m spacing) at the toe of the road RHS. The other measures are bench drainage, lined furrow ditches, concrete stone pitching, and paved side ditches to control surface water and improve the stability of the slope. On the other hand, shifting the centerline of road may be undertaken to prevent expensive remedial work and long-term stability. Based on the stability analysis, a minimum safety factor of 1.8 is obtained after the application of remedial measures

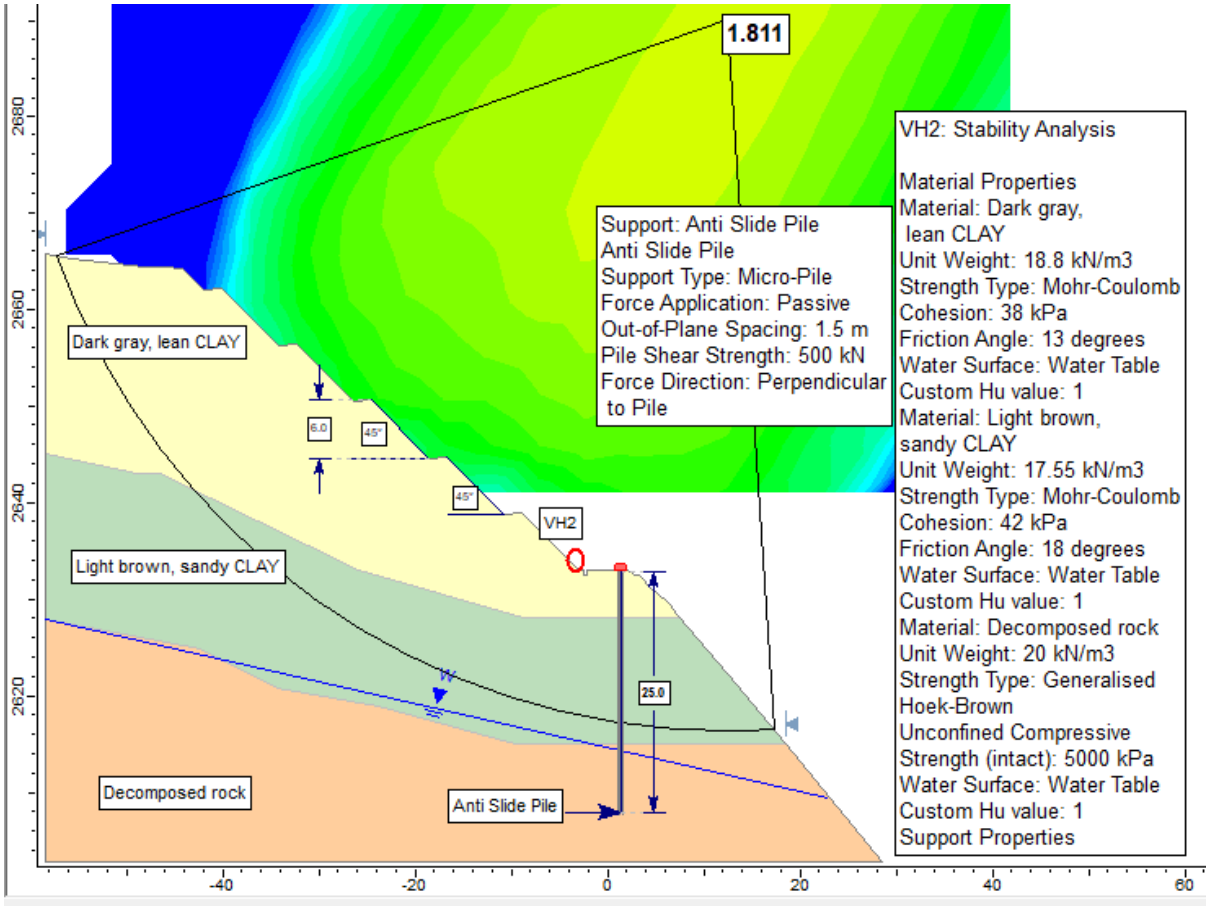

Figure 68: Stability analysis output with remedial measure along VH2, Km53+160

VH3 [Km57+600]

Based on the slope failure analysis a shallow slip surface about 2.0 m below the level of road formation along this slope, caused mainly due to loss of toe support due to excavation and saturation of slope material. The solution for such causes is suggested both restraint and control measures. The proposed remedial work involves clearing of the moved material from the crest of bench and installation of a masonry retaining wall along the toe of the back slope, having an overall height of 9.0 m with 2.0 m embedment. A 1.5 m thick rock fill will be laid beneath the wall for foundation strengthening and subsurface drainage purposes. A relief channel filled with

rock will be introduced across the road at Km 57+800 to direct subsurface flow to the nearby culvert.

Other drainage measures are achieved through rock/granular backfill behind the wall, lined furrow ditch at the back of the slope, and lined chutes for collection and removal of surface runoff. Another furrow ditch, located 3 m from the stake on the slope, will convey runoff to side ditches through chutes to minimize erosion.

Accordingly, a minimum safety factor of 1.59 is obtained after the application of remedial measure.

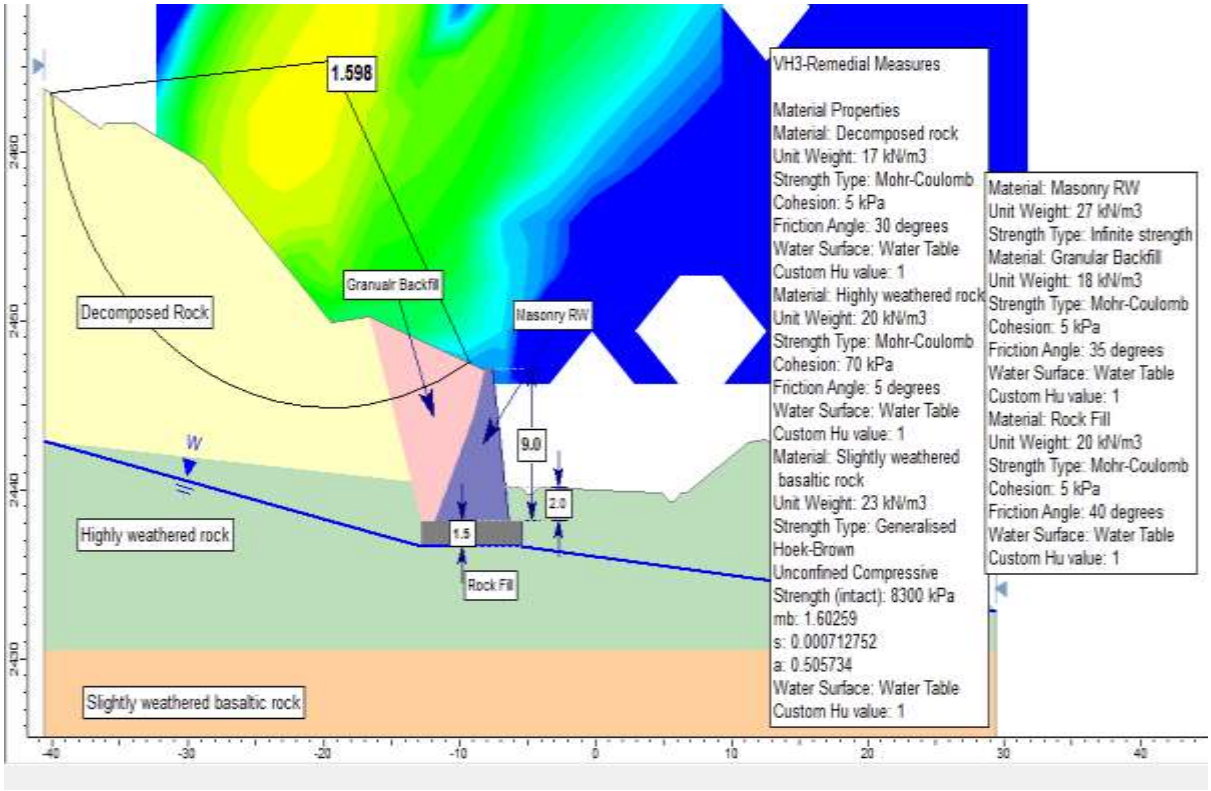

Figure 69: Stability analysis output with remedial measure along VH3, Km57+600

VH4 [65+620]

The slope stability analysis shows that the slip surface is within the colluvium deposit, with most of it caused by surface erosion resulting from uncontrolled surface runoff. This also shows that the slide is shallow seated with no predicted movement in the bedrock strata. Therefore, careful control of surface water flow is of highest priority in this section to minimize erosion and resulting slope failure of the side slope. As corrective action, paving along rivers in pipe culvert outlets is suggested for runoff control. MSE retaining wall of 12.0m height is also suggested for enhancing resistance of slope against sliding. Analysis of slope stability considering these remedial works is shown in Figure 70. Based on the stability analysis, a minimum safety factor of 1.67 is obtained after the application of remedial measure.

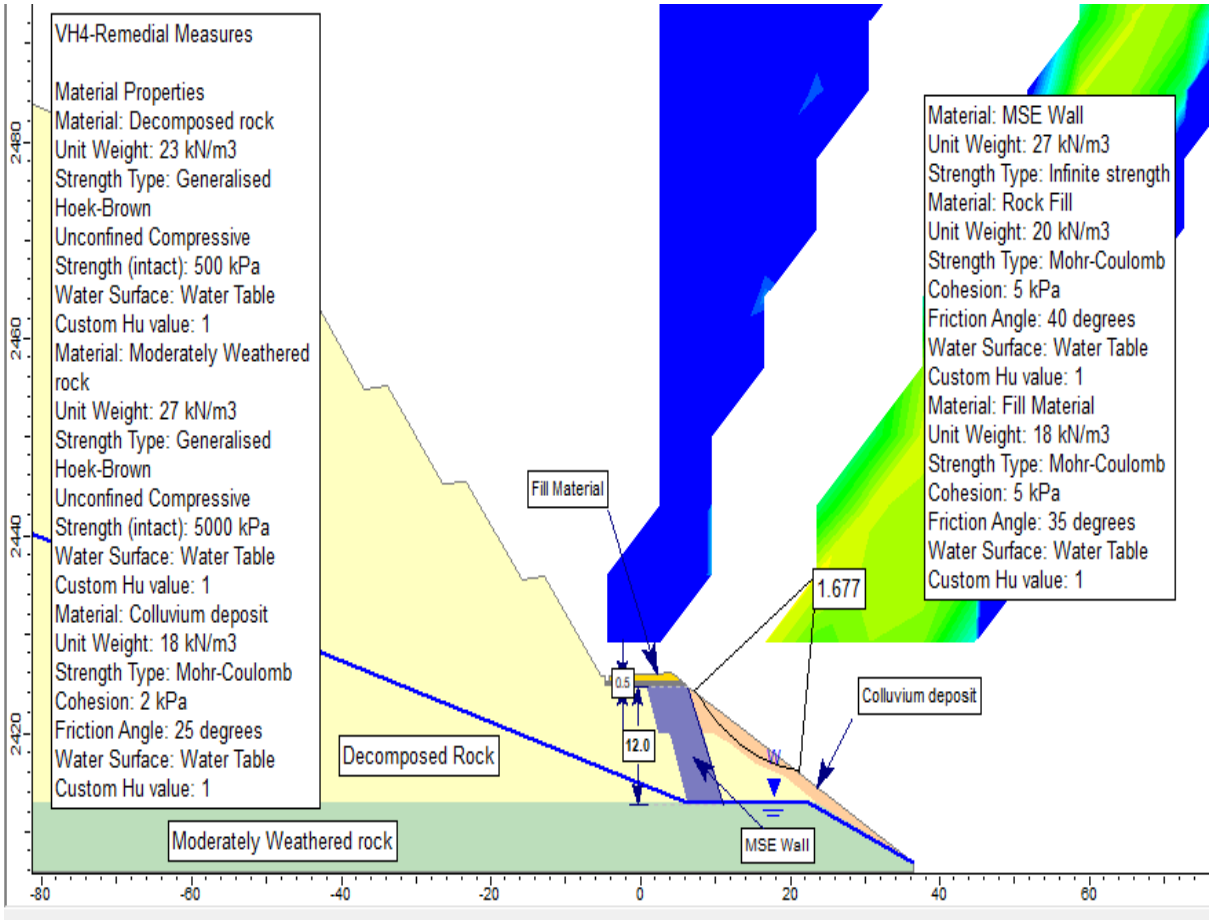

Figure 70: Stability analysis output with remedial measure along VH4, Km65+620

5.9 SYNTHESIS OF ALL THE RESULTS

This section summarizes the results of slope stability analysis using the LE method and landslide susceptibility maps produced using the FR and WoE models. To give a thorough grasp of the landslide prone areas along the study area, the results of statistical susceptibility modeling and deterministic stability analysis will be cross validated and interpreted.

The Frequency Ratio (FR) model identified the key factors as slope angle, lithology, and distance to roads. High FR values (greater than 2) were observed on steep, road cut slopes that had colluvial deposits and weathered tuff. The Weights of Evidence (WOE) analysis confirmed these findings by assigning strong positive weights to the same factor classes. It also showed that changes in land use and land cover had a greater effect, especially on bushland slopes with poor drainage. About 17.82% FR and 27.0% WOE of the study area was mapped as high to very high susceptibility. This highlights the strong spatial agreement between the FR and WOE models.

Table 15: Summary of stability analysis findings (FOS) values and failure types

Hazard Zone	Section	FoS (Dry)	FoS (wet)	Failure Type	Remarks
Moderate	M1, Km20+510	1.15	0.96	Shallow rotational	Stable under dry condition
	M2, Km35+220	1.11	0.94	Shallow rotational	Stable under dry condition
High	H1, km17+160	1.11	0.90	Deep rotational	Fails under wet condition
	H2, km63+400	1.06	0.88	Deep rotational	Near critical
Very High	VH1, km52+200	0.90	0.747	Deep rotational	Unstable
	VH2, km53+160	0.83	0.64	Complex	Very unstable
	VH3, km57+600	0.94	0.68	Rotational	Highly unstable
	VH4, km65+620	0.78	0.54	Translational	Requires urgent action

Limit Equilibrium Method (LEM) analysis of representative slopes within these statistically defined high and very high susceptibility zones showed factors of safety (FoS) ranging from 0.54 to 0.90 under saturated conditions. This confirms unstable conditions. In contrast, slopes in moderate susceptibility zones had FoS values of 0.94 to 0.96 under nearly saturated conditions (Table 15). The relationship between low FoS values and high susceptibility classes shows that combining FR, WOE, and LE methods improves the reliability of susceptibility maps. It also provides both spatial probability and a mechanical basis for targeted mitigation planning.

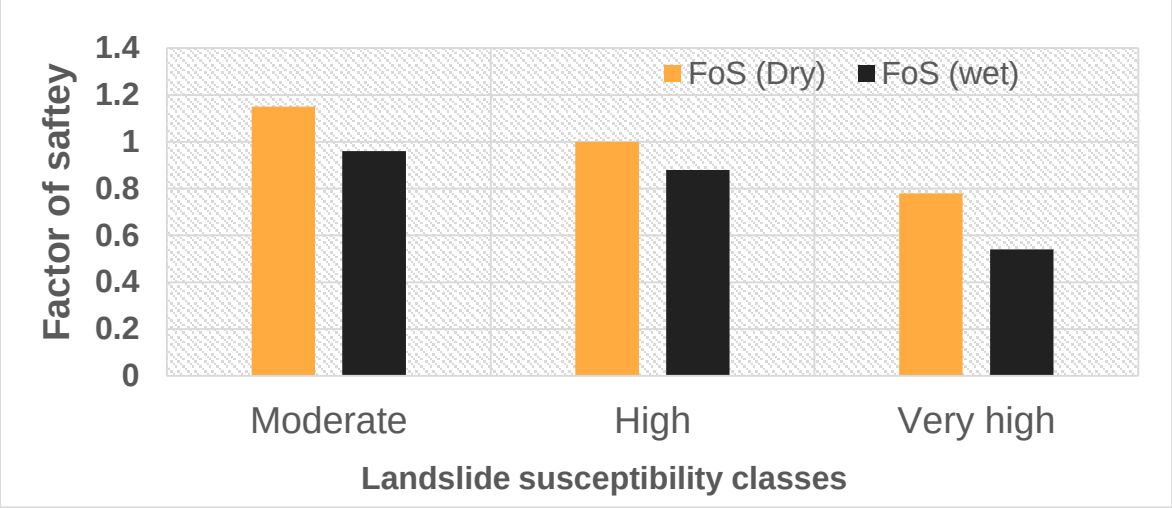

Figure 71: Synthesis of landslide susceptibility mapping and factor of safety

Therefore, the following mitigation measures were recommended based on the integrated results of the statistical susceptibility maps effectively identify where landslides are likely to occur, While LEM provides insight into why and under what conditions failure may happen. This combined analysis strengthens the confidence in both approaches and supports their

application in future mitigation planning, route selection, and hazard zoning along the project corridor.

Table 16: Summary of mitigation measures and respective FOS results

Hazard zone	**Slope section**	**Mitigation measures**	**Height, m**	**FoS**
Moderate	M1, Km20+510	Masonry retaining wall + drainage	7.0 m	1.82
	M2, Km35+220	Masonry retaining wall + drainage	6.0 m	1.54
High	H1, km17+160	Masonry retaining wall + drainage	8.5m	1.74
	H2, km63+400	Concrete retaining wall + drainage	12.0m	1.51
Very High	VH1, km52+200	Antislide pile + drainage	18.0m	1.61
	VH2, km53+160	Antislide pile + drainage	25.0m	1.81
	VH3, km57+600	Masonry retaining wall + drainage	9.0m	1.59
	VH4, km65+620	MSE wall + drainage	12.0m	1.67

Previous investigations along the study area have attempted mitigation measures such as gabion walls, retaining structures, and surface drainage systems. However, these interventions proved inadequate because active landslides were linked to unmapped old landslide bodies, the depths and geometries of failure surfaces were poorly understood, and surface and shallow groundwater conditions were not sufficiently characterized, leading to pore-water pressure build-up. In addition, unpaved roadside ditches triggered gully erosion, the local soil and rock properties were not adequately studied, and prolonged heavy rainfall further destabilized unconsolidated slopes. These shortcomings demonstrate that earlier efforts were largely reactive and based on incomplete understanding of the failure mechanisms.

Therefore, this study is designed to address these gaps by systematically identifying active and old landslides, analyzing failure surfaces through back-analysis and subsurface investigation, integrating hydrogeological assessments, and characterizing local soil and rock properties. By doing so, it aims to provide more reliable and site-specific recommendations for slope stabilization and drainage management that overcome the limitations of previous approaches.

6 CONCLUSION AND RECOMMENDATIONS

6.1 CONCLUSIONS

The study area was involved comprehensive literature review, geological and geotechnical assessments, and detailed site investigations. A geological map was generated using fieldwork, satellite imagery, and t 1: 50,000 geological maps of the Jimma Sheet, identifying dominant lithological units such as upper/middle/lower trachyte flows, basalt flows, and colluvial-alluvial deposits. Significant structural features such as NW-SE, NNW-SSE, and N-S trending faults and joint sets were also mapped, with joint dips ranging from shallow to steep inclinations. Soil samples were tested in the field and laboratory. Results revealed fine grained, highly plastic soils with natural moisture content between 22.8%–42.0%, and over 80% passing the 0.075 mm sieve. Plasticity indices ranged from 18.0% to 35.5%, and shear strength parameters (c = 5–38 kN/m², φ = 5–30°) indicated variable strength and poor subgrade conditions. Soils were classified as CH, CL, MH, and ML based on USCS soil classification suggesting that low engineering performance and landslide susceptibility.

The assessment of landslide inventory in the study area shows that the area is affected by debris/earth flow, debris/earth slide, gully erosion and pavement defects. The major conditioning factors and their corresponding subclasses were identified and prioritized during field traverses. By producing thematic maps each causative factors numerical values were assigned for each class and subclass using FR and WOE models. The final produced LSM from FR, the total area was categorized into the following susceptibility zones; (a) very Low (34.17% or 61.51 km²), (b) low (27.78% or 50.0 km²), (c) moderate (20.23% or 36.41 km²), (d) high (9.92% or 17.86 km²), and (e) very high (7.89% or 14.21 km²). on the other hand, the LSM derived from WOE resulted in the following categories: very low (26.1% or 47.2 km²), low (28.1% or 50.9 km²), moderate (21.7% or 39.2 km²), high (14.9% or 27.0 km²), and very high (9.20% or 16.6 km²). The LSM maps were validated using both the overlay method with landslide inventory and the ROC-AUC approach. Out of the 120 inventoried landslides, 70% were used for the overlay method, with 74.53% of the FR landslides falling in high and very high susceptibility zones, compared to 72.26% for the WoE method. Furthermore, the AUC values calculated for FR and WOE were 0.802 (80.2%) and 0.791 (79.1%), respectively.

Slope stability analyses, which revealed that the factor of safety (FoS) decreases from moderate to very high susceptibility zones. In moderate hazard zones, the FoS ranged from 1.11 to 1.15 when dry to 0.94 to 0.96 when saturated, indicating decreased stability. FoS values in high-

hazard zones ranged from 0.88 to 0.90 when saturated and from 1.06 to 1.11 when dry, indicating instability in both conditions. With FoS values between 0.78 and 0.94 (dry) and 0.54 and 0.94 (saturated), very high-hazard zones were the most unstable, supporting the high vulnerability shown on the susceptibility maps and highlights the vulnerability of highly plastic, moisture-sensitive soils, especially fat clays.

Appropriate remedial measures, including mechanically stabilized earth (MSE) walls, retaining walls, anti-slide piles, and integration with surface/subsurface drainage systems, were recommended based on failure mechanisms and verified through post-remedial stability analysis.

6.2 RECOMMENDATIONS

The Bonga – Felegeselam road is repeatedly affected by earth slides, debris flows, and asphalt cracking and bulging especially in saturated conditions i.e. during the summer season. To address this, it is recommended to remove failed masses, flatten steep slopes, and construct retaining structures that intercept slip surfaces. Proper backfilling of these structures is essential, and subsurface trench drains should be installed below the pavement to intercept water before it damages the road. Furthermore, road maintenance and siltation removal in the study area are not routine tasks and require significant attention.

The upper back slope material within the cut section and crossing drainages along most of the project road has poor resistance to erosion. Hence, emphasis should be given on how to effectively remove the rain water from the back slope.

In addition, using appropriate vegetation cover will help protect the back slope material from surface erosion by surface runoff. Additionally, constructing unlined furrow ditches should be avoided in order to minimize infiltration of the surface water in to the cut slopes and the collected water should be dissipated through lined chutes to the side ditches or wherever appropriate.

Further to this, the control of spoil disposal on the road side is of utmost concern, because it has been aggravating the condition of landslide and slope failures. Hence spoils should be regulated, ensuring materials are placed exclusively in geotechnically verified and environmentally approved sites.

Last but not least, all remedial measures shall be carried out during the dry season to prevent the reactivation and further aggravation of the landslide and slope failures.

However, the landslide inventory was largely based on field observations and Google Earth imagery; integration of high-resolution satellite data is recommended to improve spatial accuracy. Additionally, the limited number of soil samples may not fully represent the variability across the corridor. Future work should include more extensive subsurface investigations and real-time monitoring to capture the dynamic behavior of slopes and improve the reliability of mitigation strategies.

7 REFERENCES

Abay, A., & Barbieri, G. (2012). Landslide susceptibility and causative factors evaluation of the landslide area of Debresina, in the southwestern Afar escarpment, Ethiopia. Journal of Earth Science and Engineering, 2(3).

Abay, A., Barbieri, G., & Woldearegay, K. (2019). GIS-based Landslide Susceptibility Evaluation Using Analytical Hierarchy Process (AHP) Approach: The Case of Tarmaber District, Ethiopia. Momona Ethiopian Journal of Science, 11(1), 14. https://doi.org/10.4314/mejs.v11i1.2

Abbate, E., Bruni, P., & Sagri, M. (2015). Geology of Ethiopia: A review and geomorphological perspectives. Landscapes and Landforms of Ethiopia, 33–64.

Abebe, B., Dramis, F., Fubelli, G., Umer, M., & Asrat, A. (2010). Landslides in the Ethiopian highlands and the Rift margins. Journal of African Earth Sciences, 56(4), 131–138. https://doi.org/10.1016/j.jafrearsci.2009.06.006

Ahmed, B. (2015). Landslide susceptibility mapping using multi-criteria evaluation techniques in Chittagong Metropolitan Area, Bangladesh. Landslides, 12(6), 1077–1095. https://doi.org/10.1007/s10346-014-0521-x

Aleotti, P., & Chowdhury, R. (1999). Landslide hazard assessment: Summary review and new perspectives. Bulletin of Engineering Geology and the Environment, 58(1), 21–44. https://doi.org/10.1007/s100640050066

Ali, S., Biermanns, P., Haider, R., & Reicherter, K. (2019). Landslide susceptibility mapping by using a geographic information system (GIS) along the China–Pakistan Economic Corridor (Karakoram Highway), Pakistan. Natural Hazards and Earth System Sciences, 19(5), 999–1022. https://doi.org/10.5194/nhess-19-999-2019

Anbalagan, R. (1992). Landslide hazard evaluation and zonation mapping in mountainous terrain. Engineering Geology, 32(4), 269–277. https://doi.org/10.1016/0013-7952(92)90053-2

Asrat, A., Barbey, P., & Gleizes, G. (2001). The Precambrian geology of Ethiopia: A review. Africa Geoscience Review, 8(3/4), 271–288.

Atkinson, P. M., & Massari, R. (1998). GENERALISED LINEAR MODELLING OF SUSCEPTIBILITY TO LANDSLIDING IN THE CENTRAL APENNINES, ITALY. Computers & Geosciences, 24(4), 373–385. https://doi.org/10.1016/s0098-

3004(97)00117-9

Ayalew, L. (1999). The effect of seasonal rainfall on landslides in the highlands of Ethiopia. Bulletin of Engineering Geology and the Environment, 58, 9–19.

Ayalew, L., & Yamagishi, H. (2004). Slope failures in the Blue Nile basin, as seen from landscape evolution perspective. Geomorphology, 57(1–2), 95–116.

Ayalew, L., Yamagishi, H., & Ugawa, N. (2004). Landslide susceptibility mapping using GIS-based weighted linear combination, the case in Tsugawa area of Agano River, Niigata Prefecture, Japan. Landslides, 1, 73–81.

Aydin, A. (2009). ISRM Suggested method for determination of the Schmidt hammer rebound hardness: Revised version. International Journal of Rock Mechanics and Mining Sciences, 46(3), 627–634. https://doi.org/10.1016/j.ijrmms.2008.01.020

Ayele, A. (2017). Probabilistic seismic hazard analysis (PSHA) for Ethiopia and the neighboring region. Journal of African Earth Sciences, 134, 257–264. https://doi.org/10.1016/j.jafrearsci.2017.06.016

Ayele, A., Jacques, E., Kassim, M., Kidane, T., Omar, A., Tait, S., Nercessian, A., De Chabalier, J.-B., & King, G. (2007). The volcano–seismic crisis in Afar, Ethiopia, starting September 2005. Earth and Planetary Science Letters, 255(1–2), 177–187. https://doi.org/10.1016/j.epsl.2006.12.014

Ayenew, T., & Barbieri, G. (2005). Inventory of landslides and susceptibility mapping in the Dessie area, northern Ethiopia. Engineering Geology, 77(1–2), 1–15. https://doi.org/10.1016/j.enggeo.2004.07.002

Baeza, C., & Corominas, J. (2001). Assessment of shallow landslide susceptibility by means of multivariate statistical techniques. Earth Surface Processes and Landforms, 26(12), 1251–1263. https://doi.org/10.1002/esp.263

Barton, N., Lien, R., & Lunde, J. (1974). Engineering classification of rock masses for the design of tunnel support. Rock Mechanics Felsmechanik M�canique Des Roches, 6(4), 189–236. https://doi.org/10.1007/bf01239496

Basharat, M., Shah, H. R., & Hameed, N. (2016). Landslide susceptibility mapping using GIS and weighted overlay method: A case study from NW Himalayas, Pakistan. Arabian Journal of Geosciences, 9(4), 292. https://doi.org/10.1007/s12517-016-2308-y

Berhane, G., Gebrehiwot, A., & Abay, A. (2023). Landslide susceptibility mapping in the Adwa

Volcanic Mountain Plugs, Northern Ethiopia: A comparative analysis of frequency ratio and analytical hierarchy process methods. Geomatics, Natural Hazards and Risk, 14(1), 2281244. https://doi.org/10.1080/19475705.2023.2281244

Berhane, G., Kebede, M., Alfarah, N., Hagos, E., Grum, B., Giday, A., & Abera, T. (2020). Landslide susceptibility zonation mapping using GIS-based frequency ratio model with multi-class spatial data-sets in the Adwa-Adigrat Mountain chains, northern Ethiopia. Journal of African Earth Sciences, 164, 103795. https://doi.org/10.1016/j.jafrearsci.2020.103795

Bieniawski, Z. T. (1989). Engineering Rock Mass Classifications: A Complete Manual for Engineers and Geologists in Mining, Civil, and Petroleum Engineering. John Wiley & Sons.

Bobrowsky, P., VanDine, D., & Couture, R. (2014). Landslide Guidelines and Best Practices for Professional Engineers and Geoscientists. In G. Lollino, M. Arattano, M. Giardino, R. Oliveira, & S. Peppoloni (Eds.), Engineering Geology for Society and Territory—Volume 7 (pp. 229–232). Springer International Publishing.

Broeckx, J., Vanmaercke, M., Duchateau, R., & Poesen, J. (2017). A landslide susceptibility map of Africa. 27.

Caine, N. (1980). The Rainfall Intensity: Duration Control of Shallow Landslides and Debris Flows. Geografiska Annaler. Series A, Physical Geography, 62(1/2), 23. https://doi.org/10.2307/520449

Campbell, R. H. (1975). Soil slips, debris flows, and rainstorms in the Santa Monica Mountains and vicinity, southern California (Professional Paper). US Geological Survey. https://doi.org/10.3133/pp851

Capitani, M., Ribolini, A., & Bini, M. (2013). The slope aspect: A predisposing factor for landsliding? Comptes Rendus Geoscience, 345(11), 427–438. https://doi.org/10.1016/j.crte.2013.11.002

Carrara, A., BITELLI, G., & CARLA, R. (1997). Comparison of techniques for generating digital terrain models from contour lines. International Journal of Geographical Information Science, 11(5), 451–473. https://doi.org/10.1080/136588197242257

Çellek, S. (2020). Effect of the Slope Angle and Its Classification on Landslide. Copernicus GmbH. https://doi.org/10.5194/nhess-2020-87

Chau, K. T., Sze, Y. L., Fung, M. K., Wong, W. Y., Fong, E. L., & Chan, L. C. P. (2004). Landslide hazard analysis for Hong Kong using landslide inventory and GIS. Multidimensional Geospatial Technology for the Geosciences, 30(4), 429–443. https://doi.org/10.1016/j.cageo.2003.08.013

Chen, H., & Lee, C. F. (2003). A dynamic model for rainfall-induced landslides on natural slopes. Geomorphology, 51(4), 269–288. https://doi.org/10.1016/S0169-555X(02)00224-6

Chen, W., Zhang, S., Li, R., & Shahabi, H. (2018). Performance evaluation of the GIS-based data mining techniques of best-first decision tree, random forest, and naïve Bayes tree for landslide susceptibility modeling. Science of The Total Environment, 644, 1006–1018. https://doi.org/10.1016/j.scitotenv.2018.06.389

Choi, J.-H., Edwards, P., Ko, K., & Kim, Y.-S. (2016). Definition and classification of fault damage zones: A review and a new methodological approach. Earth-Science Reviews, 152, 70–87. https://doi.org/10.1016/j.earscirev.2015.11.006

Chung, C.-J. F., & Fabbri, A. G. (2003). Validation of Spatial Prediction Models for Landslide Hazard Mapping. Natural Hazards, 30(3), 451–472. https://doi.org/10.1023/B:NHAZ.0000007172.62651.2b

Coduto, D. P., Yeung, M.-C., & Kitch, W. A. (2011). Geotechnical engineering: Principles and practices (2nd ed). Pearson.

Cornforth. (2005). Landslides in Practice: Investigation, Analysis, and Remedial/Preventative Options in Soils. Wiley.Com.

Corominas, J., van Westen, C., Frattini, P., Cascini, L., Malet, J.-P., Fotopoulou, S., Catani, F., Van Den Eeckhaut, M., Mavrouli, O., Agliardi, F., Pitilakis, K., Winter, M. G., Pastor, M., Ferlisi, S., Tofani, V., Hervás, J., & Smith, J. T. (2014). Recommendations for the quantitative analysis of landslide risk. Bulletin of Engineering Geology and the Environment, 73(2), 209–263. https://doi.org/10.1007/s10064-013-0538-8

Crozier. (1986). Landslides: Causes, Consequences and Environment. London: Croom Helm Australia Pty. Ltd.

Crozier, M. J., & Glade, T. (2005). Landslide Hazard and Risk: Issues, Concepts and Approach. In T. Glade, M. Anderson, & M. J. Crozier (Eds.), Landslide Hazard and Risk (1st ed., pp. 1–40). Wiley. https://doi.org/10.1002/9780470012659.ch1

Cruden, D. M. (1991). A simple definition of a landslide. Bulletin of the International Association of Engineering Geology, 43(1), 27–29. https://doi.org/10.1007/bf02590167

Cruden & Varnes. (1996). Landslide types and processes (Vol. 247). transportation research board, US national academy of sciences.

Dahal, R. K., Hasegawa, S., Nonomura, A., Yamanaka, M., Dhakal, S., & Paudyal, P. (2008). Predictive modelling of rainfall-induced landslide hazard in the Lesser Himalaya of Nepal based on weights-of-evidence. Geomorphology, 102(3), 496–510. https://doi.org/10.1016/j.geomorph.2008.05.041

Dai, F. C., & Lee, C. F. (2001). Terrain-based mapping of landslide susceptibility using a geographical information system: A case study. Canadian Geotechnical Journal, 38(5), 911–923. https://doi.org/10.1139/t01-021

Dai, F. C., Lee, C. F., & Ngai, Y. Y. (2002). Landslide risk assessment and management: An overview. Engineering Geology, 64(1), 65–87. https://doi.org/10.1016/S0013-7952(01)00093-X

Davidson, D. (1983). The mechanism of feather pattern development in the chick: I. The time of determination of feather position. Development, 74(1), 245–259.

Deere, D. U. (1964). Rock Quality Designation (RQD) After Twenty Years.

Dubois, J.-M. M. (1987). Crozier, Michael J. (1986): Landslides: Causes, Consequences and Environment, Croom Helm, London, xvi + 252 p., 75 fig., 36 tabl., 14 x 22 cm, 25£. Géographie physique et Quaternaire, 41(3), 409. https://doi.org/10.7202/032702ar

Duncan, J. M. (1996). State of the Art: Limit Equilibrium and Finite-Element Analysis of Slopes. Journal of Geotechnical Engineering, 122(7), 577–596. https://doi.org/10.1061/(asce)0733-9410(1996)122:7(577)

Duncan, J. M. (2014). Soil Strength and Slope Stability (1st ed). John Wiley & Sons, Incorporated.

Duncan & Wright. (2005). Soil Strength and Slope Stability.

FAO. (1993). The state of food and agriculture. 1993.

Fell, R., Corominas, J., Bonnard, C., Cascini, L., Leroi, E., & Savage, W. Z. (2008). Guidelines for landslide susceptibility, hazard and risk zoning for land use planning. Landslide Susceptibility, Hazard and Risk Zoning for Land Use Planning, 102(3), 85–98. https://doi.org/10.1016/j.enggeo.2008.03.022

Fisseha, S., & Mewa, G. (2016). Road failure caused by landslide in north Ethiopia: A case study from Dedebit – Adi-Remets Road segment. Journal of African Earth Sciences, 118, 65–74. https://doi.org/10.1016/j.jafrearsci.2016.02.022

Fredlund, D. G., & Rahardjo, H. (1993). An overview of unsaturated soil behavior. Geotechnical Special Publication, 1–1.

Fumagalli, M. (2025). Rainfall-dependent susceptibility mapping for shallow landslides: Data-driven and physically-based modelling under climate change.

Gani, N. D., Abdelsalam, M. G., Gera, S., & Gani, M. R. (2009). Stratigraphic and structural evolution of the Blue Nile Basin, northwestern Ethiopian plateau. Geological Journal, 44(1), 30–56.

Gariano, S. L., & Guzzetti, F. (2016). Landslides in a changing climate. Earth-Science Reviews, 162, 227–252.

Gerra, S., & Hailemariam, M. (2000). Geology of The Nekemte Area. GSE.

Ghosh, S., van Westen, C. J., Carranza, E. J. M., Jetten, V. G., Cardinali, M., Rossi, M., & Guzzetti, F. (2012). Generating event-based landslide maps in a data-scarce Himalayan environment for estimating temporal and magnitude probabilities. Integration of Technologies for Landslide Monitoring and Quantitative Hazard Assessment, 128, 49–62. https://doi.org/10.1016/j.enggeo.2011.03.016

Gill, P., Stewart, K., Treasure, E., & Chadwick, B. (2008). Methods of data collection in qualitative research: Interviews and focus groups. British Dental Journal, 204(6), 291–295. https://doi.org/10.1038/bdj.2008.192

Griffiths, D. V., & Lane, P. A. (1999). Slope stability analysis by finite elements. Géotechnique, 49(3), 387–403. https://doi.org/10.1680/geot.1999.49.3.387

Guzzetti, F., Carrara, A., Cardinali, M., & Reichenbach, P. (1999). Landslide hazard evaluation: A review of current techniques and their application in a multi-scale study, Central Italy. Geomorphology, 31(1), 181–216. https://doi.org/10.1016/S0169-555X(99)00078-1

Guzzetti, F., Gariano, S. L., Peruccacci, S., Brunetti, M. T., & Melillo, M. (2022). Rainfall and landslide initiation. In Rainfall (pp. 427–450). Elsevier.

Guzzetti, F., Reichenbach, P., Ardizzone, F., Cardinali, M., & Galli, M. (2006). Estimating the quality of landslide susceptibility models. Geomorphology, 81(1), 166–184. https://doi.org/10.1016/j.geomorph.2006.04.007

Hailu, S., Deribew, K. T., Teferi, E., Moisa, M. B., Roba, Z. R., Dagne, S. S., & Woldetsadik, M. (2024). Spatial assessment employing fusion logistic regression and frequency ratio models to monitor landslide susceptibility in the upper Blue Nile basin of Ethiopia: Muger watershed. Environmental Systems Research, 13(1), 54.

Hearn, G. J. (2019). Slope hazards on the Ethiopian road network. Quarterly Journal of Engineering Geology and Hydrogeology, 52(3), 295–311. https://doi.org/10.1144/qjegh2018-058

Hoek, E., & Brown, E. T. (1980). Empirical strength criterion for rock masses. Journal of the Geotechnical Engineering Division, 106(9), 1013–1035.

Hosmer, D. W., & Lemeshow, S. (2000). Applied Logistic Regression (1st ed.). Wiley. https://doi.org/10.1002/0471722146

Howard, A. K. (1987). The revised ASTM standard on the description and identification of soils. Geotechnical Testing Journal, 10(4), 229–234.

Huabin, W., Gangjun, L., Weiya, X., & Gonghui, W. (2005). GIS-based landslide hazard assessment: An overview. Progress in Physical Geography: Earth and Environment, 29(4), 548–567. https://doi.org/10.1191/0309133305pp462ra

Huang, Y., Meng, L., & Ampuero, J.-P. (2012). A dynamic model of the frequency-dependent rupture process of the 2011 Tohoku-Oki earthquake. Earth, Planets and Space, 64(12), 1061–1066. https://doi.org/10.5047/eps.2012.05.011

Hungr, O., Leroueil, S., & Picarelli, L. (2014). The Varnes classification of landslide types, an update. Landslides, 11(2), 167–194. https://doi.org/10.1007/s10346-013-0436-y

Hutchinson. (1991). Periglacial and slope processes.: Vol. 7(1). Geological Society, London, Engineering Geology Special Publications.

Hutchinson, M. F. (1995). Interpolating mean rainfall using thin plate smoothing splines. International Journal of Geographical Information Systems, 9(4), 385–403. https://doi.org/10.1080/02693799508902045

Intarawichian, N., & Dasananda, S. (2010). ANALYTICAL HIERARCHY PROCESS FOR LANDSLIDE SUSCEPTIBILITY MAPPING IN LOWER MAE CHAEM WATERSHED, NORTHERN THAILAND. 7(3).

Kanungo, D. P., & Sharma, S. (2014). Rainfall thresholds for prediction of shallow landslides around Chamoli-Joshimath region, Garhwal Himalayas, India. Landslides, 11(4), 629–638. https://doi.org/10.1007/s10346-013-0438-9

Katz, O., Reches, Z., & Roegiers, J.-C. (2000). Evaluation of mechanical rock properties using a Schmidt Hammer. International Journal of Rock Mechanics and Mining Sciences, 37(4), 723–728. https://doi.org/10.1016/s1365-1609(00)00004-6

Kaur, N., Dhawan, M., Sharma, I., & Pati, P. K. (2016). Interdependency of Reactive Oxygen Species generating and scavenging system in salt sensitive and salt tolerant cultivars of

rice. BMC Plant Biology, 16(1), 131. https://doi.org/10.1186/s12870-016-0824-2

Kazmi, D., Qasim, S., Harahap, I. S. H., Baharom, S., Mehmood, M., Siddiqui, F. I., & Imran, M. (2017). Slope Remediation Techniques and Overview of Landslide Risk Management. Civil Engineering Journal, 3(3), 180–189. https://doi.org/10.28991/cej-2017-00000084

Kazmin, V. (1972). Granulites in Ethiopian basement. Nature Physical Science, 240(100), 90–92.

Kazmin, V., Shifferaw, A., & Balcha, T. (1978). The Ethiopian basement: Stratigraphy and possible manner of evolution. Geologische Rundschau, 67, 531–546.

Keefer, D. K. (2002). [No title found]. Surveys in Geophysics, 23(6), 473–510. https://doi.org/10.1023/a:1021274710840

Kieffer, B., Arndt, N., Lapierre, H., Bastien, F., Bosch, D., Pecher, A., Yirgu, G., Ayalew, D., Weis, D., & Jerram, D. A. (2004). Flood and shield basalts from Ethiopia: Magmas from the African superswell. Journal of Petrology, 45(4), 793–834.

Komac, M. (2006). A landslide susceptibility model using the Analytical Hierarchy Process method and multivariate statistics in perialpine Slovenia. Geomorphology, 74(1), 17–28. https://doi.org/10.1016/j.geomorph.2005.07.005

Kumar, R., & Anbalagan, R. (2015). Landslide susceptibility zonation in part of Tehri reservoir region using frequency ratio, fuzzy logic and GIS. Journal of Earth System Science, 124(2), 431–448. https://doi.org/10.1007/s12040-015-0536-2

Lee, S., & Min, K. (2001). Statistical analysis of landslide susceptibility at Yongin, Korea. Environmental Geology, 40(9), 1095–1113. https://doi.org/10.1007/s002540100310

Lee, S., & Pradhan, B. (2007). Landslide hazard mapping at Selangor, Malaysia using frequency ratio and logistic regression models. Landslides, 4(1), 33–41.

Lee, S., & Talib, J. A. (2005). Probabilistic landslide susceptibility and factor effect analysis. Environmental Geology, 47(7), 982–990. https://doi.org/10.1007/s00254-005-1228-z

Lee W. Abramson, Thomas S. Lee, & Sunil Sharma,. (2002). Slope Stability and Stabilization, (2nd ed.).

Manzo, G., Tofani, V., Segoni, S., Battistini, A., & Catani, F. (2013). Application of GIS Techniques for Landslide Susceptibility Assessment at Regional Scale. In C. Margottini, P. Canuti, & K. Sassa (Eds.), Landslide Science and Practice: Volume 1: Landslide Inventory and Susceptibility and Hazard Zoning (pp. 459–465). Springer Berlin Heidelberg. https://doi.org/10.1007/978-3-642-31325-7_59

McColl, S. T. (2022). Chapter 2—Landslide causes and triggers. In T. Davies, N. Rosser, & J. F. Shroder (Eds.), Landslide Hazards, Risks, and Disasters (Second Edition) (pp. 13–41). Elsevier. https://doi.org/10.1016/B978-0-12-818464-6.00011-1

Merla, G., Abbate, E., Azzaroli, A., Bruni, P., Canuti, P., Fazzuoli, M., Sagri, M., & Tacconi, P. (1979). A Geological Map of Ethiopia and Somalia: 1973; 1: 2.000. 000 and Comment with a Map of Major Landforms. Centro Stampa Firenze.

Meten, M., PrakashBhandary, N., & Yatabe, R. (2015). Effect of Landslide Factor

Combinations on the Prediction Accuracy of Landslide Susceptibility Maps in the Blue Nile Gorge of Central Ethiopia. Geoenvironmental Disasters, 2(1), 9. https://doi.org/10.1186/s40677-015-0016-7

Moeyersons, J., Nyssen, J., Van den Eeckhaut, M., Haile, M., Deckers, J., & Poesen, J. (2019). Mass Movements and Argilliturbation in Dogu'a Tembien. In J. Nyssen, M. Jacob, & A. Frankl (Eds.), Geo-trekking in Ethiopia's Tropical Mountains: The Dogu'a Tembien District (pp. 303–317). Springer International Publishing. https://doi.org/10.1007/978-3-030-04955-3_20

Mohr, P. (1963). Occurrence of Karroo system sediments in Ethiopia. Nature, 199(4898), 1086–1086.

Monteleone, S., & Sabatino, M. (2014). Hydrogeological hazards and weather events: Triggering and evolution of shallow landslides. International Soil and Water Conservation Research, 2(2), 23–29. https://doi.org/10.1016/S2095-6339(15)30003-4

Moradi, S., & Rezaei, M. (2014). A GIS-based comparative study of the analytic hierarchy process, bivariate statistics and frequency ratio methods for landslide susceptibility mapping in part of the Tehran metropolis, Iran.

Nechyba, M., Vařilová, Z., Kotva, P., Kropáček, J., & Zvelebil, J. (2016). Combined methods for risk assessment of mass movement and erosion susceptibility in the Ethiopian highlands. AUC GEOGRAPHICA, 51(1), 17–28. https://doi.org/10.14712/23361980.2016.2

Nyssen, J., Poesen, J., & Deckers, J. (2009). Land degradation and soil and water conservation in tropical highlands. Contains Papers from HighLand 2006: Land Degradation and Soil and Water Conservation in Tropical Highlands, Mekelle, Ethiopia, 21-25 September 2006, 103(2), 197–202. https://doi.org/10.1016/j.still.2008.08.002

Nyssen, J., Poesen, J., Moeyersons, J., Luyten, E., Veyret-Picot, M., Deckers, J., Haile, M., & Govers, G. (2002). Impact of road building on gully erosion risk: A case study from the northern Ethiopian highlands. Earth Surface Processes and Landforms: The Journal of the British Geomorphological Research Group, 27(12), 1267–1283.

Pal, S. C., & Chowdhuri, I. (2019). GIS-based spatial prediction of landslide susceptibility using frequency ratio model of Lachung River basin, North Sikkim, India. SN Applied Sciences, 1(5), 416. https://doi.org/10.1007/s42452-019-0422-7

Pardeshi, S. D., Autade, S. E., & Pardeshi, S. S. (2013). Landslide hazard assessment: Recent trends and techniques. SpringerPlus, 2(1), 523. https://doi.org/10.1186/2193-1801-2-523

Petley, D. (2012). Global patterns of loss of life from landslides. Geology, 40(10), 927–930.

Polemio, M., & Petrucci, O. (2012). The occurrence of floods and the role of climate variations from 1880 in Calabria (Southern Italy). Natural Hazards and Earth System Sciences, 12(1), 129–142. https://doi.org/10.5194/nhess-12-129-2012

Popescu, M. (2001). A suggested method for reporting landslide remedial measures. Bulletin of Engineering Geology and the Environment, 60(1), 69–74. https://doi.org/10.1007/s100640000084

Pourghasemi, H. R., Jirandeh, A. G., Pradhan, B., Xu, C., & Gokceoglu, C. (2013). Landslide susceptibility mapping using support vector machine and GIS at the Golestan Province, Iran. Journal of Earth System Science, 122(2), 349–369. https://doi.org/10.1007/s12040-013-0282-2

Raghuvanshi, T. K., Ibrahim, J., & Ayalew, D. (2014). Slope stability susceptibility evaluation parameter (SSEP) rating scheme – An approach for landslide hazard zonation. Special Volume of the 24th Colloquium of African Geology, 99, 595–612. https://doi.org/10.1016/j.jafrearsci.2014.05.004

Redshaw, P., Dijkstra, T., Free, M., Jordan, C., Morley, A., & Fraser, S. (2017). Landslide risk assessment for the built environment in sub-Saharan Africa. 5–12.

Regmi, N. R., Giardino, J. R., & Vitek, J. D. (2010). Assessing susceptibility to landslides: Using models to understand observed changes in slopes. Geomorphology, 122(1–2), 25–38.

Reichenbach, P., Busca, C., Mondini, A. C., & Rossi, M. (2014). The Influence of Land Use Change on Landslide Susceptibility Zonation: The Briga Catchment Test Site (Messina, Italy). Environmental Management, 54(6), 1372–1384. https://doi.org/10.1007/s00267-014-0357-0

Rengers, F. K., McGuire, L. A., Kean, J. W., Staley, D. M., & Hobley, D. E. J. (2016). Model simulations of flood and debris flow timing in steep catchments after wildfire. Water Resources Research, 52(8), 6041–6061. https://doi.org/10.1002/2015wr018176

Roslee, R., Jamaludin, T. A., & Simon, N. (2017). Landslide Vulnerability Assessment (LVAs): A Case Study from Kota Kinabalu, Sabah, Malaysia. Indonesian Journal on Geoscience, 4(1), 49–59. https://doi.org/10.17014/ijog.4.1.49-59

Rotaru, A., Oajdea, D., & Răileanu, P. (2007). Analysis of the Landslide Movements. 1(3).

Saaty. (1980). The analytic hierarchy process: Planning, priority setting, resource allocation. McGraw-Hill International Book Co.

Saaty, T. L. (2008). Decision making with the analytic hierarchy process. International Journal of Services Sciences, 1(1), 83. https://doi.org/10.1504/ijssci.2008.017590

Saha, A. K., Gupta, R. P., & Arora, M. K. (2002). GIS-based Landslide Hazard Zonation in the Bhagirathi (Ganga) Valley, Himalayas. International Journal of Remote Sensing, 23(2), 357–369. https://doi.org/10.1080/01431160010014260

Seyed, A. H., Reza, L., Majid, L., Ataollah, K., & Aidin, P. (2011). The effect of terrain factors on landslide features along forest road. African Journal of Biotechnology, 10(64), 14108–14115. https://doi.org/10.5897/ajb11.856

Sharp. (1958). Mudflow of 1941 at Wrightwood, southern California. (5th ed., Vol. 64). Geological Society of America Bulletin.

Sidle, R. C., & Ochiai, H. (2006). Landslides: Processes, Prediction, and Land Use (1st ed., Vol. 18). Wiley.

Spall, H. (1981). Earthquake History of Ethiopia and the Horn of Africa. Bulletin of the

Seismological Society of America, 71(2), 573–574. https://doi.org/10.1785/BSSA0710020573

Stokes, A., Douglas, G. B., Fourcaud, T., Giadrossich, F., Gillies, C., Hubble, T., Kim, J. H., Loades, K. W., Mao, Z., McIvor, I. R., Mickovski, S. B., Mitchell, S., Osman, N., Phillips, C., Poesen, J., Polster, D., Preti, F., Raymond, P., Rey, F., … Walker, L. R. (2014). Ecological mitigation of hillslope instability: Ten key issues facing researchers and practitioners. Plant and Soil, 377(1), 1–23. https://doi.org/10.1007/s11104-014-2044-6

Terranova, O., Antronico, L., & Gullà, G. (2007). Landslide triggering scenarios in homogeneous geological contexts: The area surrounding Acri (Calabria, Italy). Geomorphology, 87(4), 250–267. https://doi.org/10.1016/j.geomorph.2006.09.021

Terzaghi, K. (1950). Mechanism of Landslides. In S. Paige (Ed.), Application of Geology to Engineering Practice (p. 0). Geological Society of America. https://doi.org/10.1130/Berkey.1950.83

Terzaghi, K. (1953). Fifty Years of Subsoil Exploration. Harvard University. https://books.google.com.et/books?id=gIEJMMpa0zgC

Tsige, D., Quezon, E. T., & Woldearegay, K. (2017). Geotechnical conditions and stability analysis of landslide prone area: A case study in Bonga town, South-Western Ethiopia. International Journal of Scientific & Engineering Research, 8(4), 239–248.

Turner, A. K., & Schuster, R. L. (1996). Landslides: Investigation and Mitigation. National Academy Press.

UNDRR. (2025). Global Assessment Report. https://www.undrr.org/gar/gar2025

USGS. (2004). Landslide Types and Processes. https://pubs.usgs.gov/fs/2004/3072/

van Westen, C. J., Castellanos, E., & Kuriakose, S. L. (2008). Spatial data for landslide susceptibility, hazard, and vulnerability assessment: An overview. Landslide Susceptibility, Hazard and Risk Zoning for Land Use Planning, 102(3), 112–131. https://doi.org/10.1016/j.enggeo.2008.03.010

Van Westen, C. J., Rengers, N., & Soeters, R. (2003). Use of Geomorphological Information in Indirect Landslide Susceptibility Assessment. Natural Hazards, 30(3), 399–419. https://doi.org/10.1023/B:NHAZ.0000007097.42735.9e

Varnes. (1978). Slope movement types and processes. Special report (Vol. 176).

Varnes, D. (1984). Landslide hazard zonation: A review of principles and practice.

Wang, X., & Niu, R. (2010). Landslide intelligent prediction using object-oriented method. Soil Dynamics and Earthquake Engineering, 30(12), 1478–1486. https://doi.org/10.1016/j.soildyn.2010.06.017

Woldearegay, K. (2013). Review of the occurrences and influencing factors of landslides in the highlands of Ethiopia: With implications for infrastructural development. Momona Ethiopian Journal of Science, 5(1), 3–31.

Woldearegay, K. (2025). Characteristics of Landslides Affecting Road Networks in Ethiopia: Evidence from 25 Years Research, Practice and Documentation. Progress in Landslide

Research and Technology, Volume 3 Issue 2, 2024, 359–373. https://doi.org/10.1007/978-3-031-72736-8_25

Woldearegay, K., Riedmueller, G., Schubert, W., & Mogessie, A. (2004). Controlling parameters and failure mechanisms of a large-scale landslide in Ethiopia. Felsbau, 22(3), 46–55.

Woldearegay, K., Schubert, W., Klima, K., & Mogessie, A. (2005, May 31). Landslide hazards mitigation strategies in the northern highlands of Ethiopia.: International Conference on Landslide Risk Management.

Wu & Sidel. (1995). A distributed slope stability model for steep forested basins. 31, 2097-2110,

Wyllie, D. C., & Mah, C. (2004). Rock Slope Engineering: Fourth Edition. CRC Press.

Yalcin, A. (2008). GIS-based landslide susceptibility mapping using analytical hierarchy process and bivariate statistics in Ardesen (Turkey): Comparisons of results and confirmations. CATENA, 72(1), 1–12. https://doi.org/10.1016/j.catena.2007.01.003

Yalcin, A., Reis, S., Aydinoglu, A. C., & Yomralioglu, T. (2011). A GIS-based comparative study of frequency ratio, analytical hierarchy process, bivariate statistics and logistics regression methods for landslide susceptibility mapping in Trabzon, NE Turkey. CATENA, 85(3), 274–287. https://doi.org/10.1016/j.catena.2011.01.014

Yermukhanbetov, K., Yazitova, A., & Yagiz, S. (2021). Comparison of strength-based rock brittleness indices with the brittleness index measured via Yagiz's approaches. IOP Conference Series: Earth and Environmental Science, 833(1), 012038. https://doi.org/10.1088/1755-1315/833/1/012038

Zhou, G. G. D., Cui, P., Chen, H. Y., Zhu, X. H., Tang, J. B., & Sun, Q. C. (2013). Experimental study on cascading landslide dam failures by upstream flows. Landslides, 10(5), 633–643. https://doi.org/10.1007/s10346-012-0352-6

8 APPENDICES

8.1 APPENDIX 1: LANDSLIDE INVENTORY DATA

Table 17: Landslide Inventory Data Sheet

ID	Easting [m]	Northing [m]	Area [Sq.m]	Size	Type	Lithology
L001	201283.70	796595.41	368.86	Small	Earth Slide	Middle Trachyte
L002	201428.94	796282.76	1874.85	Small	Earth Slide	Middle Trachyte
L003	201626.16	794572.83	5240.47	Medium	Earth Slide	Upper Trachyte
L004	202580.31	793207.76	5338.73	Medium	Earth Slide	Upper Trachyte
L005	201965.94	796801.32	2077.86	Medium	Earth Slide	Middle Trachyte
L006	202263.42	795699.86	892.92	Small	Earth Slide	Upper Trachyte
L007	203419.96	795923.03	972.04	Small	Earth Slide	Upper Trachyte
L008	202977.68	794458.10	3687.49	Medium	Earth Slide	Upper Trachyte
L009	203145.26	794107.93	914.32	Small	Debris Slide	Upper Trachyte
L010	203313.60	794021.92	16048.88	Medium	Earth Slide	Upper Trachyte
L011	203446.08	793909.06	6724.52	Medium	Earth Slide	Upper Trachyte
L012	203537.02	793929.49	2356.33	Medium	Earth Slide	Upper Trachyte
L013	204058.65	794464.39	27904.52	Large	Earth Slide	Upper Trachyte
L014	203553.44	793614.37	1679.25	Small	Earth Slide	Upper Trachyte
L015	203559.26	793545.81	779.80	Small	Earth Slide	Upper Trachyte
L016	203476.44	793524.38	5242.90	Medium	Debris Flow	Upper Trachyte
L017	204386.00	793105.07	120542.98	Large	Earth Slide	Colluvium deposit
L018	205070.11	792546.37	7385.72	Medium	Earth Slide	Upper Trachyte
L019	204943.44	792768.63	5281.87	Medium	Earth Slide	Upper Trachyte
L020	205277.93	792368.04	15006.77	Medium	Debris Flow	Upper Trachyte
L021	205194.92	791180.23	40940.21	Large	Debris Flow	Upper Trachyte
L022	203695.71	791781.38	27592.24	Large	Debris Flow	Alluvial deposit
L023	206817.44	793292.60	55004.77	Large	Earth Slide	Upper Trachyte
L024	206251.08	791529.13	2055.03	Medium	Earth Slide	Upper Trachyte
L025	205955.92	789706.18	70978.48	Large	Debris Flow	Upper Trachyte
L026	207306.77	788812.14	19112.19	Medium	Debris Flow	Upper Trachyte
L027	207444.26	789623.26	66090.63	Large	Earth Slide	Upper Trachyte
L028	209271.53	789099.42	7341.11	Medium	Earth Slide	Lower Trachyte
L029	208703.10	790728.32	6515.71	Medium	Debris Flow	Lower Trachyte
L030	209842.66	787647.54	2099.28	Medium	Debris Flow	Lower Trachyte
L031	207071.83	787311.64	863.96	Small	Earth Slide	Upper Trachyte
L032	207778.95	788293.45	1129.99	Small	Earth Slide	Upper Trachyte
L033	209836.07	788136.82	363.13	Small	Earth Slide	Lower Trachyte
L034	210444.40	788158.59	1158.28	Small	Earth Slide	Lower Trachyte
L035	209878.91	785466.11	1418.89	Small	Earth Slide	Lower Trachyte
L036	209998.45	785624.45	1090.86	Small	Earth Slide	Lower Trachyte
L037	210305.87	786726.54	575.02	Small	Debris Flow	Lower Trachyte
L038	211406.43	786390.35	1288.39	Small	Debris Flow	Lower Trachyte
L039	210464.22	787743.59	528.92	Small	Earth Slide	Lower Trachyte
L040	210934.94	788062.29	3194.23	Medium	Earth Slide	Alluvial deposit
L041	211381.01	788681.06	607.27	Small	Debris Flow	Alluvial deposit
L042	211878.65	789430.17	966.65	Small	Debris Flow	Lower Trachyte

ID	Easting [m]	Northing [m]	Area [Sq.m]	Size	Type	Lithology
L043	209995.07	788317.87	3579.35	Medium	Earth Slide	Lower Trachyte
L044	211177.08	788107.76	2659.27	Medium	Earth Slide	Lower Trachyte
L045	212180.45	788183.29	11343.58	Medium	Earth Slide	Lower Trachyte
L046	212074.81	788344.72	7559.37	Medium	Earth Slide	Lower Trachyte
L047	212262.94	788013.60	1885.80	Small	Earth Slide	Lower Trachyte
L048	212267.79	787821.30	2628.53	Medium	Creeping	Lower Trachyte
L049	212488.72	787527.59	440.74	Small	Earth Slide	Lower Trachyte
L050	213990.72	789061.05	1305.95	Small	Debris Flow	Lower Trachyte
L051	214839.04	788750.44	826.28	Small	Debris Flow	Alluvial deposit
L052	215005.67	788673.83	241.88	Small	Debris Flow	Alluvial deposit
L053	216216.40	789096.21	406.18	Small	Debris Flow	Alluvial deposit
L054	213182.76	787418.47	6613.83	Medium	Creeping	Lower Trachyte
L055	213118.31	787581.51	7603.25	Medium	Debris Flow	Lower Trachyte
L056	213285.24	787592.95	1098.69	Small	Debris Slide	Lower Trachyte
L057	214283.02	787866.68	3421.49	Medium	Debris Flow	Lower Trachyte
L058	214709.47	787529.61	6074.59	Medium	Debris Flow	Lower Trachyte
L059	214705.42	787352.67	4334.84	Medium	Earth Slide	Lower Trachyte
L060	215685.14	787219.59	11475.49	Medium	Debris Flow	Lower Trachyte
L061	216023.46	787272.95	735.47	Small	Debris Slide	Lower Trachyte
L062	216533.26	787581.59	11975.06	Medium	Debris Flow	Lower Trachyte
L063	216743.01	787372.24	5387.85	Medium	Debris Slide	Lower Trachyte
L064	218102.86	787229.42	21905.51	Large	Debris Slide	Lower Trachyte
L065	218256.95	789616.40	389.20	Small	Earth Slide	Alluvial deposit
L066	219414.73	789966.74	10744.43	Medium	Earth Slide	Alluvial deposit
L067	218271.49	788524.33	1114.55	Small	Debris Flow	Alluvial deposit
L068	217019.17	789282.84	1847.89	Small	Debris Flow	Lower Trachyte
L069	217706.98	786290.33	11860.27	Medium	Complex	Lower Trachyte
L070	218020.58	786372.26	1382.79	Small	Debris Flow	Lower Trachyte
L071	218620.47	786258.46	3335.43	Medium	Debris Flow	Lower Trachyte
L072	216264.37	786097.24	2383.43	Medium	Complex	Lower Trachyte
L073	220936.86	786069.04	1504.65	Small	Earth Slide	Lower Trachyte
L074	221116.43	785959.42	6299.87	Medium	Complex	Lower Trachyte
L075	221303.78	785322.50	2089.86	Medium	Earth Slide	Lower Trachyte
L076	221706.69	784532.23	1283.63	Small	Earth Slide	Lower Trachyte
L077	222343.87	783041.35	1257.87	Small	Earth Slide	Upper Trachyte
L078	222636.50	783151.05	417.45	Small	Debris Flow	Upper Trachyte
L079	222526.11	785259.70	2529.70	Medium	Earth Slide	Upper Trachyte
L080	222749.24	785175.47	14034.40	Medium	Complex	Upper Trachyte
L081	223119.23	784868.65	3564.49	Medium	Earth Slide	Upper Trachyte
L082	223204.79	785109.50	1006.51	Small	Debris Flow	Upper Trachyte
L083	223615.54	784972.47	13545.31	Medium	Earth Slide	Upper Trachyte
L084	224055.78	785351.12	3584.57	Medium	Debris Flow	Upper Trachyte
L085	223865.15	784876.85	2769.30	Medium	Earth Slide	Upper Trachyte
L086	223986.87	784712.63	8002.62	Medium	Earth Slide	Upper Trachyte
L087	224158.76	784799.50	9918.73	Medium	Complex	Upper Trachyte
L088	224319.69	784788.93	11174.51	Medium	Complex	Upper Trachyte
L089	224452.34	784904.71	27800.72	Large	Complex	Colluvium deposit
L090	224548.61	785244.41	7671.82	Medium	Debris Flow	Colluvium deposit

ID	Easting [m]	Northing [m]	Area [Sq.m]	Size	Type	Lithology
L091	224283.14	784383.22	5198.31	Medium	Debris Flow	Colluvium deposit
L092	224911.00	783761.59	1729.24	Small	Debris Flow	Middle basalt
L093	224973.21	783839.83	2850.10	Medium	Debris Flow	Middle basalt
L094	224850.40	783687.89	1751.75	Small	Debris Flow	Middle basalt
L095	224675.95	783522.05	4717.42	Medium	Debris Flow	Upper Trachyte
L096	224565.41	783473.18	2349.35	Medium	Debris Flow	Upper Trachyte
L097	224510.22	783339.40	2185.93	Medium	Debris Flow	Upper Trachyte
L098	225100.75	782724.30	3615.88	Medium	Complex	Middle basalt
L099	223889.42	782548.87	2512.46	Medium	Debris Flow	Upper Trachyte
L100	223857.11	783393.61	3474.72	Medium	Debris Flow	Colluvium deposit
L101	223653.87	783608.03	3159.82	Medium	Debris Flow	Upper Trachyte
L102	223503.29	782799.77	10372.42	Medium	Complex	Upper Trachyte
L103	223091.73	781765.23	9240.99	Medium	Debris Flow	Upper Trachyte
L104	219419.87	784921.12	6004.24	Medium	Earth Slide	Lower Trachyte
L105	217548.26	784940.21	6918.81	Medium	Complex	Alluvial deposit
L106	226767.42	784414.92	609.54	Small	Debris Flow	Alluvial deposit
L107	226632.10	784712.66	1472.47	Small	Debris Flow	Alluvial deposit
L108	226574.78	784745.67	615.95	Small	Debris Flow	Alluvial deposit
L109	226315.52	784739.61	285.40	Small	Earth Slide	Middle basalt
L110	225510.90	786337.45	10336.61	Medium	Debris Flow	Colluvium deposit
L111	225466.88	786038.39	2905.95	Medium	Debris Flow	Upper Trachyte
L112	225613.75	786124.53	3959.54	Medium	Debris Flow	Colluvium deposit
L113	225305.58	786256.53	6346.17	Medium	Debris Flow	Upper Trachyte
L114	224994.54	786020.36	3903.99	Medium	Debris Flow	Colluvium deposit
L115	225895.73	786176.01	25816.22	Large	Debris Flow	Upper Trachyte
L116	225860.40	786515.76	6032.22	Medium	Debris Flow	Upper Trachyte
L117	225935.34	786658.77	859.27	Small	Debris Flow	Upper Trachyte
L118	226358.65	786565.37	19527.50	Medium	Debris Flow	Colluvium deposit
L119	226902.80	786697.46	4549.00	Medium	Earth Slide	Upper Trachyte
L120	228344.57	787008.94	6519.03	Medium	Debris Flow	Upper Trachyte

8.2 APPENDIX 2: DISCONTINUITY DATA

Table 18: Discontinuity Data

Chainage, km	Coordinates			Joint Sets	Orientations (Deg.)		
	Easting, m	Northing, m	Elevation, m		Strike	Dip	Dip direction
57+600	794048.51	794048.51	2438	Set-1	60	45	330
				Set-2	250	30	340
63+400	794048.51	794048.51	2494	Set-1	110	40	200
				Set-2	300	40	210
				Set-3	140	45	230
65+620	784908.6	784908.6	2412	Set-1	240	85	330
				Set-2	160	75	250

8.3 APPENDIX 3: CLIMATE DATA

Table 19: Climate data (Mean Monthly & Mean Annual Rainfall)

Stations		Months												MARF
	Year	Jan	Feb	Mar	Apr	May	Jun	Jul	Aug	Sep	Oct	Nov	Dec	
Amaya	**2000**	9.7	12.7	47.7	177.1	198.6	117.0	246.3	218.5	157.3	214.7	39.7	21.2	1460.6
	2001	19.8	42.7	149.4	196.8	244.3	215.6	260.2	212.8	237.4	163.8	40.2	17.7	1800.6
	2002	73.9	19.0	206.6	129.3	205.9	169.7	171.1	178.8	137.3	146.3	20.0	134.5	1592.4
	2003	46.3	79.5	109.9	140.9	116.4	236.6	239.8	324.1	229.0	114.1	49.7	30.2	1716.5
	2004	88.1	42.7	74.8	184.8	222.7	154.6	228.7	258.4	184.3	190.5	78.3	51.2	1759.1
	2005	37.4	16.8	209.2	188.0	344.5	154.1	274.9	186.7	210.0	192.4	68.1	6.0	1887.9
	2006	21.3	102.2	206.1	190.6	254.9	194.1	230.2	327.3	153.1	237.2	77.2	101.2	2095.3
	2007	66.1	61.1	160.5	174.0	221.6	185.0	275.5	212.4	273.4	126.9	20.8	6.5	1783.7
	2008	37.6	35.6	54.0	177.6	269.5	169.2	276.3	269.1	208.2	252.8	99.4	19.8	1869.0
	2009	53.6	48.4	113.1	161.5	175.3	146.7	186.4	225.7	133.4	231.5	53.9	70.0	1599.5
	2010	34.1	121.0	191.1	155.6	276.7	205.9	216.1	212.2	236.1	78.9	43.2	20.1	1791.0
	2011	14.6	29.1	107.5	198.8	339.4	210.5	238.9	276.4	263.1	81.2	185.1	16.5	1961.1
	2012	10.4	18.3	82.2	213.7	173.1	190.5	310.5	198.1	259.3	72.0	89.6	20.5	1638.4
	2013	46.0	39.0	163.4	223.9	204.0	179.8	244.7	278.3	284.2	175.5	128.6	6.8	1974.2
	2014	14.6	54.2	221.5	289.2	374.2	143.5	174.6	309.4	262.7	254.3	73.6	21.4	2193.3
	2015	30.1	34.2	111.5	244.7	284.3	228.7	229.6	180.8	184.7	209.5	141.0	54.8	1934.0
	2016	17.4	43.5	73.1	250.0	234.7	162.1	180.3	216.8	109.8	213.9	59.2	17.0	1577.7
	2017	12.0	186.1	147.8	141.7	240.3	144.2	226.7	192.3	293.1	280.5	81.9	10.1	1956.8
	2018	9.7	179.3	94.3	336.1	279.7	192.1	129.7	258.3	155.6	119.3	77.4	24.7	1856.2
	2019	8.0	102.2	201.1	282.2	355.1	287.9	338.0	269.3	197.1	292.7	171.7	68.9	2574.2
	2020	53.2	133.8	183.0	185.0	221.8	178.7	198.5	268.2	193.8	125.9	55.9	25.3	1823.2
	2021	15.2	70.9	42.8	213.8	289.3	134.4	195.4	240.5	262.3	113.7	14.5	42.0	1635.0

	2022	39.0	55.0	86.3	199.4	172.2	134.2	167.3	218.9	192.7	191.2	47.3	43.6	1547.1
	2023	14.3	36.3	220.1	316.0	276.0	158.1	179.6	172.0	271.8	364.5	213.4	33.6	2255.7
	MMRF	**33.6**	**68.0**	**141.6**	**216.1**	**259.8**	**186.7**	**235.6**	**248.1**	**221.3**	**193.2**	**83.9**	**37.5**	**2108.7**
Bonga	**Year**	**Jan**	**Feb**	**Mar**	**Apr**	**May**	**Jun**	**Jul**	**Aug**	**Sep**	**Oct**	**Nov**	**Dec**	**MARF**
	2000	15.5	13.9	52.9	178.6	221.8	129.2	177.3	136.2	163.7	176.4	92.4	34.3	1392.2
	2001	19.2	76.4	143.8	195.0	228.2	204.0	242.2	206.7	169.7	154.3	81.9	36.4	1757.8
	2002	54.8	24.5	155.4	173.7	150.0	194.5	129.5	149.4	123.1	163.9	45.7	192.3	1556.8
	2003	44.9	65.7	128.2	161.5	80.8	248.8	162.2	215.2	222.2	127.7	112.9	60.4	1630.6
	2004	88.2	27.7	68.8	167.7	184.8	168.2	198.9	185.7	217.8	125.0	166.0	90.1	1688.7
	2005	27.1	18.1	176.1	177.6	229.4	170.3	252.7	161.6	204.9	153.8	101.8	12.8	1686.1
	2006	29.5	91.6	205.8	165.5	221.0	215.4	226.9	221.0	152.3	182.5	148.5	120.6	1980.7
	2007	57.1	77.7	152.9	163.3	227.5	177.0	206.9	164.6	247.4	102.7	71.4	13.4	1661.8
	2008	71.7	65.7	63.4	240.3	225.6	200.6	190.8	213.3	177.5	182.4	116.2	50.2	1797.5
	2009	72.0	57.4	155.9	205.0	180.0	186.9	134.3	166.2	168.6	183.0	100.3	95.9	1705.7
	2010	42.9	129.9	169.6	174.9	255.3	231.7	178.2	169.0	225.7	72.4	74.9	53.8	1778.2
	2011	22.8	33.0	86.9	218.2	302.6	252.9	228.3	210.3	273.2	89.8	176.5	38.8	1933.2
	2012	16.2	17.2	91.6	193.7	174.7	225.9	222.6	177.7	205.7	101.6	164.2	60.2	1651.2
	2013	41.8	56.3	118.0	163.3	259.4	163.8	202.2	196.8	226.7	137.1	184.2	11.2	1761.0
	2014	21.9	61.8	179.7	320.8	271.8	162.1	177.9	208.7	192.8	203.4	112.9	29.8	1943.6
	2015	40.1	53.5	132.8	233.7	247.6	217.3	200.1	130.5	183.1	171.7	161.1	72.7	1844.2
	2016	24.4	34.2	79.3	225.1	264.5	160.4	191.0	193.3	127.5	150.5	69.5	28.1	1547.8
	2017	13.3	187.9	102.7	160.9	191.2	171.3	176.7	165.3	280.2	266.9	74.5	15.6	1806.5
	2018	14.6	116.5	109.4	214.1	232.8	189.6	155.5	207.9	163.1	91.8	104.6	33.1	1633.0
	2019	11.3	93.5	197.4	225.2	260.3	284.8	244.5	196.8	191.5	297.8	217.8	48.2	2269.1
	2020	46.3	118.3	141.8	178.3	211.8	182.6	219.5	195.3	174.6	136.4	84.5	55.9	1745.2
	2021	36.1	99.3	79.2	189.3	238.1	213.5	179.9	198.5	218.2	123.8	39.9	99.4	1715.4
	2022	40.1	61.0	93.6	203.7	221.0	163.7	172.3	205.7	199.5	155.2	73.8	69.9	1659.4

	2023	24.9	42.4	217.0	265.3	244.7	186.5	190.5	189.9	275.6	261.3	256.3	46.6	2200.9
	2024	0.0	0.0	0.0	0.0	0.0	0.0	0.0	0.0	0.0	0.0	0.0	0.0	**1841.1**
	MMRF	**38.1**	**70.6**	**134.9**	**208.5**	**231.5**	**204.4**	**202.7**	**194.2**	**208.0**	**165.7**	**123.1**	**59.5**	
	Year	**Jan**	**Feb**	**Mar**	**Apr**	**May**	**Jun**	**Jul**	**Aug**	**Sep**	**Oct**	**Nov**	**Dec**	**MARF**
	2000	13.5	18.4	65.0	186.1	243.1	114.1	226.1	179.5	179.0	257.8	72.0	28.6	1583.2
	2001	23.2	64.4	168.0	221.9	265.1	222.7	247.3	209.3	230.6	166.3	73.4	15.5	1907.6
	2002	67.3	29.9	209.0	157.1	189.8	189.8	151.3	169.9	141.9	159.1	35.7	196.0	1696.7
	2003	57.9	108.4	128.6	153.3	102.2	249.8	213.2	291.0	239.8	131.9	79.6	41.9	1797.6
	2004	98.4	51.1	95.2	178.5	233.9	155.4	230.5	234.6	233.6	170.0	117.3	52.5	1851.2
	2005	39.0	23.1	246.8	190.3	320.8	156.1	258.5	194.2	200.8	205.2	91.8	7.9	1934.6
	2006	25.2	135.9	244.5	186.8	256.1	208.9	237.6	275.3	158.0	249.1	115.8	123.1	2216.4
	2007	75.4	94.5	183.7	193.7	247.3	176.4	249.9	206.4	301.6	136.7	45.1	8.7	1919.5
	2008	59.1	79.2	59.9	221.8	281.0	176.8	246.0	290.6	212.1	264.4	97.5	26.1	2014.6
	2009	79.1	68.5	148.7	213.8	215.5	165.1	170.8	204.5	154.6	242.5	78.9	85.4	1827.4
	2010	41.7	177.6	208.5	179.5	307.9	210.0	197.8	205.2	243.7	83.3	53.5	52.3	1961.2
Felegeselam	2011	21.3	56.2	105.7	227.4	378.1	254.7	261.4	273.3	301.8	105.1	218.8	23.7	2227.5
	2012	14.5	29.9	106.2	239.4	213.2	215.3	314.4	217.5	274.7	110.4	144.9	36.8	1917.2
	2013	45.2	51.0	144.7	215.3	227.4	165.8	238.5	261.7	298.7	185.9	175.8	8.5	2018.6
	2014	18.5	84.4	211.3	314.2	364.4	159.4	180.1	294.2	261.7	275.9	101.0	31.2	2296.2
	2015	38.4	62.3	132.5	265.2	290.7	230.0	232.3	174.0	193.5	254.2	180.9	77.2	2131.2
	2016	24.9	48.9	101.9	241.7	269.6	174.3	193.2	225.9	118.2	185.9	56.4	21.6	1662.5
	2017	13.7	252.4	166.6	158.3	247.1	169.1	213.2	198.6	287.6	343.2	90.8	13.4	2154.0
	2018	12.9	192.2	119.1	312.1	324.8	211.2	157.5	273.6	180.8	129.1	89.5	29.9	2032.6
	2019	10.6	136.7	202.9	266.8	342.5	304.0	330.0	246.2	214.2	321.9	214.6	81.1	2671.4
	2020	66.0	176.8	161.6	176.4	226.7	175.4	217.0	266.2	209.6	161.9	78.9	55.4	1971.8
	2021	32.6	109.2	66.9	209.4	282.3	182.9	199.7	254.9	242.5	136.3	29.5	71.0	1817.1
	2022	44.2	69.7	97.8	231.0	223.1	149.3	170.3	210.8	203.5	219.7	79.8	52.9	1752.0
	2023	23.8	53.0	263.7	314.6	282.7	183.5	184.4	196.9	298.2	387.7	262.8	44.3	2495.6

	2024	0.0	0.0	0.0	0.0	0.0	0.0	0.0	0.0	0.0	0.0	0.0	0.0	**2278.9**
	MMRF	**45.1**	**103.5**	**173.3**	**250.2**	**301.7**	**219.0**	**253.4**	**264.5**	**256.2**	**232.6**	**123.1**	**56.4**	
schadda	Year	**Jan**	**Feb**	**Mar**	**Apr**	**May**	**Jun**	**Jul**	**Aug**	**Sep**	**Oct**	**Nov**	**Dec**	**MARF**
	2000	10.6	14.0	58.0	171.2	232.9	118.7	216.9	202.9	148.0	260.2	49.8	23.1	1506.4
	2001	20.8	42.7	163.8	227.0	253.4	203.0	215.4	199.4	224.2	175.2	48.9	22.6	1796.4
	2002	71.4	24.4	213.3	146.9	183.6	160.6	151.6	159.5	129.6	173.2	25.9	187.7	1627.6
	2003	50.9	79.3	111.2	147.3	108.9	230.7	223.4	307.6	206.6	135.2	56.7	40.2	1698.0
	2004	88.9	39.5	76.7	179.7	230.0	139.0	218.0	235.8	194.6	170.7	121.4	46.0	1740.3
	2005	35.9	19.5	221.8	174.3	348.5	148.3	260.2	182.6	168.9	206.7	78.7	7.2	1852.6
	2006	19.4	106.7	230.4	170.3	261.1	179.8	217.8	285.6	141.6	246.3	117.4	143.6	2120.1
	2007	71.1	70.5	181.7	191.9	250.3	171.8	236.7	205.4	269.1	151.1	32.8	8.4	1840.7
	2008	47.0	56.2	56.5	210.4	271.9	171.1	235.0	273.3	206.4	278.5	109.7	23.3	1939.1
	2009	61.8	53.3	135.7	189.1	215.9	144.1	146.2	203.7	151.1	250.8	70.3	82.0	1703.9
	2010	41.6	145.1	196.8	168.8	304.4	188.5	195.1	187.7	223.5	91.0	46.4	36.6	1825.4
	2011	16.3	42.6	101.3	215.6	389.5	218.2	244.5	268.5	275.6	109.5	211.4	22.8	2115.7
	2012	12.1	21.7	86.1	245.4	188.3	191.8	300.8	207.2	240.9	107.3	110.0	37.3	1748.9
	2013	46.1	40.5	152.4	238.3	203.0	181.2	245.0	261.6	285.2	228.0	169.3	8.5	2058.9
	2014	17.9	58.0	225.1	326.1	395.9	149.4	161.7	287.1	243.5	304.3	84.0	24.8	2277.8
	2015	34.4	38.8	126.7	263.3	281.4	223.0	224.4	173.8	191.1	295.7	183.4	67.1	2103.2
	2016	18.7	43.8	81.0	280.4	245.5	169.6	172.2	210.7	120.8	234.1	65.2	19.5	1661.7
	2017	17.2	213.8	158.8	154.8	255.1	145.6	211.9	185.1	279.9	333.7	99.5	12.1	2067.5
	2018	11.4	187.9	114.8	340.1	329.7	208.3	128.2	259.5	161.7	130.6	94.4	32.3	1998.9
	2019	9.4	107.9	194.8	279.8	356.7	294.4	330.9	242.2	198.9	345.2	197.0	82.3	2639.5
	2020	59.2	133.1	201.9	187.7	247.0	184.3	202.0	278.3	208.7	156.0	77.6	49.7	1985.5
	2021	23.7	92.5	64.0	216.0	262.9	138.8	184.1	241.0	253.5	164.6	21.7	60.2	1723.0
	2022	36.6	58.5	104.1	228.1	226.9	126.8	165.3	187.3	198.2	228.3	69.0	53.0	1682.0
	2023	21.8	42.5	258.6	335.2	290.0	171.2	170.5	180.3	278.8	401.7	236.6	51.8	2439.1
	MMRF	**36.7**	**75.3**	**152.9**	**229.9**	**275.3**	**185.1**	**219.9**	**235.9**	**217.4**	**225.1**	**103.4**	**49.7**	**2197.7**

8.4 APPENDIX 4: BOREHOLE LOGS

Project	Contractor	Sub Contractor	Consultant
Bonga-Ameya-Chida Road Project, Lot-I: Bonga - Felegeselam	Zhongmei Engineering Group LtD.	CWCE PLC	DANA Consulting Engineers PLC

Location/Chainage: 17+160	Drilling Method: Dry boring	Water level: 10.50
Coordinates (E/N): 203195 793858	Core diameter (mm): 97(0.0-8.0)mm, 75mm (8.0-15.0m)	Sheet: 1 of 1
Ground Elevation (masl.): 2105	Casing type & depth: Hw	BH Inclination: -90
Borehole No.: BH-15	Date Started: 26-May-2019	Bit type: Carbide/Diamond
Total Depth (m): 15	Date Completed: 31-May-2019	Type of Rig: Convetional

Depth (m)	Core run	TCR (%)	SCR (%)	RQD (%)	Sample Depth	Sample Type	SPT	N	SPT graph N-value	Soil/Rock description	Soil/Rock symbole	Core photographs
0												
1	1.00	100										
2	2.00	100			1.5 1.95	D	2,2,7	9				
3	3.00	100			3 3.45	D	2,2,3	5		Soft to firm, wet, silty CLAY with some Boulders		5
4	4.00	100										
5	5.00	100										
	5.40	0										
6	6.00	100			6 6.45	D	1,1,1	2				
7	7.00	100										
8	8.00	100			7.5 7.8	UD					7.80	
9	9.00	100			8.5 8.95	D	11,14,21	35		Very stiff, light gray mottled orange, moist, clayey SILT (TUFF)		10
10	10.00	100									10.50	
11	11.00	100	98	0	11 11.07	D RC				Weak, dark gray, very closely jointed & highly fractured BASALT, BASALT infilling with dark gray clay		15
12	12.00	100	98	0								
13	13.00	100	98	0								
14	14.00	100	98	0								
15	15.00	100	98	0							15.00	

Site Photograph

Driller: Eshetu Yasin

Logged by: Hagos k/Mariam

Checked by: Kassahun Zergaw

Note:
D=Disturbed Sample (Split spoon)
UD=Undisturbed Sample
RC=Rock Core Sample
SPT=Standard Penetration Test
SCR=Solid Core Recovery
RQD=Rock Quality Designation
HF= Highly Fractured

Project	Contractor	Sub Contractor	Consultant
Bonga-Ameya-Chida Road Project, Lot-I: Bonga - Felegeselam	Zhongmei Engineering Group LtD.	CWCE PLC	DANA Consulting Engineers PLC

Location/Chainage: 20+510	Drilling Method: Dry/Wash boring		Water level: 4.50
Coordinates (E/N): 205215 792144	Core diameter (mm): 97(0.0-9.0)mm, 75mm (9.0-15.0m), (15.0-20.0)64mm		Sheet: 1 of 1
Ground Elevation (masl.): 2287	Casing type & depth: Hw	BH Inclination: -90	
Borehole No.: BH-11	Date Started: 15-May-2019	Bit type: Carbide/Diamond	
Total Depth (m): 20	Date Completed: 24-May-2019	Type of Rig: Convetional	

Depth (m)	Core run	TCR (%)	SCR (%)	RQD (%)	Sample Depth	Sample Type	SPT	N	SPT graph N-value	Soil/Rock description	Soil/Rock symbole	Core photographs
0–1	1.00	100										
1–2	2.00	100										
2–3	3.00	100			2.3 2.7	UD				Firm to very stiff, light brown, moist, high plastic, fat CLAY with sand (CH).		
3–4	4.00	100										
4–5	5.00	100			4.5 4.95	D	3,5,18	23				
5–6	6.00	100			6 6.45	D	1,3,3	6				
6–7	7.00	100									7.50	
7–8	8.00	100			7.5 7.95	D	3,5,7	12				
8–9	9.00	95								Stiff, dark gray, lean CLAY (CL) with some boulders.		
9–10	10.00	95			9 9.05		50,R	50				
10–11	11.00	100									11.00	
11–12	12.00	100										
12–13	13.00	100			12 12.45	D	15,29,40	69		Very stiff reddish brown, fat CLAY with sand (CH).		
13–14	14.00	100			13.5 13.95	D	17,30,39	69				
14–15	15.00	100									15.00	
15–16	16.00	100			15.5 15.55	D	50,R	50				
16–17	17.00	100								Very stiff, light gray, gravelly lean CLAY with sand (CL), weathred product of RHYOLITE)		
17–18	18.00	100										
18–19	19.00	100			18.5 18.56	D	50,R	50				
19–20	20.00	100									20.00	

Site Photograph

Driller: Eshetu Yasin

Logged by: Hagos k/Mariam

Checked by: Kassahun Zergaw

Note:

D=Disturbed Sample (Split spoon)
UD=Undisturbed Sample
RC=Rock Core Sample
SPT=Standard Penetration Test
SCR=Solid Core Recovery
RQD=Rock Quality Designation
HF= Highly Fractured

Project	Contractor	Sub Contractor	Consultant
Bonga-Ameya-Chida Road Project	Zhongmei Engineering Group LtD.	CWCE PLC	DANA Consulting Engineers PLC

Location/Chainage: 35+220	Drilling Method: Dry/Wash boring	Water level: 6.0
Coordinates (E/N): 212195 78758	Core diameter (mm): 97(0.0-4.50), 75 (4.50-20.0m)	Sheet: 1 of 1
Ground Elevation (masl.): 1715	Casing type & depth: Hw	BH Inclination: -90
Borehole No.: BH-10	Date Started: 14-Apr-2019	Bit type: Carbide/Diamond
Total Depth (m): 20	Date Completed: 21-Apr-2019	Type of Rig: Convetional

Depth (m)	Core run	TCR (%)	SCR (%)	RQD (%)	Sample Depth	Sample Type	SPT	N	Soil/Rock description
0	0.70	100							Backfill for road pavement
1	1.00	100							
2	2.00	100			1.5 1.95	D	9,6,9	15	Stiff to hard, dark grey to dark brown, lean CLAY(CL) with some gravel
3	3.00	100			3 3.45	D	2,3,5	8	
4	4.00	100			4.5 4.95	D	2,3,4	7	
5	5.00	100			6 6.45	D	5,5,5	10	
6	6.00	100			7.15 7.35	UD D	6,12,26	38	
7	7.00	100			7.5 7.95	UD			Hard, reddish brown, fat CLAY (CH) with some silt
8	8.00	100			9 9.3	D	15,21,23	44	
9	9.00	100			9.3 9.75	D	23,24,30	54	
10	10.00	100			10.5 10.95				
11	11.00	100			12 12.15	D	50/R	50	Hard, light brown mottled grey and orange, lean CLAY (CL) with some gravel
12	12.00	100			13.5 13.65	D	50/R	50	
13	13.00	100			15 15.45	D	19,23,27	50	
14	14.00	100			16.5 16.95	D	23,27,33	60	
15	15.00	100			18 18.45	D	15,19,23	42	
16	16.00	100							
17	17.00	100							
18	18.00	100							
19	19.00	100							
20	20.00	100							

SPT graph: N-value (4, 24, 44)

Soil/Rock symbole: 0.70; 7.50; 10.00; 20.00

Core photographs: 5; 10; 15; 20

Site Photograph

Driller: Eshetu Yasin

Logged by: Hagos k/Mariam

Checked by: Kassahun Zergaw

Note:

D=Disturbed Sample (Split spoon)
UD=Undisturbed Sample
RC=Rock Core Sample
SPT=Standard Penetration Test
SCR=Solid Core Recovery
RQD=Rock Quality Designation
HF= Highly Fractured

Project	Contractor	Sub Contractor	Consultant
Bonga-Ameya-Chida Road Project; Lot-II: Felegeselam-Ameya-Chida	Zhongmei Engineering Group LtD.	CWCE PLC	UNICONE

Location/Chainage: 52+200	Drilling Method: Dry/Wash boring	Water level: Nill
Coordinates (E/N): 223919 784540	Core diameter (mm): 97(0.0-2.50)mm, 75mm (2.50-20.75m)	Sheet: 1 of 1
Ground Elevation (masl.): 2685	Casing type & depth: Hw/9	BH Inclination: -90
Borehole No.: BH-08	Date Started: 21-Apr-2019	Bit type: Carbide/Diamond
Total Depth (m): 20.75	Date Completed: 1-May-2019	Type of Rig: Wireline, XYT-3B

Depth (m)	Core run	TCR (%)	SCR (%)	RQD (%)	Sample Depth	Sample Type	SPT	N	SPT graph N-value	Soil/Rock description	Soil/Rock symbole	Core photographs
0										Back fill	0.50	
1	1.00	100										
2	2.00	100			1.5 1.95	D	2,4,4	8		Very stiff to hard, light gray mottled orange, sandy lean CLAY with Gravel (CL), around 8.0m some seepage)		
3	3.00	100			3 3.45	D	4,2,4	6				
4	4.00	100										
5	5.00	100			4.5 4.95	D	10,17,13	30				
6	6.00	100										
7	7.00	70			6 6.45	D	9,12,11	23			6.50	
8	8.00	70			7.5 7.95	D	10,14,15	29				
9	9.00	75										
10	10.00	75										
11	11.00	75								very dense, dark gray, moist, clayey SAND with Gravel (SC) and boulders.		
12	12.00	80										
13	13.00	80			12 12.45	D	12,14,17	31				
14	14.00	80			13.5 13.95	D	14,19,23	42				
15	15.00	80			15 15.45	D	10,15,18	33				
16	16.00	80										
17	17.00	80			16.5 16.95	D	12,17,24	41				
18	18.00	80										
19	19.00	80			18 18.45	D	13,16,22	38				
20	20.00	80										
21	20.75	60			19.45 19.5	D	10,14,20	34		Very hard, light yellow, moist, lean CLAY (CL) a product of altered Rhyolite with Tuff	20.75	

Site Photograph

Driller: Gashaw Adem

Logged by: Hagos k/Mariam

Checked by: Kassahun Zergaw

Note:

D=Disturbed Sample (Split spoon)
UD=Undisturbed Sample
RC=Rock Core Sample
SPT=Standard Penetration Test
SCR=Solid Core Recovery
RQD=Rock Quality Designation
HF= Highly Fractured

Project	Contractor	Sub Contractor	Consultant
Bonga-Ameya-Chida Road Project, Lot-2: Felegeselam-Ameya-Chida	Zhongmei Engineering Group LtD.	CWCE PLC	UNICONE

Location/Chainage: 53+160	Drilling Method: Dry/Wash boring	Water level: 8.0
Coordinates (E/N): 224290 784711	Core diameter (mm): 75 mm(0.0-29.00m)	Sheet: 1 of 2
Ground Elevation (masl.): 2640	Casing type & depth: Hw/10	BH Inclination: -90
Borehole No.: BH-02	Date Started: 11-Jun-2019	Bit type: Carbide/Diamond
Total Depth (m): 29	Date Completed: 18-Jun-2019	Type of Rig: Wireline, XYT-3B

Depth (m)	Core run	TCR (%)	SCR (%)	RQD (%)	Sample Depth	Sample Type	SPT	N	SPT graph N-value	Soil/Rock description	Soil/Rock symbole	Core photographs
0	0.5	98								Very soft, light yellow, lean clay with sand (CL), product of RHYOLITE/Trachayte		
1	1.00	98										
2	2.00	98			1.5 1.95	D	1,1,1	2			2.00	
3	3.00	100			3 3.45	D	4,3,3	6				
4	4.00	100										
5	5.00	100			4.5 4.95	D	8,9,3	12				5
6	5.50	100			6 6.45	D	7,8,12	20				
7	7.00	100										
8	8.00	100										
9	9.00	100			8.6 8.8	UD D	9,7,3	10		Stiff to very stiff, brown mottled gray, highly plastic, moist, sandy lean CLAY with Gravel (CL) and boulders		
10	10.00	100			9 9.45							10
11	11.00	98										
12	12.00	98			12 12.45	D	3,7,3	10				
13	13.00	100										
14	14.00	98										

Site Photograph

Driller: Gashaw Adem

Logged by: Hagos k/Mariam

Checked by: Kassahun Zergaw

Note:

D=Disturbed Sample (Split spoon)
UD=Undisturbed Sample
RC=Rock Core Sample
SPT=Standard Penetration Test
SCR=Solid Core Recovery
RQD=Rock Quality Designation
HF= Highly Fractured

Project	Contractor	Sub Contractor	Consultant
Bonga-Ameya-Chida Road Project, Lot-2: Felegeselam-Ameya-Chida	Zhongmei Engineering Group LtD.	CWCE PLC	UNICONE

Location/Chainage: 53+160	Drilling Method: Dry/Wash boring	Water level: 8.0
Coordinates (E/N): 224290 784711	Core diameter (mm): 75 mm(0.0-29.00m)	Sheet: 2 of 2
Ground Elevation (masl.): 2640	Casing type & depth: Hw/10	BH Inclination: -90
Borehole No.: BH-02	Date Started: 11-Jun-2019	Bit type: Carbide/Diamond
Total Depth (m): 29	Date Completed: 18-Jun-2019	Type of Rig: Wireline, XYT-3B

Depth (m)	Core run	TCR (%)	SCR (%)	RQD (%)	Sample Depth	Sample Type	SPT	N	SPT graph N-value	Soil/Rock description	Soil/Rock symbole	Core photographs
15	15.00											15
16	16.00	80										
17	17.00	80			16.5 16.95	D	7,9,12	21			17.50	
18	18.00	100										
19	19.00	40										
20	20.00	80			19.45 19.5	D	17,32,20	52				20
21	21.00	98			21 21.45	D	12,14,13	27				
22	22.00	95										
23	23.00	95			22.5 22.95	D	12,18,22	40		Very stiff to hard, dry, light brown mottled orange, low plastic, sandy lean CLAY (CL) (Altered RHYOLITE)		25
24	24.00	100			24 24.45	D	17,24,45	69				
25	25.00	98			25 25.95	D	23,30,50	80				
26	26.00	98										
27	27.00	100										
28	28.00	100									29.00	29
29	29.00	100										

Site Photograph

Driller: Gashaw Adem

Logged by: Hagos k/Mariam

Checked by: Kassahun Zergaw

Note:

D=Disturbed Sample (Split spoon)
UD=Undisturbed Sample
RC=Rock Core Sample
SPT=Standard Penetration Test
SCR=Solid Core Recovery
RQD=Rock Quality Designation
HF= Highly Fractured

Borehole Data Collection Format for Foundation Investigation

CORE/GE/RF/086/B

CORE Consulting Engineers Plc
Tel: 251-11-3-206032,251-11-3-727013
Fax: 251-1-2306033 P.O.Box
Email: coreconsult@ethionet.et
Addis Ababa, Ethiopia

BOREHOLE LOG

BH: BH-1

SHEET: 1 of 1

PROJECT: Felege Selam - Ameya - Chida Road Project
CLIENT: Zhongmei Engineering Group Ltd.
SITE LOCATION: 57+600 - 57+660
BH COORDINATE(UTM-Adindan Datum)
EASTING: 226809.12
NORTHING: 786514.03
GROUND ELEVATION(m): 2442.47

DRILLING TYPE: Rotary Drilling
INCLINATION: Vertical
TOTAL DEPTH DRILLED: 17.5m
GWL: Not Encountered
FLUSHING SYSTEM: Water
DATE STARTED: 25/03/2019
DATE COMPLETED: 27/03/2019

Elevation (m)	Depth (m)	Run Length	TCR	RQD	Penetration Rate (minute)	Hole dia.	Sampling	SPT	GWL	Graphic Log	Field Description of Soil/Rock	Photo
2442	0	1.5	100		4	100	D	5/7/7			Light to Brownish gray decomposed rock resembles a silty clay /clayey silt soil with gravel	
2441	2	1.5	100		2			7/15/17				
2440												
2439	4	1.5	100		2			8/18/30				
2438		0.7	100		1							
2437	6	1.3	100		3			R				
2436		1	100		9			R				
2435	8										7.5	
2434		1.5	100	45	37						Grayish, highly weathered, highly fractured basaltic rock	
2433	10	0.5	100	33	18							
2432		1.1	100	14	26	86						
2431	12	1	100	35	15						12.1	
2430		0.7	100	64	21		R				Grayish, slightly weathered, moderately fractured, strong basaltic rock	
2429		1.2	100	86	18							
2428	14	1	100	67	19						15.15	
2427		0.6	33	0	9						Reddish silty clay soil (Paleosol) 15.6	
2426	16	1.9	80	75	46						Grayish, highly weathered, moderately fractured basaltic rock	
2425	18										17.5	

BH = Borehole
N = Blows/30cm
SPT = Standatd Penetration test
USCS = Unified Soil Classifcation System

RQD = Rock Quality Designation
TCR = Total Core Recovery
GWL = Ground Water Level

D Distrubed Sample
U Undistrubed Sample
R Rock Sample

REMARK:_____

LOGED BY: _____
APPROVED BY: _____
SCALE: _____

Borehole Data Collection Format for Foundation Investigation

CORE/GE/RF/086/B

CORE Consulting Engineers Plc
Tel: 251-11-3-206032,251-11-3-727013
Fax: 251-1-2306033 P.O.Box
Email: coreconsult@ethionet.et
Addis Ababa, Ethiopia

BOREHOLE LOG

BH: BH-2

SHEET: 1 of 1

PROJECT: Felege Selam - Ameya - Chida Road Project
CLIENT: Zhongmei Engineering Group Ltd.
SITE LOCATION: 63+550 - 63+640
BH COORDINATE(UTM-Adindan Datum)
EASTING: 231171.17
NORTHING: 787148.56
GROUND ELEVATION(m): 2461.73

DRILLING TYPE: Rotary Drilling
INCLINATION: Vertical
TOTAL DEPTH DRILLED: 28.0m
GWL: 8.4m
FLUSHING SYSTEM: Water
DATE STARTED: 22/03/2019
DATE COMPLETED: 27/03/2019

Elevation (m)	Depth (m)	Run Length	TCR	RQD	Penetration Rate (minute)	Hole dia.	Sampling	SPT	GWL	Graphic Log	Field Description of Soil/Rock	Photo
2461	0	0.6	100		1						Light to dark brown gravel mixture with fews, cobbles and boulders 2	
2460	2	1.8	100		13							
2459		0.9	100		6							
2458	4	0.7	100		4							
2457		0.8	93		8							
		0.4	100		12							
2456	6	0.6	100		8		D				Light brown decomposed rock resembles a clayey gravel soil.	
2455		1.3	100		26							
2454	8	0.7	100		7				8.4 ▽			
2453		0.7	100		15							
2452		0.7	100		8							
	10	0.8	83		5							
		0.5	100		3			R				
2451		1	100	92	21			✳			11.3	
2450	12	0.5	100	60	12						Slightly weathered moderately fractured strong fresh grayish basaltic rock	
2449		0.9	82	66	1							
2448		0.9	87	47	30		R					
	14	0.6	87	60	19	89						
2447		0.6	73	30	20							
		0.4	88	25	22							
2446	16	0.6	82	20	16						16	
2445		0.4	100	65	65			22/R			Light to dark brown very stiff clay soil mixed with gravels and remnant decomposed rock	
2444		0.8	100		50			✳				
2443	18	0.9	100		54		D				19	
		0.5	40		17			R				
2442		1.7	100		37			✳			Brownish very stiff clayey silty sand soil with gravels and remnant decomposed rock	
2441	20	0.55	86		20			R			21.2	
								✳				
2440		0.8	94	26	8							
	22	0.5	90	20	20							
2439		0.5	94	76	20		R				Slightly weathered, moderately fractured, strong, fresh, grayish basaltic rock	
2438		0.7	100	91	23						24	
	24	0.8	100	100	30							
2437		1	95		21						Light to dark brown stiff clayey silt soil mixed with remnant decomposed rock	
		0.5	10		10							
2436	26						D				27	
2435		1	10		17							
2434	28	1	90		20						Light brownish clayey silt soil mixed with decomposed rock 28	

BH = Borehole
N = Blows/30cm
SPT = Standatd Penetration test
USCS = Unified Soil Classifcation System

RQD = Rock Quality Designation
TCR = Total Core Recovery
GWL = Ground Water Level

D Distrubed Sample
U Undistrubed Sample
R Rock Sample

REMARK:_____

LOGED BY:_____
APPROVED BY:_____
SCALE:_____

Borehole Data Collection Format for Foundation Investigation

CORE/GE/RF/086/B

CORE Consulting Engineers Plc
Tel: 251-11-3-206032,251-11-3-727013
Fax: 251-1-2306033 P.O.Box
Email: coreconsult@ethionet.et
Addis Ababa, Ethiopia

BOREHOLE LOG

BH: BH-2

SHEET: 1 of 1

PROJECT: Felege Selam - Ameya - Chida Road Project
CLIENT: Zhongmei Engineering Group Ltd.
SITE LOCATION: 65+600 - 65+750
BH COORDINATE(UTM-Adindan Datum)
EASTING: 230305.15
NORTHING: 788737.92
GROUND ELEVATION(m): 2429.89

DRILLING TYPE: Rotary Drilling
INCLINATION: Vertical
TOTAL DEPTH DRILLED: 20.0m
GWL: 0.0m
FLUSHING SYSTEM: Water
DATE STARTED: 01/04/2019
DATE COMPLETED: 03/04/2019

Elevation (m)	Depth (m)	Run Length	TCR	RQD	Penetration Rate (minute)	Hole dia.	Sampling	SPT	GWL	Graphic Log	Field Description of Soil/Rock	Photo
2429	0	0.75	100		1						Light brown clayey sand mixed with decomposed and fragmented coarse gravel size rock 1.5	
		0.75	100		1			3/2/2				
2428	2	0.75	0		2	110						
2427		0.75	0		1			1				
2426	4	1.5	57		2			2/1/1				
2425		1.5	100		2							
2424	6							1/1				
2423		1.5	0		2			1/1/1			Dark silty sand soil mixed with coarse gravel size, sub angular shaped rock fragments (flow like viscous fluid)	
2422	8	1.5	100		2							
2421								1				
2420	10	0.5	0		2		D	1/1				
2419		0.5	0		1							
2418	12	1	70		4	89		2/1/1				
2417		1.5	35		3			3/3/5				
2416	14	1.5	93		3							
2415								R			15	
2414	16	1	100		4						Dark to light gray, decomposed vesicular basaltic rock resembles a clayey sand soil.	
		0.5	100		4			11/18/34				
2413		0.5	100		6							
2412	18	0.5	100		4			20/R				
2411		1.5	100		7							
2410	20	0.5	100		3			R			20	

BH = Borehole
N = Blows/30cm
SPT = Standatd Penetration test
USCS = Unified Soil Classifcation System

RQD = Rock Quality Designation
TCR = Total Core Recovery
GWL = Ground Water Level

D Distrubed Sample
U Undistrubed Sample
R Rock Sample

REMARK:

LOGED BY:
APPROVED BY:
SCALE:

8.5 APPENDIX 5: LABORATORY ANALYSIS SUMMARY

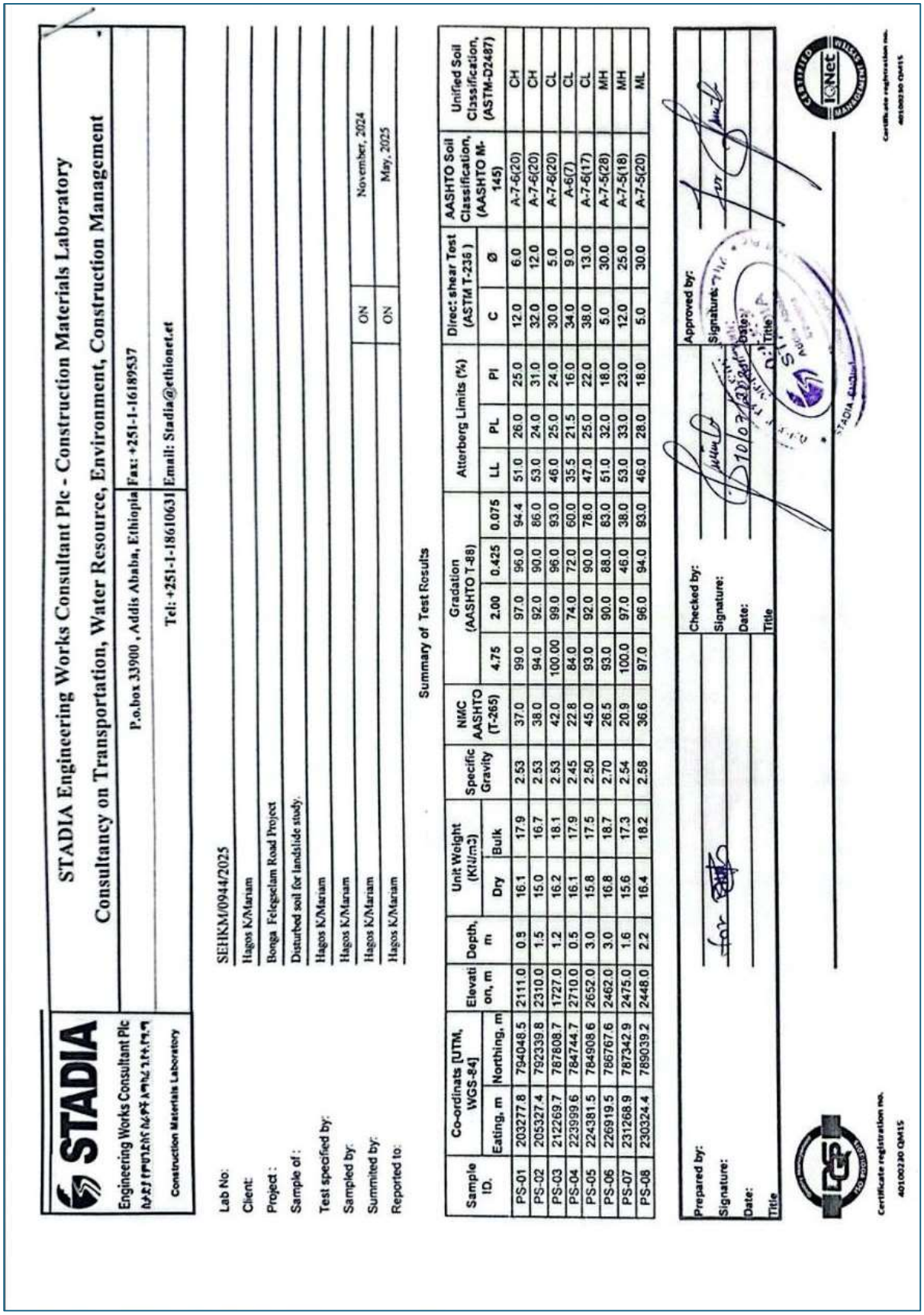

STADIA

STADIA Engineering Works Consultant Plc - Construction Materials Laboratory

Consultancy on Transportation, Water Resource, Environment, Construction Management

Engineering Works Consultant Plc
አዲስ ምህንድስና አማካሪ ድርጅት ኃ.የ.ተ.የ.ግ.ማ

Construction Materials Laboratory

P.o.box 33900 , Addis Ababa, Ethiopia | Fax: +251-1-16189537

Tel: +251-1-18610631 | Email: Stadia@ethionet.et

Lab No: SEHKM/0944/2025

Client: Hagos K/Mariam

Project : Bonga Felegselam Road Project

Sample of : Disturbed soil for landslide study.

Test specified by: Hagos K/Mariam

Sampled by: Hagos K/Mariam

Summited by: Hagos K/Mariam — ON — November, 2024

Reported to: Hagos K/Mariam — ON — May, 2025

Summary of Test Results

Sample ID.	Co-ordinats [UTM, WGS-84]		Elevation, m	Depth, m	Unit Weight (KN/m3)		Specific Gravity	NMC AASHTO (T-265)	Gradation (AASHTO T-88)			Atterberg Limits (%)			Direct shear Test (ASTM T-238)		AASHTO Soil Classification, (AASHTO M-145)	Unified Soil Classification, (ASTM-D2487)
	Easting, m	Northing, m			Dry	Bulk			4.75	2.00	0.425	0.075	LL	PL	PI	C	Ø	
PS-01	203277.8	794048.5	2111.0	0.9	16.1	17.9	2.53	37.0	99.0	97.0	96.0	94.4	51.0	26.0	25.0	12.0	6.0	A-7-6(20)	CH
PS-02	205327.4	792339.8	2310.0	1.5	15.0	16.7	2.53	38.0	94.0	92.0	90.0	86.0	53.0	24.0	31.0	32.0	12.0	A-7-6(20)	CH
PS-03	212269.7	787808.7	1727.0	1.2	16.2	18.1	2.53	42.0	100.00	99.0	96.0	93.0	46.0	25.0	24.0	30.0	5.0	A-7-6(20)	CL
PS-04	223999.6	784744.7	2710.0	0.5	16.1	17.9	2.45	22.8	84.0	74.0	72.0	60.0	35.5	21.5	16.0	34.0	9.0	A-6(7)	CL
PS-05	224381.5	784908.6	2652.0	3.0	15.8	17.5	2.50	45.0	93.0	92.0	90.0	78.0	47.0	25.0	22.0	38.0	13.0	A-7-6(17)	CL
PS-06	226919.5	786767.6	2462.0	3.0	16.8	18.7	2.70	26.5	93.0	90.0	88.0	83.0	51.0	32.0	18.0	5.0	30.0	A-7-5(28)	MH
PS-07	231268.9	787342.9	2475.0	1.6	15.6	17.3	2.54	20.9	100.0	97.0	46.0	38.0	53.0	33.0	23.0	12.0	25.0	A-7-5(18)	MH
PS-08	230324.4	789039.2	2448.0	2.2	16.4	18.2	2.58	36.6	97.0	96.0	94.0	93.0	46.0	28.0	18.0	5.0	30.0	A-7-5(20)	ML

Prepared by: | Checked by: | Approved by:

Signature: | Signature: | Signature:

Date: | Date: | Date:

Title | Title | Title

Certificate registration no. 4010030 QM15

8.6 APPENDIX-6: REMEDIAL MEASURES DRAWINGS

Slope H1, Km17+160

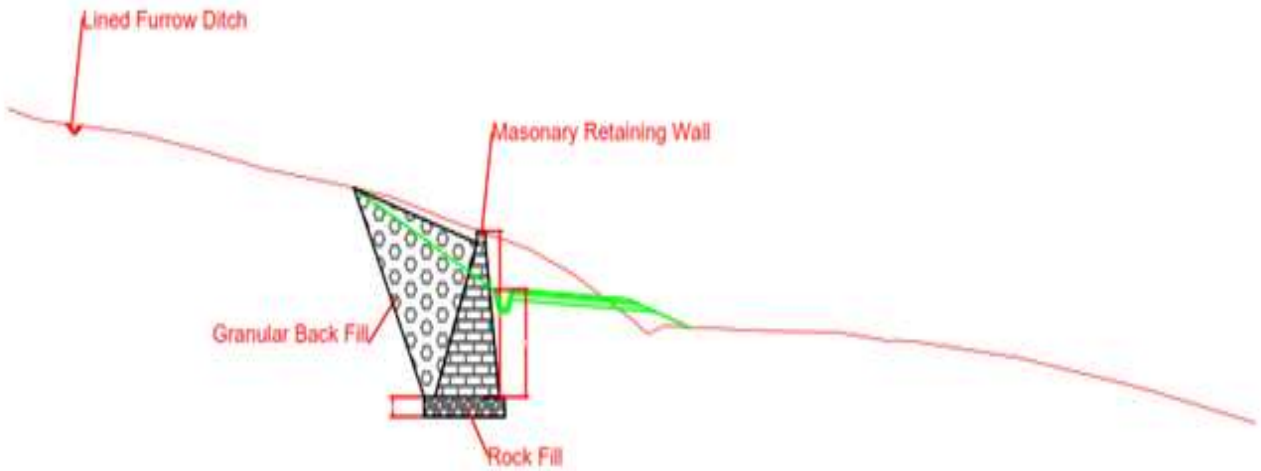

NOTES:

1.All dimension are in meters , quantity dimension are in square meters.
2.Remove,trim and level part of the failed mass(displaced material) slope mainly above the first bench to 2H:1V
3.Rock/granular backfill should be used behind retaining wall
4.Relief channel filled with rock shall be introduced across the road around km17+020.
5.Provide lined Furrow ditch at the slope stake of the flattened slope

Slope M1, Km20+510

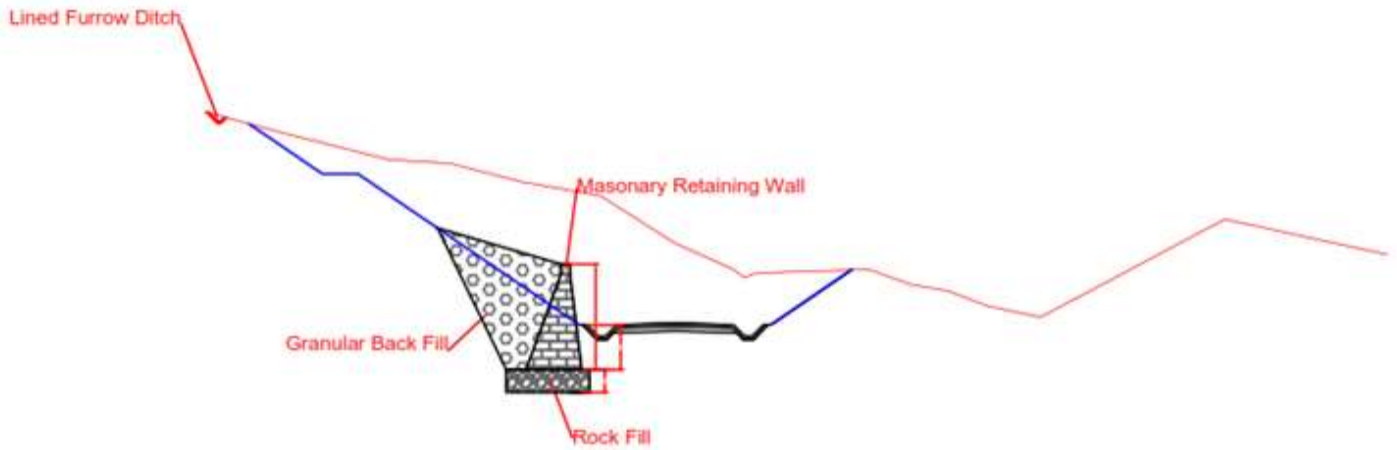

NOTES:

1.All dimension are in meters , quantity dimension are in square meters.
2.Remove,trim and level part of the failed mass(displaced material) slope mainly above the first bench to 2H:1V
3.Rock/granular backfill should be used behind retaining wall
4.Relief channel filled with rock shall be introduced across the road around km20+410.
5.Provide lined Furrow ditch at the slope stake of the flattened slope

Slope M2, Km35+220

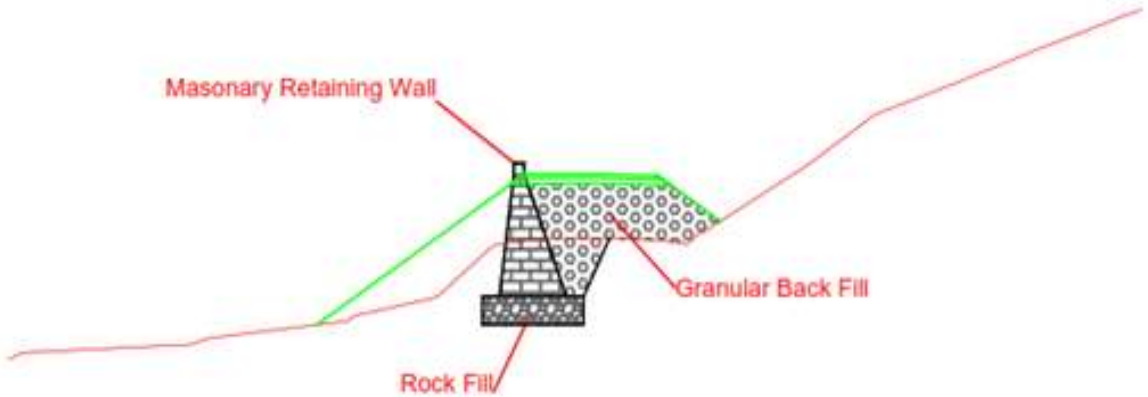

NOTES:

1.All dimension are in meters , quantity dimension are in square meters.
2.Remove,trim and level part of the failed mass(displaced material) mainly the asphalt road
3.Rock/granular backfill should be used behind retaining wall
4.Pave side ditch shall be introduced in the RHS.

NOTES:

1.All dimension are in meters , quantity dimension are in square meters.
2.Remove,trim and level part of the failed mass slope mainly above the first bench to 2H:1V
3.Rock/granular backfill should be used below the road level at least 60cml
4.Provide lined Furrow ditch at the slope stake of the flattened slope and bench drain

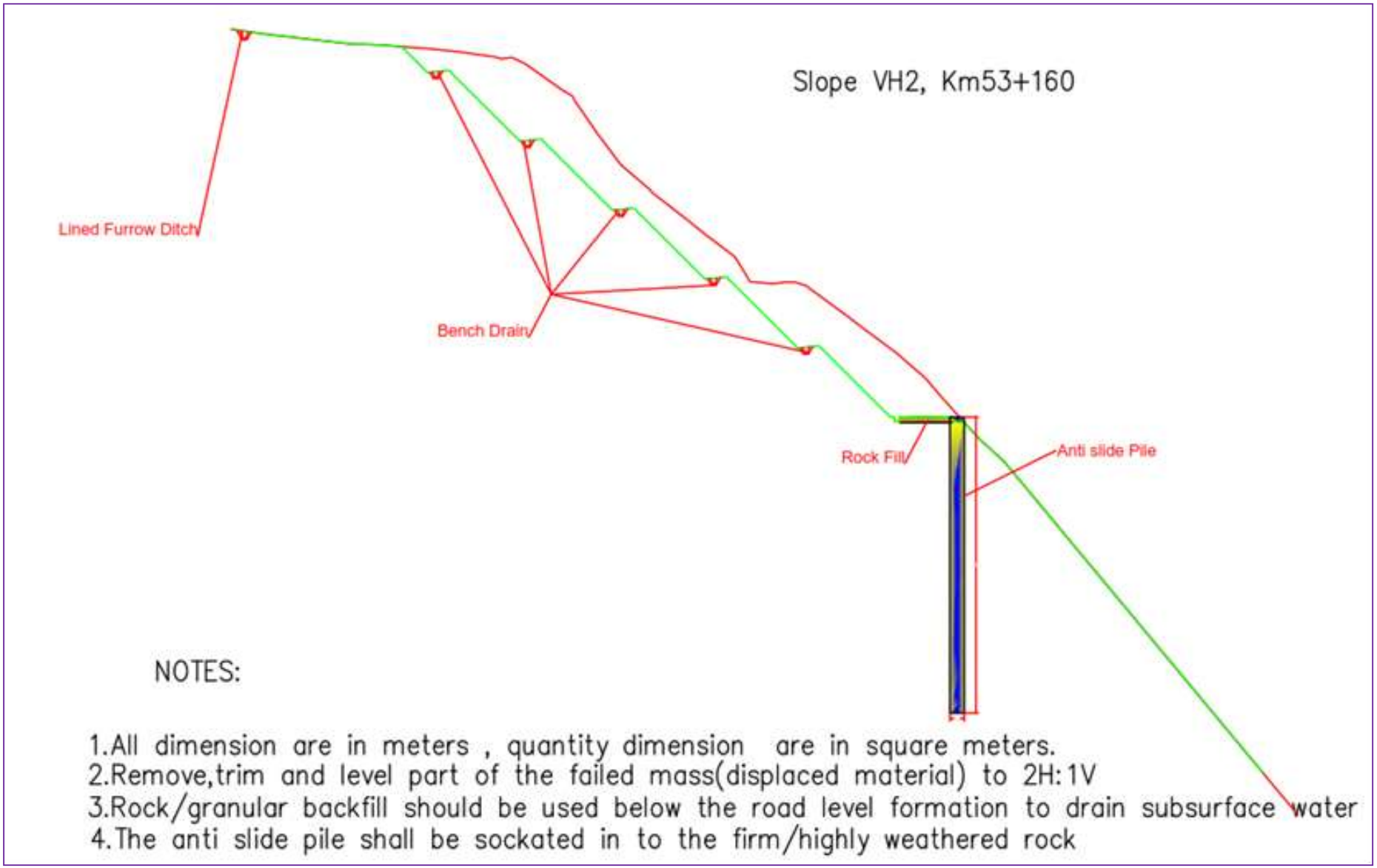
Slope VH2, Km53+160
Lined Furrow Ditch
Bench Drain
Rock Fill
Anti slide Pile
NOTES:
1.All dimension are in meters , quantity dimension are in square meters.
2.Remove,trim and level part of the failed mass(displaced material) to 2H:1V
3.Rock/granular backfill should be used below the road level formation to drain subsurface water
4.The anti slide pile shall be sockated in to the firm/highly weathered rock

Slope VH3, Km57+600

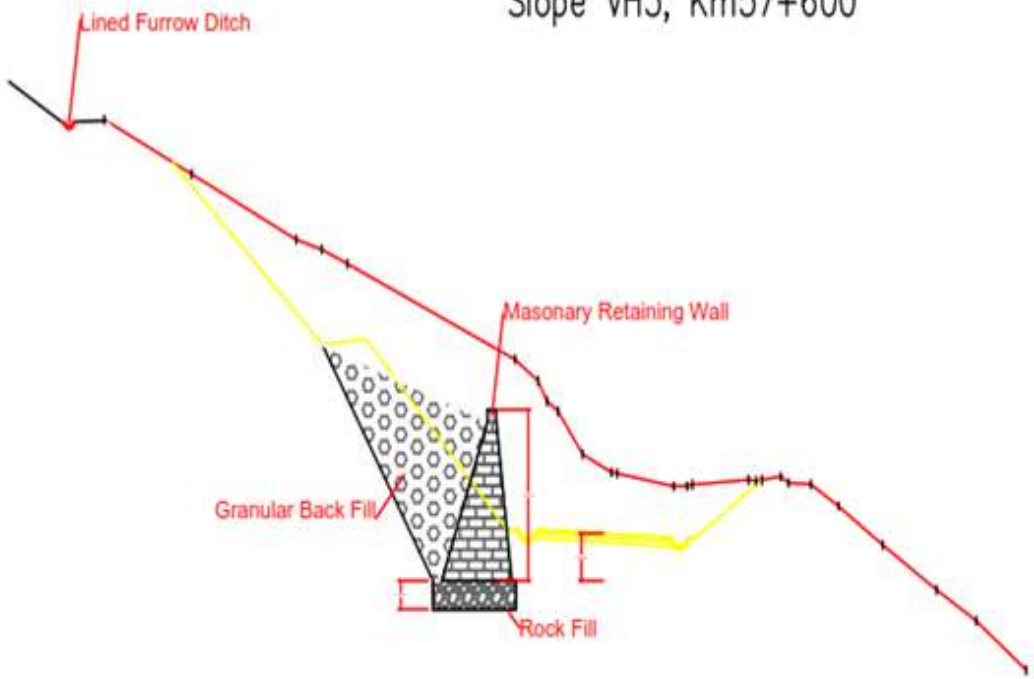

NOTES:

1.All dimension are in meters , quantity dimension are in square meters.
2.Remove,trim and level part of the failed mass(displaced material) slope mainly above the first bench to 2H:1V
3.Rock/granular backfill should be used behind retaining wall
4.Relief channel filled with rock shall be introduced across the road around km57+600.
5.Provide lined Furrow ditch at the slope stake of the flattened slope

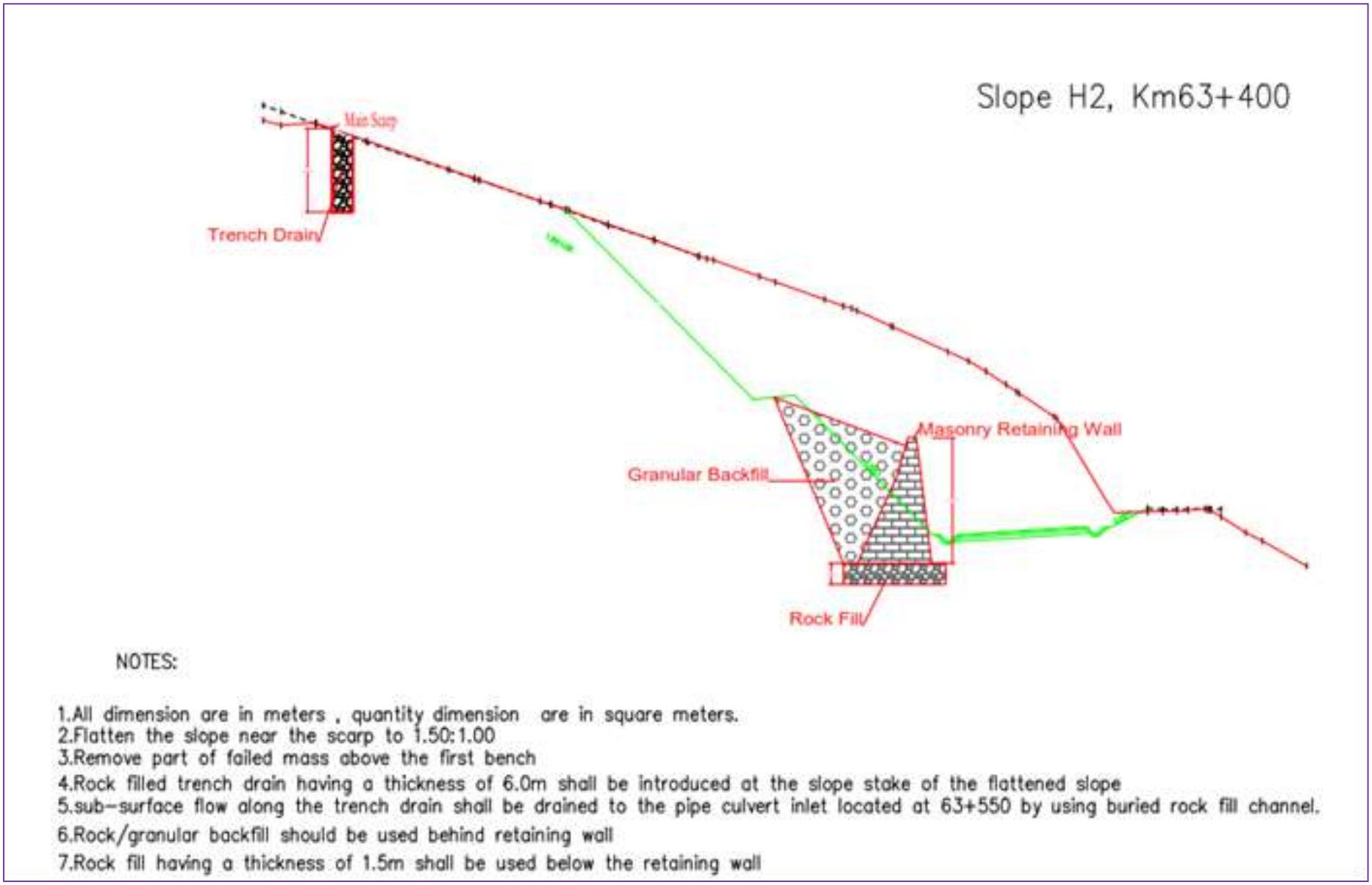
Slope H2, Km63+400
Main Scarp
Trench Drain
Masonry Retaining Wall
Granular Backfill
Rock Fill
NOTES:
1.All dimension are in meters , quantity dimension are in square meters.
2.Flatten the slope near the scarp to 1.50:1.00
3.Remove part of failed mass above the first bench
4.Rock filled trench drain having a thickness of 6.0m shall be introduced at the slope stake of the flattened slope
5.sub-surface flow along the trench drain shall be drained to the pipe culvert inlet located at 63+550 by using buried rock fill channel.
6.Rock/granular backfill should be used behind retaining wall
7.Rock fill having a thickness of 1.5m shall be used below the retaining wall

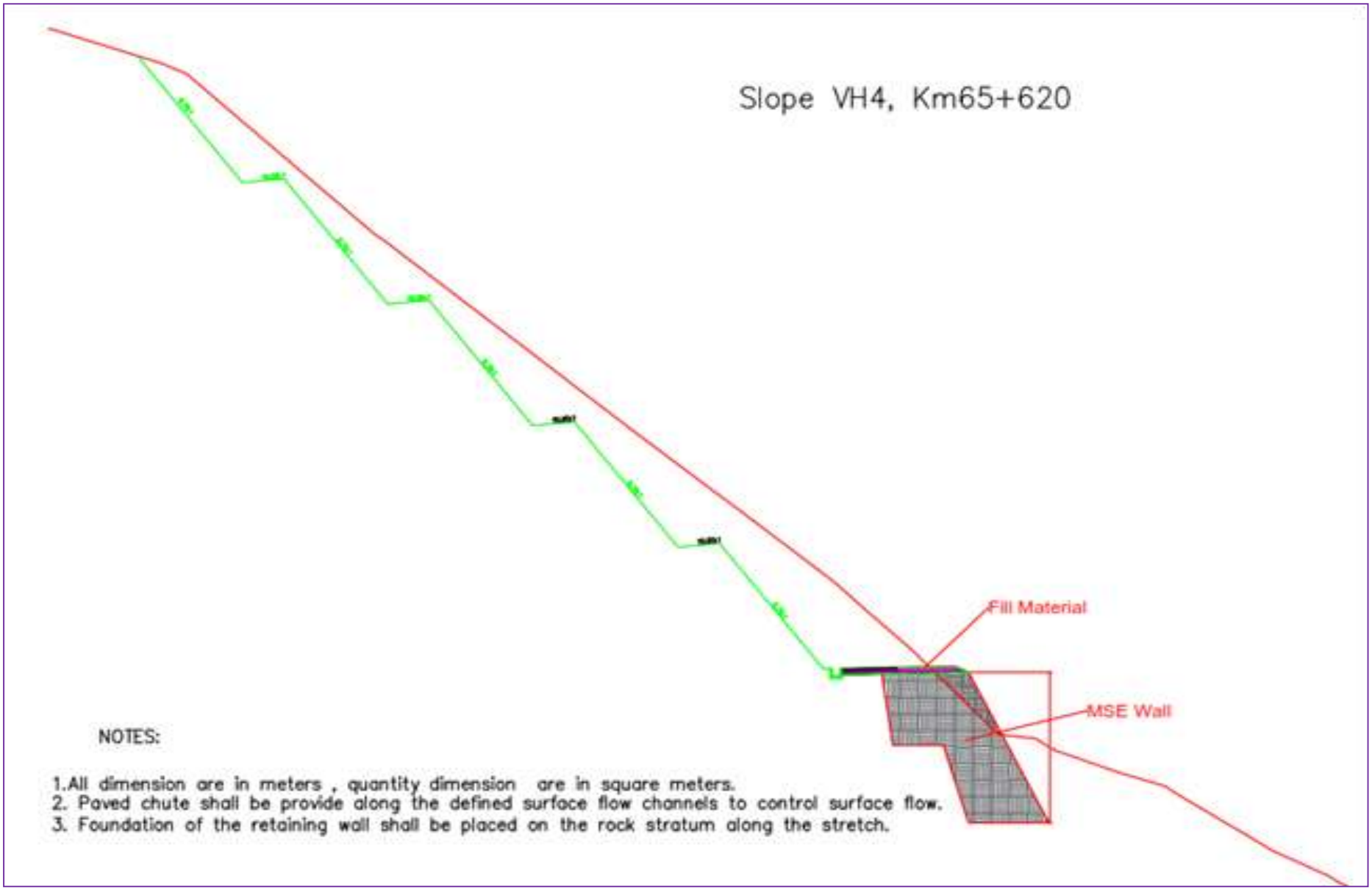
Slope VH4, Km65+620
Fill Material
MSE Wall
NOTES:
1.All dimension are in meters , quantity dimension are in square meters.
2. Paved chute shall be provide along the defined surface flow channels to control surface flow.
3. Foundation of the retaining wall shall be placed on the rock stratum along the stretch.